THE NON-DESTRUCTIVE TESTING OF ADHESIVELY BONDED STRUCTURES

by

C.C.H. Guyott

A thesis submitted to the University of London
for the degree of Doctor of Philosophy
and for the Diploma of Imperial College

Department of Mechanical Engineering
Imperial College of Science and Technology
London SW7

November 1986

Abstract

In spite of its potential advantages, the use of adhesive bonding in primary structure has been limited by the lack of non-destructive testing procedures to guarantee the reliablity of the joint. The three main types of defect that are commonly found in adhesive joints have been identified, the first type being complete voids, porosity and disbonds in the adhesive layer, the second type of defect being poor cohesive strength i.e. a weak adhesive layer, whilst the final type is low adhesion strength or a weak bond between the adhesive and the adherends.

At present there is only one commercially available instrument, the Fokker Bond Tester Mk II, that attempts to predict the cohesive strength of a joint. However, an investigation into the sensitivity of the instrument has shown that it is not able to detect changes in adhesive modulus and thickness, and hence cohesive strength, unless the adhesive layer has either much lower modulus or a significantly higher thickness than is commonly employed in high stength applications. There is therefore a need for the development of improved testing techniques.

The technique of ultrasonic spectroscopy has been thoroughly investigated and used to measure the resonant frequencies of plain plates and joints. A model was developed to predict the resonant frequencies and mode shapes of plain plates and joints, the predicted values showing excellent agreement with the measured resonant frequencies over a wide range of adhesive properties.

The tests reported here also show that measurements of the resonant frequencies of adhesive joints obtained using ultrasonic spectroscopy can be used to detect changes in adhesive thickness and modulus, accuracies of approximately 10% in thickness and 20% in modulus being obtained in joints typical of those used in primary structure. Consequently, it has been demonstrated that ultrasonic spectroscopy can be used to monitor the cohesive properties of a joint, a change from the normal values indicating a fault in the process control and a likely reduction in the cohesive strength of the joint.

Since there is no method suitable for the non-destructive detection of poor adhesion strength this problem is currently overcome by careful control of the surface preparation procedures. Further work is now required to develop a satisfactory method of testing for poor adhesion strength once the joint has been manufactured.

Acknowledgements

I would like to give particular thanks Dr Peter Cawley for his encouragement and guidance throughout my period of research. I am indebted to Prof. Bob Adams and John Skinner of Bristol University, for their advice and help in the manufacture of the adhesive joints. I would also like to acknowledge the advice and help given by Dr Tony Kinloch and the technical staff of the Mechanical Engineering Department in the preparation of test specimens.

In addition, I would like to thank Dr Peter Lloyd and Dr David Bruce at the Royal Aircraft Establishment for the arranging lone of equipment and for their advice.

Many thanks are also due to Josephine, my wife, for helping with a large proportion of the typing and more importantly for the valuable encouragement that she has given.

I would also like to take the opportunity of thanking British Aerospace Kingston and the SERC for their support in the funding of this research work.

The work presented here has formed the basis of the following papers :-

C.C.H. Guyott, P.Cawley, and R.D. Adams, "The Non-destructive Testing of Adhesively Bonded Structure: A Review", Journal of Adhesion v20 n2, pp129-159, 1986.

C.C.H.Guyott, P.Cawley, and R.D.Adams, "Use of the Fokker Bond Tester on Joints with Varying Adhesive Thickness", in proceedings of the International Conference on Structural Adhesives in Engineering, (I. Mech. E.), 2-4 July 1986, Bristol University.

C.C.H. Guyott, P. Cawley, and R.D. Adams, "Vibration Characteristics of the Mk II Fokker Bond Tester Probe", Ultrasonics Int. v24, pp318-324, 1986.

Contents

PART ONE - REVIEW

Chapter One

PART TWO - THE FOKKER BOND TESTER Mk II

Chapter Two

Chapter Three

PART THREE - ULTRASONIC SPECTROSCOPY

Chapter Four

Chapter Five

Experimental Results for a Plain Plate at Normal Incidence 134

Chapter Six

Chapter Seven

Experimentally Measured Spectra of Adhesive Joints 168

Chapter Eight

PART FOUR - CONCLUSIONS AND FURTHER WORK

Chapter Nine

Chapter Ten

Appendix

Nomenclature

A	Area of the adhesive or adherend over which deformation occurs = $\pi D^2/4$
A_P	Amplitude of incident pulse
A_1, A_2, etc	Amplitude of wave potential (subscript refers to wave type)
a_1, a_2, etc	Asymmetric Lamb modes of a plain plate
B_1, B_2, etc	Amplitude of wave potential (subscript refers to wave type)
C_1, C_2, etc	Amplitude of wave potential (subscript refers to wave type)
c	Longitudinal velocity in liquid
c_L	Longitudinal wave velocity (in a plain plate)
c_S	Shear wave velocity (in plain plate)
c_1, c_2	Longitudinal velocity (subscripts refer to material i.e. 1 - adherend, 2 - adhesive)
c', c''	Generalised wave velocity
D	Diameter of probe
D_1, D_2, etc	Amplitude of wave potential (subscript refers to wave type)
E_A	Modulus of adhesion layer
E_r	Calculated error between the predicted and measured frequencies of the joint
E_{res}	Resonant Bar modulus
E_1, E_2	Young's Modulus (subscripts refer to material i.e. 1 - adherend, 2 - adhesive)
E'_1, E'_2	Apparent modulus (subscripts refer to material i.e. 1 - adherend, 2 - adhesive)
$F_j(\omega)$	Harmonic force input at position j
F_{Ln}	Frequency of n^{th} longitudinal or through thickness mode of plate
F_{Sm}	Frequency of m^{th} shear mode of plate
f_d	Frequency of disc membrane resonance
f_m	Frequency of the mass-spring-mass model for the first mode of the joint
f_n	Predicted frequency of n^{th} mode of joint
f_{n1}, f_{n2}	Predicted frequency of the half power points for n^{th} mode of the joint
f_n *	Measured frequency of the n^{th} mode of the joint
f_{ny}	Nyquist frequency
f_S	Sampling frequency
$H_{ij}(\omega)$	Frequency response function
i	Direction of propagation of the wave front (1- downwards, 2 - upwards)
j	Interface number (1 - top of plate, 2 - bottom of plate)

K_A	Stiffness of adhesion zone
l_A	Thickness of the plain plate
l_p	Length of the probe used in the model of the Fokker Bond Tester
l_1, l_3	Thickness of the adherends
l_2	Thickness of the adhesive
N	Number of points in the Fast Fourier Transform
N_h	Harmonic number for axisymmetric finite element work
n	Number of longitudinal mode
m	Number of shear mode
p	Start mode for error matrix calculation
Q	Damping factor
q	Finish mode for error matrix calculation
R_A	Increase in the amplitude of the second echo from the top of the adhesive in the presence of a disbond
R_d	Defect radius
R_{ij}	Reflection coefficient for the potential of the longitudinal wave front
R^*_{ij}	Reflection coefficient for the potential of the shear wave front
R'_{ij}	Reflection mode conversion efficiency for the potential of longitudinal waves to shear waves
R''_{ij}	Reflection mode conversion efficiency for the potential of shear waves to longitudinal waves
R_{press}	Pressure reflection coefficient
S_A, S_B	Measured frequencies of the shear modes of the joint
s_1, s_2, etc	Symmetric Lamb modes of a plain plate
T	Overall record length used for the Fast Fourier Transform
T_d	Duration of the digitised record length
T_{ij}	Transmission coefficient for the potential of the longitudinal wave front
T'_{ij}	Transmission mode conversion efficiency for the potential of longitudinal waves to shear waves
T''_{ij}	Transmission mode conversion efficiency for the potential of shear waves to longitudinal waves
T_L	Transmission time of a longitudinal wave through a plain plate
T_P	Duration of incident pulse
T_{press}	Pressure transmission coefficient
T_S	Transmission time of a shear wave through a plain plate
t	Time
t_A	Thickness of adhesion zone

u_i	Displacement of structure at position i
u_x, u_y, u_z	Displacement in the directions of the cartesian coordinates
v_j	Velocity of the structure at position j
$X_i(\omega)$	Response of the structure eg. the displacement or velocity etc. at position i
x,y,z	Cartesian coordinates
Z	Acoustic impedance of the couplant liquid
Z_L	Acoustic impedance of the plate for longitudinal waves
Z_S	Acoustic impedance of the plate for shear waves
Z', Z"	Generalised acoustic impedance
Z_1,Z_2	Acoustic impedance (subscripts refer to material i.e. 1 - adherend, 2 - adhesive)
z_{ij}	Mechanical impedance of the structure
α_{ij}	Mechanical receptance of the structure
α_{jj}	Mechanical point receptance of the Fokker Bond Tester probe Model
β_{jj}	Mechanical point receptance of a plain plate
δf	Frequency spacing between spectral lines
δt	Time interval
η_1, η_2, η_A	Damping factor (subscripts refer to the material i.e. 1- adherend, 2 - adhesive, A - adhesion zone)
θ, θ_L, θ_S	Direction of propagation of the wave fronts relative to the normal of the plate (subscripts refer to medium and wave type i.e. L- longitudinal wave in the plate, S - shear wave in the plate, no subscript - longitudinal wave in the liquid)
θ_e	Effective angle of incidence of the edge waves
κ, κ_L, κ_S	Wave number (subscript refers to medium and wave type i.e. L - longitudinal wave in a plate, S - shear wave in a plate)
λ	Acoustic wave length
ν	Poisson's Ratio
ρ	Density of the couplant liquid
ρ_1, ρ_2	Density (subscripts refer to the material i.e. 1- adherend, 2 - adhesive)
ρ', ρ''	Generalised material density
$\Phi_i(t)$	Longitudinal wave potential
$\Psi_i(t)$	Shear wave potential
ω	Angular frequency = $2\pi f$

PART ONE

REVIEW

CHAPTER 1
Review of Existing Non-destructive Testing Techniques for Adhesively Bonded Structures

1 Introduction

Adhesive bonding has been used extensively for many years in aerospace and other high-technology industries and has great potential for application to other areas of manufacturing. Adhesive bonding is attractive because it distributes stress over the entire bond area compared with the stress concentrations which can occur with mechanical fasteners, such as bolts and rivets. Also, the high temperatures of welding and brazing are avoided and improved appearance, together with reduced weight, can frequently be obtained.

In spite of its potential advantages, the use of adhesive bonding in primary structure has been limited by a lack of adequate non-destructive testing procedures: without such procedures, the reliability of a structure cannot be guaranteed. Such testing will usually be performed at the post-manufacture stage or at stages during manufacture; however, in more stringent applications, inspection during service may also be required.

Ideally, the non-destructive test would predict the strength of the bond. However this is very difficult to achieve, partly because a direct measurement of strength cannot be non-destructive, so it is necessary to correlate strength with other properties such as bond area, stiffness, damping etc. Also, the stress distribution in a typical adhesive joint is highly non-uniform (see for example, Adams and Peppiatt, 1974) so the strength is much more sensitive to the integrity of some areas of the joint than to others. Therefore measurement of bond area, for example and stiffness, do not necessarily give good correlations with strength. Changes in the properties do, however, give an indication that a joint may be defective.

There are three main types of defect which occur in practice; these are:-

(i) complete voids, disbonds or porosity

(ii) poor adhesion i.e. a weak bond between the adhesive and one or both adherends.

(iii) poor cohesive strength i.e. a weak adhesive layer.

Voids or large gas bubbles in the adhesive are caused either by a lack of adhesive or by the presence of foreign matter on (or even in) the adherends. Porosity of the adhesive is similar to voiding except that the size of the bubbles can be much smaller; typically having an area, in the plane of the adherends, of less than 1-2 x 10^{-6} m^2. It is usually caused by volatiles or gases trapped in the adhesive. A major problem can occur with composite adherends if these are not adequately dried before bonding as absorbed moisture can vapourise during the cure cycle to produce bubbles in the adhesive.

Disbonds or zero-volume unbonds can occur during manufacture due to the presence of a contaminant, such as grease, on an adherend. The surfaces of a disbond are generally in close proximity, or are touching, but are incapable or transferring load from the adherend to the adhesive. Disbonds also occur as a result of impact or environmental degradation after manufacture. Environmental degradation generally takes place at an interface between the adhesive and an adherend, causing the bond to fail. Resistance to this mode of failure can be improved by use of the correct surface treatment prior to bonding (Kinloch, 1983).

No reliable non-destructive test for the adhesion strength of a bond has been developed. In the aerospace industry this problem is overcome by strict control of the adherend surface preparation procedures or possibly by testing the adherend surface prior to bonding (Schliekelmann, 1972; Kim and Sutliff, 1978). This is done on the grounds that failures due to poor adhesion are always a result of inadequate surface preparation. Great care must then be taken to ensure that surface contamination does not occur between the time of the surface preparation or the test and the bonding operation.

Provided that the adherend preparation has been satisfactory, the adhesion strength of a joint is always greater than its cohesive strength. This is desirable since cohesive strength of a joint is more predictable than adhesion

strength and hence can be used in design calculations.

Poor cohesive strength of the joint is generally caused by the adhesive having the incorrect modulus or thickness. The extent of molecular cross linking in the adhesive and hence its modulus is mainly dependent on the correct mixing of the base resin and hardener and on the cure cycle that the adhesive receives. When large jigs are used to hold components during bonding, differences in temperature of the adhesive can easily occur and it is therefore possible that the adhesive will not be uniformly cured, resulting in areas of incorrect modulus.

Similarly, when jigs are used to hold the large and relatively thin adherends which are commonly used in the aerospace industry (Evans, 1985), it is difficult to ensure that a uniform pressure is applied to the joint during bonding. Areas where the applied pressure is too low will tend to have an adhesive thickness higher than the specification , while regions of high pressure will tend to produce bondlines thinner than desired.

The non-destructive measurement of cohesive properties is much less reliable than the detection of disbonds and voids. Consequently, in practice, if the cohesive properties are to be checked, destructive tests are often performed on specimens manufactured under the same conditions as the actual structure.

Since there are many widely available non-destructive techniques it is useful to examine each of them to determine their suitability for the detection of the three main catagories of defect described above. Although the majority of techniques are only suitable for the detection of complete voids and disbonds it is still important to show which are more suitable in particular circumstances than others.

2 Time Domain Ultrasonics

2.1 Basis of the Technique

The monitoring of ultrasonic echoes in the time domain forms one of the most widely used methods of non-destructive testing. It is commonly used for the detection of disbonds and voids in composites. The method is also used for the detection of disbonds, bond line voids and porosity in adhesive joints

(Hagemaier, 1971; 1972). Furthermore time domain methods are being investigated as a method of predicting the cohesive properites of the adhesive (Rose *et al.*, 1983), which is discussed in Section 2.5.

An incident pulse of ultrasound will be reflected and transmitted, (assuming normal incidence, and hence no refraction), at each interface of the joint. The amplitudes of the reflected and transmitted pulses are dependent on the reflection and transmission coefficients of the interface, which may be calculated from (Brekhovskikh, 1960) :-

$$R_{press} = (Z''- Z') / (Z'+ Z'') \qquad (1.1)$$

$$T_{press} = 2Z''/ (Z'+ Z'') \qquad (1.2)$$

where R_{press} and T_{press} are the reflection and transmission coefficients for the acoustic pressure, Z' is the acoustic impedance of the medium in which the incident and reflected pulse propagate and Z'' is the acoustic impedance of the medium in which the transmitted pulse propagates, which are given by :-

$$Z' = c' \rho' \quad \text{and} \quad Z'' = c''\rho'' \qquad (1.3)$$

where c', c'' and ρ', ρ'' are the longitudinal wave velocities and densities of the respective media.

If a defect is assumed to contain air or any other low density substance then it will have a very low acoustic impedance relative to the adhesive or adherend. The reflection coefficient then approaches unity at a boundary between either an adherend or the adhesive and a defect, since $Z'' << Z'$. An incident pulse over the defect is then practically totally reflected leaving negligible energy to be transmitted through the defect. Measurement of the reflected or transmitted energy may therefore be used to indicate the presence of a defect.

Due to the severe impedance mis-match between solid materials and air, it is difficult to propagate ultrasound from a transducer through air to the test structure. It is therefore vital that there is a satisfactory couplant between the transducer and the test piece. This is often achieved by immersing the

test piece and transducer in a water bath. The ultrasound then propagates across the water filled gap (typically 25-100 mm depending on the transducer) into the test piece. Alternatively, the transducer can be held in contact with the test structure, coupling being provided by a thin layer of gel or grease.

Both methods tend to have problems since the immersion technique is often impractical for large components and buoyant honeycombs. The contact technique is slow when large areas need to be examined, and can be sensitive to contact pressure (Canella, 1973). A further alternative is that of a water jet transducer or "squirter" in which the ultrasound propagates along a water jet which surrounds the transducer, as shown in figure 1.1. However, care must be taken in the design of the squirter nozzle to ensure that spurious echoes are not generated from reflections within the water jet (Tretout *et al.*, 1985).

Techniques which monitor ultrasonic echoes can detect very small defects such as bond line porosity with a high degree of reliability. However, a major limitation arises if the couplant or some other liquid such as water or fuel is allowed to penetrate the defect. The presence of the liquid reduces the reflection coefficient and the defect becomes much more difficult to detect. When the technique is used in production control, liquid ingress can usually be prevented. However, when joints with an unknown history are examined, the results need to be interpreted with care.

Several methods of displaying the ultrasonic reflections are available, the most common being A,B and C-Scans, which can be chosen to show the defect as required. The simplest presentation is an A-Scan which shows the amplitude of the echoes or refections as a function of time (or distance, if a value for the veloctiy of sound in the medium is known), as shown in figure 1.2. An A-Scan can be obtained at each point of the work surface, the relative amplitude of the echoes being used to establish whether defects are present.

The information can also be presented as a B-Scan. The time axis of the A-Scan becomes the vertical axis in the B-Scan (see figure 1.3). Hence an image of the cross section of a component is built up. The horizontal lines in the B-Scan show areas where the echo from a feature at a particular depth exceeds a pre-set level. Information on the depth of features is therefore

produced. In the case of an adhesive disbond, echoes from interfaces below the defect are very small so gaps appear in the horizontal lines from features below the disbond.

If the amplitude of a particular echo is monitored at each point on the surface of the work, a C-Scan can be produced. Measurements at each point are taken using a scanning mechanism, which produces a plan of the defect positions but gives no information on their depth (see figure 1.4).

The automatic scanning mechanisms required to produce B and C-Scans usually employ immersion or water jet coupling whereas A-Scan devices often use the contact technique. A number of transducer configurations are used with ultrasonic time domain analysis, the commonly used ones being described below.

2.2 Through Transmission

The through-transmission technique uses separate transmitting and receiving transducers positioned either side of the structure to be tested, as shown in figure 1.5. Alignment of one transducer above the other is important and can present difficulties when large components are tested. Alignment of the transducer axis perpendicular to the surface to be tested, however, is not as critical as with other techniques. Instead of monitoring the reflections from each interface, the magnitude of the transmitted signal is often used to detect defects. The signal at the receiving transducer either reduces or disappears when a defect is present.

Through-transmission is particularly suited to the inspection of honeycomb structures. Using a pulse-echo technique (see Section 2.3), only the bonding of the top face to the core can be tested reliably, whereas using through transmission, both top and bottom bonds between skins and core can be inspected in a single test (Hagemaier, 1971).

The technique can also be used with hand held transducers for rapid production line inspection, the transducers being held against the specimens and manually adjusted to give a signal of maximum amplitude.

2.3 Pulse-Echo

The pulse-echo technique generally uses a single transducer capable of sending and receiving a pulse of ultrasound (see figure 1.6). The delay between pulses and the geometry of the transducer and water path ensure that reverberations from the transmitting crystal have died away before the echoes are received. Provided that pulses are short enough (see Section 2.4) the individual echoes from each interface can be resolved, their position and amplitude being used to detect the presence of a defect. A large proportion of ultrasound will be reflected at a defect owing to its large reflection coefficient, so echoes from features behind the defect will be reduced or disappear. The technique can use all types of coupling and is a commonly used non-destructive technique for adhesive joints.

A minor variant of the technique is obtained by using a reflector plate beneath the structure, see figure 1.7. In the absence of defects, the ultrasound passes through the structure and into the water to be reflected back up through the structure. The A-Scan then consists of groups of echoes from the structure separated by the time taken for the ultrasound to traverse the water path between the structure and reflector plate, see figure 1.8. In the presence of a defect the incident pulse is practically totally reflected at the defect, so that no ultrasound is transmitted into the water behind the structure. Consequently, the A-Scan only consists of the slowly decaying echoes from the disbond, see figure 1.9. This reflection technique can only be used with immersion coupling owing to the need for a couplant between the reflector plate and rear face of the structure.

In all pulse echo testing, alignment of the transducer axis perpendicular to the surface of the structure or reflector plate is important if off-axis reflections are to be minimised.

2.4 Ultrasonic Transducer and Equipment Requirements

Many types of ultrasonic transducer are commonly available for use with non-destructive testing equipment. For time domain analysis it is desirable to use a transducer which produces short ultrasonic pulses so that echoes from the features of a joint may be more easily resolved.

The pulse length obtained from a given transducer is dependent on the excitation pulse and on the characteristics of the receiving amplifier. Figure 1.10 shows two ultrasonic pulses from the same transducer used with different excitation pulses and receiver ranges.

Transducers are often characterised by their frequency response (or spectrum) which gives an indication of the energy available at particular frequencies when the transducer is used under certain conditions. The frequency at which the maximum energy occurs, for a particular transducer and test set, is often quoted and is typically in the range 1 - 25 MHz. It should be emphasised, however, that the pulse length produced by a transducer, and hence its performance, is not only dependent on the frequency response of the transducer but also on the pulser and amplifier used. The quoted "frequency" of the transducer is therefore not a reliable measure of performance on its own.

The exact limit of resolution of two pulses or echoes depends on both their length and shape. As a rough guide, however, resolution becomes difficult when the separation between pulses is reduced to less than the pulse length, see figure 1.11.

The resolution of individual echoes is important if the depths of defects in a multilayered structure or the position of a defect within a thick bondline is required. Clarke *et al.* (1983) showed that it is possible to distinguish between disbonds at either the top or bottom adherend/adhesive interface with a bond line thickness of approximately 0.1 mm provided pulse lengths of 0.05 μs or less are used.

The problem of resolution is less critical if large adhesive disbonds, whose position in the bond line is unimportant, are to be detected. The more commonly used transducers, giving pulse lengths of approximately 0.5 μs, are adequate for detecting disbonds in bond lines thicker than 0.2 mm. In this instance the echoes from the top and bottom of the adhesive are generally not resolved but the disbond causes multiple echoes or ringing of the ultrasonic signal (Hagemaier, 1971). The multiple echoes are caused by repeated reflections from the disbond within the top adherend, the disbond preventing

the energy of the pulse from being transmitted to the adhesive. The echoes from a disbond can readily be distinguished from the more rapidly decaying echoes produced by a sound joint, see figure 1.12.

The amplitude of the echoes from the top of the adhesive (labelled 2,3,4 etc in figure 1.12b) are often monitored when joints are C-Scanned since there magnitudes increase in the presence of a disbond as described above. For example, by assuming that the impedance of the defect is negligible, it can be shown that the ratio, R_A, of the magnitude of the second echo from the bottom of the top adherend (labelled 3 in figure 1.12b) in the presence of a disbond to that obtained from a sound joint is given by :-

$$R_A = 1/(R_{press})^2$$
$$= [\,(Z_2 + Z_1) / (Z_2 - Z_1)\,]^2 \qquad (1.4)$$

where R_{press} is the reflection coefficient at the interface between the adherend and the adhesive and Z_2 and Z_1 are the acoustic impedances of the adhesive and the adherends respectively, see eqn. (1.3).

As the adhesive thickness (l_2) increases, the first echo from the bottom of the adhesive (labelled 2a in figure 1.12b), although it may not be resolved, occurs closer to the second echo from the top of the adhesive (labelled 3). Consequently, when

$$l_2 = l_1 . c_2/c_1 \qquad (1.5)$$

where l_1 is the thickness of the top adherend, and c_2 and c_1 are the velocities in the adhesive and adherends respectively, the second echo from the top of the adhesive is coincident with the first echo from the bottom of the adhesive. When this occurs, it has the effect of reducing the amplitude of the second echo from the top of the adhesive, since the two echoes are in anti-phase.

The problem is made worse if the ultrasonic pulse shape is more complex than the simple pulse shown in figure 1.12. For example, if a pulse shape similar to that shown in figure 1.10b is used, the second echo from the top of the

adhesive (3) can increase or decrease in magnitude as the adhesive thickness is increased and the first echo from the bottom of the adhesive (2a) approaches it, the direction of the change in magnitude being dependent on the phasing of the echoes. Whilst a decrease in the magnitude of the second echo from the top of the adhesive is the opposite effect to that which occurs in the presence of a disbond or void, an increase in its magnitude due to a change in adhesive thickness can easily be mistaken for a defect. Consequently, C-scans of joints with varying adhesive thickness that are produced by monitoring the amplitude of the echoes from the top of the adhesive will show varations resulting from thickness changes and the presence of voids (Martin *et al.*, 1979).

Figure 1.13 shows the C-scans of five single lap joints with 1.6 mm thick adherends and adhesive thickness varying between 0.5 and 0.7 mm. In this instance the echo from the bottom of the adhesive and the second echo from the top of the adhesive are coincident when the adhesive thickness is approximately 0.6 mm. Destructive examination of the joints showed that there were no voids or disbonds, the variation in the C-scans being caused solely by small changes in the adhesive thickness.

It can be seen from eqn. (1.4) that problems also arise if the acoustic impedance of the adhesive (Z_2) is too low relative to that of the adherend (Z_1), i.e. R_A approaches unity when $Z_2 << Z_1$ and it becomes difficult to distinguish the defects from the good structure. For example, with aluminium adherends, the increase in amplitude of the second echo from the top face of the adhesive is under 3dB when the impedance of the adhesive is less than approximately 1.7×10^6 Kg/s.m^2. With steel adherends, the increase is less than 2dB even when high modulus epoxies (having typical impedances of $2.6\text{-}3.0 \times 10^6$ Kg/s.m^2) are used.

It is also possible to use echoes from features below the bond line for disbond location, since they will disappear in the presence of a disbond. However, in practice, it is difficult to distinguish such echoes from those produced within the top adherend, unless very short pulses are used.

2.5 Ultrasonic Echo Ratio

The methods described in Sections 2.1-2.4 are aimed at detecting defects with a high reflection coefficient i.e. disbonds, voids and porosity. However, by measuring the relative amplitude of particular echoes it has been suggested (Rose *et al.*, 1983; Alers *et al.*, 1977), that the modulus and loss factor of the materials on either side of the interface can be found.

Although limited to use on joints with thick bondlines, where the reflections from individual interfaces could be resolved, Rose and Meyer (1973) found that the time history could be used to predict bond quality. They showed that there was a relationship between the cohesive strength of the joint and the ratio of the echo from the top face of the joint to that of the echo or echoes from the adhesive. However, they also observed considerable scatter and a dependence of the ratio on the adhesive thickness.

Techniques based on the ratio between the amplitudes of the top face echo and that of the echoes from the adhesive appear to have severe limitations when the bond line thickness is variable, as it would be in practice. This limitation arises because adhesive thicknesses of approximately 0.1-0.2 mm are at the limit of resolution obtainable with most ultrasonic transducers, see Section 2.4. Consequently the echoes from the adhesive layer are a complex function of the pulse shape, the adhesive thickness and the reflection coefficients of the interfaces.

Even when the echoes from the top and bottom of the adhesive are resolved by using probes with a shorter pulse length, the magnitude of the individual echoes remains a complex function of their pulse shape, the adhesive thickness and the reflection coefficients of the interfaces. This therefore tends to make the measurement of the cohesive strength of the joint very unreliable (Rose and Meyer, 1973).

3 Ultrasonic Impedance and Spectroscopy

3.1 Principle of Operation

Measurement of the through thickness vibration characteristics of a bonded structure can be used to detect defects. Instruments working on this principle

use transducers which operate in the frequency range 0.1 - 10 MHz and excite through thickness modes of vibration of the structure via a suitable couplant.

It should be noted that through thickness resonance is quite different from membrane resonance (see Section 4.4). Membrane resonance involves flexure of the layer above a disbond, the strain in the direction perpendicular to the surface of the structure being negligible. However, the strain in through thickness modes of vibration is primarily perpendicular to the surface.

Through thickness vibration is often explained using a wavelength approach, resonance occuring when the thickness of the layer above the disbond, l_A, is equal to an integer multiple of half wavelengths. For example this occurs when

$$l_A = n\lambda/2 = n c_L/2F_{Ln} \qquad (1.6)$$

where λ is the acoustic wavelength, c_L is the longitudinal wave velocity in the layer above the disbond, and F_{Ln} is the resonant frequency of n^{th} mode of the layer.

For a solid plate, a series of equally spaced harmonics or resonances occur, each having a different deformed (mode) shape. For a given mode, the frequency of through thickness resonance increases as the thickness decreases. The early types of ultrasonic thickness gauge used this principle (Szilard, 1982) and it formed the basis of several "bond testers".

The response of a bonded joint is considerably more complex than that for a single plate, the resonances no longer being equally spaced. The natural frequencies of the joint depend on the material properties and thickness of the adherends and adhesive layer(s).

Instruments for the non-destructive testing of adhesive joints based on the measurement of the through thickness vibration properties fall into two groups: those operating at a single frequency which monitor the amplitude and/or phase of the response at this frequency and those using a range of excitiation frequencies, in which resonant frequency and amplitude changes are detected.

3.2 Single Frequency Instruments

Bond testers which operate at a single frequency are limited to the detection of disbonds or gross voiding in an adhesive joint, and are essentially ultrasonic impedance measuring instruments.

The instrument measures the response of the system comprising the transducer and the joint. By coupling the transducer to the joint, the modes occur at lower frequencies, the range in which the resonances occur being primarily governed by the transducer or probe. Different probes are used for different applications but they typically operate in the range 0.1-5 MHz.

Bond testers of this type either measure response alone, such as the 210 Bondtester manufactured by NDT Instruments - (Hagemaier, 1982), or response together with the phase between excitation and response such as the Bondscope 2100 also manufactured by NDT Instruments - (Djordjevic and Venables, 1981). In both cases, however, it is important that the instrument operates at a frequency below or at the first through thickness resonance of the good structure (Li *et al.*, 1982). The response then decreases as the probe moves from a good to a disbonded area.

If the instrument operates above the first through thickness resonance of the good structure, for example at the through thickness resonance of a disbond, it can become difficult to distinguish between disbonds at different depths in a multilayer structure. More importantly, distinguishing between disbonds and undamaged structure can also become difficult.

3.3 Fokker Bond Tester Mk II

Currently, the widely used Fokker Bond Tester Mk II is the only commercially available instrument which claims to measure the cohesive strength of a joint. It does not monitor strength directly but relies on a correlation between strength and a measured natural frequency of a probe coupled to the joint the value of which depends on the stiffness of the adhesive layer (see figure 1.14). It is important to note that the Fokker Bond Tester Mk I (Schliekelmann, 1979), which operates at a much lower frequency, is only suitable for the location of large voids and disbonds.

The Fokker Bond Tester Mk II is also commonly used to detect disbonds and voids in adhesive joints (Lord, 1985). A disbond or void in the adhesive substantially reduces the stiffness which the instrument monitors, and hence produces a significant change in the measured natural frequency. It can also give a more reliable measure of the depth of disbonds in a multi-layer structure than that obtained using the ultrasonic impedance method described in Section 3.2.

It is more difficult to predict the cohesive strengths of the joint (Curtis, 1982; Wilkinson, 1982) than to detect disbonds since the frequency shifts resulting from a change in cohesive properties such as adhesive modulus or bond line thickness are much smaller than those obtained in the presence of a disbond. Although the instrument is widely used, it remains unclear how sensitive it is to the changes in modulus and adhesive thickness encountered in practice. The instrument does not claim to detect poor adhesion between the adhesive layer and the adherends.

3.4 Ultrasonic Spectroscopy

Spectroscopic techniques give information on resonant frequency and amplitude of response over a wide range of frequencies rather than at a single frequency as described in Section 3.2. As the frequency range increases, more modes of vibration can be examined and the potential for extracting information about the bond increases.

The technique of broad band ultrasonic spectroscopy can be used to measure frequency response over a wide frequency range e.g. 1-30 MHz. For example, Haines (1976) showed that the measurement of spectra in this frequency range could be used to measure oxide thickness on the insides of pipes. Broad band ultrasonic spectroscopy has also been used to predict the cohesive properties of a joint, (Lloyd and Wadhawani, 1978; Lloyd *et al.*, 1979; Rivenez, 1984). However to date the correlation between the complex spectra and the cohesion properties has been unreliable.

4 Sonic Vibration

4.1 Principle of Operation

A family of sonic vibration techniques is used for non-destructive testing of adhesive bonded structures. Most of these depend on a defect causing a local change in stiffness and hence a change in vibrational properties of the structure. The testing methods can be split into two types, those requiring excitation and response measurement at each point tested, and those using excitation at a single point and measuring response over the whole structure.

The size of defect which can be detected is related to the wavelength employed. As the frequency increases, the wavelength decreases, and the minimum detectable size reduces. Instruments using sonic vibrations operate typically at frequencies up to 20-30 kHz, so they will not be able to find defects as small as those detectable at ultrasonic frequencies (typically up to 20 MHz).

Sonic vibration techniques will generally only detect disbonds or gross voids, their exact size depending on the depth or thickness of adherends. Although the minimum detectable size is larger, the tests are often faster than the ultrasonic techniques and they do not require a couplant between the transducer and test structure. The techniques are most sensitive to defects close to the surface of a stiff structure and are therefore well suited to the inspection of honeycomb constructions.

4.2 Coin Tap Test

The coin tap test is one of the oldest methods of non-destructive inspection. It is regularly used in the inspection of laminates and honeycomb constructions (Hagemaier and Fassbender, 1978). Until recently, however, the technique has remained largely subjective and there has been considerable uncertainty about the physical principles behind it.

The sound produced when a structure is tapped is mainly at the frequencies of the major structural modes of vibration. These modes are structural properties which are independent of the position of excitation. Consequently, if the same impulse is applied to a good area and to an adjacent defective

area, the sound produced must be very similar. Therefore the difference in sound when good and defective areas are tapped must be due to a change in the force input.

When a structure is struck with a hammer, the characteristics of the impact are dependent on the local impedance of the structure and the hammer used. The local change in structural stiffness produced by a defect changes the nature of the impact. The time history of the force applied by the hammer during the impact may be measured by incorporating a force transducer in the hammer and typical force-time histories from taps on sound and disbonded areas of an adhesively bonded structure are shown in figure 1.15. The impact on the sound structure is more intense and of a shorter duration than that on the damaged area, the impact duration on the sound structure being approximately 1 ms compared with 1.7 ms on the defective zone (Adams and Cawley, 1985).

The differences between the force pulses are more readily quantified if the frequency content of the force pulse is determined. This is achieved by carrying out a Fourier transform of the force-time records. The spectra of the force-time records in figure 1.15 are shown in figure 1.16. The impact on the damaged area has more energy at low frequencies, but the energy content falls off rapidly with increasing frequency. The impact on the sound area has a much lower rate of decrease of energy with frequency. This means that the impact on the defective area will not excite the higher structural modes as strongly as the imapct on the good zone. The sound produced will therefore be at a lower frequency and the structure will sound "dead".

The testing technique therefore involves tapping the area to be tested with an automatic, instrumented hammer designed to give a single, reproducible impact. The frequency spectrum of the impulse is then compared with that of an impulse, with the same hammer, on an area of the structure that is known to be sound. Data from a sound structure is stored in the testing instrument so that it can carry out the comparison and give an immediate indication of the integrity of the area under test (Adams and Cawley, 1985). Measurements are only based on the impact force; consequently, no transducers need be attached to the structure which avoids the coupling and alignment problems which arise with, for example, ultrasonic techniques. However, since the technique is only

sensitive to changes in local stiffness of the structure, measured perpendicular to the plane of the surface, it will only detect defects that lie parallel to the plane of the surface e.g. voids and disbonds.

A similar device, the "Acoustic Spectral Flaw Detector" (Lange,1978), uses the measurement of vibration response rather than input force. The response is measured using a transducer attached to the structure or by a microphone. However, the use of response measurements at frequencies up to membrane resonance can lead to contradictory results (Adams and Cawley, 1985).

4.3 Mechanical Impedance

The impedance method has been used for many years in the Soviet Union (Lange and Moskovenko, 1978). More recently the Acoustic Flaw Detector and the MIA 3000, developed by Inspection Instruments Limited and based on the original Soviet design, have been available in the West. The technique uses the principle of local impedance measurement to detect flaws in the plane parallel to the test surface. The point impedance, z_{jj}, of a structure, can be defined as (Cawley, 1984) :-

$$z_{jj} = F_j(\omega)/v_j \qquad (1.7)$$

where $F_j(\omega)$ is the harmonic force input to structure and v_j is the resultant velocity of the structure, both measured at point j.

Commercially available instruments generally take measurements at a single pre-set frequency, typically between 1 and 10 kHz. As the probe is moved from a good to a defective area, the impedance decreases. Figure 1.17 shows the impedance as a function of frequency for disbonds under a 3.3 mm thick aluminium skin adhesively bonded to a thick steel beam. As the base structure becomes more flexible, the impedance of a defective zone can be higher or lower than that of a good zone, depending on the frequency, so the test becomes less reliable (Cawley, 1984).

Instead of using a couplant, a dry point contact is used between the transducer and structure. This contact has a finite stiffness (Lange and Teumin, 1971)

which must be kept as high as possible, otherwise the sensitivity of the technique will be reduced.

Figure 1.18 gives an estimate of the minimum detectable defect diameter versus depth in aluminium and carbon fibre reinforced plastic structures. These curves assume a stiff base structure and that the impedance of the defective zone must be at least 3dB lower than that of the sound zone for the defect to be reliably detected. The technique is less sensitive with the composite owing to the reduced contact stiffness obtained with this material.

4.4 Membrane Resonance

A planar disbond can be modelled as a plate restrained around the edges by the surrounding structure. As the frequency of excitation increases, this plate resonates, the first mode being the membrane resonance and having a deflected shape similar to that of a diaphragm. At resonance the impedance measured over the defect reduces to a minimum and the response for a given force input increases substantially. Hence, at or close to membrane resonance, the response amplitude of a defective zone will be much higher than that of the surrounding structure. Since this resonant amplification is high, typically greater than a factor of 10 (20 dB), resonance can be detected by measurement of response alone. This can lead to inaccuracies since it assumes that the input force is roughly constant but it can simplify the measurement technique and apparatus. Although less accurate measurements are required than for the impedance method, it is important that the operating frequency is at or close to the resonant frequency of the layer(s) above the defect. The layer(s) above a defect may be modelled as a disc clamped around its edges. The resonant frequency, f_d, of such a disc is given by (Cawley, 1984) :-

$$f_d = (0.47\, l_A / R_d^2).\, [\, E_1 / \rho_1 (1 - \nu^2)\,]^{1/2} \qquad (1.8)$$

where l_A is the thickness of the layer above the defect, R_d is the defect radius, E_1 is Young's modulus, ρ_1 is the density and ν is Poisson's ratio of the layer above the defect. In practice, this frequency, f_d, would represent an upper limit, since the actual edge conditions fall somewhere between fixed and

simply supported.

The typical maximum operating frequency of instruments of this type is 20-30 kHz. If 1.6 mm aluminium adherends are assumed then the minimum detectable defect diameter (i.e. at 30 kHz) would be approximately 23 mm. At 10 kHz, this size would increase to 40 mm.

The original Fokker Bond Tester (Type I), described by Schliekelmann (1972), operates on this principle and uses white noise excitation in the range 0.5-10 kHz. The more commonly used Mk II, or model 70 operates at a much higher frequency and on a different principle, see Section 3.3. In the original version of the instrument the transmitting and receiving transducers are housed in the same probe which requires no couplant. The ratio between the transmitted and received energy is displayed on a meter and is used to identify defects.

The Harmonic Bond Tester manufactured by the Shurtronics Corp. operates at a single frequency (Hagemaier,1972) and was developed by Boeing from the Eddy Sonic Test System (Botsco, 1968). The excitation is via induced eddy-currents which require no couplant. However, part of the structure under test must be electrically conducting to support the eddy-currents. The response is measured by a microphone in the eddy-current coil (Phelan, 1972). The interaction between the original and induced fields produces vibration at double the frequency applied to the coil, giving an excitation frequency of 28 kHz. A single excitation frequency is also used in the "acoustic amplitude" method developed by Lange (1976).

To be sure that defects are detected, it is important that they are excited at or close to their membrane resonance. If the excitation is at frequencies over a broad range, (white noise), then this can be achieved. However, if the excitation is at a single frequency, there is a high probability of missing defects.

4.5 Vibrothermography

The technique of vibrothermography (or active thermography) monitors the surface temperature of a component as it is cyclically stressed. A defect will cause a local rise in temperature due to either frictional heating at its

internal surfaces or hysteretic energy dissipation. An infra-red thermal imaging camera is usually used to measure the temperature of the component by representing the isotherms on its surface as a series of colours or tones.

Heating can occur during low frequency fatigue testing i.e. at 1-2 Hz. Pye and Adams (1981) showed, however, that if a component is excited at a resonant frequency the input forces required are much smaller than in fatigue testing and the method becomes feasible for non-destructive testing in the field.

Henneke and Reifsnider (1982) located disbonds in composites by exciting them at their membrane resonances (see Section 4.4). At frequencies of up to 13 kHz, the disbonds could be made to show up as hot spots. As the frequency was increased further, the membrane resonance was passed, heating ceased, and the damage was not detectable.

Vibrothermography has the potential advantage of being able to monitor the response of large areas when exciting at only one location. The method depends on a local temperature rise for damage location. Since this is controlled by the thermal conductivity of the component, the sensitivity of the technique will be reduced as the conductivity rises. Pye and Adams (1981) found that damage was more difficult to detect in carbon fibre composites than in glass fibre constructions for this reason.

Current infra-red cameras are able to resolve differences in surface temperatures of typically 0.1°C which probably limits them to the detection of disbonds in composite adherends, rather than metal ones.

Holographic techniques can also be used to locate defects over large areas in a similar way to vibrothermography. Holographic interferometry (Fagot *et al.*, 1980) enables the very small discontinuities in surface displacement, which occur at a defect when a component is stressed, to be measured. Although rapid inspection is possible, the technique is still under development and equipment costs are high.

5 Passive Thermography

Passive thermography uses the same technique as vibrothermography, see

Section 4.5, to measure the surface temperature of a component. However passive thermography monitors the response of the structure to thermal transients created by an external heat source.

Either heating or cooling transients can be used to detect disbonds and voids in bonded panels. Heating transients can be induced by heating the back surface of the structure and measuring temperature changes at the front. Defective areas are cooler owing to the lower conduction through voids. Heating transients can also be created by heating on the same side as the camera; the defects then appear as hotter areas. Cooling transients can be used in a similar manner by applying an aerosol freezer spray to the surface to be tested.

There are significant differences between one and two sided examination; heating the back face and monitoring the temperature at the front enables deeper defects to be detected. Heating and monitoring the temperature at the same surface however, can produce better results with near surface defects. It is important to note that thermal transients must be used because a defect would have a negligible effect on steady state heat transfer. In practice these thermal transients have to be recorded since a temperature difference sufficiently large for detection may only exist for a brief period. The use of video recording techniques has greatly simplified this process (Reynolds and Wells, 1984).

The sensitivity of the method is reduced, like vibrothermography, as conductivity increases. Difficulties can also arise if the surface to be tested has areas of different emissivity though this effect can be reduced by spraying the surface under examination matt black.

The technique can be used to detect delaminations and voids in composites (McLaughlin *et al.*, 1980) and has also been used successfully with aluminium adherends. Schliekelmann (1979) reports that voids of 25 x 25 mm can be detected below 0.5 mm thick aluminium adherends.

Although the cost of thermographic equipment is high, such techniques have the potential advantage of testing large areas rapidly.

6 X-Radiography

X-Radiography is commonly used for locating defects in welded and cast components. Radiography has also been used to locate bond-line porosity in carbon composite joints (Clarke *et al.*, 1983). However, if porosity is to be reliably detected, the absorption of radiation in the adhesive has to be increased by incorporating a filler in it, such as aluminium powder.

The technique cannot be used effectively when a material with high absorption is used as either of the adherends. The much greater absorption in, for example aluminium, would mask small changes resulting from voids in the adhesive and thus make them undetectable.

The location of disbonds in joints is more difficult because the thickness of a defect parallel to the beam is substantially less than for porosity. Disbond location can be improved, however, by using a radio-opaque penetrant such as zinc iodide. The technique is more commonly used to locate impact damage in composites (Sendeckyj, 1983) and requires a surface point of entry for the penetrant, which is not always present in adhesive joints.

7 Discussion

A variety of methods is available for the detection of complete disbonds in adhesive joints, some of which are more suitable in particular circumstances than others. The high frequencies used with ultrasonic time domain techniques are especially suited to the detection of small defects such as bond line porosity. Consequently, the technique is commonly used in conjunction with immersion coupling or a water jet probe and a C-Scan display to produce a defect map of a component.

The ultrasonic C-Scanning of relatively large components, although capable of detecting small defects, can be time consuming and expensive and the method is more commonly used for post-manufacture than for in-service testing. Ultrasonic C-Scan frames are also available for use on small areas of in-service components. They are commonly used with a gel couplant or a water jet probe and can be useful when a component cannot be immersed.

Larger defects than porosity, such as voids and disbonds, do not require the accurate scanning facility of a C-Scan rig and can often be detected by hand scanning. Again a gel couplant or jet probe is often used, the defects being detected using an A-Scan presentation. Such techniques are relatively adaptable and can be used either after manufacture or in service. A similar set-up, used with a B-Scan display can be valuable for showing defect depth in a multi-layered joint.

Since a complex rig and immersion tank are likely to be a major capital expense, it is important to decide whether its accurate scanning facility is necessary. If bond line porosity can be eliminated reliably, by experience and process control, then larger defects may be more economically located by an ultrasonic hand scanning technique.

The applications of the ultrasonic impedance technique are very similar to those of time domain ultrasonics mentioned above. Ultrasonic impedance devices have been used with both C-Scan rigs and hand scanning; however, since most operate at low ultrasonic frequencies (0.1 - 2 MHz), they will not be able to detect such small defects as bond line porosity. Also instruments of this type can give misleading results if defects at other depths are encountered. However, the widely used Fokker Bond Tester Mk II which measures the natural frequency of the probe coupled to the joint, rather than the amplitude and phase of the impedance at a single frequency, can be used to monitor defect depth.

Ultrasonic impedance instruments also require a couplant between the transducer and the test structure, and as with all techniques which need a couplant, it is important to prevent the ingress of any liquid into a defect, or it can become very difficult to detect.

Techniques based on the use of sonic vibrations will only be able to detect disbonds or gross voiding of the adhesive layer, although they do offer some potential advantages over the ultrasonic techniques. Methods which use single point excitation and a non-contacting, scanning measurement system, such as vibrothermography and holography, have the particular advantage that large areas can be inspected rapidly. Unfortunately, the equipment required tends to be very expensive. It is very probable that the thermographic system used in

vibrothermography will be more expensive than an ultrasonic C-Scan rig. Nevertheless, in large scale applications where the techniques have the required sensitivity, the costs are likely to be justified.

The other sonic vibration techniques, which require excitation at each test point, are slower than those requiring excitation at a single point. However, they have the advantage over the high frequency ultrasonic methods that a dry point contact between the probe and the structure is satisfactory, so no coupling fluid is required. They are therefore easier to apply, particularly in situ, for example on an aircraft wing. The techniques are also particularly suited to the inspection of honeycomb constructions. The mechanical impedance method operates at a single excitation frequency so the computational requirements are small. This means the probe can be moved over the surface of the structure giving a continuous reading. Unfortunately there are dangers in using only one frequency. The techniques based on the membrane resonance of the layer above the defect are quick, but problems arise with defects whose natural frequencies are above the frequency range of the instrument. The probability of missing defects is greatly increased if excitation is confined to a single frequency or a narrow band.

The automated coin-tap method requires a spectrum to be computed at each point. This means that the inspection rate is of the order of ten positions per second. However, the reliability is improved by looking at more than one frequency and, since the tapping head only makes instantaneous contact with the structure, problems of alignment and clamping force, which can arise with the impedance technique, do not occur. Most of the vibration methods described can be used with a hand held probe or with a scanning frame to produce a C-Scan presentation.

Passive thermography offers similar advantages to those of vibrothermography and is likely to cost approximately the same. However, unlike vibrothermography, passive thermography does not require any attachment to the structure to be tested nor that it should be excited over a broad range of frequencies.

X-Radiography is well established in other areas of non-destructive testing, particularly in the quality control of welds and castings. Unfortunately, its

application to the non-destructive testing of joints is limited to cases where the absorption in the adherends is low, such as when composite adherends are used. Results can be enhanced by using a radio-opaque penetrant but this is not generally practical for voids and disbonds. However, the technique can be useful in research to determine the size and position of defects accurately.

No reliable non-destructive test for the adhesion strength of a joint has been developed. In the aerospace industry, this is overcome by strict control of the adherend surface preparation procedures and by testing the adherend surface prior to bonding. This is done on the grounds that failures due to poor adhesion are always the result of inadequate surface preparation. Great care must then be exercised to ensure that the surfaces are not contaminated between such a test and the bonding operation.

Two techniques being examined for quantifying adhesion strength, although not truly non-destructive, are those of acoustic emission and the debonding of weak joints. Work by Curtis (1975) and Hill (1977) suggests that acoustic emission counts can be used to detect adhesion failure prior to fracture, as a joint is loaded. Another approach (Knollman *et al.*, 1982) classifies weak adhesion strength by attempting to debond a joint with high energy ultrasound. Weak bonds would fail and could be detected as disbonds whereas bonds with a high adhesion strength would be unaffected. It is probable that such a test would only be able to separate very low from high adhesion strengths but in practice it is likely that this is all that is required.

The non-destructive evaluation of cohesive strength is also extremely unreliable at present. Currently, the Fokker Bond Tester MK II is the only commercially available instrument which claims to measure cohesive strength. However, it is not clear how sensitive the instrument is to typical changes in adhesive modulus and thickness.

The technique of broad band ultrasonic spectroscopy uses a similar basic principle to the Fokker Bond Tester in that it measures the through thickness resonant frequencies and amplitudes of a joint. However, unlike the Fokker Bond Tester, which only monitors the resonant frequencies of at most two modes of the joint, ultrasonic spectroscopy gives information on many modes (typically 10 to 20) of the joint. Since each of these modes is dependent on the

cohesive properties it is likely that a better correlation with cohesive strength would be obtained with ultrasonic spectroscopy than with the Fokker Bond Tester.

8 Conclusions

No single method of detecting disbonds and voids is universally applicable. Since it is likely to take longer and cost more to find smaller defects, it is important to know the size of the smallest defect which must be detected. This size, together with the type of testing environment, i.e. post-manufacture or in-service, and the structure to be tested, will help to determine which type of technique is the most applicable.

The sonic vibration techniques are particularly useful in circumstances where the use of the coupling fluids required for ultrasonic testing is undesirable. They are frequently used for the inspection of honeycomb constructions to which they are particularly suited. Ultrasonic techniques, however, are generally able to detect smaller defects than those using sonic vibrations. If rapid inspection of large areas is required, then a thermographic technique can offer substantial advantages.

No reliable non-destructive technique currently exists for measuring the adhesion and cohesive strength of a bonded joint, so it is often assumed that a joint is serviceable provided it is free from voids and disbonds. Poor cohesive properties and low adhesion strength are generally avoided by careful surface preparation and process control, but joint design has to be conservative to allow for variation in these properties. Consequently, to enable the potential advantages of adhesive joints to be fully utilised it is important that techniques for the non-destructive evaluation of both cohesive and adhesion strength are developed.

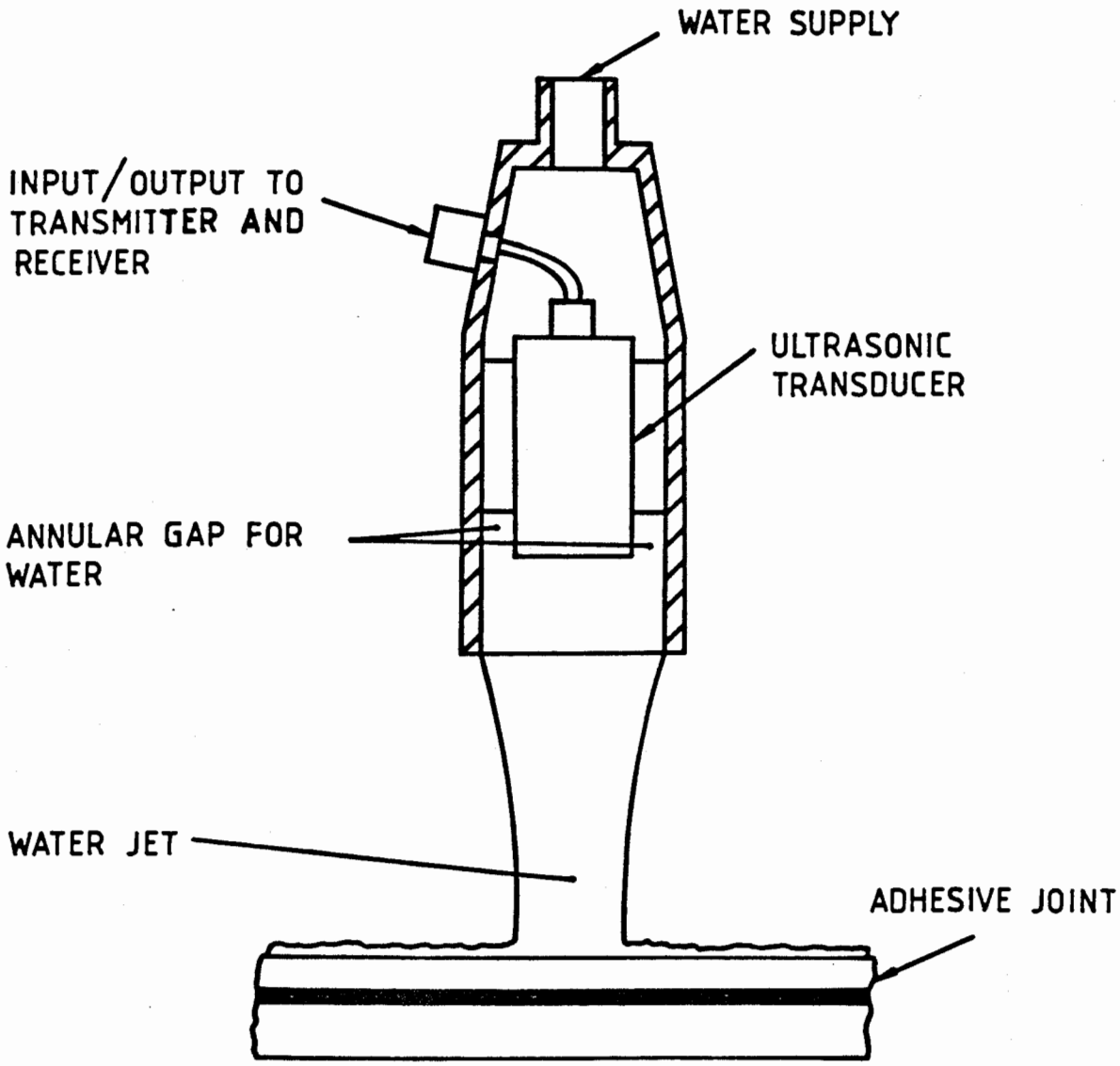

Figure 1.1 **Typical Ultrasonic Water Jet Transducer**

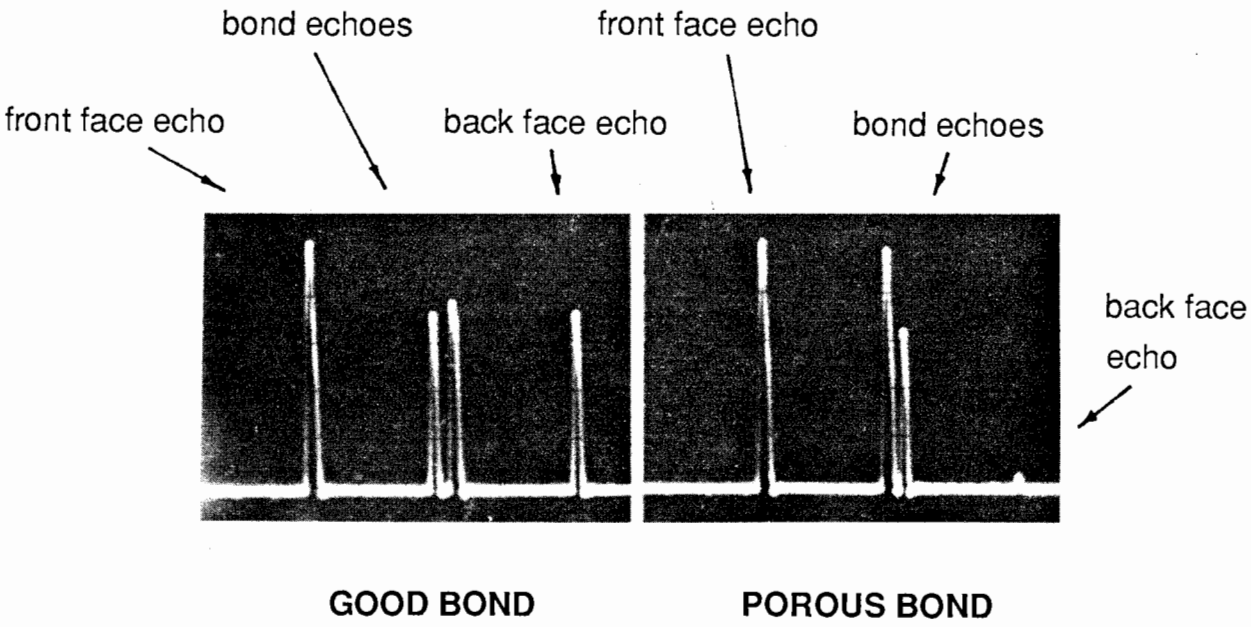

Figure 1.2 **Typical A-Scan from a Carbon Fibre Composite Lap Joint** (overall joint thickness of 3.7 mm) from Clarke *et al.* (1983).

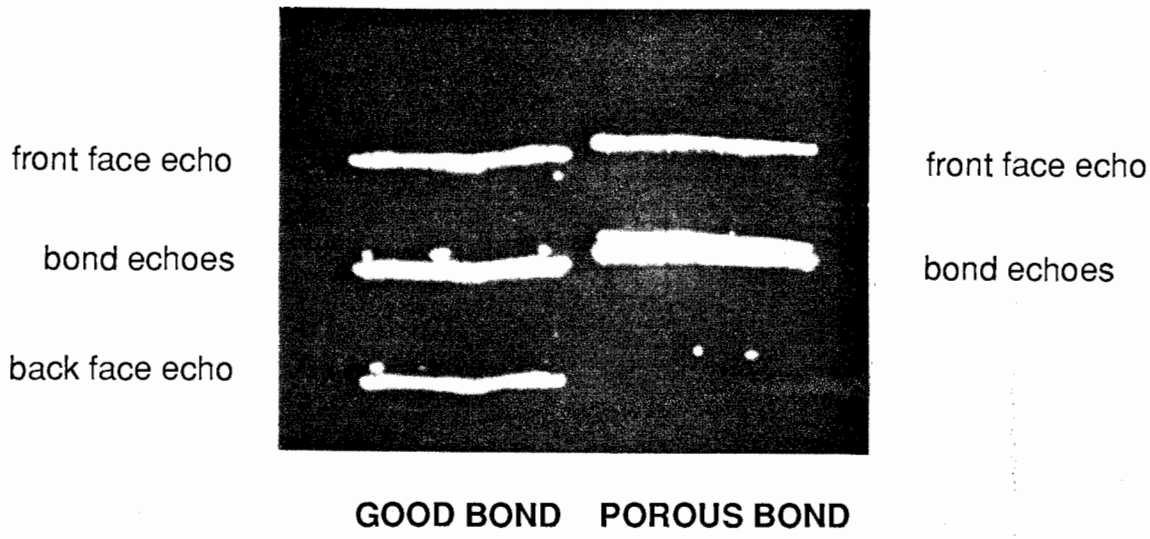

Figure 1.3 **Typical B-Scan from a Carbon Fibre Composite Lap Joint** (overall joint thickness of 3.7 mm) from Clarke *et al.* (1983).

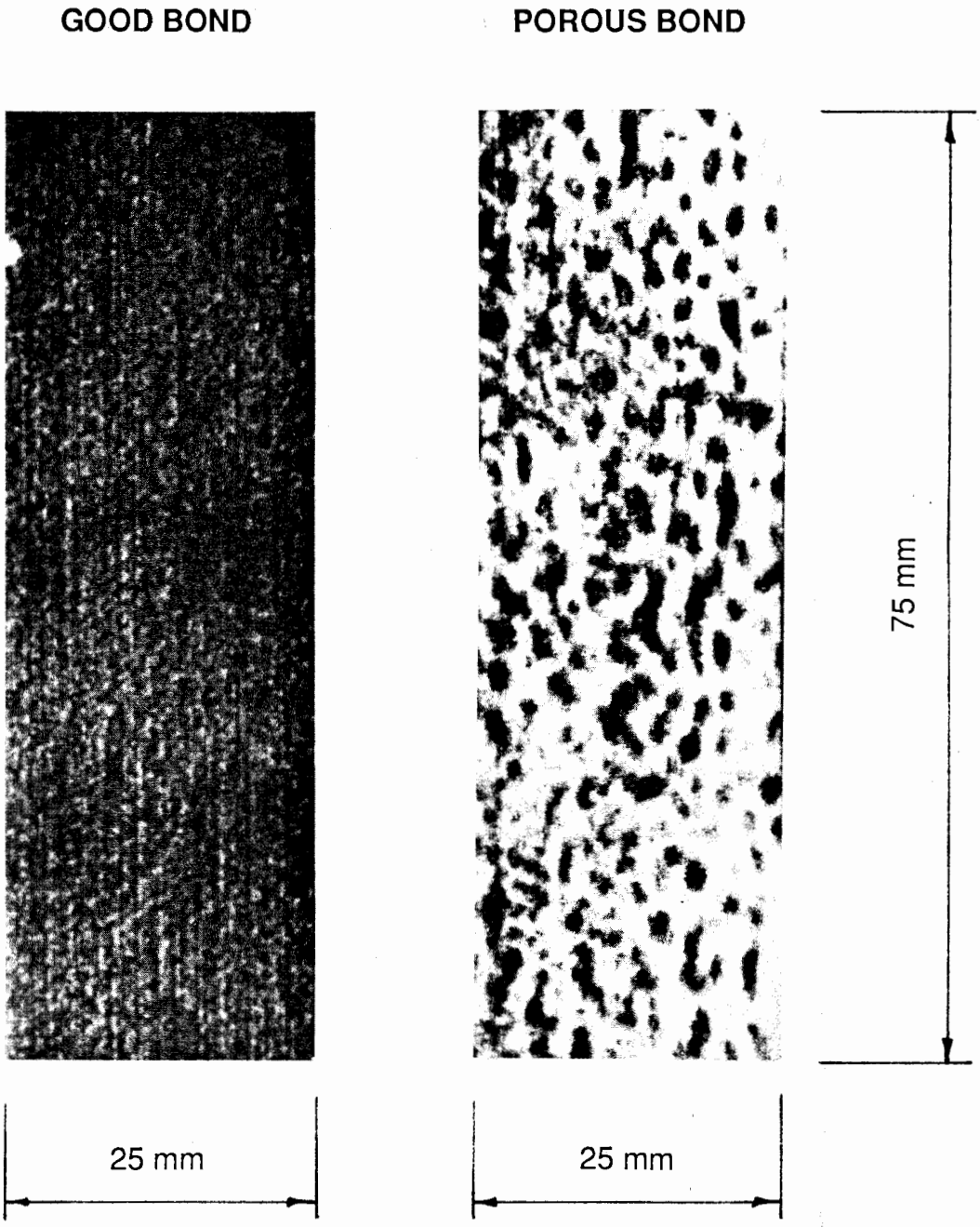

Figure 1.4 **Typical C-Scan from a Carbon Fibre Composite Lap Joint** (overall joint thickness of 3.7 mm) from Clarke *et al.* (1983).

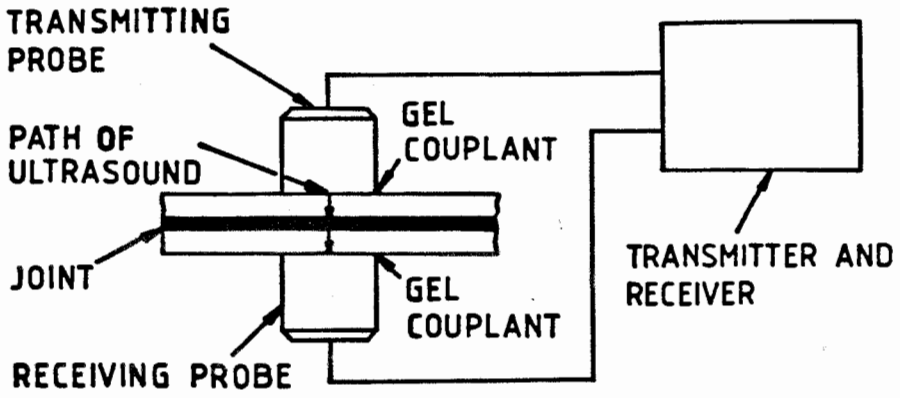

Figure 1.5 Configuration of Transducers for the Ultrasonic Through Transmission Technique

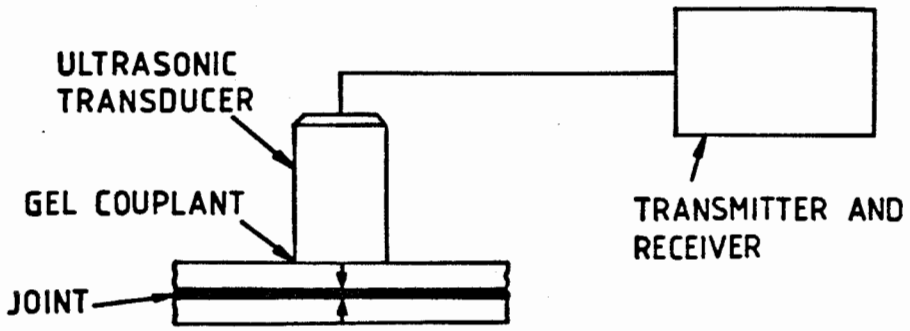

Figure 1.6 Configuration of Transducers for the Ultrasonic Pulse Echo Technique

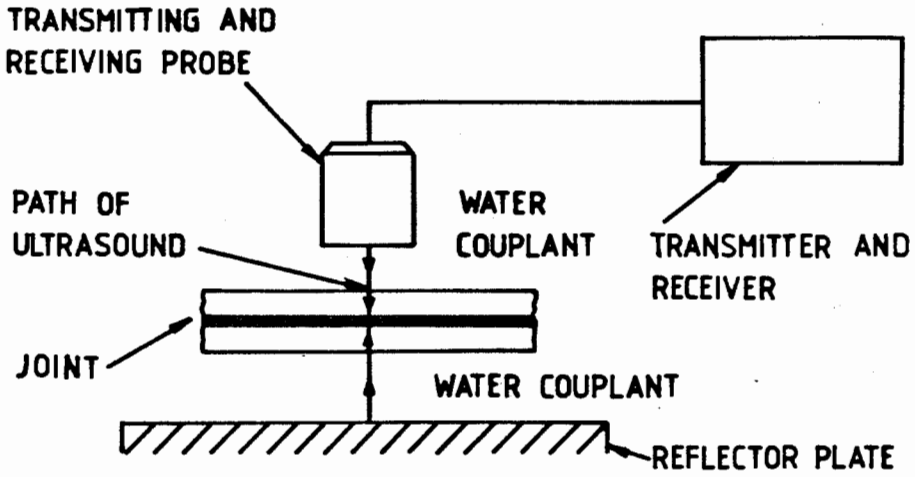

Figure 1.7 Configuration of Transducers for the Ultrasonic Reflection Technique

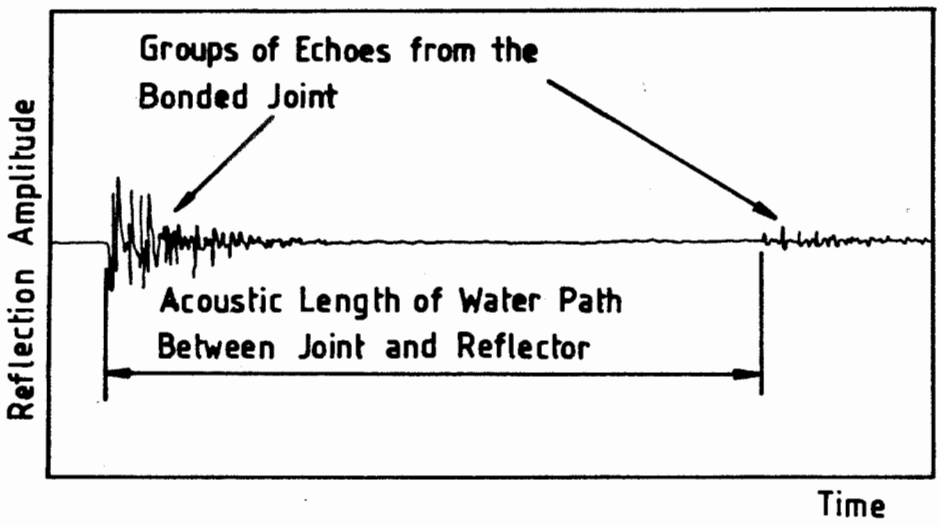

Figure 1.8 A-Scan from a Sound Joint using the Reflection Technique

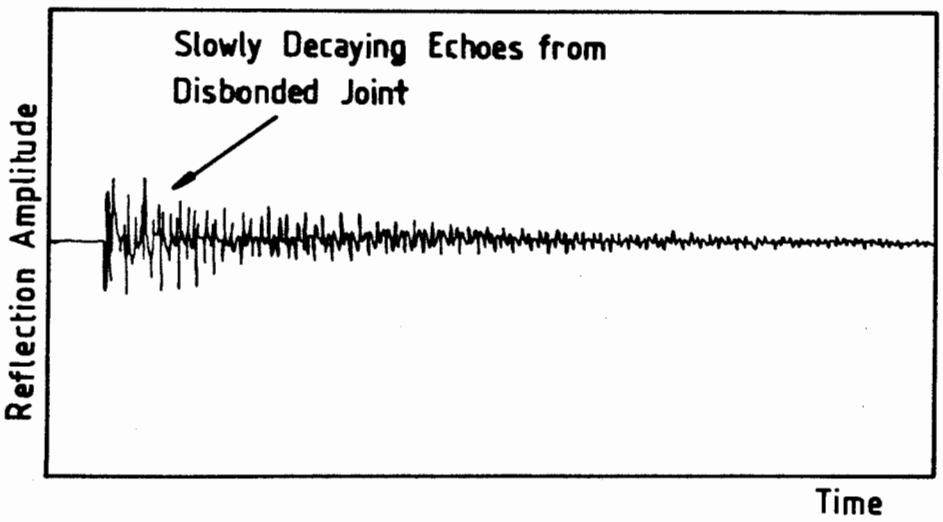

Figure 1.9 A-Scan from a Disbonded Joint using the Reflection Technique

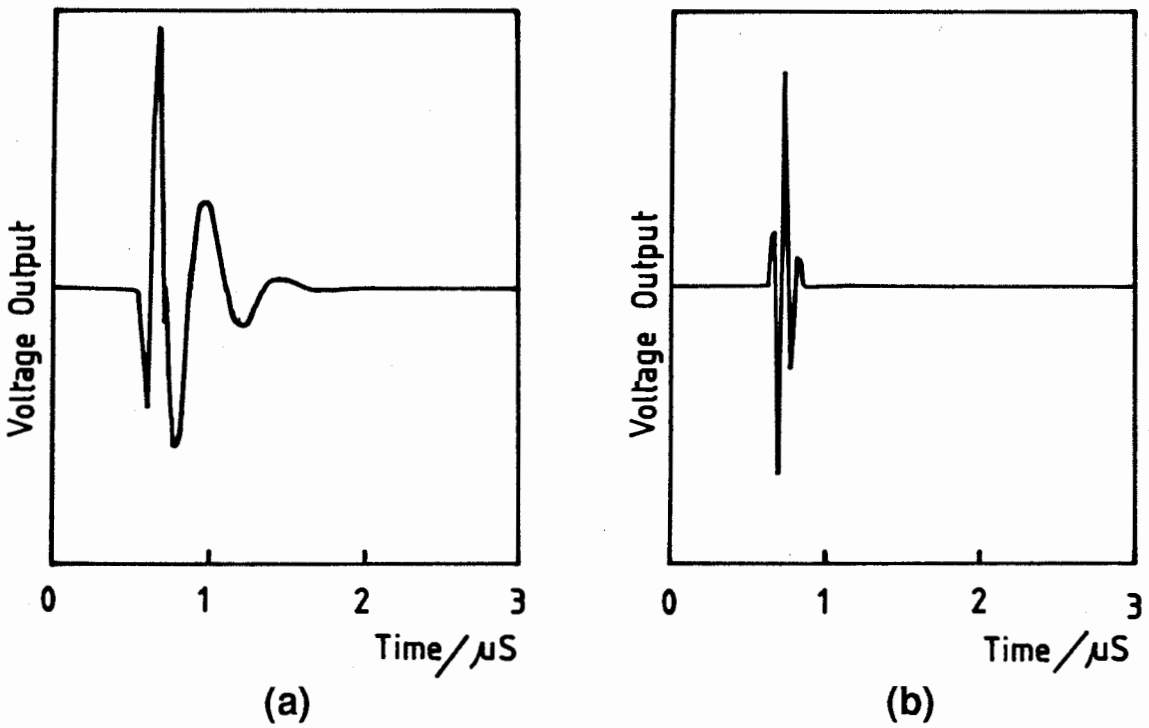

Figure 1.10 **<u>Transducer Output Voltage - Reflection off Flat Surface separated from a 10 MHz Transducer by approximately 25 mm of Water</u>** (a) 450v excitation pulse and a 2.25 MHz 'Narrow Band' receiver (b) 200v Excitation Pulse and a 10 MHz 'Narrow Band' receiver

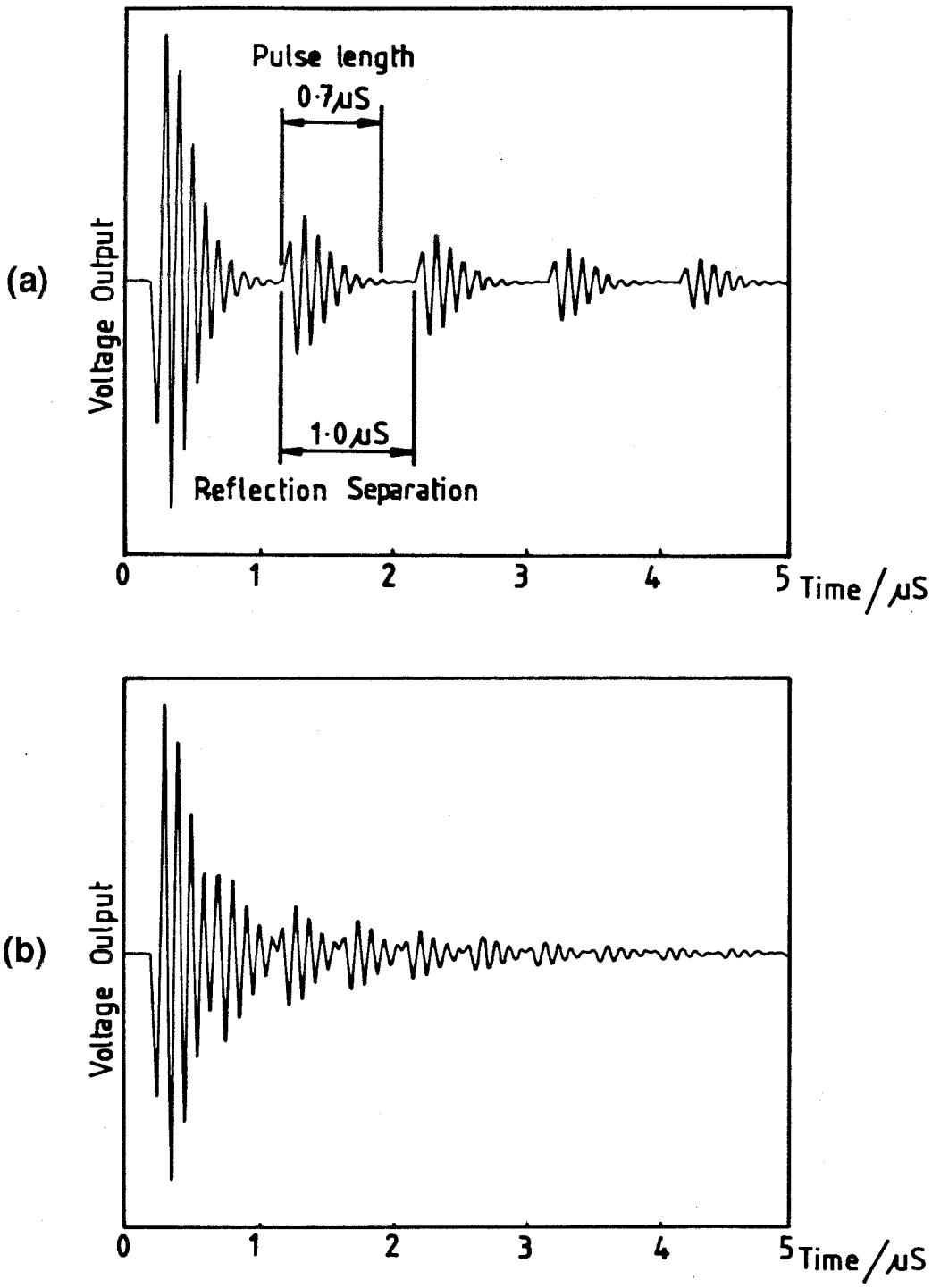

Figure 1.11 **Resolution of Ultrasonic Pulses from a 10 MHz Probe** (a) reflections 1.0μs apart - from a 3.2 mm aluminium plate in water (b) reflections 0.46μs apart - from a 1.5 mm aluminium plate in water

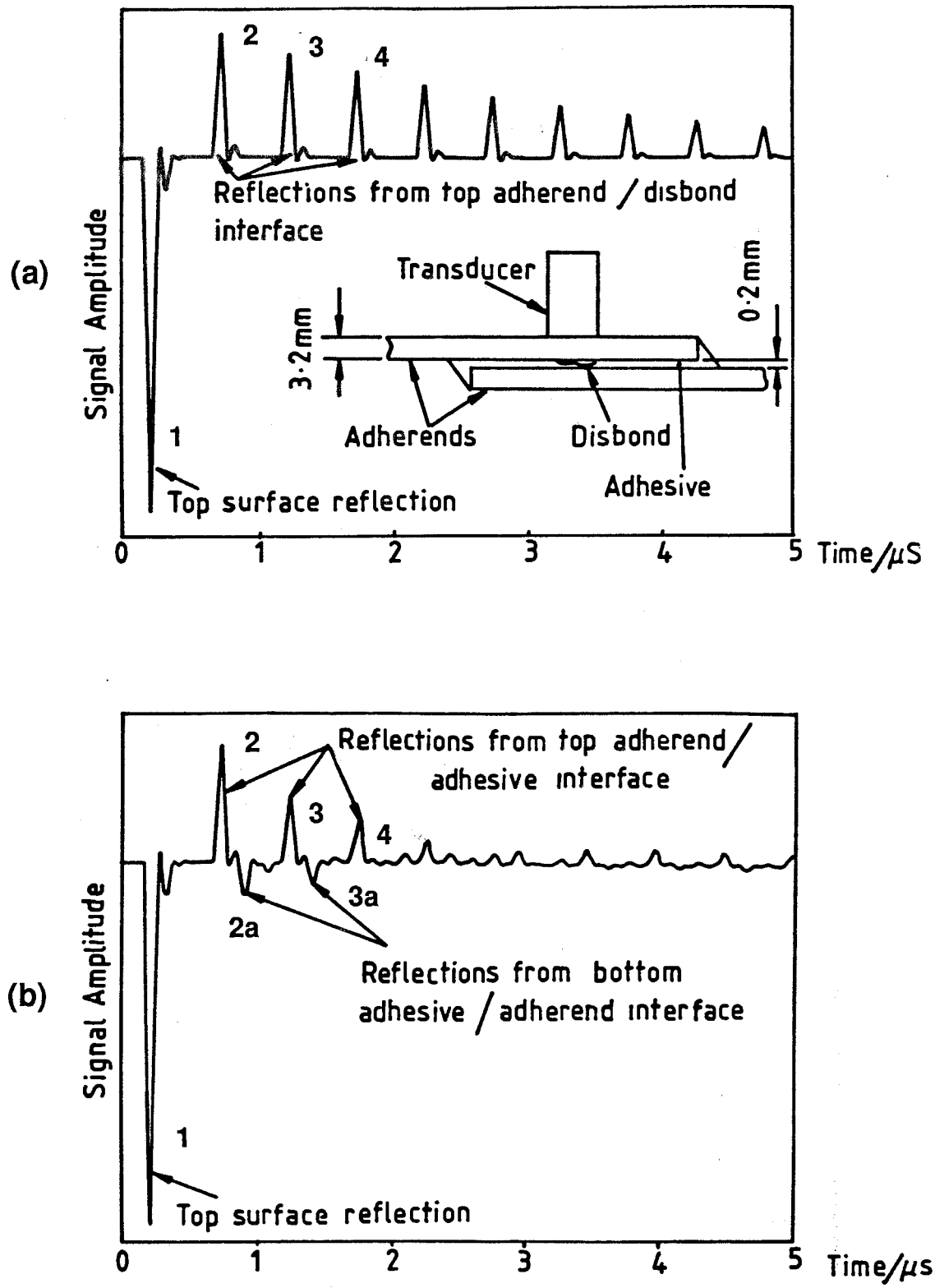

Figure 1.12 **A-Scans showing the Transducer Voltage against Time** (a) a Disbonded joint (b) a Sound Adhesive Joint

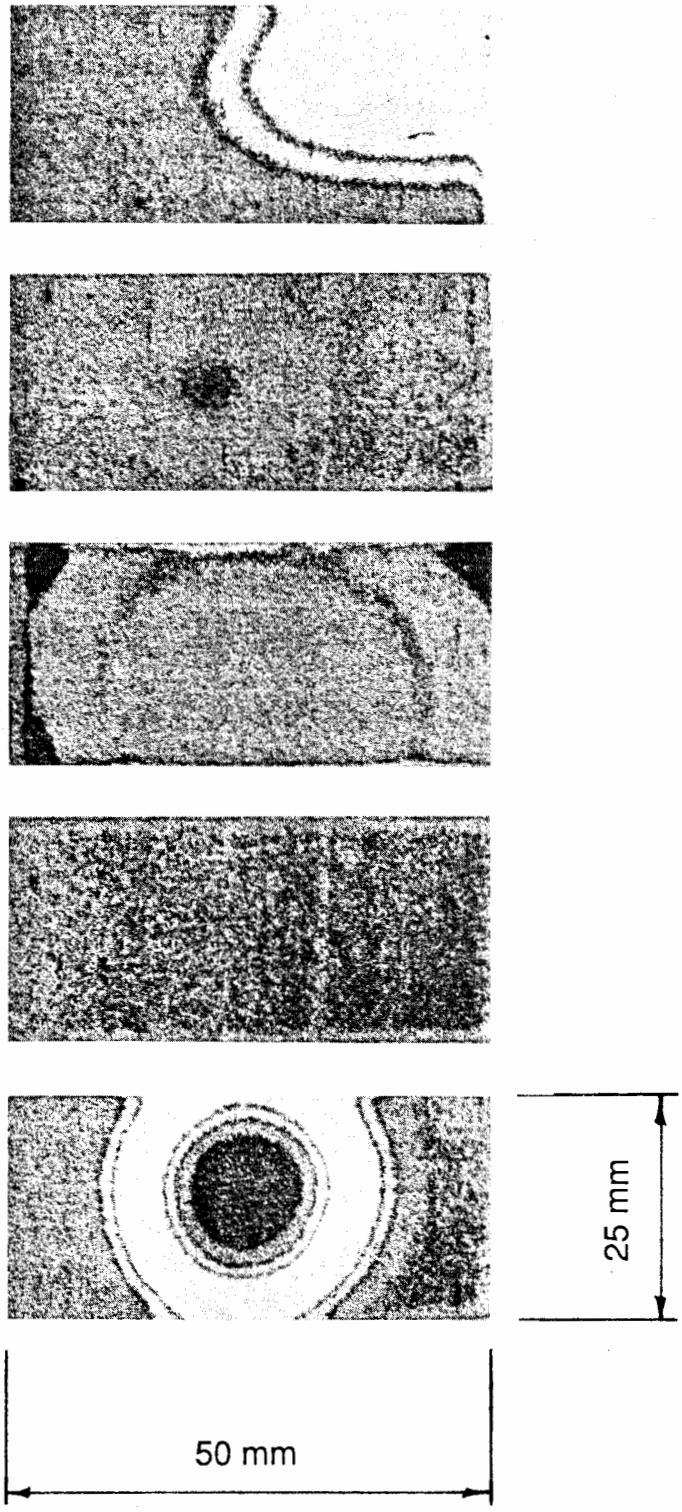

Figure 1.13 C-Scans of five Single-Lap Joints with Varying Adhesive Thickness.

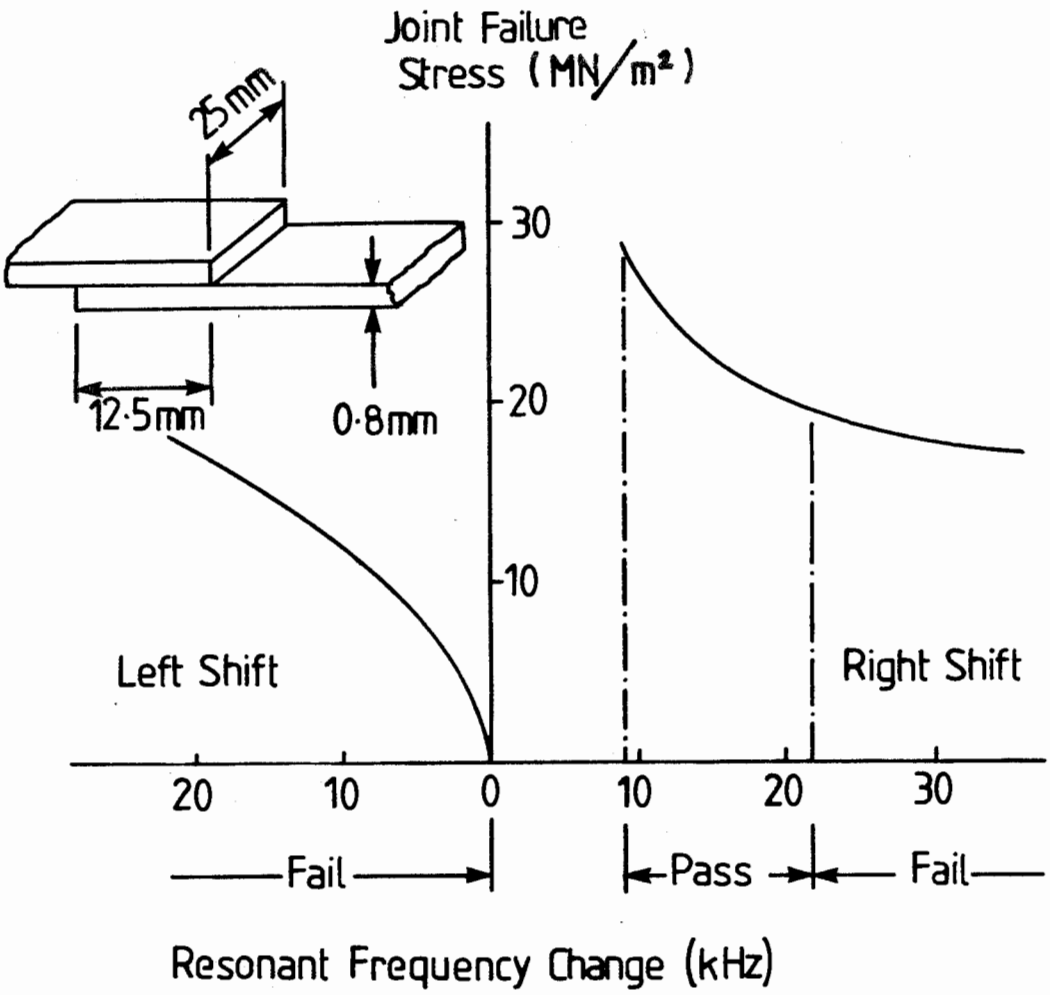

Figure 1.14 **Example of a Correlation Curve between Resonant Frequency Changes and Failure Stress for a Fokker Bond Tester MK II** A 'Right Shift' is a decrease in frequency and a 'Left Shift' is an increase in frequency

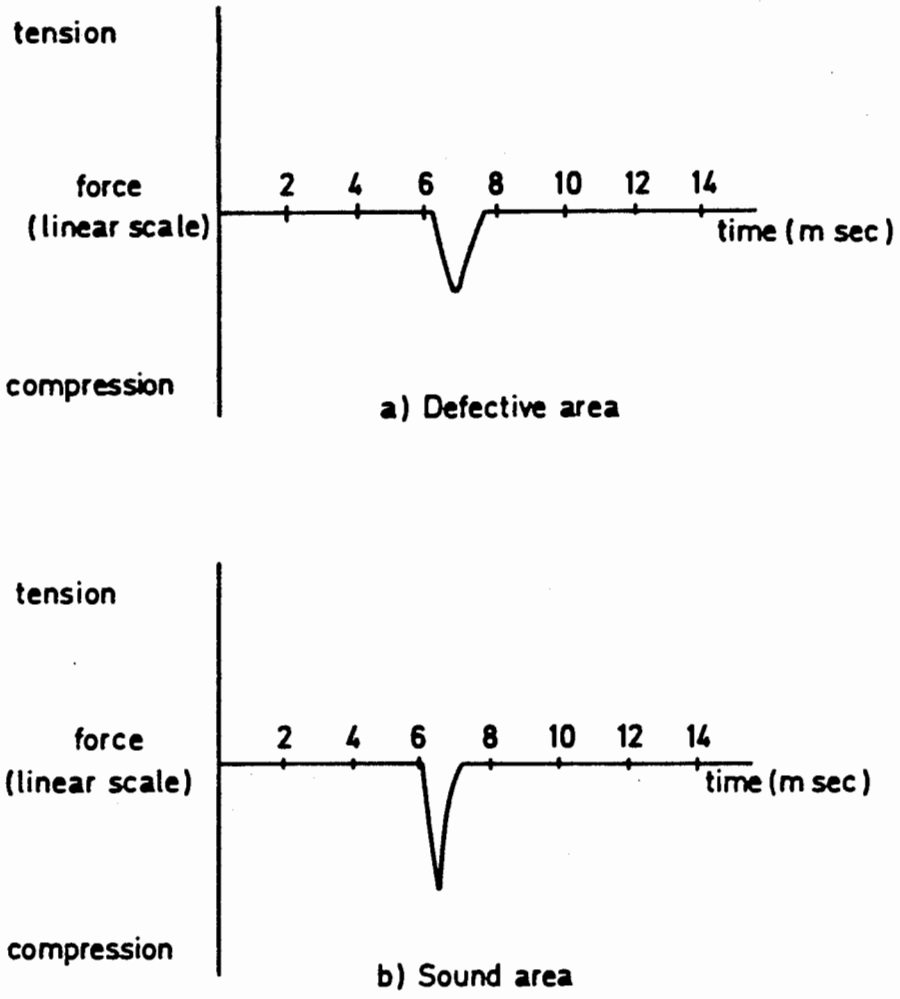

Figure 1.15 **Force Time Records for Impacts on Disbonded and Sound Areas of an Adhesive Joint**

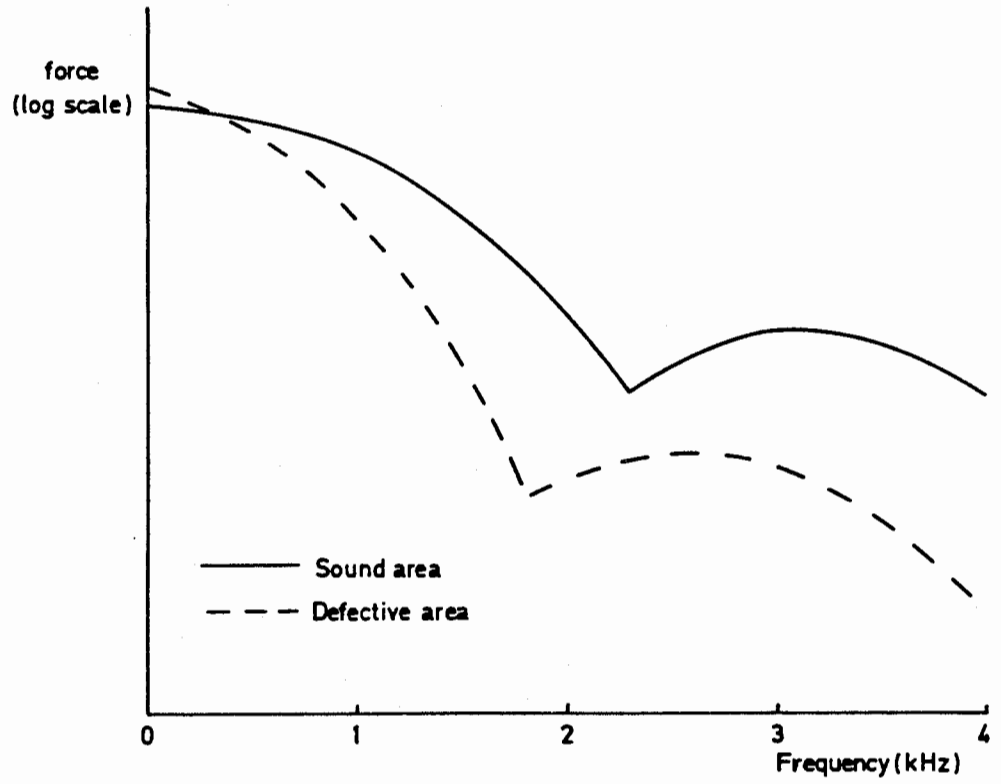

Figure 1.16 **Spectra of the Time Records shown in Figure 1.15**

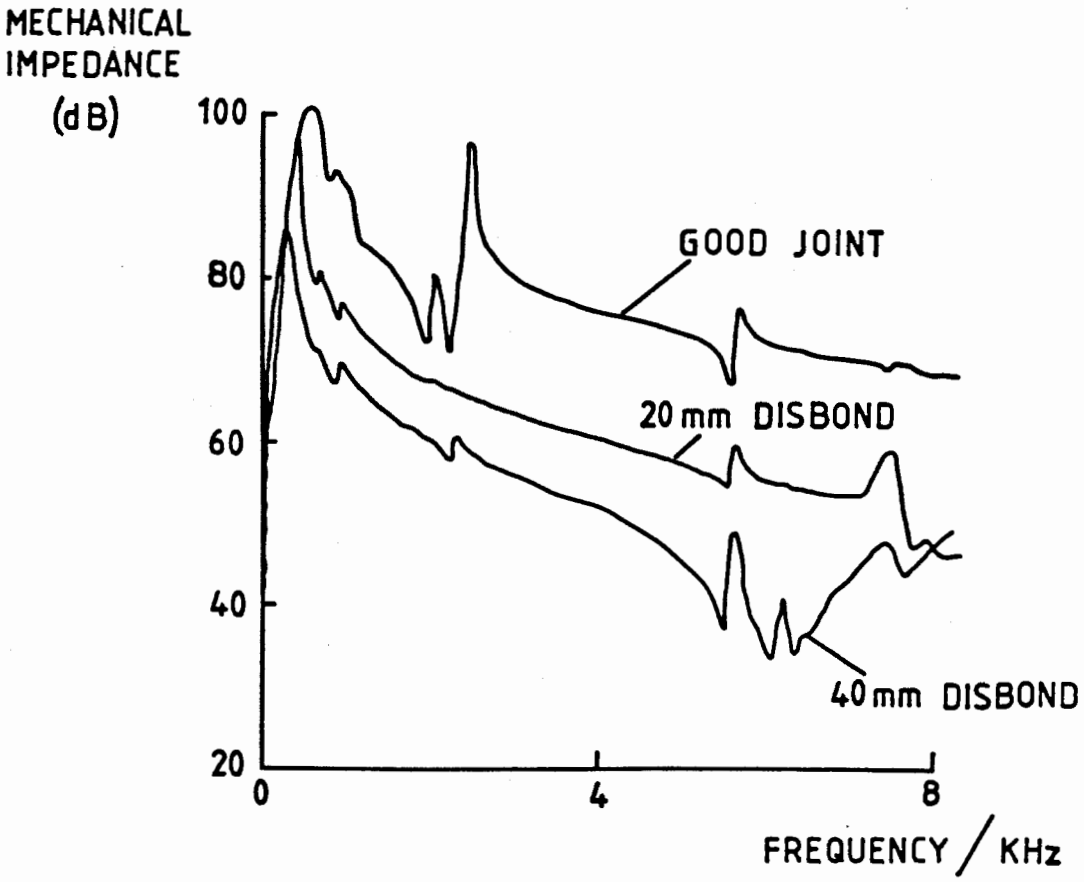

Figure 1.17 **Mechanical Impedance as a function of Frequency for a Thick Beam with an Adhesively Bonded Skin 3.3 mm Thick**

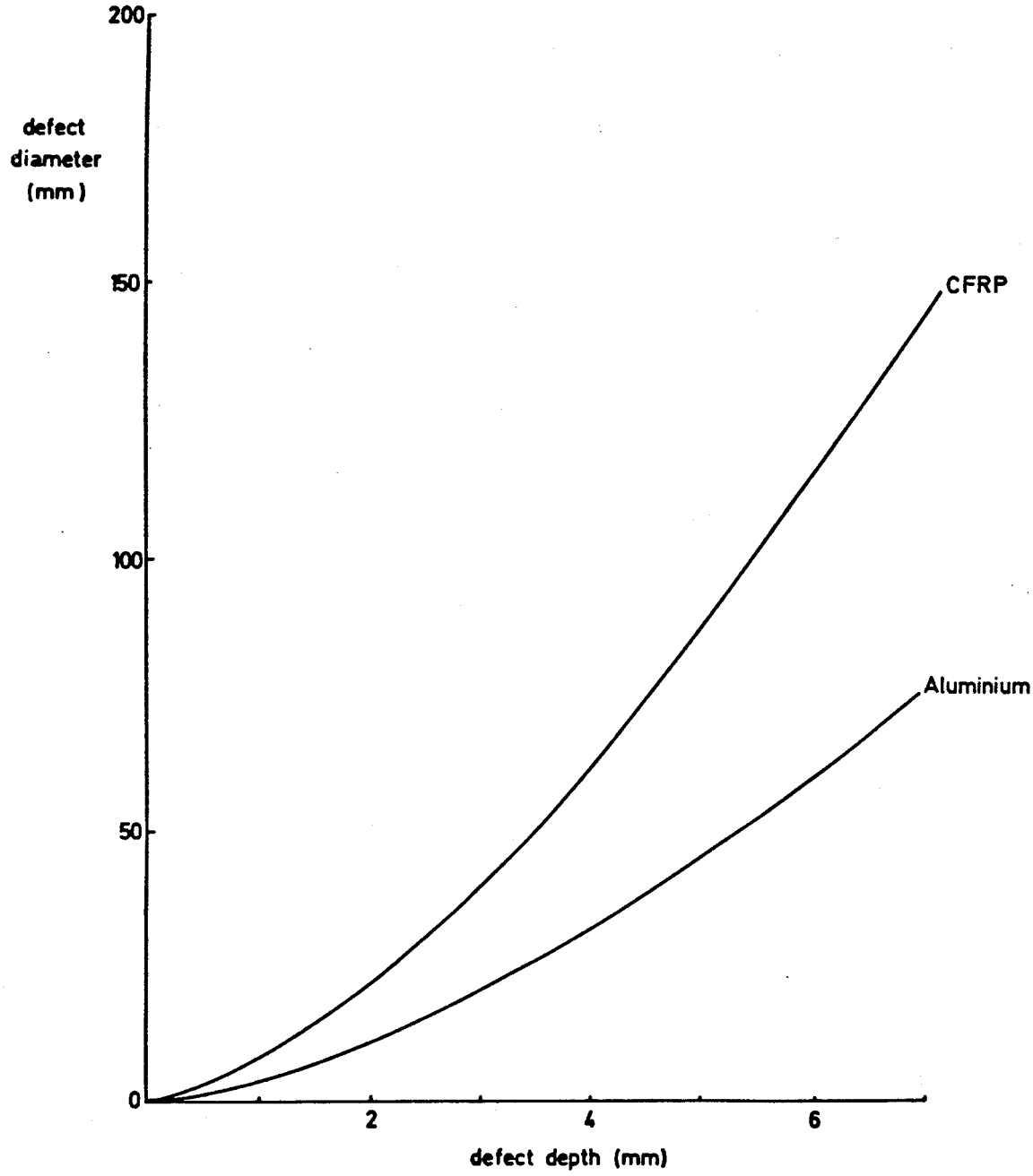

Figure 1.18 Minimum Detectable Defect Diameter against Depth in Aluminium and Carbon Fibre Composite assuming a 3dB Reliability in Impedance Measurements

PART TWO

THE FOKKER BOND TESTER Mk II

CHAPTER 2

Operation of the Fokker Bond Tester Mk II and the Vibration Properties of its Transducer

1 Introduction

It was shown in Chapter 1 that the Fokker Bond Tester Mk II is the only commercially available instrument that attempts to non-destructively measure the cohesive strength of a joint. Ying and Li (1979) conducted an investigaton into the working principle of the Fokker Bond Tester Mk II. They modelled the probe as a cylinder in axial resonance to which was attached the joint, modelled as a mass-spring-mass system. However the suitablity of the Fokker Bond Tester for measuring the cohesive strength of joints with different thicknesses and types of adhesive remains unclear.

Since the instrument is commonly used in industry to test adhesive joints, it was decided to carry out an investigation of the physical principles behind it, and to assess the sensitivity of the instrument when used on metal to metal joints bonded with different thicknesses and types of adhesive. This chapter describes the instrument and reports an investigation of the vibration characteristics of the transducer used. The operation of the instrument is discussed in Chapter 3.

2 Description of the Fokker Bond Tester Mk II

The Fokker Bond Tester Mk II uses a probe, see figure 2.1, which is coupled by a thin layer of liquid or gel to the component being tested. The probe consists of a cylindrical polarised piezoelectric (barium titanate) crystal, with electrodes on its top and bottom faces. The crystal is lightly supported by three hooked springs which also act as contacts for the electrodes. A number of crystals are available with different overall sizes and diameter to length ratios. Thicker adherends, and hence greater overall joint thicknesses, require larger crystals. Crystals with a diameter to length ratio of 1.5 or less, such as the 3412 and 3814, are used for testing sheet to sheet joints, whereas crystals for use on honeycomb to skin bonds, such as the 3414, have a larger diameter to length ratio. Table 2.1 gives the dimensions and diameter to length

ratio of three commonly used crystals (3412, 3814 and 3414).

When a voltage is applied across the electrodes on the crystal, the piezoelectric material is strained. Thus, when an alternating voltage is applied, the crystal vibrates at the same frequency as the applied voltage. The impedance of the crystal varies with frequency and decreases to a minimum at its resonant frequencies. In the electrical circuit used in the Fokker Bond Tester, the crystal is in series with a resistance, the voltage supplied to the resistance and crystal being roughly constant. Hence, the voltage across the resistance reaches a maximum at the resonant frequency of the crystal since the impedance of the crystal reaches a minimum.

Similarly, when the probe is placed on a specimen, the voltage across the resistance reaches a maximum at the resonant frequency of the system comprising the crystal and specimen. This is because the effective impedance of the crystal now reaches a minimum at the resonant frequency of the system comprising the crystal and component.

It is not clear exactly how the crystal deforms when it is repeatedly polarised over its top and bottom faces using continuous wave excitation; however it is likely that the most strongly excited modes will be those where there is axisymmetric axial deformation of the crystal. The modes of the crystal with non-axisymmetric axial deformation will be less strongly excited, and modes with relatively small axial deformation are only likely to be weakly excited.

In the operation manual of the instrument, Rienks (1972) states that there are two main resonant frequencies of the crystal, the deformation of the crystal in one mode being primarily radial and in the other largely axial, as shown in figure 2.2. The deformation in these modes cannot be either purely radial or purely axial since the Poisson's ratio effect ensures that deformation in one axis is accompanied by deformation in the others. Rienks refers to these two modes as the radial and axial modes of the crystal.

The Fokker Bond Tester has two displays, the A and B-Scales (Rienks, 1972). The A-Scale displays the frequency response of the probe (or the probe with the specimen coupled to it) over the pre-set frequency range, with frequency increasing from right to left, see figure 2.3. The change in resonant frequency

can be obtained from this display. The B-Scale gives an indication of resonant amplitude. The older versions of the instrument used a cathode ray tube for the A-Scale and an anologue meter for the B-Scale. However, a new version uses a digital display for both the A and B Scales.

The Fokker Bond Tester sweeps the voltage applied to the crystal over a frequency range which can be pre-set between approximately 10 and 80 kHz depending on the crystal used. The centre of the range depends primarily on the resonant frequencies of the crystal, and typically falls between 50kHz and 0.5MHz. The operation manual (Rienks, 1972) says that the centre frequency should be chosen so that the mode shape of the crystal corresponds with the radial mode when sheet to sheet joints are inspected and with the axial mode when honeycomb to skin joints are inspected. However, it is the axial motion of either the radial or axial mode that would be most strongly coupled, via the thin layer of liquid or gel, to the joint being inspected.

Since it is likely that the frequency response of the crystal is more complex than Rienks (1972) suggests, it was decided to clarify which mode or modes of the probe are used to excite the joint under examination. This was done by measuring the response of typical crystals and comparing the results with values predicted using finite element analysis.

3 Predicted Resonant Frequencies and Mode Shapes of the Crystal

Finite element analysis was used to predict the resonant frequencies and mode shapes of the crystals in the operating frequency range of the Fokker Bond Tester. The element used in the analysis was an axisymmetric version of the 8-node isoparametric element described by, for example, Zienkiewicz (1971). This element allows quadratic displacement variations along both its major dimensions. A 4x4 mesh was employed which was considered to be sufficiently fine to represent the modest curvatures seen in the lower modes of vibration. The analysis was run using the FINEL finite element package developed at Imperial College (Hitchins, 1984) and was run on a CDC Cyber 170/855 machine.

As is standard in analyses using axisymmetric elements, the displacements

were assumed to vary as Cos $N_h\theta$ around the circumference of the crystal. Hence, N_h=0 gives axisymmetric modes while N_h=1,2,3... gives modes in which the shape of the circumference is distorted.

The predicted resonant frequencies for probe 3814, with a diameter to length ratio of 1.5 are given in table 2.2. The results shown are for the four analyses with N_h=0,1,2,3. The frequencies of the modes with N_h=4 were predicted to be above the frequency range of interest.

The absolute values of the natural frequencies are dependent on the modulus and Poisson's ratio of the piezoelectric material. These properties were obtained by measuring the transit time of an ultrasonic pulse from a 10 MHz probe through a crystal. Knowing the thickness of the crystal, it was possible to calculate the longitudinal (c_L) and shear (c_S) wave velocity, which were found to be 5795 and 2937 m/s respectively. The Poisson's ratio was calculated to be 0.320 from the ratio of shear to longitudinal wave velocity (Kolsky, 1963). The Young's modulus (E) is given by (Kolsky, 1963) :

$$E = \rho c_S^2 (3c_L^2 - 4c_S^2) / (c_L^2 - c_S^2) \qquad (2.1)$$

where ρ is the density of the crystal. This gave a value of 122 GN/m^2 for the Young's modulus.

The predicted mode shapes of probe 3814 corresponding to the resonances at 264.2kHz, 292.5kHz, 296.9kHz, 323.1kHz and 351.6kHz, are shown in figure 2.4. Each of these modes has significant axial deformation and they are all likely to be excited when the crystal is polarised over its top and bottom faces.

The other modes in the range 200-400kHz predicted by finite element analysis have negligble axial deformation compared to the modes shown in figure 2.4. For example, the axisymmetric (N_h=0) mode predicted at 229.9kHz consists primarily of torsional deformation and is unlikely to be significantly excited when the crystal is polarised over its top and bottom faces.

The predicted resonant frequencies of the larger crystal, also with a diameter

to length ratio of 1.5, (3412) are given in table 2.3, the predicted mode shapes of probe 3412 being similar to the corresponding mode shapes of crystal 3814.

The resonant frequencies and corresponding mode shapes of probe 3414, which has a diameter to length ratio of 3.0, were also predicted using finite element analysis. In this instance there are many modes with N_h=0,1,2,3 and 4 in the frequency range of interest, the resonant frequencies of the axisymmetric modes (N_h=0) with significant axial deformation being given in table 2.4.

The predicted mode shapes of probe 3414 corresponding to the resonances at 160.8kHz, 337.1kHz, 415.5kHz and 456.1kHz, are shown in figure 2.5. Each of these modes is axisymmetric (N_h=0) and has significant axial deformation; consequently they are all likely to be excited when the crystal is polarised over its top and bottom faces.

As can be seen from the predicted resonant frequencies in tables 2.2-2.4, there are many more modes of vibration of each crystal in the operating range in the Fokker Bond Tester than the two suggested by Rienks (1972). In addition all the mode shapes predicted by finite element analysis are more complex than those suggested by Rienks (1972).

4 The Measured Frequency Response of the Crystal

The frequency response of the probe was measured independently by varying the frequency of an alternating voltage applied to the crystal, in series with a 330Ω resisitor, as shown in figure 2.6. A micro-computer was used to control both the function generator, which supplied a harmonic voltage to the crystal, and the voltmeter, which measured the voltage across the resistor. The resonant frequencies of the crystal occurred when the voltage across the resistor reached a maximum.

The frequency response of each of the crystals was also obtained from the A-Scale of a Fokker Bond Tester Model 70 and was found to be similar to that obtained from the system shown in figure 2.6. However, since the Fokker Bond Tester does not give a direct measure of frequency, but only the change in frequency, it was more difficult to measure the resonant frequencies of the crystal using the Fokker Bond Tester. Difficulties were also encountered in

obtaining an accurate frequency calibration of the cathode ray tube A-Scale display. This error, together with the difficulty of using the display introduced further errors (up to approximately 5%) in the measurement of frequency response using the Fokker Bond Tester. A later version of the instrument (Model 80L) use a digital display for the A-Scale which helps to reduce this error.

The measured frequency response of probe 3814, which has a diameter to length ratio of 1.5, is shown in figure 2.7. The values of the resonant frequencies, defined as maxima in the voltage across the resistor, obtained from this curve are given in table 2.2. The strongly excited mode shown in figure 2.7, which occurs at 277.8kHz corresponds to the axisymmetric (N_h=0) mode predicted at 292.5kHz. As can be seen from its predicted mode shape shown in figure 2.4b, there is both axial and radial deformation of the crystal with the top and bottom faces moving in opposite phase. The amplitude of the radial motion is slightly greater than that of the axial motion so the mode shape is fairly similar to that of the radial mode described by Rienks (1972). There are also a number of smaller resonances in the range 200-400kHz which correspond to other predicted modes of the crystal.

The frequency response for the larger probe (3412) with the same diameter to length ratio as probe 3814 was also measured, the resonant frequencies being given in table 2.3. The frequency response was similar in form to that of the smaller probe, but with the resonances occurring at lower frequencies. In this case the strongly excited axisymmetric (N_h=0) mode occurred at 148.8kHz.

It was anticipated that there would be some discrepancy between the predicted and measured natural frequencies due to a variation (up to 5%) in the dimensions of nominally identical crystals and inaccuracies in the measured Young's modulus of the crystal. The Young's modulus used in the analysis was measured at 10 MHz whereas the modes of interest of the crystal were in the range 200-400 kHz. However, although the absolute values of the measured and predicted resonant frequencies vary by as much as 10% the relative values should be correct. Therefore, the predicted and measured frequencies for all the modes are compared with those of the axisymmetric (N_h=0) mode described above. Table 2.2 shows that there is good agreement between theory and experiment on the relative positions of the modes.

The measured change in resonant frequency due to variation in the dimensions of the crystals depends on the mode of the crystal. However, a variation of approximately 1.5% in the major axisymmetric mode was found between nominally identical 3412 crystals.

The frequency response for probe 3414, which has a diameter to length ratio of 3.0, is shown in figure 2.8 and the measured resonant freqencies of the major modes are given in table 2.4. The frequency response has a different form to that of probe 3814 with many resonant frequencies in the range 100-500kHz and a major resonance at 403.2kHz. The predicted mode shapes corresponding to the main resonances seen in figure 2.8 are shown in figure 2.5 The predicted and measured resonant frequencies relative to those of the axisymmetric (N_h=0) mode predicted at 160.8kHz are also shown in table 2.4. This shows that there is good agreement between theory and experiment on the relative position of the strongly excited modes shown in figure 2.5.

5 Investigations on Large Scale Model of Crystal

It is very difficult to measure the mode shapes of a small object such as the crystal and, since there are discrepancies between the mode shapes predicted using finite element analysis and those suggested by Rienks (1972), it was decided to test a large model of the crystal on which the mode shapes could be measured. The model of the crystal consisted of an aluminium cylinder having a diameter of 216 mm and a length of 144 mm, giving it a similar geometry to that of crystals 3412 and 3814.

5.1 Predicted Mode Shapes

The finite element analysis was repeated four times, to give the modes with N_h=0,1,2,3, for the aluminium cylinder using a similar element to that employed for the analysis of the crystal. Standard values for Young's modulus of 68.9 GN/m^2 and Poisson's ratio of 0.355 were used. Table 2.5 gives the predicted resonant frequencies of the aluminium cylinder. The predicted mode shapes were similar to those predicted for the corresponding modes of crystals 3412 and 3814. However, the modes of the aluminium cylinder do not neccessarily occur in the same frequency order as those of the crystal since

the Poisson's ratios of the materials are different.

5.2 Measured Resonant Frequencies and Mode Shapes

The natural frequencies of a structure correspond to the maxima in the frequency response function, $H_{ij}(\omega)$, which is defined by :-

$$H_{ij}(\omega) = X_i(\omega)/F_j(\omega) \qquad (2.2)$$

where ω is the frequency, F_j is the force applied at position j and X_i is the corresponding response at position i.

The deflected shape (mode shape) at a particular resonant frequency may be obtained by measuring the frequency response (transfer) function, at the appropiate frequency, between a reference position and a series of points on different parts of the structure. The relative values of the frequency response function at the different points then gives the deflected (mode) shape of the structure.

The required frequency response functions may be measured either by applying a force at the reference position and measuring the response due to this force at a series of positions, or by measuring the response at the reference point due to a force applied at a series of different points. The method which is most convenient depends on the measuring system employed.

In this case, impact excitation via a hammer with a force gauge in its head was used, the response being measured by an accelerometer attached to the model. It was therefore convenient to measure the response at the reference point and to apply the force, via the impact, at different points. The frequency response function was obtained by passing the force and acceleration signals into a two channel spectrum analyser (Bruel and Kjaer type 2032) via two charge amplifiers. The measurement system is shown in figure 2.9 and the technique is described in more detail by, for example, Ewins (1984).

The measured resonant frequencies of the aluminium cylinder are given in table 2.5. There is a small discrepancy between the predicted and measured

natural frequencies which is assumed to be due to errors in the values of the material properties used in the theoretical analysis. The predicted and measured natural frequencies of all modes relative to those of the major axisymmetric N_h=0 mode are also shown in table 2.5 and it can be seen that there is excellent agreement between the relative values.

The predicted N_h=0 mode at 10.62kHz was not detected in practice since this mode consisted primarily of torsional deformation, with negligble axial or radial deformation, and hence could not easily be excited.

The mode shapes of the aluminium cylinder at 12.685kHz, 13.925kHz, 14.120kHz, 15.650kHz and 16.510kHz were determined using the technique outlined above and agreed very closely with the corresponding predicted mode shapes shown in figure 2.4 for a crystal of similar geometry to the model.

6 Discussion

The excellent agreement obtained between the predicted and measured mode shapes of the aluminium model strongly indicates that the predicted mode shapes for the crystal are accurate. Rienks (1972) states that there are two main modes of the crystal which he terms the radial and axial modes. However the measured frequency responses, see figures 2.7 and 2.8, show that there are many modes in the operating frequency range. Similarly, the mode shapes predicted and measured in this investigation are more complex than the simple shapes given by Rienks (1972).

In the frequency range used to inspect sheet to sheet joints, the major mode of crystals 3412 and 3814 which is excited has the deflected shape shown in figure 2.4b. This is the major axisymmetric (N_h=0) mode of the crystal and there is deformation in both the radial and axial directions. However, when the probe is coupled to the joint by a thin layer of liquid or gel, little of the radial motion will be transmitted to the joint. Instead, the joint will be primarily excited by axial motion of the crystal and the area below the probe will vibrate in the through thickness direction.

The most strongly excited mode of probe 3414, used in inspection of skin to honeycomb core bonds, is that shown in figure 2.5c, which has predominantly

axial motion and is analogous to the axial mode described by Rienks (1972). This is different from the mode shape of the most strongly excited mode of crystals 3412 and 3814 which is shown in figure 2.4b. However, the mode of crystal 3414 which occurs at 160.4kHz has the mode shape shown in figure 2.5a which is similar to the major mode of crystals 3412 and 3814.

7 Conclusions

It has been shown that there is good agreement between the measured and predicted resonant frequencies for the crystals and the model of the crystal. In addition the measured and predicted mode shapes for the model of the crystal also showed excellent agreement.

There is therefore strong evidence to show that the frequency response of Fokker Bond Tester probes is quite complex, there being a number of modes in the frequency range of interest, which have more complex mode shapes than those suggested by Rienks (1972).

Crystal Type	Crystal Diameter/mm	Crystal Length/mm	Diameter/ Length ratio
3412	19.05	12.75	1.5
3814	9.50	6.40	1.5
3414	19.05	6.40	3.0

Table 2.1 Dimensions of Typical Crystals

Predicted Frequency kHz	% Change from the mode at 292.5 kHz	N_h	Measured Frequency kHz	% Change from the mode at 277.8 kHz
175.7	-39.9	2	not detected	-
229.9	-21.4	0	- " -	-
231.1	-21.0	2	- " -	-
260.4	-11.0	1	244.4	-12.0
261.1	-10.7	1	not detected	-
264.2	-9.7	0	252.8	-9.0
292.5	0.0	0	277.8	0.0
296.9	+1.5	3	283.0	+1.8
323.1	+10.5	2	306.0	+10.2
342.9	+17.2	1	not detected	-
348.5	+19.1	1	- " -	-
351.6	+20.2	3	334.1	+20.3

Table 2.2 **Predicted and Measured Resonant Frequencies for Probe 3814 with a Diameter-to-Length Ratio of 1.5**

Predicted Frequency kHz	% Change from the mode at 146.3 kHz	N_h	Measured Frequency kHz	% Change from the mode at 148.8 kHz
87.4	-40.3	2	not detected	-
115.3	-21.2	0	- " -	-
115.3	-21.2	2	- " -	-
130.3	-10.9	1	130.6	-12.2
130.3	-10.9	1	not detected	-
131.5	-10.1	0	132.3	-11.1
146.3	0.0	0	148.8	0.0
147.9	+1.1	3	152.0	+2.2
161.9	+10.7	2	not detected	-
172.0	+17.6	1	- " -	-
174.2	+19.1	1	- " -	-
175.4	+19.9	3	176.5	+18.6

Table 2.3 **Predicted and Measured Resonant Frequencies for Probe 3412 with a Diameter-to-Length Ratio of 1.5**

Predicted Frequency kHz	% Change from the mode at 160.8 kHz	N_h	Measured Frequency kHz	% Change from the mode at 160.4 kHz
160.8	0.0	0	160.4	0.0
337.1	+109.6	0	346.8	+116.2
415.5	+158.4	0	403.2	+151.4
456.1	+183.6	0	457.1	+185.0

Table 2.4 **Predicted and Measured Resonant Frequencies for Probe 3414 with a Diameter-to-Length Ratio of 3.0**

Predicted Frequency kHz	% Change from the mode at 13.48 kHz	N_h	Measured Frequency kHz	% Changefrom the mode at 14.120 kHz
8.01	-40.6	2	8.245	-41.6
10.57	-21.6	2	10.925	-22.6
10.62	-21.2	0	not detected	-
12.00	-11.0	1	12.285	-13.0
12.01	-10.9	1	12.530	-11.3
12.35	-8.4	0	12.685	-10.2
13.48	0.0	0	14.120	0.0
13.56	+0.6	3	13.925	-1.4
14.94	+10.8	2	15.650	+10.8
16.08	+19.3	3	16.510	+16.9

Table 2.5 **Predicted and Measured Resonant Frequencies for the Crystal Model with a Diameter-to-Length Ratio of 1.5**

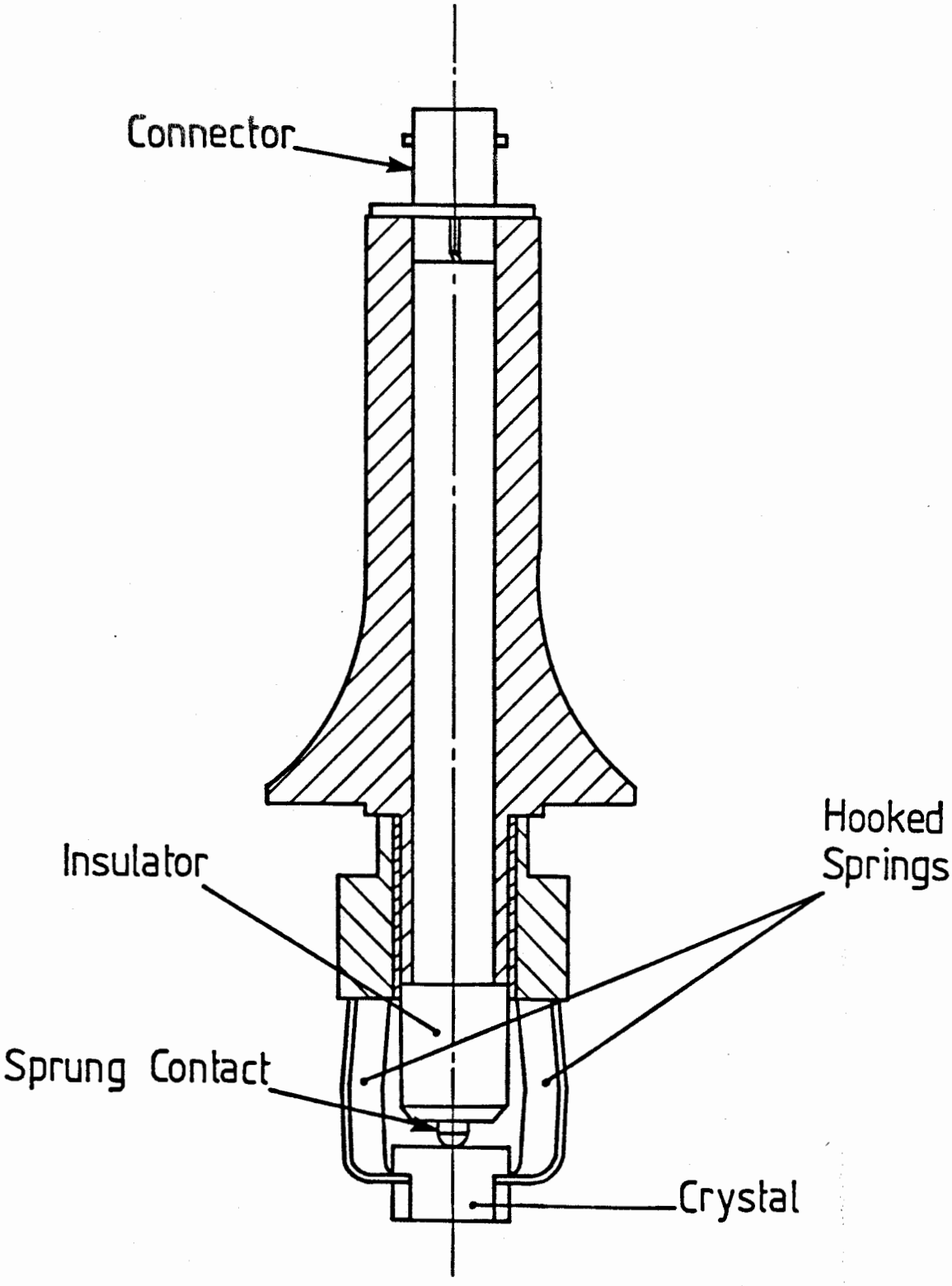

Figure 2.1 **Cross Section of Fokker Bond Tester Mk II Probe**

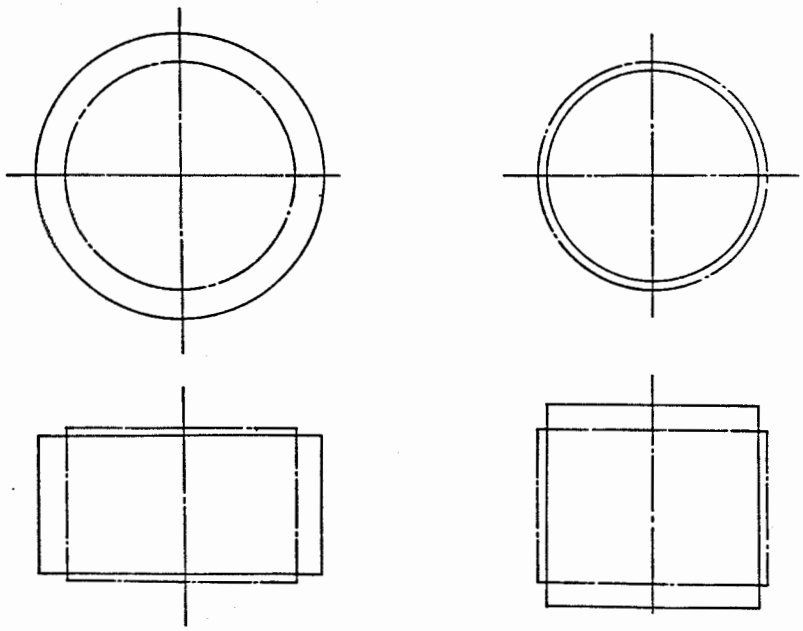

(a) Radial Mode (b) Axial Mode

Figure 2.2 **Deformed Shapes of Crystal after Rienks (1972)**
upper view - plan view of top of crystal
lower view - diametral cross-section of crystal
chain line - undeformed shape of crystal
solid line - deformed shape of crystal

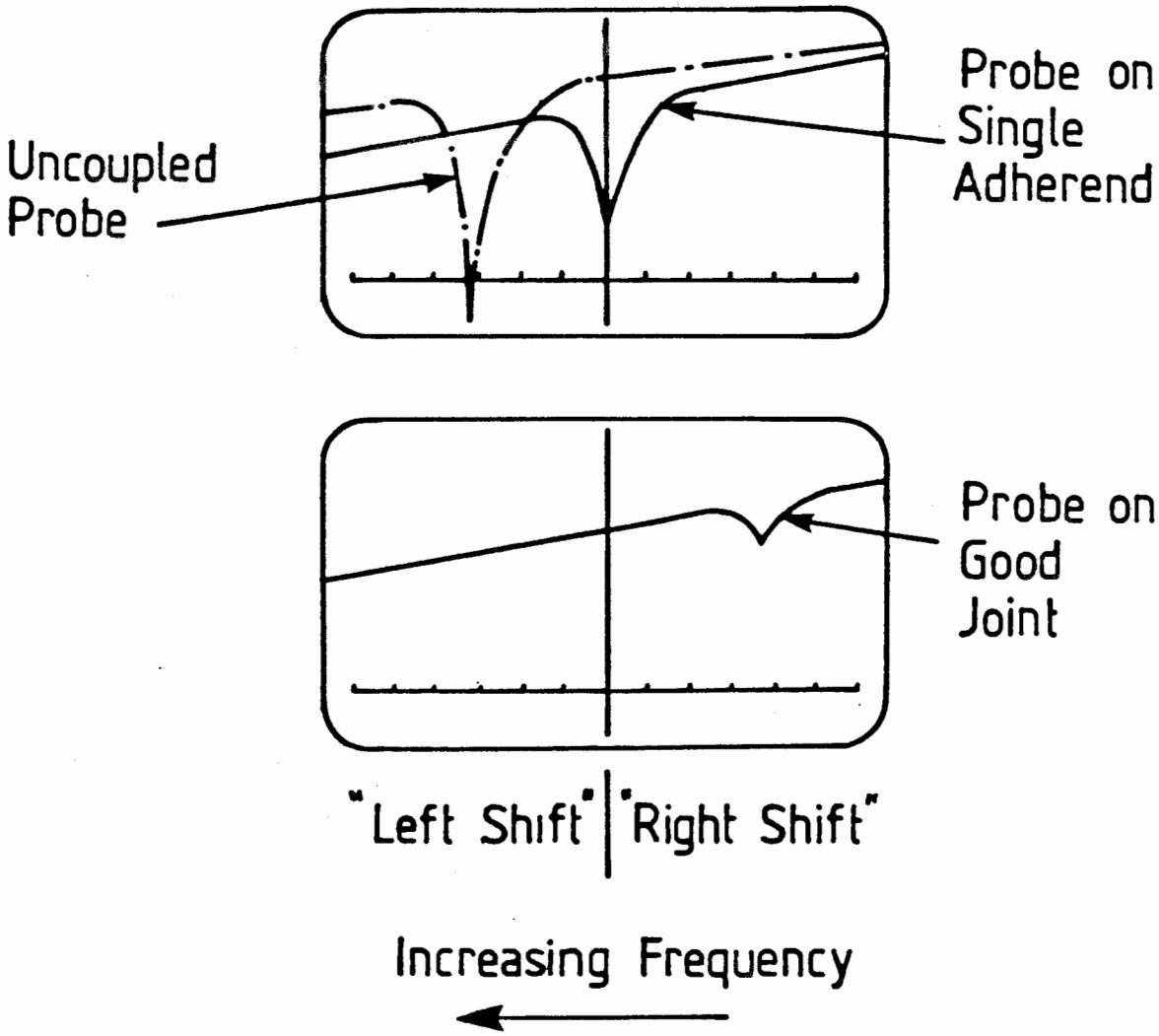

Figure 2.3 **A-Scale Display of Probe on Good Joint and Plate from Fokker Bond Tester Mk II**

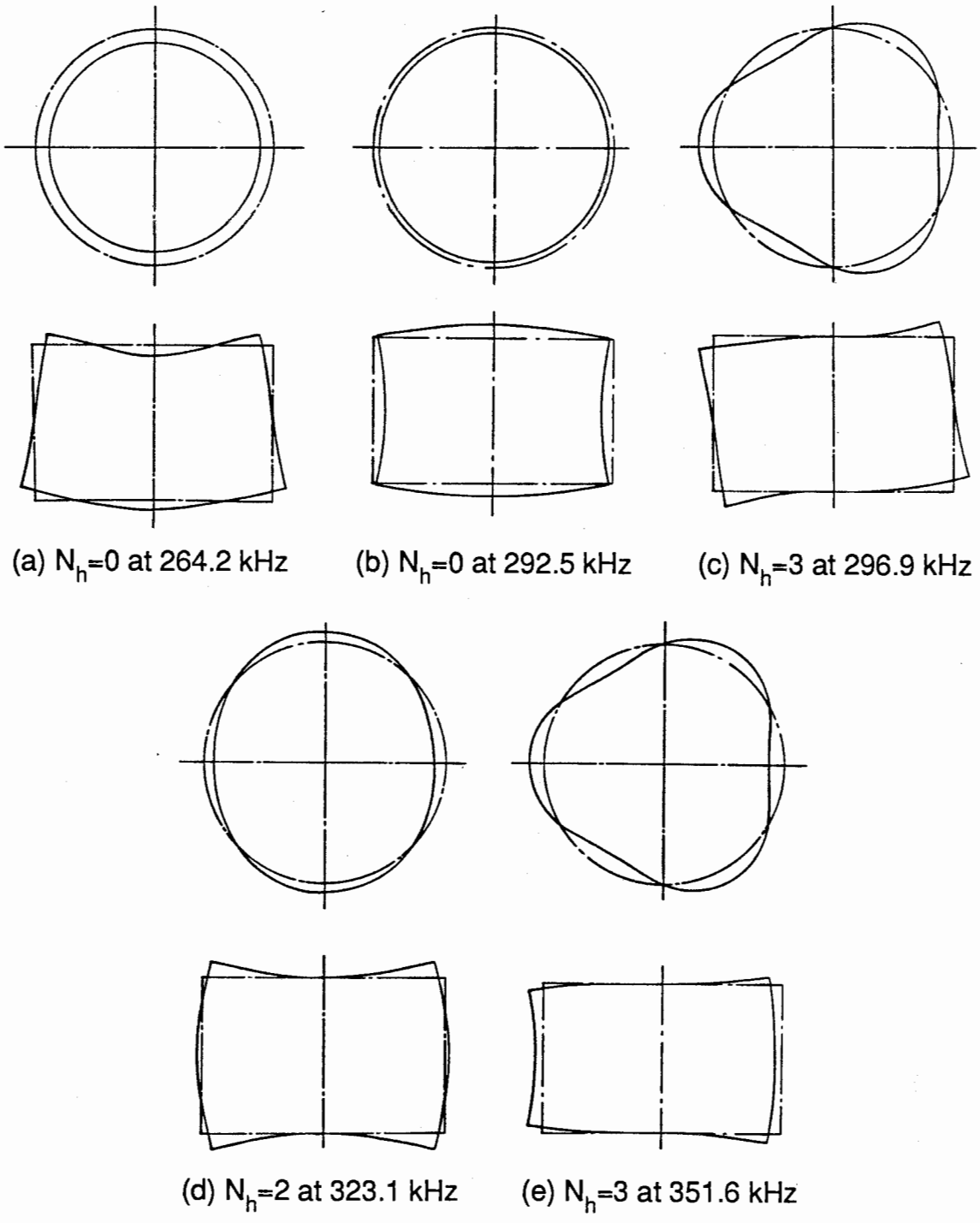

Figure 2.4 **Predicted Deformed Shapes of Crystal 3814 with a Diameter to Length Ratio of 1.5**

upper view - plan view of top of crystal
lower view - diametral cross-section of crystal
chain line - undeformed shape of crystal
solid line - deformed shape of crystal

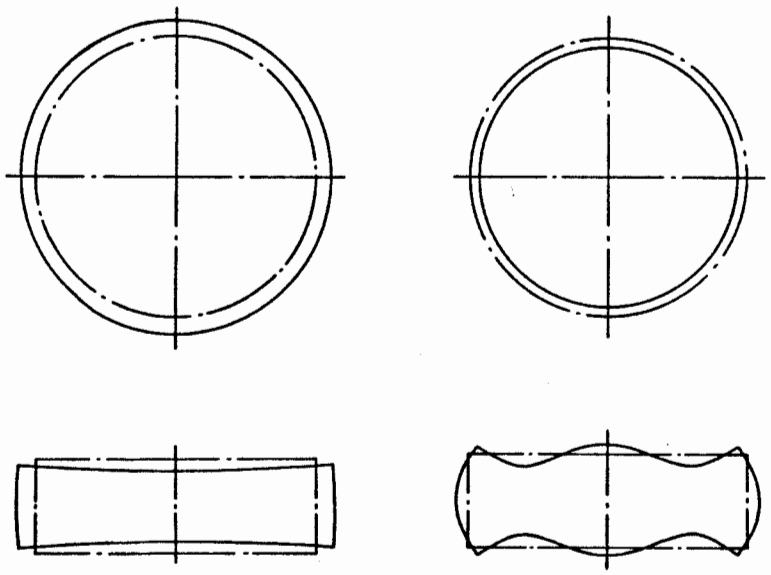

(a) N_h=0 at 160.8kHz (b) N_h=0 at 337.1 kHz

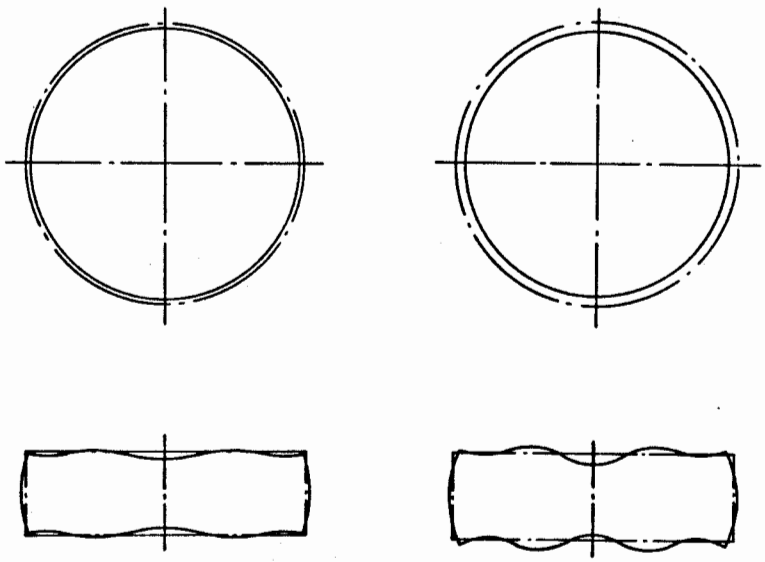

(c) N_h=0 at 415.5 kHz (d) N_h=0 at 456.1 kHz

Figure 2.5 **Predicted Deformed Shapes of Crystal 3414 with a Diameter to Length Ratio of 3.0**

upper view - plan view of top of crystal
lower view - diametral cross-section of crystal
chain line - undeformed shape of crystal
solid line - deformed shape of crystal

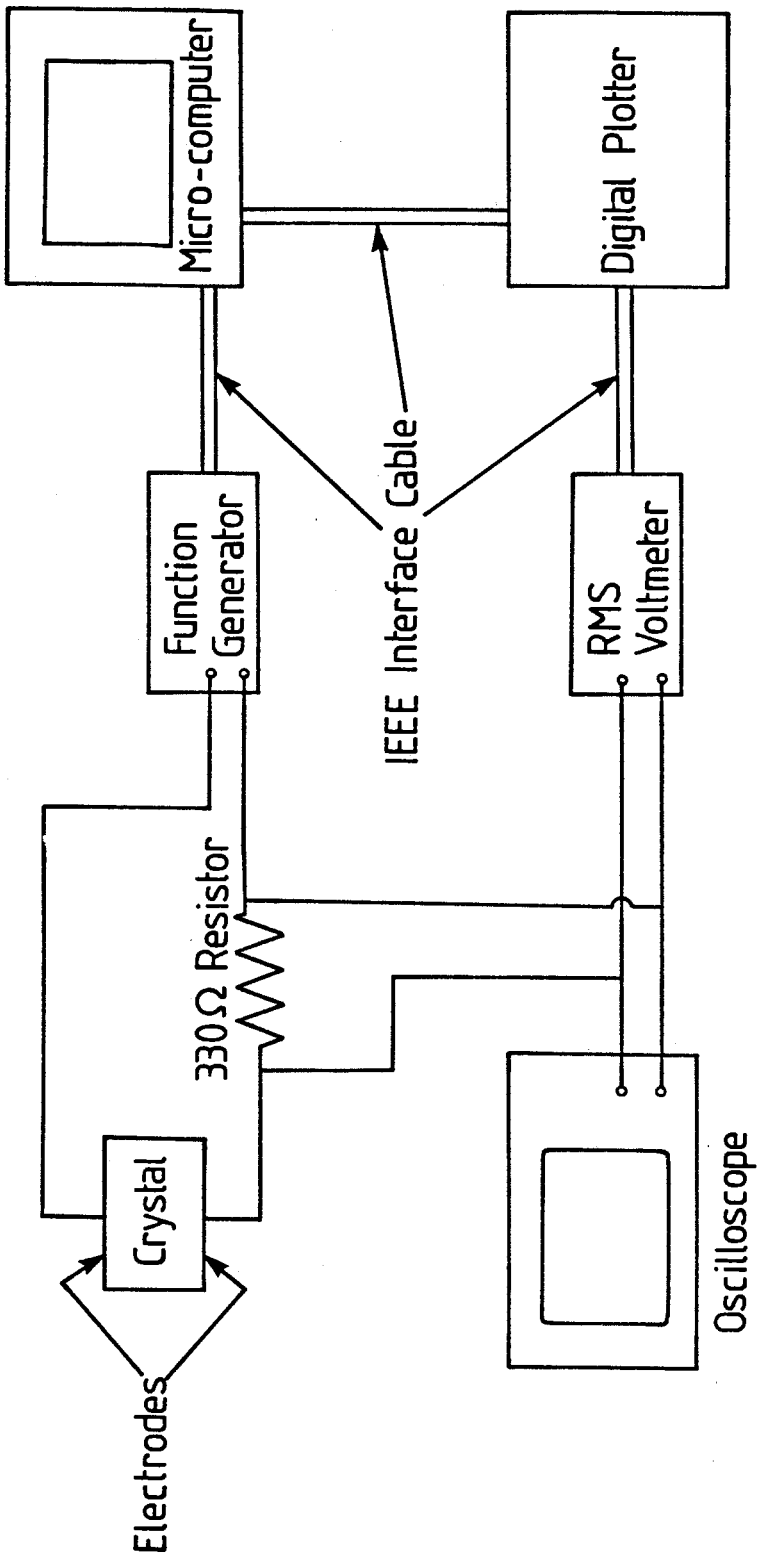

Figure 2.6 **Schematic Diagram of Apparatus**

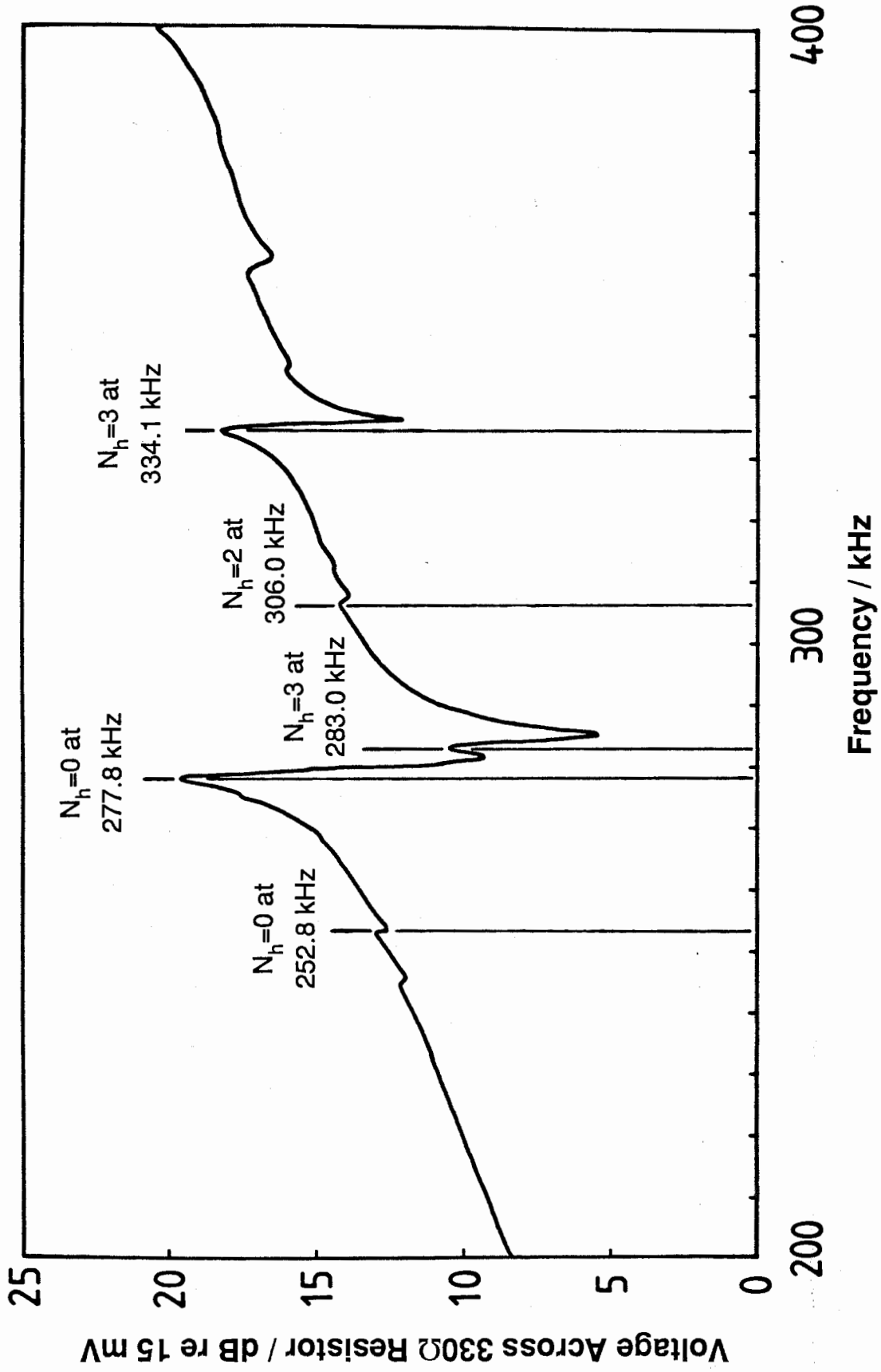

Figure 2.7 **Measured Frequency Response of Probe 3814 with a Diameter to Length Ratio of 1.5**

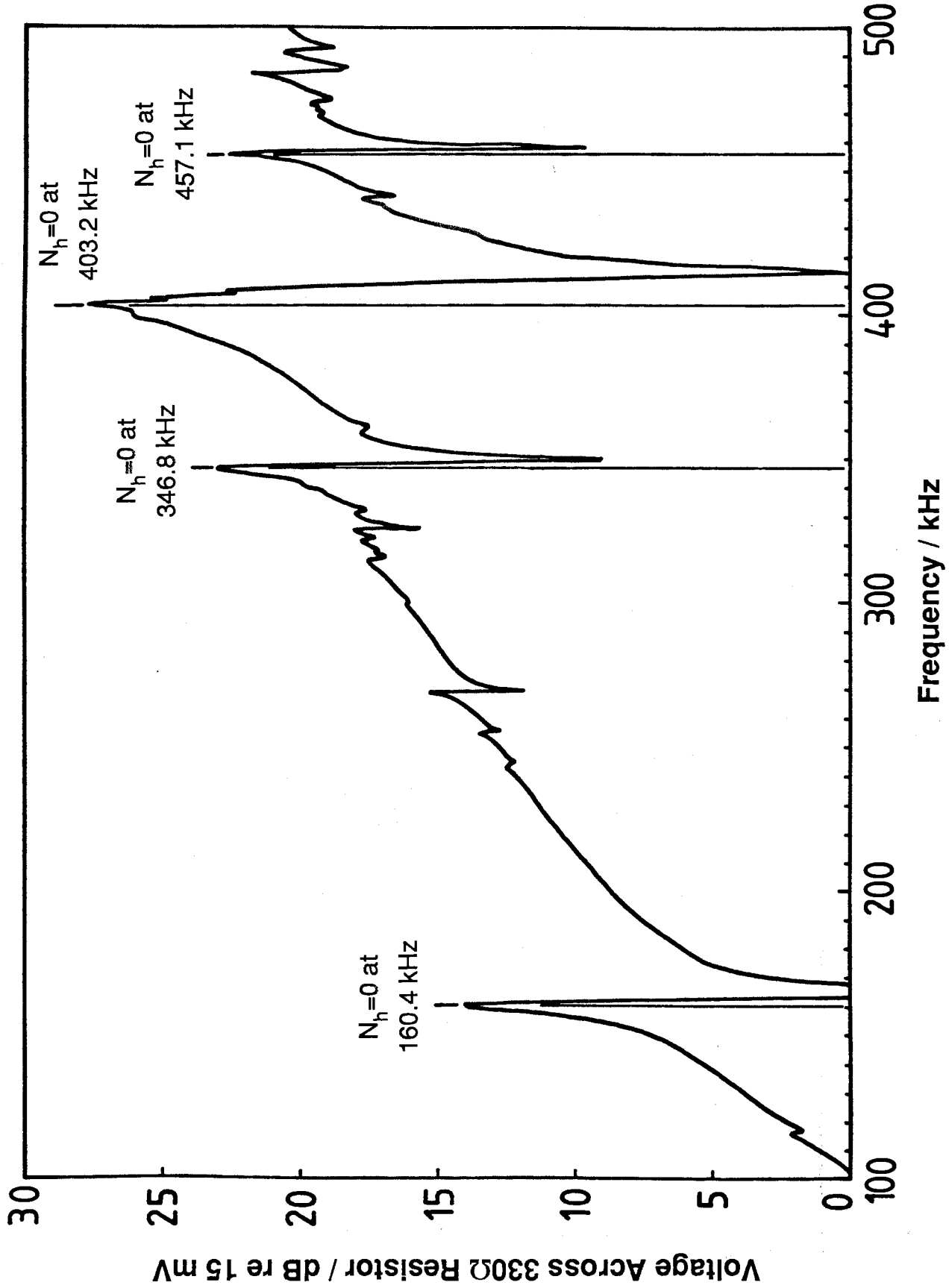

Figure 2.8 **Measured Frequency Response of Probe 3414 with a Diameter to Length Ratio of 3.0**

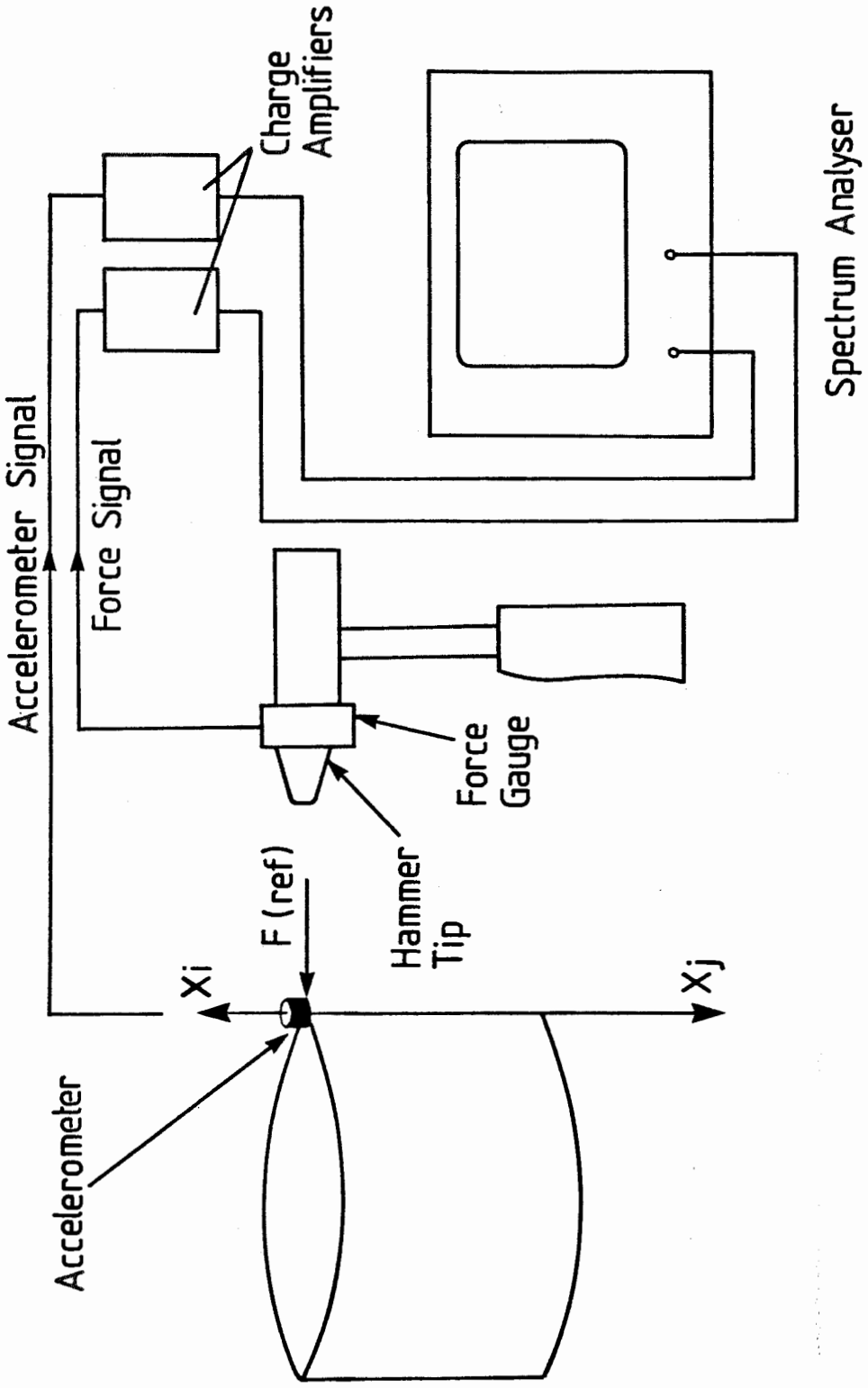

Figure 2.9 **Schematic Diagram of the Apparatus used to Measure the Frequency Response Function**

CHAPTER 3

Use of the Fokker Bond Tester Mk II

1 Introduction

When the Fokker Bond Tester Mk II is used to predict the cohesive strength of a sheet to sheet joint the instrument is initially adjusted so that the resonance of the probe coupled to a single adherend lies at the centre of the A-Scale. The amplitude is also adjusted to give a B-Scale reading of 100. When the probe is coupled to the joint, the resonant frequency changes and the amplitude decreases; a decrease in frequency is called a "Right-Shift" and an increase a "Left-Shift", see figure 2.3. The Fokker Bond Tester uses the resonant frequency changes on the A-Scale to predict the cohesive strength of the joint.

When the probe is coupled to a honeycomb panel, the change in resonant frequency, and hence A-Scale reading, between that obtained with the probe coupled to the skin alone and that with the skin bonded to the honeycomb is negligible. However, the resonant amplitude, or B-Scale reading, for a good bond between the skin and the core is lower than that obtained when the probe is coupled to the skin alone (Curtis, 1982).

The measured resonant frequency of a sheet to sheet joint can either be above or below that of the single adherend. This frequency will depend both on the modulus and on the thickness of the adhesive layer . However, the cohesive strength of a joint does not correlate with adhesive modulus and thickness in the same way. Consequently, a test for cohesive strength must be able to distinguish between adhesive thickness and modulus changes.

In order to determine the sensitivity of the Fokker Bond Tester to typical changes in adhesive modulus and thickness it was decided to measure the resonant frequencies of the probe coupled to various joints and to compare these results with those predicted using a simple model. However, before the response of the probe coupled to the joints was determined, it was useful to examine the response of the probe coupled a plain plate which is a much simpler system than an adhesive joint.

2 Resonant Frequency of the Probe on a Plain Plate

The measured frequency response of a type 3814 probe is shown in figure 2.7. In addition to a large resonance at 277.8kHz, which is the major axisymmetric mode of the crystal, there are a number of smaller resonances in the range 200-400kHz, see Chapter 2 for details.

The frequency response for the larger probe (3412) was measured in a similar way to that used for probe 3814. The frequency response was similar in form to that of the smaller probe, but with the resonances occurring at lower frequencies. In this case, the major axisymmetric mode occurred at 148.8kHz.

When the probe is coupled to a flat plate, the probe no longer vibrates independently, so the modes of the complete system must be considered. Only axial motion is coupled efficiently to the plate by the couplant: very little radial motion will be transmitted. The vibration of the plate is therefore primarily in the through thickness direction. At the high frequencies under consideration, the motion is mainly in the region directly below the probe. The plate may therefore conveniently be modelled as a solid cylinder in axial vibration whose diameter, D, equals that of the probe and whose length, l_A, is the thickness of the plate. The apparent modulus, E'_1, of the plate at a frequency of around 5MHz was measured as 111 GN/m^2 by obtaining the transit time of an ultrasonic pulse from a 5MHz probe. Knowing the thickness of the plate, the wave velocity can readily be calculated and the apparent modulus is given by :-

$$E'_1 = c_1^2 \rho_1 \qquad (3.1)$$

where c_1 is the ultrasonic longitudinal wave velocity in the plate or adherend and ρ_1 is the density of the plate.

It was shown in Chapter 2 that the modes of the crystal are fairly complicated, and it would be difficult to model the coupling of these modes to the plate via the gel. It was therefore decided to use a very simple model of the probe.

Since the major mode of the probe involves a significant amount of axial vibration which is axisymmetric, and as it is chiefly axial motion which is transmitted to the plate, the probe was also modelled as a solid cylinder in axial vibration. The diameter, D, and density, ρ_P, of the cylinder were taken as the values measured on the probe itself and the apparent modulus, E'_P, of 178 GN/m^2 was measured using a similar technique to that used for the plate. The length of the cylinder, l_P, was then chosen so that the first axial resonant frequency of the cylinder coincided with the major axisymmetric mode of the probe as discussed earlier.

It should be emphasised that this model is only approximate and cannot take account of the modes of the crystal other than the axisymmetric one. The model therefore breaks down at frequencies close to the resonant frequencies of these other modes.

Since the models of the plate and the probe were similar, the properties of the system comprising the probe attached to the plate could readily be predicted by adding the two models together using receptance analysis, (see figure 3.1).

The receptance, α_{ij}, of a structure is defined (Bishop and Johnson, 1960) as :-

$$\alpha_{ij} = u_i/F_j \qquad (3.2)$$

where u_i is the displacement at position i resulting from an harmonic force F_j applied to the structure at position j. Consequently, the receptance of a structure reaches a maximum at the resonant frequencies of the structure. The direct or point receptance of the probe at the point of coupling to the plate, j, is α_{jj}, and that of the the plate, β_{jj}. These are given (Bishop and Johnson, 1960) as follows :-

$$\alpha_{jj} = -1 / (AE'_P \Lambda_P \tan (\Lambda_P l_P)) \qquad (3.3)$$

$$\text{and } \beta_{jj} = -1 / (AE'_1 \Lambda_1 \tan (\Lambda_1 l_1)) \qquad (3.4)$$

where the area $A = \pi D^2/4$, $\Lambda_P = \omega (\rho_P/E'_P)^{1/2}$ and $\Lambda_1 = \omega (\rho_1/E'_1)^{1/2}$. It can readily be shown (Bishop and Johnson, 1960) that the resonant frequencies of the combined system of the probe coupled to the plate are given by :-

$$\alpha_{jj} + \beta_{jj} = 0 \qquad (3.5)$$

The effect of coupling the probe to a plate is similar to that of increasing the length of the cylinder used to model the probe. Consequently, the resonant frequency of the system comprising the probe coupled to the plate is lower than that for the probe on its own.

The resonant frequency for a probe on plates of different thicknesses was predicted, using eqn. (3.5), for probes 3412 and 3814. Figures 3.2 and 3.3 show the predicted frequencies together with the corresponding values measured using the system described in Chapter 2 and shown in figure 2.6.

When the plate thickness, and hence resonant frequency reduction, is small it is easy to locate a resonant peak, see figure 3.4. Consequently, there is good agreement between the predicted and measured frequencies.

However, as the plate thickness increases, the resonant frequency of the probe coupled to the plate decreases further and it approaches the frequency of other modes of the crystal. Coupling of the modes then occurs and the measured frequency response becomes very complicated, making the location of a resonant peak difficult, as shown in figure 3.5. When mode coupling occurs, the simple model used to predict the frequency reduction becomes invalid and the measured frequencies show some deviation from the predicted values.

The resonant amplitude of the probe coupled to a plain plate was found to be sensitive to the thickness of the couplant layer, and hence to the load applied to the probe. Although the couplant thickness did not appear to change the resonant frequency, it became difficult to locate a resonant peak when the amplitude diminished. Similarly, a poor finish on the surface to which the probe was coupled caused by, for example, heavy scratching, also caused the resonant amplitude to decrease.

3 Predicted Resonant Frequency of the Probe on a Joint

Since a simple model of the probe and a plain plate gave very satisfactory results, it was decided to adopt a similar model to predict the behaviour of the probe on an adhesive joint. The joint was modelled as three solid cylinders in axial vibration joined end-on, the diameter of the cylinders (D) being that of the probe, see figure 3.1. The lengths of the first and third cylinders, l_1 and l_3, were the thicknesses of the top and bottom adherends respectively, while the length of the second cylinder, l_2, was the thickness of the adhesive. The apparent moduli and densities of the cylinders were those of the adherends or adhesive, see the Appendix for details. The model of the probe was the same as that used to predict its response when coupled to a plain plate.

The response of the complete system comprising the probe coupled to the joint was again found by receptance analysis in a similar way to that used for the probe and plate, (Bishop and Johnson, 1960). Since the model of the probe was the same as that used in the earlier work, this analysis again becomes invalid at frequencies close to the modes of the probe which are not modelled by a cylinder in axial vibration.

When the stiffness of the adhesive layer was high, the predicted behaviour of the probe on the joint was similar to that of the probe on a plain plate of thickness equal to that of the whole joint. At high adhesive stiffnesses, only the first mode of vibration of the probe and the joint was predicted to be within the frequency range of interest.

However, as the adhesive stiffness was reduced, the adhesive layer became the major flexibility in the system and vibration could occur with the probe and adherends acting effectively as rigid bodies. The first mode of vibration therefore tended towards that of a simple mass-spring-mass system, with the mass of the bottom adherend coupled by a spring, the adhesive, to the mass of the probe plus the top adherend. At low adhesive stiffnesses, this mode fell below the frequency range of interest, but the second mode of vibration came into the operating frequency range. In this second mode of vibration, the probe and the top adherend no longer moved as a rigid body and, as the stiffness of the adhesive layer was reduced, the bottom adherend was effectively

decoupled from the system. The frequency of this mode was then asymptotic to that predicted earlier for the probe on a plain plate of thickness equal to that of the top adherend alone.

Hence, depending on the adhesive stiffness, the mode of vibration of the probe on the joint which falls in the operating frequency range may either be the first or second mode of the model described above. At some intermediate stiffnesses, both modes are found. In the subsequent discussion, these modes are referred to as the first and second modes. They should not be confused with the different modes of the probe itself. Indeed, the effective operating range of the instrument is centred on the major axisymmetric mode of the probe and the model is only valid close to this frequency.

The frequency of the second mode is always above or equal to that of the probe on a plain plate of the same thickness as the top adherend. Since the Fokker Bond Tester uses the frequency of the probe on an adherend as a reference, the second mode appears as an increase in frequency or a "Left-Shift" on the Fokker Bond Tester A-Scale. At higher adhesive stiffnesses, where the second mode is above the operating range and the first mode is monitored, the measured resonant frequency is below that of the probe on a plate of the same thickness as the joint and, as the stiffness increases, it becomes asymptotic to this value. As the reference frequency is taken as the probe on a single adherend, all these frequencies are seen as "Right-Shifts" (decreases in frequency) on the A-Scale.

The resonant frequencies of the first two modes for both the smaller (3814) and larger (3412) probe coupled to a joint with 1.6 mm adherends were predicted for different adhesive moduli and thicknesses. It was found that the resonant frequencies are essentially functions of the specific adhesive stiffness, which is defined as the ratio of apparent adhesive modulus to adhesive thickness. The relationship between the natural frequencies and the specific stiffness for both probes is shown in figures 3.6 and 3.7. The resonant frequency is also a function of the adhesive density; however it was predicted that a 10% increase in density typically produces less than 0.5% change in frequency.

4 Measured Resonant Frequencies of the Probe on a Joint

The resonant frequencies for both probes 3412 and 3814 coupled to a joint were measured over a wide range of adhesive stiffnesses. The specimens used were single lap joints with 1.6 mm thick aluminium adherends which were prepared by grit blasting and degreasing. The range of specific adhesive stiffness, between 1.5×10^5 and 5×10^3 GN/m^3, was achieved by varying both the adhesive modulus and thickness. Two of the three adhesive types described in the Appendix were used for the joints, one was a typical epoxy (Type B) and the other was a "rubbery" gap filling adhesive (Type C). The epoxy is a typical high modulus adhesive (Young's modulus = 4.6 GN/m^2) whereas the gap filling adhesive represents the opposite extreme of adhesive modulus likely to be encountered in practice (Young's modulus = 0.7 GN/m^2). The adhesive thickness variation of 0.05 to 0.75 mm was obtained by shimming the joint while it cured.

The measured and predicted resonant frequencies of the joints coupled to probes 3814 and 3412 are shown as a function of specific adhesive stiffness in figures 3.6 and 3.7, the independently measured adhesive modulus and thickness being used to calculate the specific adhesive stiffness for each joint.

The adhesive modulus was independently measured at two frequencies above and below the operating frequency range of the Fokker Bond Tester, see the Appendix for details. Unfortunately neither measurement technique could be used in the operating frequency range of the Fokker Bond Tester, i.e. between 100 and 300 kHz. However, the results show that the apparent modulus of the high modulus adhesive (Type B) is practically independent of frequency between 5 kHz and 5 MHz.

The apparent modulus of the low modulus adhesive (Type C) shows a greater dependence on frequency than the Type B adhesive, but the results suggest that the modulus is also fairly constant between 300 kHz and 3 MHz. The values of apparent modulus used to calculate the specific stiffness are shown in table 3.1, it being assumed that the apparent modulus of the Type C adhesive was equal to the value measured at between 300 kHz and 5 MHz.

5 Use of the Fokker Bond Tester to Measure Cohesive Strength

Figures 3.6 and 3.7 show that there is good agreement between the general trend of the experimental results and the frequencies predicted using the receptance model. The discrepancy between the predicted frequencies and the measured results is most probably caused by the over simplified model of the probe used in the analysis since the error appears to increase when the frequency of the mode is further away from that of the probe in air.

When the main resonance approaches one of the other modes of the crystal mode coupling occurs and the frequency changes predicted by the model are then incorrect. Also, it becomes more difficult to locate the main resonant peak and the measured results show more scatter, in a similar way to that found when the probe was coupled to a plain plate, see figure 3.5. However, once the other modes have been passed, mode coupling is reduced and the predicted frequencies show fairly good agreement with the measured results.

It was difficult to locate a resonance if its amplitude was reduced by changes in probe contact pressure or surface finish in a similar way to that experienced with the probe on a plain plate.

However, the experimental results show that as the specific adhesive stiffness increases, the resonant frequency of the first mode tends towards that obtained with a plain plate of twice the adherend thickness. Indeed, the resonant frequency of the first mode is practically independent of adhesive stiffness above specific stiffnesses of around 1.5×10^4 GN/m^3 with the larger probe (3412) and above 5.0×10^4 GN/m^3 with the smaller probe (3814).

When the large probe (3412) was coupled to joints with 1.6 mm adherends, and the adhesive thickness was less than 0.2 mm, the first mode was found to be independent of the values of adhesive modulus tested. The specific adhesive stiffness of such joints was 1.8×10^4 GN/m^3 or greater. Joints made with film adhesive and cured under pressure, a technique which is commonly used in the aerospace industry (Evans, 1985), typically have adhesive thicknesses less than 0.2 mm and hence specific adhesive stiffnesses greater than 1.8×10^4 GN/m^3.

When the specific adhesive stiffness is less than 1.5 x 10^4 GN/m^3 for the large probe (3412) and less than 5.0 x10^4 GN/m^3 for the smaller probe (3814) the frequencies of both modes show more dependence on adhesive stiffness. *However, it is not possible to distinguish changes in adhesive thickness from variations in modulus.*

The strength of an adhesive joint is dependent on many variables which include the adhesive thickness, modulus and toughness. Typically, the modulus obtained with a particular adhesive (and therefore ultrasonic velocity in the adhesive), is dependent on the cure cycle and on the correct mixing of hardener and resin and correlates strongly with cohesive strength (Alers, *et al.*, 1977). The dependence of joint strength on adhesive thickness is less certain; however, very thin or thick bondlines can cause a reduction in strength (Ciba-Geigy, 1982). Consequently, joints which have the same specific adhesive stiffness but different adhesive moduli and thicknesses will not have the same strength. Therefore a non-destructive test for joint strength cannot simply rely on a measurement of the ratio of adhesive modulus to thickness.

The Fokker Bond Tester uses a different correlation curve, between cohesive strength and frequency, for each type of adhesive to be tested and it is based on the assumption that the adhesive modulus is constant and the thickness varies (Rienks, 1972). Therefore, although the adhesive stiffness changes it does not give a true correlation with cohesive strength in the presence of modulus variations. Moreover, whatever correlation there is between adhesive thickness and cohesive strength, the Fokker Bond Tester will only be able to apply it when the adhesive stiffness is less than 1.5 x 10^4 GN/m^3 for probe 3412 and less than 5.0 x 10^4 GN/m^3 for probe 3814. Above these values, the measured frequency is independent of adhesive stiffness and no correlation can be applied.

6 Use of the Fokker Bond Tester for Disbond Location

The Fokker Bond Tester is frequently used to locate disbonds in multi-layer joints (Lord, 1985). In the absence of disbonds, the response of a joint is similar to that of a flat plate of thickness equal to the overall joint thickness. When the probe is placed over a disbond, it is effectively coupled to a plate

whose thickness is that of the layers above the disbond, provided the disbond is at least as large as the probe. Hence, the resonant frequency depends on the depth of the disbond and the location of the disbond may be determined.

The maximum thickness of joint that can be tested is limited by the maximum decrease in frequency that can be reliably measured before mode coupling occurs. For the small probe (3814) the maximum thickness is approximately 1.5 mm of aluminium before mode coupling occurs and the results show significant scatter, see figure 3.3. This thickness increases to approximately 3.5 mm for the larger probe (3412).

Coupling probe 3814 to a 1.0 mm plate causes a 4.7% decrease in frequency whereas coupling probe 3412 to a similar plate produces a 2.7% decrease in frequency. Consequently, although the maximum thickness of the joint that can be examined is less with the smaller probe (3814) its sensitivity is greater than that of the larger probe (3412).

Some instruments used to find disbonds in a multilayer joint, such as the 210 Bondtester manufactured by NDT Instruments, only measure the magnitude of response of a probe similar to the Fokker probe coupled to the joint rather than the resonant frequncies. Using this method, rather than measuring the change in frequency, it can become difficult to distinguish between disbonds and the undamaged structure (Li *et al.*, 1982). The Fokker Bond Tester Mk II therefore tends to be more reliable than these instruments.

7 Conclusions

The frequencies of the first two modes of through thickness vibration for two Fokker Bond Tester probes (3412 and 3814) coupled to joints having a large range of adhesive stiffnesses have been predicted and measured, good agreement being obtained between the two sets of values.

Over a wide range of typical adhesive stiffnesses, the frequency of the first mode is independent of stiffness, and hence of adhesive modulus and thickness, and is equal to that of the probe on a plate of twice the adherend thickness. Consequently, no correlation can be made between cohesive strength and measured frequency.

At lower adhesive stiffnesses, the measured and predicted frequencies are dependent on adhesive stiffness but it is not possible to distinguish between changes in modulus and thickness. At very low adhesive stiffnesses the frequency of the second mode tends towards that of the probe on a plate of the same thickness as the adherends.

Although the investigation reported here has concentrated on the operation of the Fokker Bond Tester, the results and conclusions are equally valid for any test based on monitoring the lower natural frequencies of a transducer coupled to a joint.

Adhesive thickness and modulus have different effects on joint strength, so joints with the same adhesive stiffness may not have the same cohesive strength. Therefore, even when the resonant frequencies are dependent on adhesive stiffness, since the stiffness change may be caused by changes in either adhesive modulus or thickness or both, it is not possible to obtain a unique correlation between the measured frequencies and cohesive strength. Hence, unless adhesive thickness is carefully controlled, or is measured independently, erroneous cohesive strength predictions will result.

It has been shown that unless the adhesive in a metal to metal joint has a low specific stiffness, and the bond line thickness is monitored independently, the Fokker Bond Tester is unlikely to give an accurate measure of the cohesive strength of a joint. Consequently, since many commonly used adhesives have moderately high specific stiffness, the Fokker Bond Tester cannot reliably be used to monitor the cohesive strength of joints made with these adhesives. In the absence of any other testing instrument which claims to detect poor cohesive properties, this means that the potential advantages of adhesive bonding cannot be fully realised. There is therefore a need for the development of alternative testing techniques such as ultrasonic spectroscopy.

The Fokker Bond Tester can, however, be used successfully to locate and determine the depths of disbonds in multi-layer joints, the minimum detectable disbond diameter being approximately equal to the diameter of the probe used. The technique is limited by the maximum thickness of the joint that can be examined. For aluminium adherends this was found to be around 2.0

mm when using the smaller probe (3814) and around 3.5 mm when using the larger probe (3412). However, even larger probes are available (Rienks, 1972) which would enable thicker joints to be examined.

Adhesive Type (see Appendix for details)	Measured Apparent Modulus (E'_2) GN/m^2
B	7.2
C	3.6

Table 3.1 **Measured Apparent Moduli of the Adhesives**

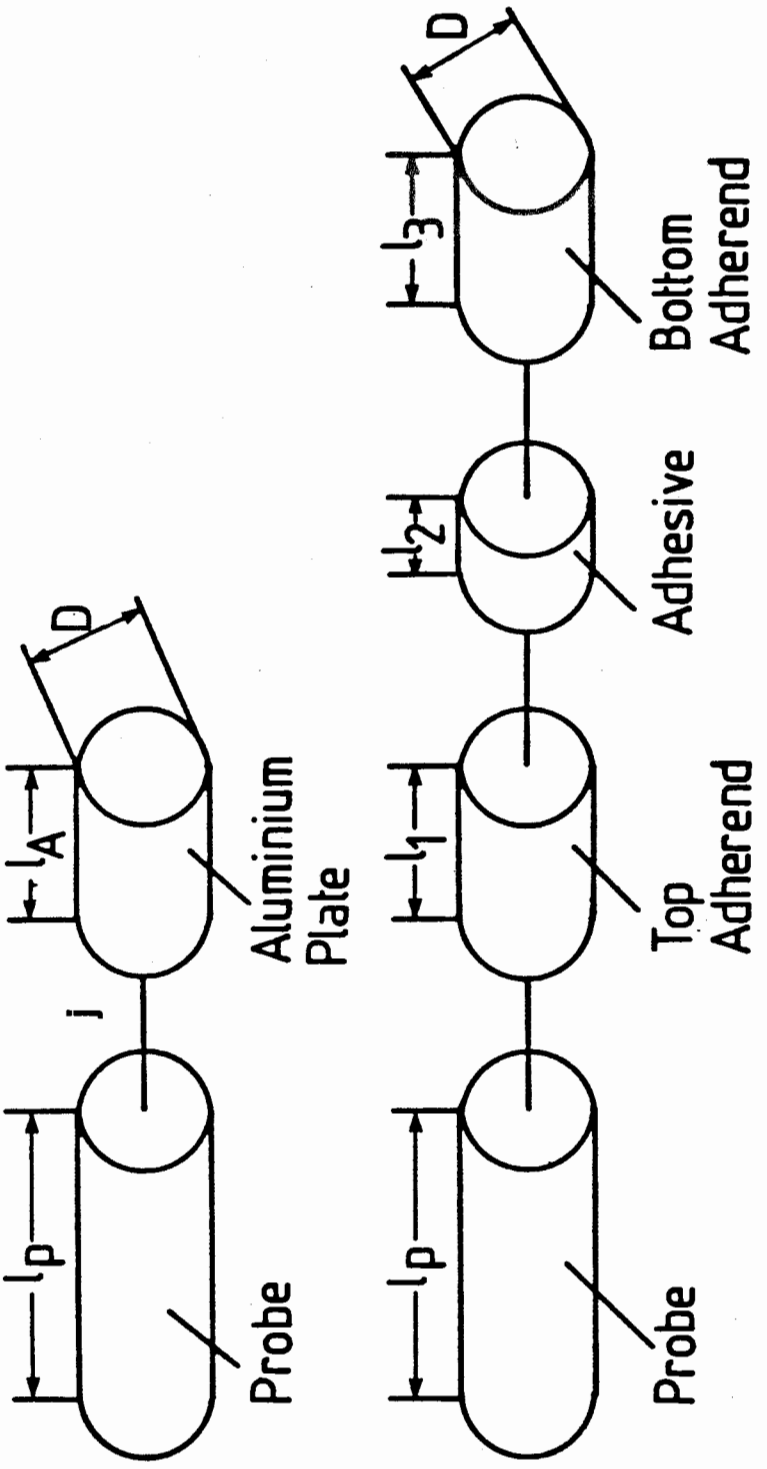

Figure 3.1 **Schematic Representation of Models Used for the Receptance Analysis**
upper view - model of probe on a plate
lower view - model of probe on a joint

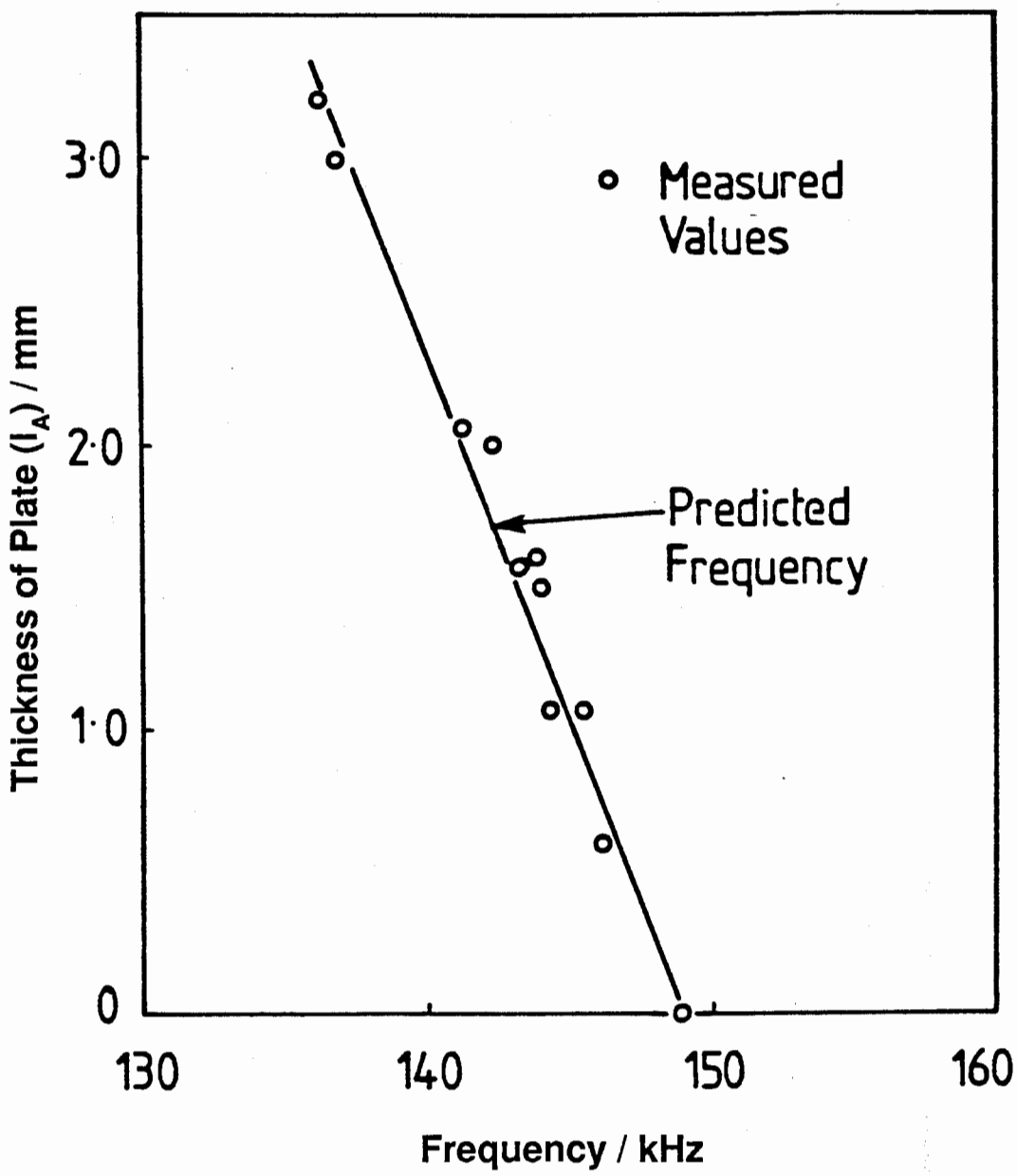

Figure 3.2 **Predicted and Measured Resonant Frequency of Probe 3412 on a Flat Plate**

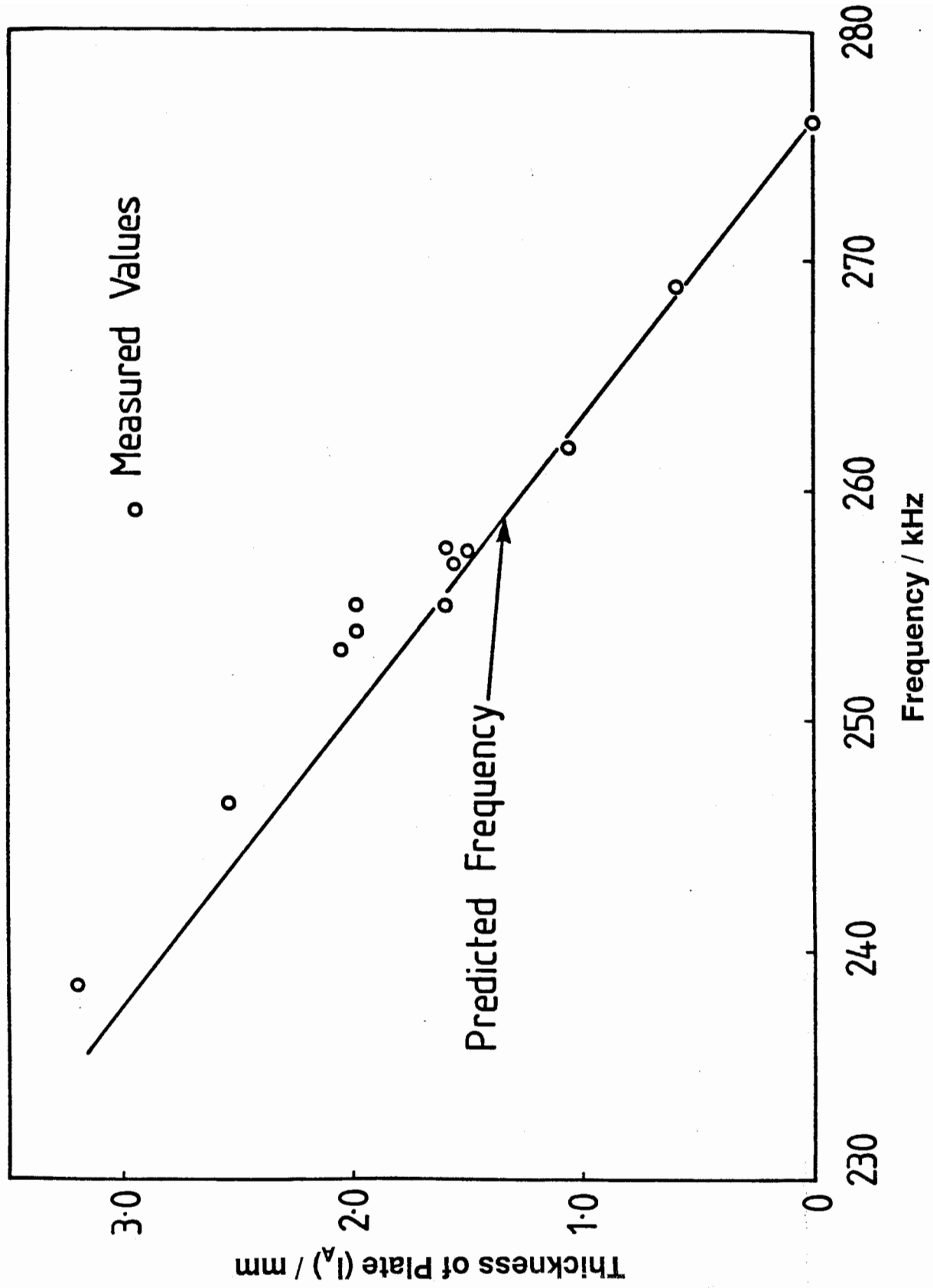

Figure 3.3 **Predicted and Measured Resonant Frequency of Probe 3814 on a Flat Plate**

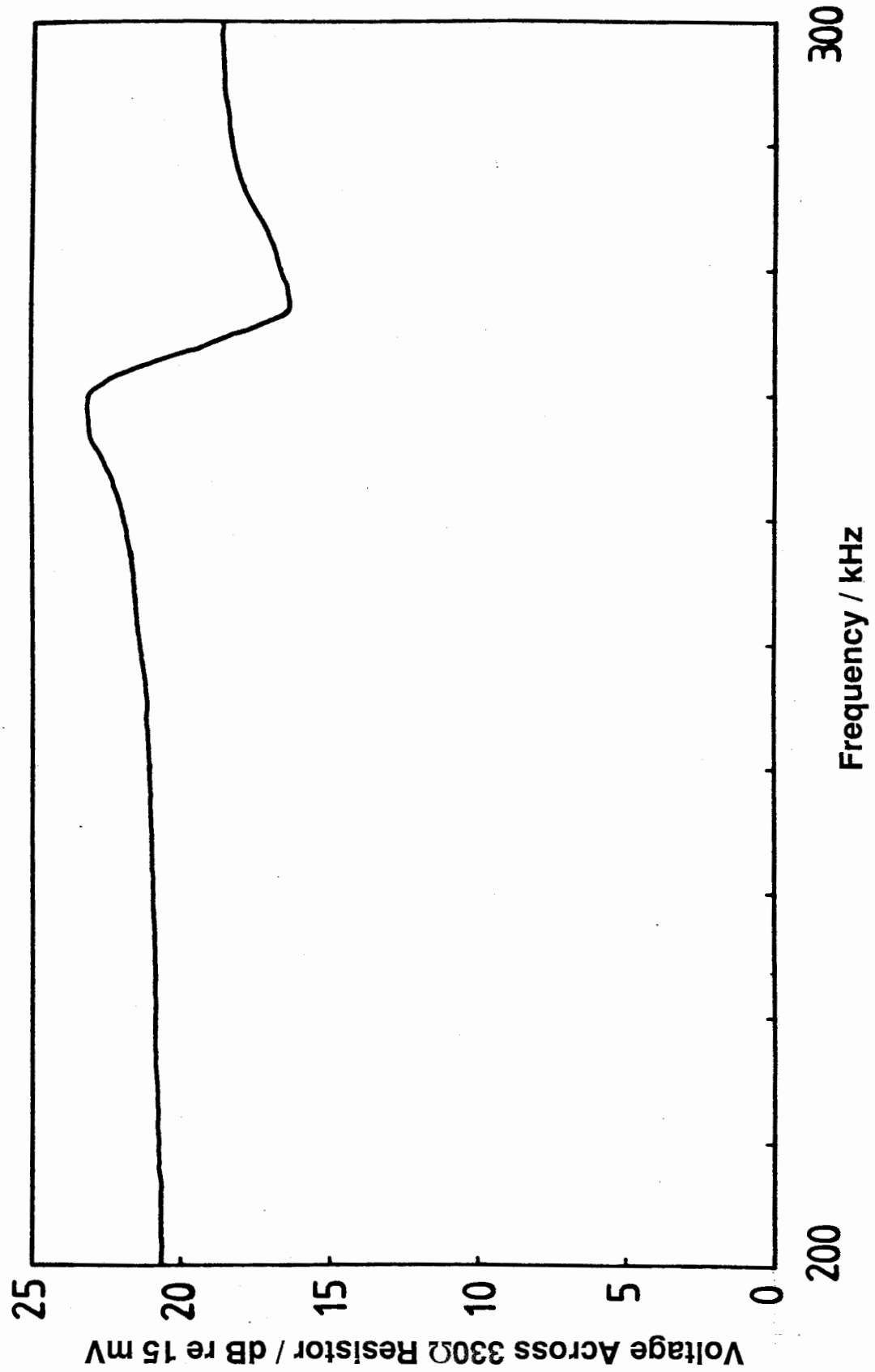

Figure 3.4 **Measured Frequency Response of Probe 3814 on 0.59 mm Plate**

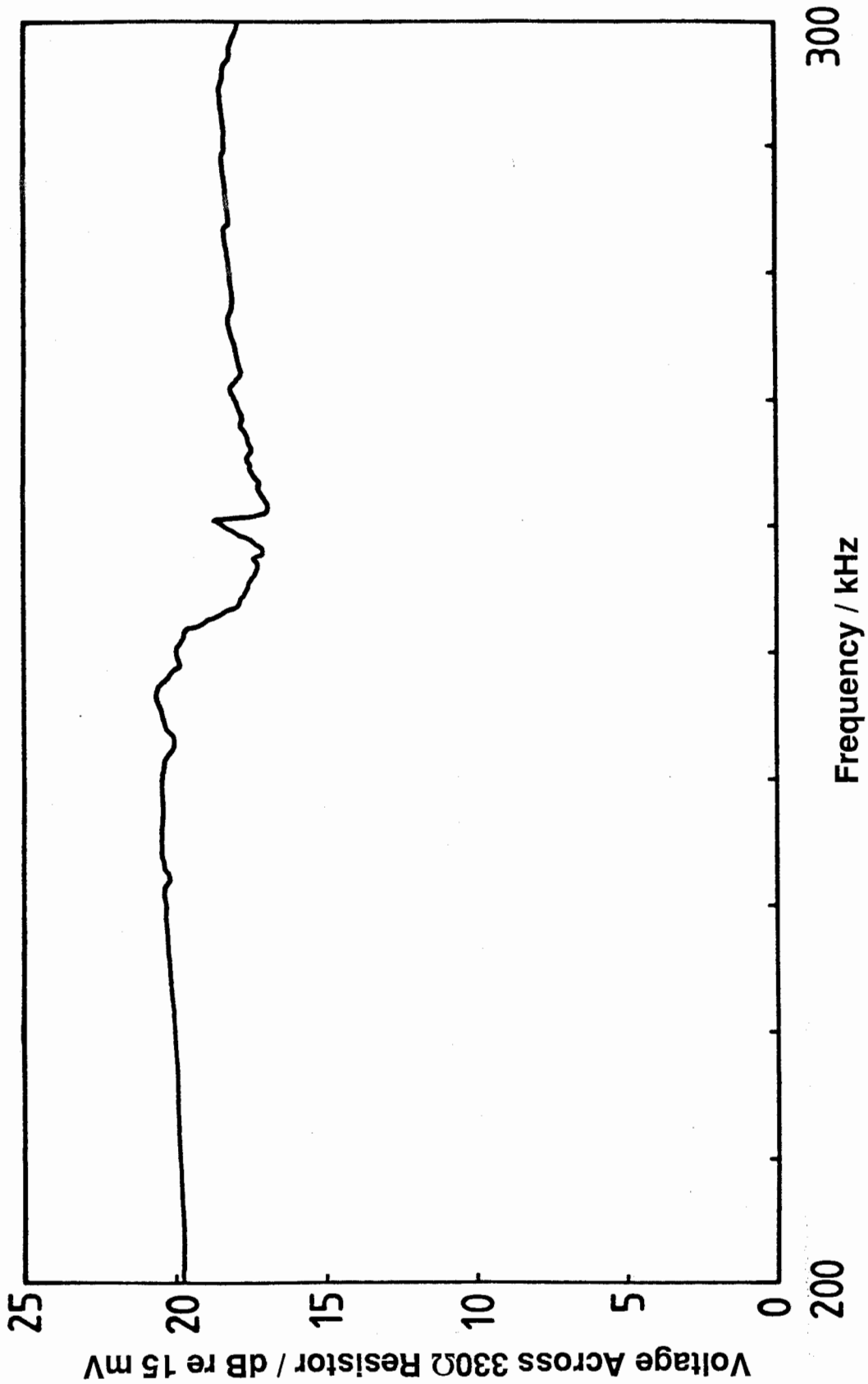

Figure 3.5 **Measured Frequency Response of Probe 3814 on 2.5 mm Plate**

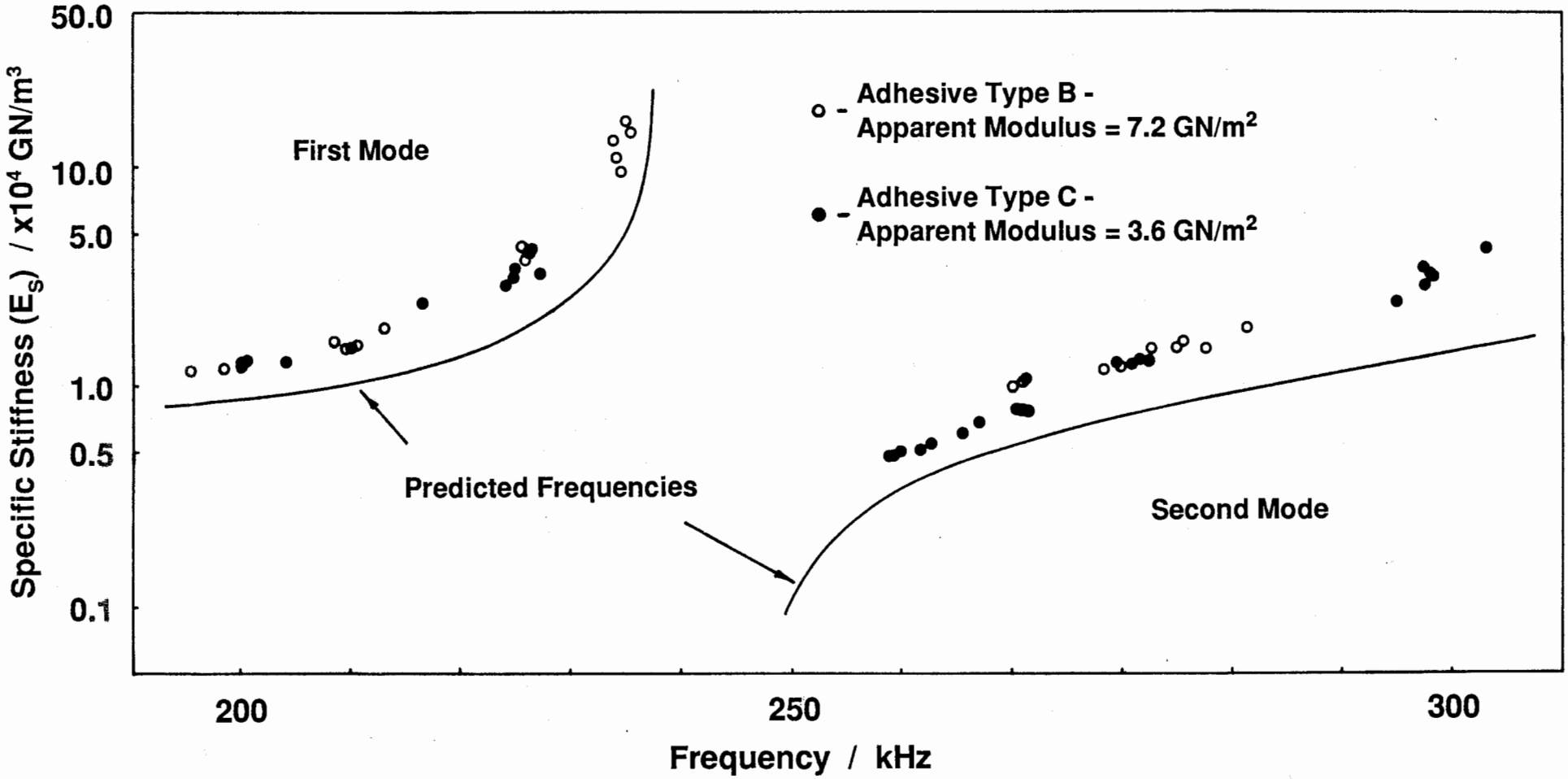

Figure 3.6 Predicted and Measured Resonant Frequency of Probe 3814 on 1.6 mm Single-Lap Joints with Different Adhesives

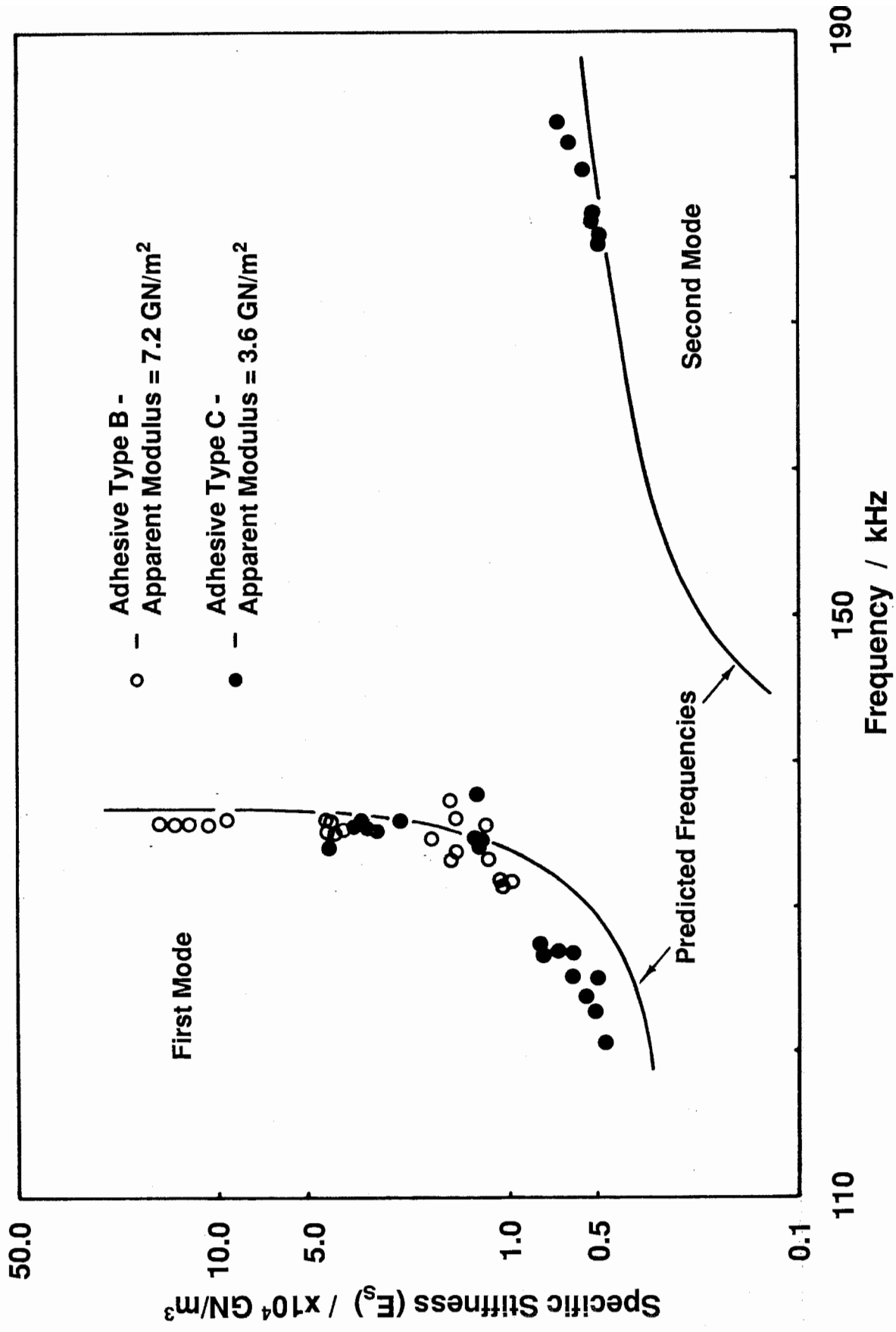

Figure 3.7 **Predicted and Measured Resonant Frequency of Probe 3412 on 1.6 mm Single-Lap Joints with Different Adhesives**

PART THREE

ULTRASONIC SPECTROSCOPY

CHAPTER 4

Theoretical Model for the Propagation of a Pulse Through a Plain Plate at Small Angles of Incidence

1 Introduction

In Chapters 2 and 3 the operation of the Fokker Bond Tester Mk II has been examined and its sensitivity to changes in adhesive modulus and thickness has been determined. It has been shown that the instrument is insensitive to changes in the adhesive modulus and thickness of typical sheet to sheet joints unless the adhesive has a very low specific stiffness (i.e. less than $1\text{-}2\text{x}10^4$ GN/m^3).

It has also been shown that even when the instrument is used on joints of very low specific stiffness, it is only sensitive to the ratio of adhesive modulus to thickness i.e. the specific stiffness of the adhesive; consequently it is unlikely to give an adequate prediction of cohesive strength. Since most joints commonly used in engineering primary structure have specific stiffnesses of $2\text{-}3\text{x}10^4$ GN/m^3 or greater, there is a need for the development of alternative testing techniques.

The most promising area for development is that of ultrasonic spectroscopy, see Chapter 1. This technique uses the same basic principle as the Fokker Bond Tester, in that it measures the through thickness resonant frequencies and amplitudes of resonant response of the joint, but it is able to monitor many more modes than the Fokker Bond Tester. Since each of these modes is dependent on adhesive thickness and modulus it is probable that the overall sensitivity would be better than the Fokker Bond Tester and that changes in modulus can be distinguished from those in thickness. However, to date, difficulties have been experienced in correlating the complex spectra with the cohesive properties of the joint (Lloyd *et al.*, 1979; Rivenez, 1984).

Before investigating the use of ultrasonic spectroscopy for the non-destructive evaluation of the cohesive properties of adhesive joints, it was decided to ensure that the ultrasonic vibration of a plain plate could be

measured and predicted satisfactorily. This required the development of a model to predict the behaviour of a pulse as it propagates through a plate, thus enabling the theoretical spectrum for the plate to be calculated.

2 Description of Pulse Propagation Model

The propagation of a pulse with a plane wave front through a flat plate immersed in liquid can be conveniently modelled by considering the propagation of a ray in a similar way to that done with optics (Bond and Saffari, 1984). It is assumed that a plane, longitudinal wave front in the liquid is incident at some small angle, θ, on the entire area of an infinitely wide plate of finite thickness, l_A, which lies parallel to the x=0 plane, see figure 4.1.

In practice, the structure of the ultrasonic pulse produced by a probe is likely to be more complex than the plane wave front (Weight and Hayman, 1978; Weight, 1984) assumed by the model. However, it will be seen (see Chapter 5) that this simple analysis provides an adequate model of the propagation of a pulse through a plate.

Following the interaction of the longitudinal wave front with the top boundary, and at an infinitesimal time δt after the arrival of the incident wave front, at time t, three new wave fronts will have been generated (see for example Brekhovskikh, 1960; Graff, 1975), as shown in figure 4.2a. To calculate the amplitudes of the three new wave fronts relative to that of the incident wave it is convenient to consider the potential of the wave (Brekhovskikh, 1960). The potential, $\Phi_i(t)$, of a wave is given by the product of the acoustic pressure and the density of the medium in which the wave propagates, consequently the pressure amplitude of a wave is proportional to its potential amplitude. The subscript of the potential, i, refers to the direction of propagation of the wave i.e. i=1 for waves propagating downwards and i=2 for waves propagating upwards, see figure 4.1.

The potential of the wave front incident on the top face of the plate, $\Phi_1(t)$, can be written as a function of time as follows :-

$$\Phi_1(t) = A_1 \exp . i [\kappa(y.\sin \theta - x.\cos \theta) - \omega t] \quad (4.1)$$

where A_1 is the amplitude of the wave, x and y are the cartesian coordinates perpendicular and parallel to the plane of the plate respectively, $i = \sqrt{-1}$, and κ is the wave number defined as $\kappa = \omega/c$ where ω is the angular frequency and c is the wave velocity in the liquid.

One of the three new wave fronts generated following the interaction of the longitudinal wave with the top face of the plate will be a reflected longitudinal wave in the liquid having an amplitude B_1 and propagating at the same angle (θ) to the normal as the incident wave. The wave potential, $\Phi_2(t+\delta t)$, of this reflected wave is given by :-

$$\Phi_2(t+\delta t) = B_1 \exp . i [\kappa(y.\sin \theta + x.\cos \theta) - \omega t] \quad (4.2)$$

The other two wave fronts propagate in the plate, one will be the transmitted longitudinal wave having an amplitude C_1 and propagating at an angle θ_L to the normal. The wave potential, $\Phi_1(t+\delta t)$, of the transmitted longitudinal wave is given by :-

$$\Phi_1(t+\delta t) = C_1 \exp . i [\kappa_L(y.\sin \theta_L - x.\cos \theta_L) - \omega t] \quad (4.3)$$

where κ_L is the wave number defined as $\kappa_L = \omega/c_L$ where c_L is the longitudinal wave velocity in the plate.

The other wave front in the plate will be a shear wave, generated by mode conversion, having an amplitude D_1 and propagating at an angle θ_S to the normal. The wave potential, $\Psi_1(t+\delta t)$, of the transmitted shear wave is given by :-

$$\Psi_1(t+\delta t) = D_1 \exp . i [\kappa_S(y.\sin \theta_S - x.\cos \theta_S) - \omega t] \quad (4.4)$$

where κ_S is the wave number defined as $\kappa_S = \omega/c_S$ where c_S is the shear wave

velocity in the plate.

The directions of propagation of the longitudinal and shear waves, θ_L and θ_S, are given by Snell's Law as follows :-

$$\sin\theta/c = \sin\theta_L/c_L = \sin\theta_S/c_S \qquad (4.5)$$

It can be shown that the amplitudes of the wave potential of the three new wave fronts (B_1, C_1, and D_1), relative to that of the incident wave (A_1) are equal to the reflection, R_{ij}, transmission, T_{ij}, and mode conversion efficiencies, T'_{ij}, for the interface and are given as follows (Brekhovskikh, 1960) :-

$$R_{21} = B_1/A_1 = (Z_L\cos^2 2\theta_S + Z_S\sin^2 2\theta_S - Z)/(Z_L\cos^2 2\theta_S + Z_S\sin^2 2\theta_S + Z) \qquad (4.6)$$

$$T_{11} = C_1/A_1 = (\rho/\rho_1) \cdot [\, 2Z_L\cos 2\theta_S / (Z_L\cos^2 2\theta_S + Z_S\sin^2 2\theta_S + Z)] \qquad (4.7)$$

$$T'_{11} = D_1/A_1 = -(\rho/\rho_1) \cdot [\, 2Z_L\sin 2\theta_S / (Z_L\cos^2 2\theta_S + Z_S\sin^2 2\theta_S + Z)] \qquad (4.8)$$

where R_{21} and T_{11} are the reflection and transmission coefficients of the longitudinal wave respectively and T'_{11} is the transmission mode conversion efficiency for longitudinal to shear waves. Z, Z_L, and Z_S are the acoustic impedances for the liquid, and the longitudinal and shear waves in the plate respectively, and are given by :-

$$Z = \rho c/\cos\theta, \qquad Z_L = \rho_1 c_L/\cos\theta_L, \qquad Z_S = \rho_1 c_S/\cos\theta_S \qquad (4.9)$$

where ρ is the density of the liquid, and ρ_1 is the density of the plate. The subscripts, i and j, of the reflection, and transmission coefficients and mode conversion efficiencies refer to the direction of propagation and the interface respectively. For example, i=1 for waves propagating downwards and i=2 for waves propagating upwards and j=1 at the top surface of the plate and j=2 at the bottom surface, see figure 4.1.

At normal incidence when $\theta=0$ eqns. (4.6-4.8) simplify to give :-

$$R_{21} = (Z_L - Z) / (Z_L + Z) \qquad (4.10)$$

$$T_{11} = (\rho/\rho_1) \cdot [2Z_L / (Z_L + Z)] \qquad (4.11)$$

$$T'_{11} = 0 \qquad (4.12)$$

From eqn. (4.12) it can be seen that no shear waves are generated in the plate at normal incidence.

When a longitudinal wave front within the plate, of amplitude A_2, is incident, at an angle θ_L, on the lower interface between the plate and the liquid (j=2), there are there are three further wave fronts generated, see figure 4.2b. One is the transmitted longitudinal wave in the liquid having an amplitude C_2, and propagating at an angle θ to the normal. The other two wave fronts are in the plate, one being the reflected longitudinal wave having an amplitude B_2, and propagating at an angle θ_L to the normal, and the other being the reflected shear wave having an amplitude D_2, generated by mode conversion, and propagating at an angle θ_S to the normal.

In a similar way to that shown above, the amplitude of the wave potential of the three new wave fronts (B_2, C_2, and D_2), relative to that of the incident longitudinal wave in the plate (A_2), are given by :-

$$R_{22} = B_2/A_2 = (Z+Z_S\sin^2 2\theta_S - Z_L\cos^2 2\theta_S)/(Z_L\cos^2 2\theta_S + Z_S\sin^2 2\theta_S + Z) \qquad (4.13)$$

$$T_{12} = C_2/A_2 = (c\cos\theta_L / c_L\cos\theta\cos^2 2\theta_S) \cdot (1 - R_{12}) \qquad (4.14)$$

$$R'_{22} = D_2/A_2 = (c_S/c_L)^2 \cdot (\sin 2\theta_L / \cos 2\theta_S) \cdot (1 - R_{12}) \qquad (4.15)$$

where R_{22} and T_{12} are the reflection and transmission coefficients of the longitudinal wave respectively and R'_{22} is the reflection mode conversion efficiency for longitudinal waves to shear waves.

When a shear wave front within the plate of amplitude A_3 is incident, at an angle θ_S, on the interface between the plate and the liquid there are three further wave fronts generated, see figure 4.2c. One is the transmitted longitudinal wave in the liquid having an amplitude C_3, generated by mode conversion and propagating at an angle θ to the normal. The other two wave fronts are in the plate, one being the reflected shear wave with an amplitude B_3, and propagating at an angle θ_S to the normal. The other wave front in the plate is a reflected longitudinal wave having an amplitude D_3, generated by mode conversion, and propagating at an angle θ_L to the normal.

Similarly, the amplitude of the wave potential of the three new wave fronts (B_3, C_3, and D_3), relative to that of the incident shear wave (A_3) in the plate, are given as follows :-

$$R^*_{22} = B_3/A_3 = - (Z_L\cos^2 2\theta_S - Z_S\sin^2 2\theta_S + Z)/(Z_L\cos^2 2\theta_S + Z_S\sin^2 2\theta_S + Z) \qquad (4.16)$$

$$T''_{12} = C_3/A_3 = (\tan\theta / 2\sin^2\theta_S) \,.\, (1 + R^*_{12}) \qquad (4.17)$$

$$R''_{22} = D_3/A_3 = - (c_L/c_S)^2 .\, (\cos 2\theta_S / \sin 2\theta_L) \,.\, (1 + R^*_{12}) \qquad (4.18)$$

where R^*_{22} is the reflection coefficient for shear waves, and T''_{12} and R''_{22} are the transmission and reflection mode conversion efficiencies for shear to longitudinal waves respectively.

At normal incidence $\theta=0$ and eqns. (4.13-4.18) simplify in a similar way to eqns. (4.6-4.8) and they show that there is no mode conversion between shear and longitudinal waves, or vice versa. Hence, at normal incidence, the reflection and transmission coefficients and the mode conversion efficiencies become:-

$$R_{22} = (Z - Z_L) / (Z_L + Z) \qquad (4.19)$$

$$T_{12} = (c/c_L) \,.\, [2Z_L / (Z_L + Z)] \qquad (4.20)$$

$$R'_{22} = 0 \qquad (4.21)$$

$$R^*_{22} = -1 \qquad (4.22)$$

$$T''_{12} = 0 \qquad (4.23)$$

$$R''_{22} = 0 \qquad (4.24)$$

From consideration of the symmetry of the plate it can readily be shown that the reflection coefficient, R_{12}, for a longitudinal wave incident on the lower face of the plate from the liquid (i.e. i=1 and j=2) is equal to the reflection coefficient (R_{21}) for a similar wave at the upper face (i.e. with i=2 and j=1). A similar argument produces equalities for the other reflection and transmission coefficients and the mode conversion effciencies, thus giving the following expressions :-

$$\begin{aligned} &R_{11} = R_{22}, \quad T_{11} = T_{22}, \quad T'_{11} = T'_{22}, \\ &R_{12} = R_{21}, \quad T_{12} = T_{21}, \quad R'_{11} = R'_{22}, \\ &R^*_{11} = R^*_{22}, \quad T''_{12} = T''_{21}, \quad R''_{11} = R''_{22} \end{aligned} \qquad (4.25)$$

In practice it is useful to be able to determine the amplitude of the longitudinal waves or their acoustic pressure, in the liquid above and below the plate, as a function of time since this is what would be received by a transducer placed above or below the plate. As the acoustic pressure is proportional to the wave potential in the liquid, the response of a transducer placed above the plate is proportional to the wave potential in the liquid at the top face of the plate i.e. $\Phi_2(t+\delta t)$. Simarly, at the bottom face the response of the transducer is proportional to the wave potential in the liquid at the bottom face of the plate i.e. $\Phi_1(t+\delta t)$.

At the top face of the plate the wave potentials of the emitted wave fronts, $\Phi_1(t+\delta t)$, $\Phi_2(t+\delta t)$, $\Psi_1(t+\delta t)$, and $\Psi_2(t+\delta t)$, can be written (Brekhovskikh, 1960) as functions of the longitudinal and shear wave potentials incident on the interface ($\Phi_1(t)$, $\Phi_2(t)$, and $\Psi_2(t)$) as follows :-

$$\Phi_1(t+\delta t) = \Phi_1(t).\, T_{11} + \Phi_2(t).\, R_{11} + \Psi_2(t).\, R''_{11} \qquad (4.26)$$

$$\Phi_2(t+\delta t) = \Phi_1(t).\, R_{21} + \Phi_2(t).\, T_{21} + \Psi_2(t).\, T''_{21} \quad (4.27)$$

$$\Psi_1(t+\delta t) = \Phi_1(t).\, T'_{11} + \Phi_2(t).\, R'_{11} - \Psi_2(t).\, R^*_{11} \quad (4.28)$$

$$\Psi_2(t+\delta t) = 0 \quad (4.29)$$

Similarly, at the bottom face of the plate the potential of the emmited wave fronts, $\Phi_1(t+\delta t)$, $\Phi_2(t+\delta t)$, $\Psi_1(t+\delta t)$, and $\Psi_2(t+\delta t)$, can be written as follows :-

$$\Phi_1(t+\delta t) = \Phi_1(t).\, T_{12} + \Phi_2(t).\, R_{12} + \Psi_1(t).\, T''_{12} \quad (4.30)$$

$$\Phi_2(t+\delta t) = \Phi_1(t).\, R_{22} + \Phi_2(t).\, T_{22} + \Psi_1(t).\, R''_{22} \quad (4.31)$$

$$\Psi_1(t+\delta t) = 0 \quad (4.32)$$

$$\Psi_2(t+\delta t) = \Phi_1(t).\, R'_{22} + \Phi_2(t).\, T'_{22} - \Psi_1(t).\, R^*_{22} \quad (4.33)$$

The respective reflection and transmission coefficients and the mode conversion efficiencies for each interface are given by eqns. (4.6-4.8), (4.13-4.15) and (4.16-4.18). Note that since the shear modulus and hence shear velocity in a liquid is zero, the potentials of the shear wave front in the liquid above and below the plate, is also zero, see eqn. (4.29) and (4.32).

At normal incidence eqns (4.26-4.29) and (4.30-4.33) simplify since the mode conversion efficiencies, given by eqns. (4.12), (4.21), (4.23), (4.24) are zero. In this case the wave potentials at the top face of the plate are given by :-

$$\Phi_1(t+\delta t) = \Phi_1(t).\, T_{11} + \Phi_2(t).\, R_{11} \quad (4.34)$$

$$\Phi_2(t+\delta t) = \Phi_1(t).\, R_{21} + \Phi_2(t).\, T_{21} \quad (4.35)$$

$$\Psi_1(t+\delta t) = 0 \quad (4.36)$$

and at the bottom face of the plate :-

$$\Phi_1(t+\delta t) = \Phi_1(t).\, T_{12} + \Phi_2(t).\, R_{12} \quad (4.37)$$

$$\Phi_2(t+\delta t) = \Phi_1(t).\, R_{22} + \Phi_2(t).\, T_{22} \quad (4.38)$$

$$\Psi_2(t+\delta t) = 0 \quad (4.39)$$

Figure 4.3a shows schematically how an incident longitudinal pulse at normal

incidence propagates through a 2.2 mm thick glass plate immersed in water. This shows the incident and emmited ray paths drawn at non-normal incidence for clarity. The magnitude of the longitudinal wave potential above and below the plate was calculated as a function of time by adding the incident wave potentials, using eqns. (4.34-4.35) and (4.37-4.38), at each instant that a wave front reached an interface of the plate. The material properties used to calculate the transmission and reflection coefficients and the mode conversion efficiencies are given in table 4.1.

The incident plane wave was modelled as pulse of unit magnitude and duration, T_p. The amplitude of the pulse, A_p, as a function of time, is given by :-

$$\text{for } 0 \le t \le T_p, \quad A_p = \sin^2(\pi t / T_p) \qquad \text{and for } t > T_p, \quad A_p = 0 \qquad (4.40)$$

This shape of pulse has less energy at higher frequencies than a similar duration square pulse, consequently the problem of aliasing (Newland, 1984) could be avoided when the spectra of the echoes from the plate were calculated, see Section 3.

The calculated magnitude of the longitudinal wave potential above a 2.2 mm glass plate, as a function of time, and resulting from an incident pulse of 0.1 ms duration, is plotted in figure 4.3b. The magnitude of the potential is proportional to that of the echoes received by a transducer in pulse echo mode (see Chapter 1). Similarly, the magnitude of the longitudinal wave potential below the plate, see figure 4.3c, is proportional to that of the echoes received by the receiving transducer in through transmission mode (see Chapter 1).

In the pulse echo case, the first echo from a plate is only dependent on R_{21} whereas subsequent echoes are dependent on R_{11}, R_{22}, T_{11} and T_{21} (note that $R_{11}=R_{22}$ as explained above). When Z is less than Z_L, as it is in the case for a glass plate immersed in water, R_{21} is positive and R_{11} (= R_{22}) is negative, see eqns (4.10) and (4.19). Since T_{11} and T_{21} are always positive, all the echoes, except the first one, are in negative phase. Hence, the first echo is opposite in phase to the subsequent ones in pulse echo mode.

In the through transmission case, the echoes are only dependent on T_{11} and T_{12}, which are always positive, and $(R_{22})^n$, where n=2,4,6 etc which is again always positive; consequently the phase of the echoes is the same.

Figure 4.4a shows a schematic representation of how a longitudinal wave pulse incident on a 2.2 mm glass plate at an angle of 2° generates longitudinal and shear waves within the plate. The magnitude of the longitudinal wave potential above and below the plate is shown in figures 4.4b and 4.4c and was calculated as a function of time by adding the incident wave potentials using eqns. (4.26-4.28), (4.30-4.31) and (4.33) in a similar way to that done at normal incidence.

When the angle of incidence is only 2°, the echoes received from the plate are still dominated by the reflection of the longitudinal wave within the plate and are similar to those obtained at normal incidence, see figure 4.3. However, even at these small angles of incidence, shear waves are generated by mode conversion of the longitudinal waves. Subsequently, the shear waves undergo another mode conversion back to longitudinal waves to form the additional echoes, 2a,2b etc and Ia, IIa etc, shown in figure 4.4.

The arrival times of the calculated echoes are dependent on the times, T_L and T_S, taken for the longitudinal and shear waves to traverse the plate. These times are given by :-

$$T_L = l_A / c_L . \cos \theta_L \qquad (4.41)$$

$$T_S = l_A / c_S . \cos \theta_S \qquad (4.42)$$

For example the second main longitudinal echo, labelled 2 on figure 4.4b, occurs at a time $2T_L$ after the first echo (labelled 1) since it results from a pulse that makes two traverses of the plate as a longitudinal wave. Figure 4.4a shows that the first echo received at the top of the plate resulting from mode conversion (labelled 2a), consists of the superposition of two pulses. One pulse is the result of mode conversion of the incident longitudinal wave to a shear wave at the top face followed by mode conversion back to give a reflected longitudinal wave at the bottom face. The second pulse is the result

of mode conversion of the longitudinal wave at the bottom face to give a reflected shear wave followed by mode conversion at the top face to give the transmitted longitudinal wave. In both cases the pulse makes one traverse of the plate as a shear wave and one as a longitudinal wave, consequently they arrive at the top face of the plate at the same instant, at a time (T_L+T_S) after the first main echo, when they are superimposed on each other to form a single echo.

The second echo (2b) resulting from mode conversion to be received at the top of the plate makes both traverses of the plate as a shear wave, see figure 4.4b, and arrives at a time $2T_S$ after the first main echo (1). The echo is the result of mode conversion of the incident longitudinal wave at the top face of the plate to give a shear wave. The shear wave is reflected off the bottom of the plate and is then converted back to longitudinal wave at the top of the plate.

The predicted time history, in pulse echo mode, from a 1.6 mm thick aluminium plate immersed in water, caused by an incident plane wave at 2°, is shown in figure 4.5. The ratio between the longitudinal and shear velocities for aluminium is approximately 2:1, see table 4.1, compared with approximately 1.7:1 for the glass plate shown in figure 4.4. Consequently, the transit time of a shear wave in aluminium, T_S, is approximately twice that of the longitudinal wave, T_L, at small angles of incidence (i.e. $T_S \approx 2T_L$).

The first mode converted echo (2a), received at the top face of the plate, now occurs approximately $3T_L$ after the first echo (1) since it makes one traverse of the plate as a shear wave and one as a longitudinal wave. Therefore the mode converted echo (2a) occurs approximately mid way between the second (2) and third (3) main reflections which have made two and four traverses of the plate as longitudinal waves respectively.

The second mode converted echo, received at the top face of the plate, which makes two traverses of the plate as a shear wave is not seen in aluminium and other materials where the longitudinal wave velocity is approximately twice the shear wave velocity. This is because the mode converted echo arrives at the same time as the much larger main reflection (3).

3 Spectra of the Predicted Longitudinal Wave Potentials

Figures 4.6a and 4.6b show the spectra produced from the Fourier Transform of the calculated time histories, shown in figures 4.3b and c, for a 2.2 mm glass plate at normal incidence, in pulse echo and through transmission modes respectively. The frequencies of the maxima and minima are identical, and are controlled by the the spacing between subsequent echoes in the time series. These frequencies, F_{Ln}, are those of the longitudinal or through thickness resonances of the plate i.e. the deformation is predominantly perpendicular to the plane of the plate and are given by :-

$$F_{Ln} = nc_L/2l_A \qquad \text{with } n=1,2,3\ldots \text{ etc.} \qquad (4.43)$$

where n is the number of the through thicknesss mode of the plate.

The resonances occur as maxima or minima depending on the phase relationship between the echoes in the time domain. When the echoes are of the same phase, as they are in the case of through transmission (figure 4.3c), the resonances occur as maxima in the frequency domain. When the first, much larger, echo (1) is in the opposite phase to the subsequent echoes, as it is in the case of pulse echo (see figure 4.3b), the resonances occur as minima in the frequency domain.

Figures 4.7a and b show the spectra of the calculated time histories, shown in figure 4.4, for the 2.2 mm glass plate at an angle of incidence of 2°. In this instance, in addition to the longitudinal, or through thickness modes, of the plate discussed above, and occuring at frequencies given by eqn. (4.43), there are also some shear modes of the plate which are excited by mode conversion.

The shear modes of the plate also involve through thickness deformation of the plate except that in this instance the deformation is parallel to the plane of the plate, rather than perpendicular to it as in the case of the longitudinal modes. However, since the deformation perpendicular to the plane of the plate is greater in the longitudinal modes than the shear modes the longitudinal modes are commonly refered to as simply through thickness modes. The deformed shapes of the plates (mode shapes) will be discussed in more detail in Section 4.

The frequencies of the shear modes of the plate at normal incidence can be predicted, in a similar way to that used for the through thickness modes, and they occur at frequencies, F_{sm}, given by:-

$$F_{sm} = mc_S/2l_A \qquad \text{with m=1,2,3... etc.} \qquad (4.44)$$

where m is the number of the shear mode of the plate. It is important to note, however, that in this instance the shear modes of the plate are not excited at normal incidence since there is no mode conversion.

The frequencies given by eqns. (4.43) and (4.44) are also the frequencies of the asymptotes of the dispersion curves of a plate (see for example Fiorito *et al.*, 1979; Pitts *et al.,* 1976 and Schoch, 1953), which occur at normal incidence (infinite phase velocity). Figure 4.8 shows the symmetric (eg. s_1, s_2 etc.) and asymmetric (eg. a_1, a_2 etc.) dispersion curves for a 1.6 mm thick aluminium plate for angles of incidence up to 8°. The classification of the curves as symmetric and asymmetric refers to the deformation of the plate and is explained in greater detail in Section 4.

At small angles of incidence ($\theta \approx 2°$), the spectra obtained from the predicted longitudinal wave potentials show that not all the shear modes of the plate, obtained from eqn. (4.44) or from the dispersion curves, are excited. For example, the spectra of the glass plate, see figures 4.7a and b, show that the shear modes of the plate given by eqn. (4.44) with m=5,10 etc. do not appear to be excited. Also, the shear modes with m=1,4,6,9,11 etc. are only weakly excited compared to the modes with m=2,3,7,8. It is possible that the shear modes with m=5,10 etc. are not seen in the spectra because they occur close to the longitudinal modes of the plate given by eqn. (4.43) with n=3,6, etc., see figure 4.7. However, the more strongly excited shear modes, that occur at frequencies given by eqn. (4.44) with m=2,3,7,8 etc., also occur close to the longitudinal modes of the plate i.e. those given by eqn. (4.43) with n=1,2,4,5 etc.

The spectrum of the aluminium plate, see figure 4.9, also shows that some of the shear modes are not excited. In this instance the shear modes that occur at frequencies, given by eqn. (4.44) with m=4,8 do not appear to be excited and

that the modes with m=1,3,5,7,9 are only weakly excited.

The longitudinal and shear modes of a plate that occur at non-normal angles of incidence can also be predicted by using the equations for the ratio of transmitted to incident energy given by Schoch, (1952) and Fiorito *et al.*, (1979). These equations show (Izbicki *et al.*, 1984 and Rothe, 1986) that the modes given by the dispersion curves are not all excited at small angles of incidence, in a similar way to that found with the predicted spectra shown in figures 4.7 and 4.9.

The shear modes of the plate described above are only excited because there is some mode conversion of the incident longitudinal wave to shear waves at non-normal incidence. If it were possible to excite the plate with a shear wave directly then it would be expected that all the shear modes of the plate would be excited.

4 Mode Shapes of the Plate

Figures 4.10a and 4.10b show the mode (deformed) shapes of an element from the cross section of the plate at the frequencies of the first longitudinal mode and first shear mode, given by eqns (4.43) and (4.44) with n and m=1 (calculated using the technique described by Bishop and Johnson, 1960) . Here, u_x represents the displacement perpendicular to the plane of the plate, or in a through thickness direction, and u_y represents the displacement parallel to the plane of the plate or shear deformation. In both cases, the strain is given by the rate of change of displacement with distance (see for example Benham and Warnock, 1978); consequently the longitudinal strain is given by $\partial u_x/\partial x$ and the shear strain is given by $[(\partial u_y/\partial x) + (\partial u_x/\partial y)]$; however, in this instance $\partial u_x/\partial y = 0$.

In the first longitudinal or through thickness mode of the plate, see figure 4.10a, there is a node (point of zero motion) on the mid-plane of the plate, the displacement above this point being in anti-phase to that below it; consequently the deformation of the plate is symmetrical about its mid-plane in this mode.

In the first shear mode of the plate see figure 4.10b, the node also lies on its mid-plane. However, since the shear displacements are in anti-phase above and below the mid-plane the deformation of the plate is asymmetric about its mid-plane in this mode.

The mode shapes of the plate at the frequencies of the second longitudinal and second shear mode given by eqns. (4.43) and (4.44) with n=2 and m=2, are shown in figures 4.11a and b respectively. The displacements in the longitudinal mode, see figure 4.11a, now have the same phase above and below the mid-plane of the plate, hence the deformation of the plate is asymmetric about its mid-plane in this mode. Although the displacements of the shear mode also have the same phase above and below the mid-plane of the plate, see figure 4.11b, the deformation of the plate is symmetric about its mid-plane in this mode.

Consequently, longitudinal modes of the plate given by eqn. (4.43) with n=1,3,5 etc have deformation of the plate which is symmetric about about its mid-plane. However, the shear modes given by eqn. (4.44) with m=1,3,5 etc have deformation of the plate which is asymmetric about its mid-plane. Similarly, longitudinal modes of the plate given by eqn. (4.43) with n=2,4,6 etc have deformation of the plate which is asymmetric about about its mid-plane and the shear modes given by eqn. (4.44) with m=2,4,6 etc have deformation which is symmetric about its mid-plane.

When shown on a dispersion curve the modes of a plate are generally identified as either symmetric e.g. s_1, s_2 etc or asymmetric modes e.g. a_1, a_2 etc (Fiorito *et al.*, 1979; Pitts *et al.*, 1976; Schoch, 1953). These modes of the plate are normally called Lamb modes. As can be seen in figure 4.8, which shows the Lamb modes for an 1.6 mm thick aluminium plate in vacuum, the first mode to occur (a_1) is asymptotic to the frequency of the shear mode, given by eqn. (4.43) with m=1, which has asymmetric deformation about the mid-plane of the plate. The next two modes occur close together, the lower being the longitudinal mode (s_1) given by eqn. (4.42) with n=1, and the higher mode being the shear mode (s_2) given by eqn (4.43) with m=2, consequently both modes have deformation which is symmetric about the mid-plane of the plate.

The fourth mode (a_2) of the plate is a shear mode with m=3 and hence is an asymmetric mode. The fifth and sixth modes (a_3 and s_3) of the plate occur close together, see figure 4.8, and are longitudinal and shear modes with n=2 and n=4 respectively. Consequently, the deformation is asymmetric in the fifth mode and symmetric in the sixth.

5 Conclusions

A model of the propagation of a pulse through plate at small angles of incidence has been developed so that the echoes received from a plate can be predicted, and the spectrum of the echoes calculated. This has shown that at zero incidence there is no mode conversion of the incident longitudinal wave to a shear wave, and that only the longitudinal or through thickness modes of the plate are excited. However, at non-normal incidence new echoes appear in the time domain, resulting from mode conversion of the longitudinal and shear waves at the surfaces of the plate. This mode conversion excites shear modes of the plate, in addition to the longitudinal modes found at normal incidence.

At small angles of incidence ($\theta<2°$) it has been shown that the frequencies of the longitudinal and shear modes of the plate can be approximated by using eqns. (4.43) and (4.44) respectively. These frequencies also represent the asymptotes of the dispersion curves. However, it was shown that some of the shear modes, given by eqn. (4.44) and the dispersion curves, were not found in the spectra predicted using the pulse propagation model. This result has also been verified by other authors (Izbicki *et al.*, 1984 and Rothe, 1986) by evaluating the ratio of incident to transmitted energy for the plate.

For a glass plate, the shear modes that were not excited at small angles of incidence are those given by eqn. (4.44) with m=5,10 etc, which correspond to the asymmetric Lamb modes a_4 and a_8 etc. For an aluminium plate it is the shear modes with m=4,8 etc which correspond to the symmetric Lamb modes s_3 and s_6 etc that are not excited at small angles of incidence.

Material	Longitudinal Velocity (c_L) m/s	Shear Velocity (c_S) m/s	Density (ρ or ρ_1) kg/m^3	Ratio of Longitudinal to Shear Velocity
glass	5770	3392	2440	1.701
aluminium	6342	3132	2720	2.025
water	1493	-	1000	-

Table 4.1 Material Properties

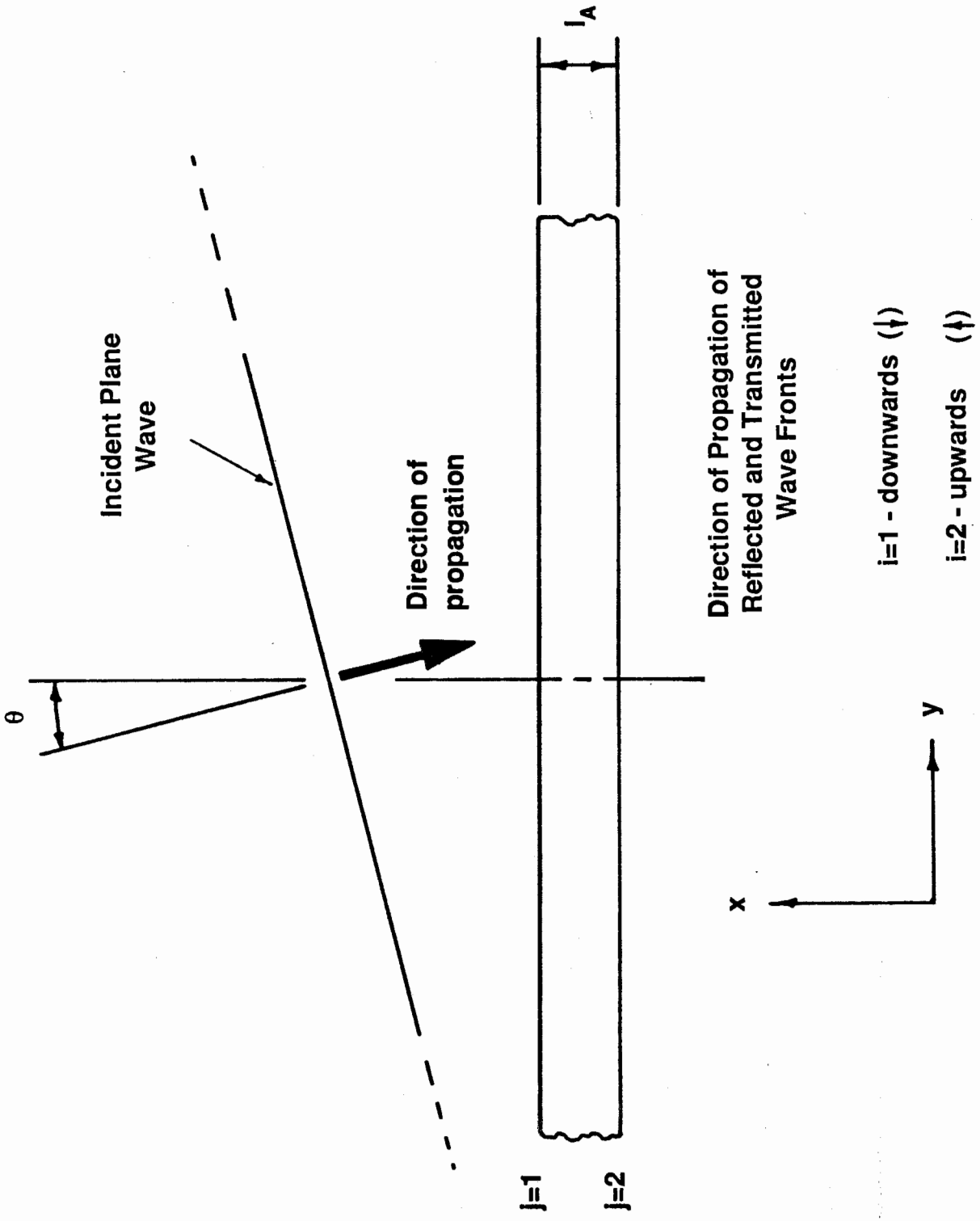

Figure 4.1 **Schematic Representation of Plane Wave approaching the Plate**

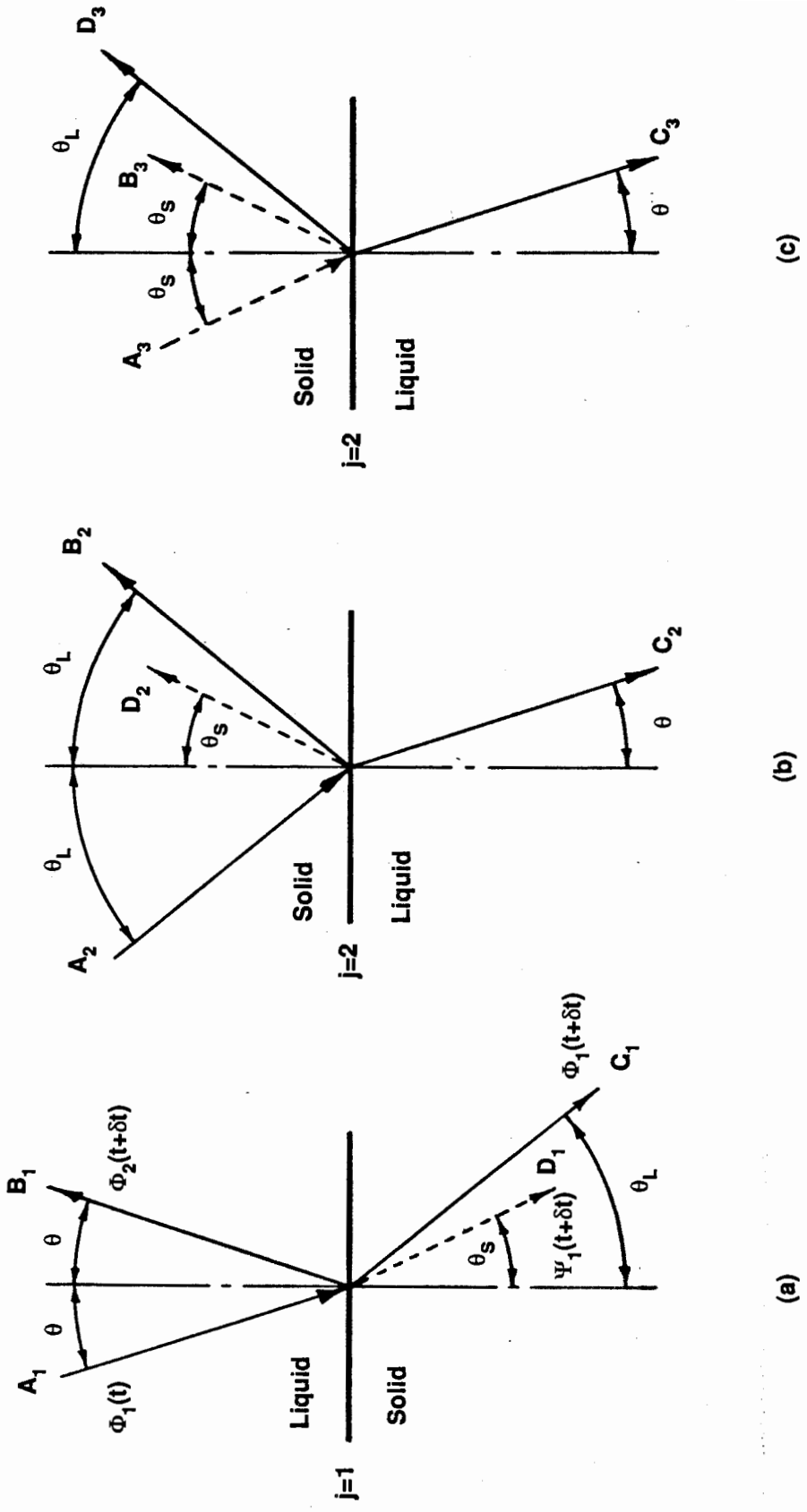

Figure 4.2 **Schematic Representation of Mode Conversion at Non-Normal Angles of Incidence**

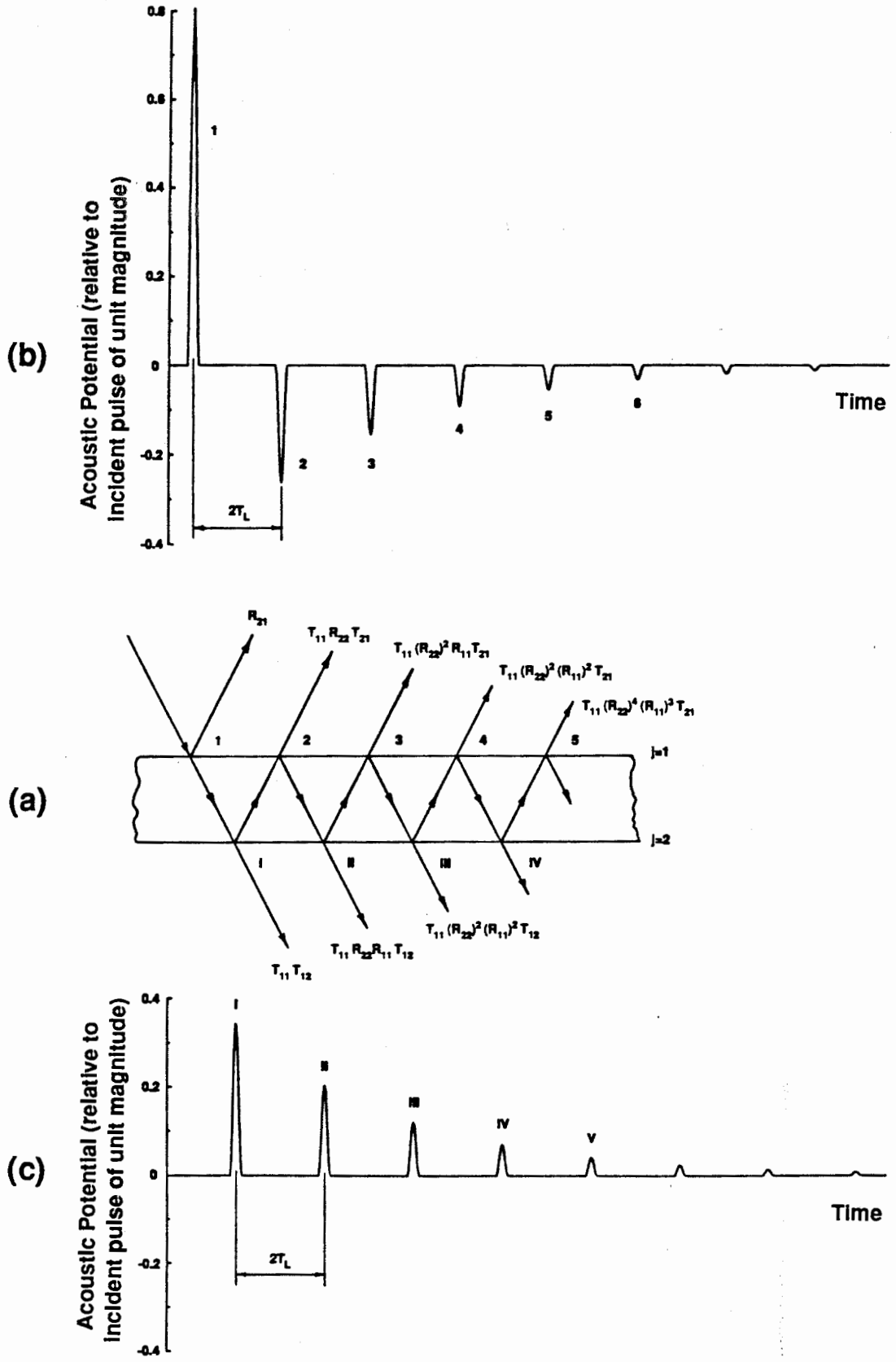

Figure 4.3 **Echoes from 2.2mm Thick Glass Plate at Normal Incidence** (a) wave path in plate (drawn at non-normal incidence for clarity) (b) wave pattern in liquid above the plate (c) wave pattern in liquid below the plate

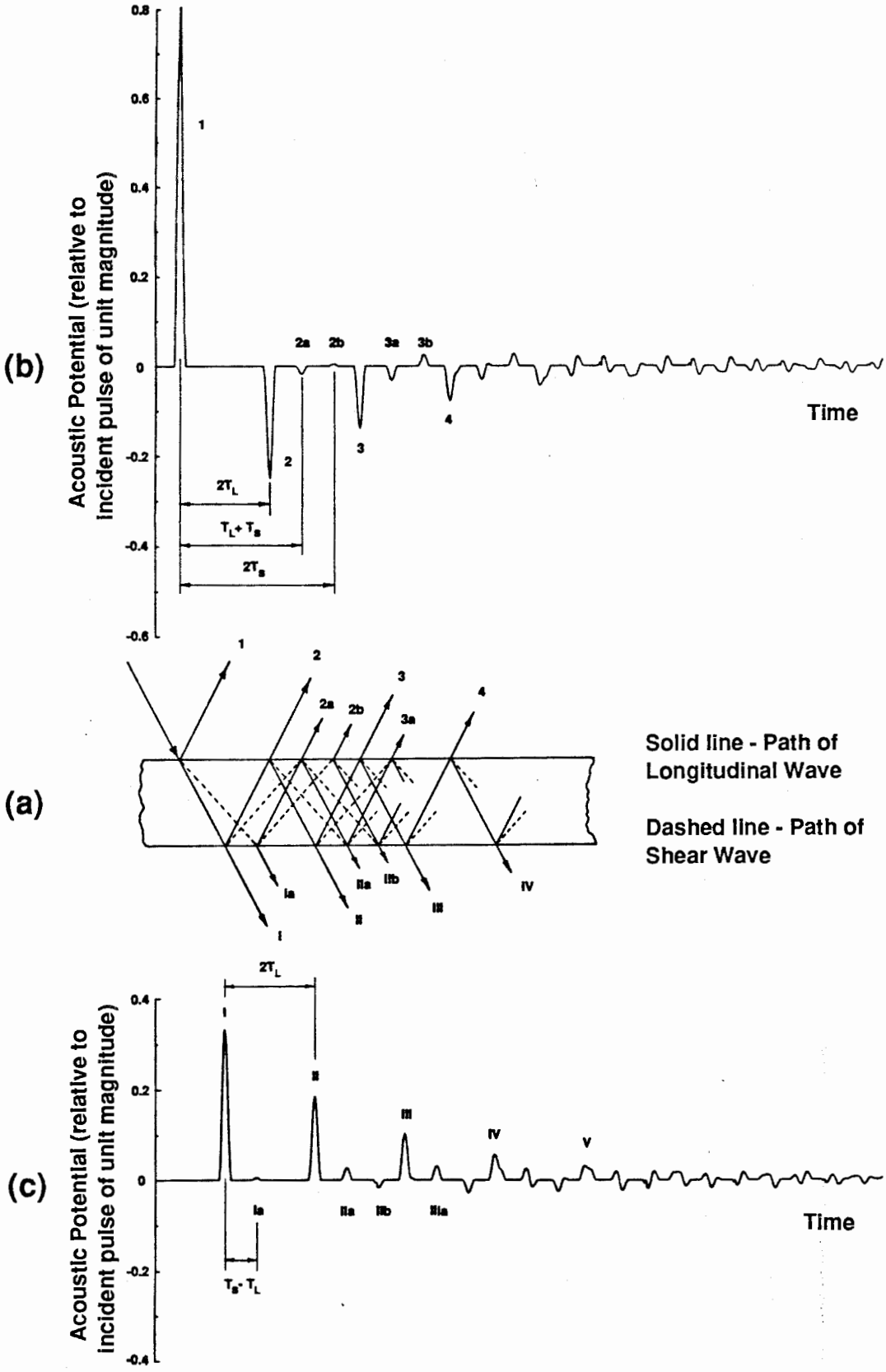

Figure 4.4 **Echoes from 2.2mm Thick Glass Plate at θ=2°** (a) wave path in plate (drawn at arbitrary angle for clarity) (b) wave pattern in liquid above plate (c) wave pattern in liquid below plate

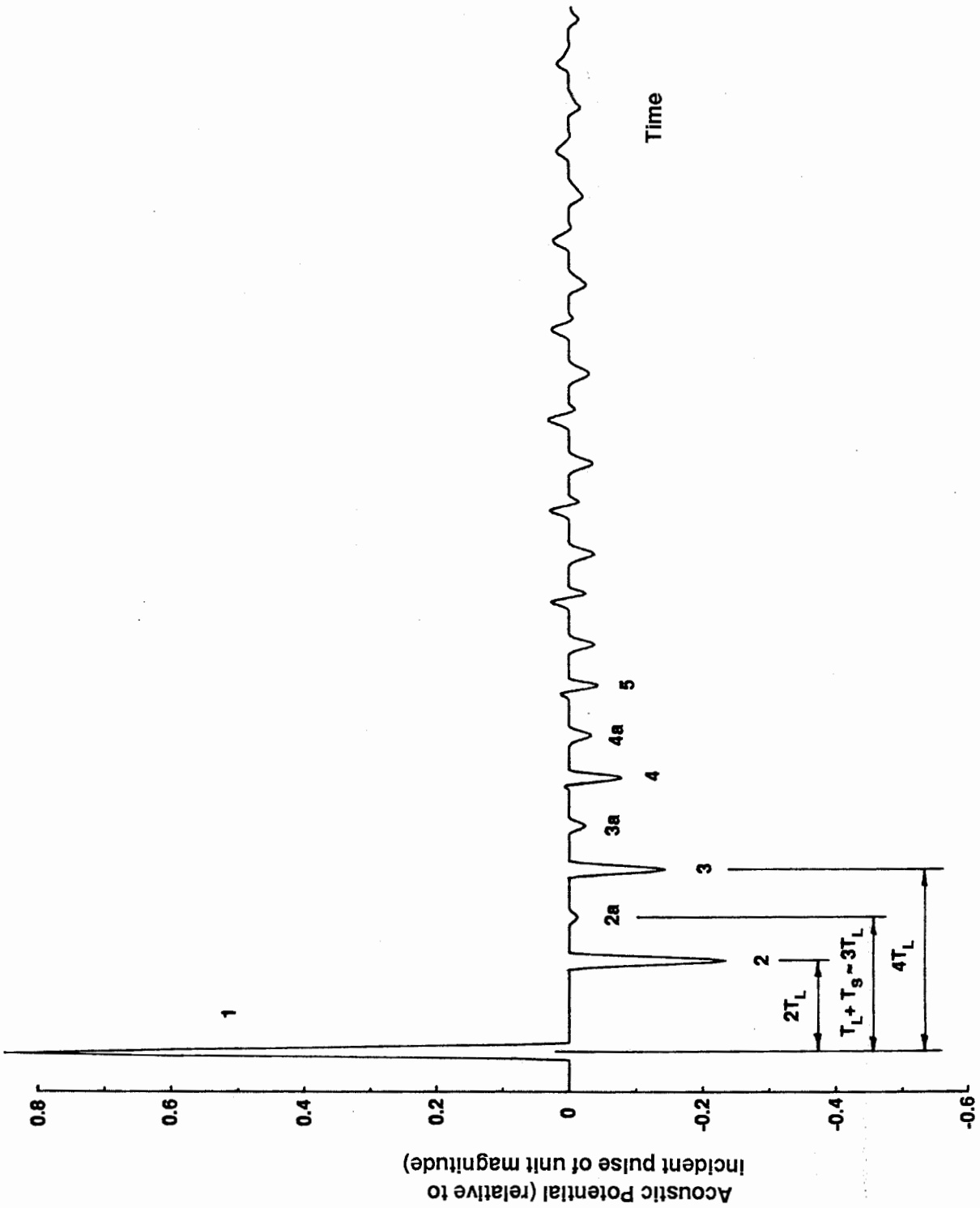

Figure 4.5 **Echoes from 1.6mm Thick Aluminium Plate at θ=2°in pulse echo mode**

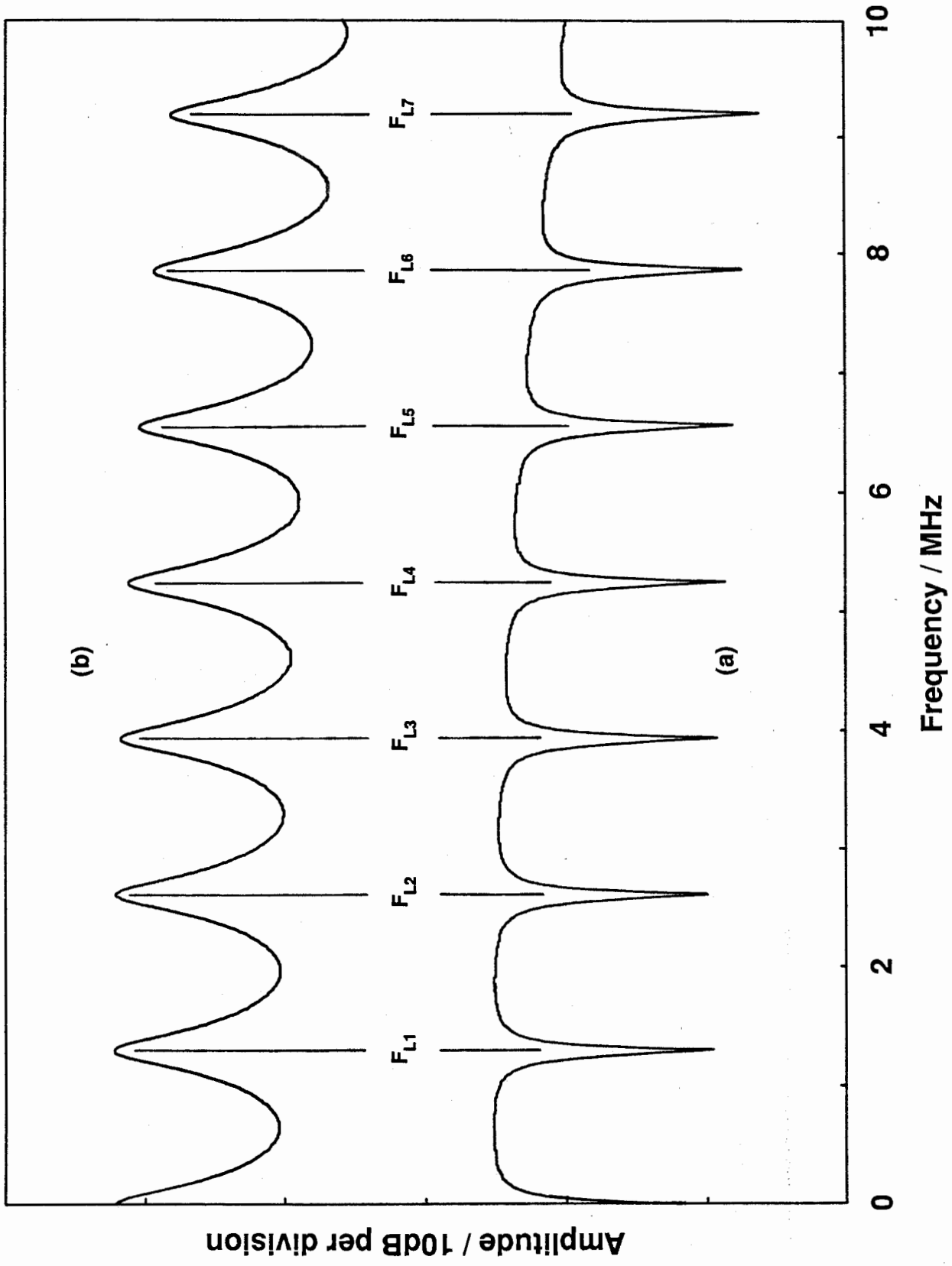

Figure 4.6 **Spectra from 2.2mm Thick Glass Plate at Normal Incidence** (a) from wave pattern above plate (b) from wave pattern below plate

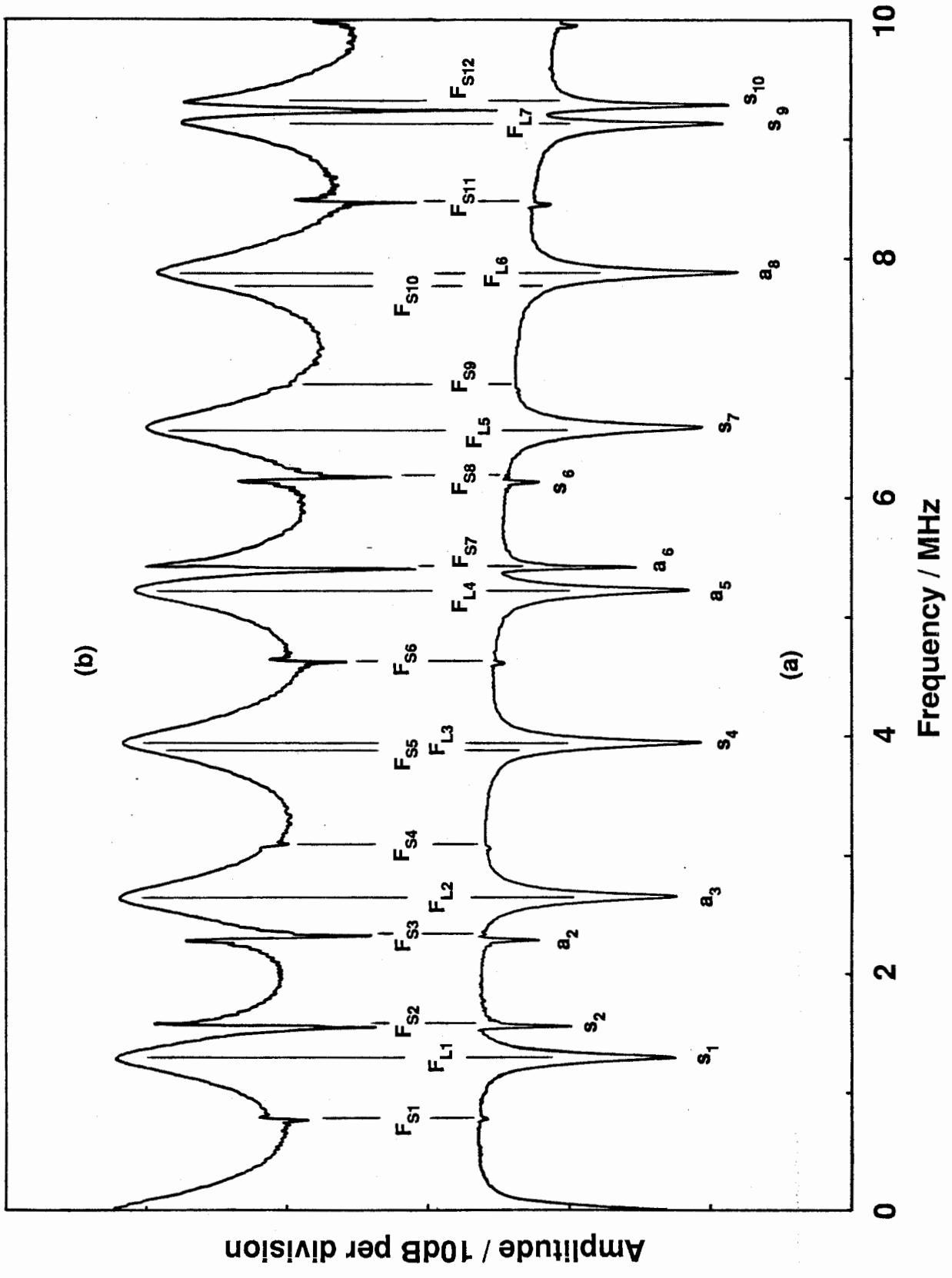

Figure 4.7 **Spectra from 2.2mm Thick Glass Plate at θ=2°** (a) from wave pattern above plate (b) from wave pattern below plate

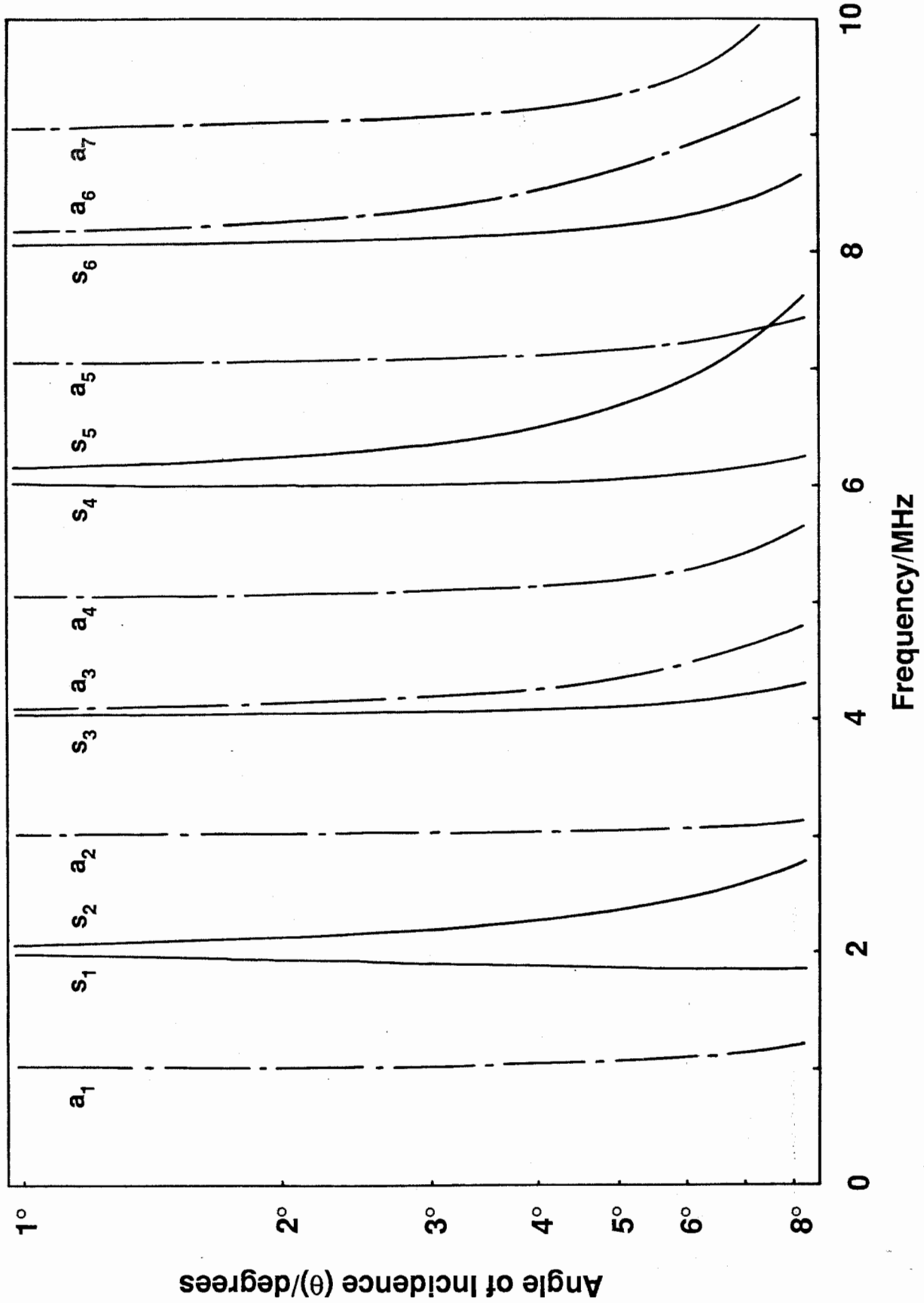

Figure 4.8 **Dispersion Curve for 1.6mm Thick Aluminium Plate**

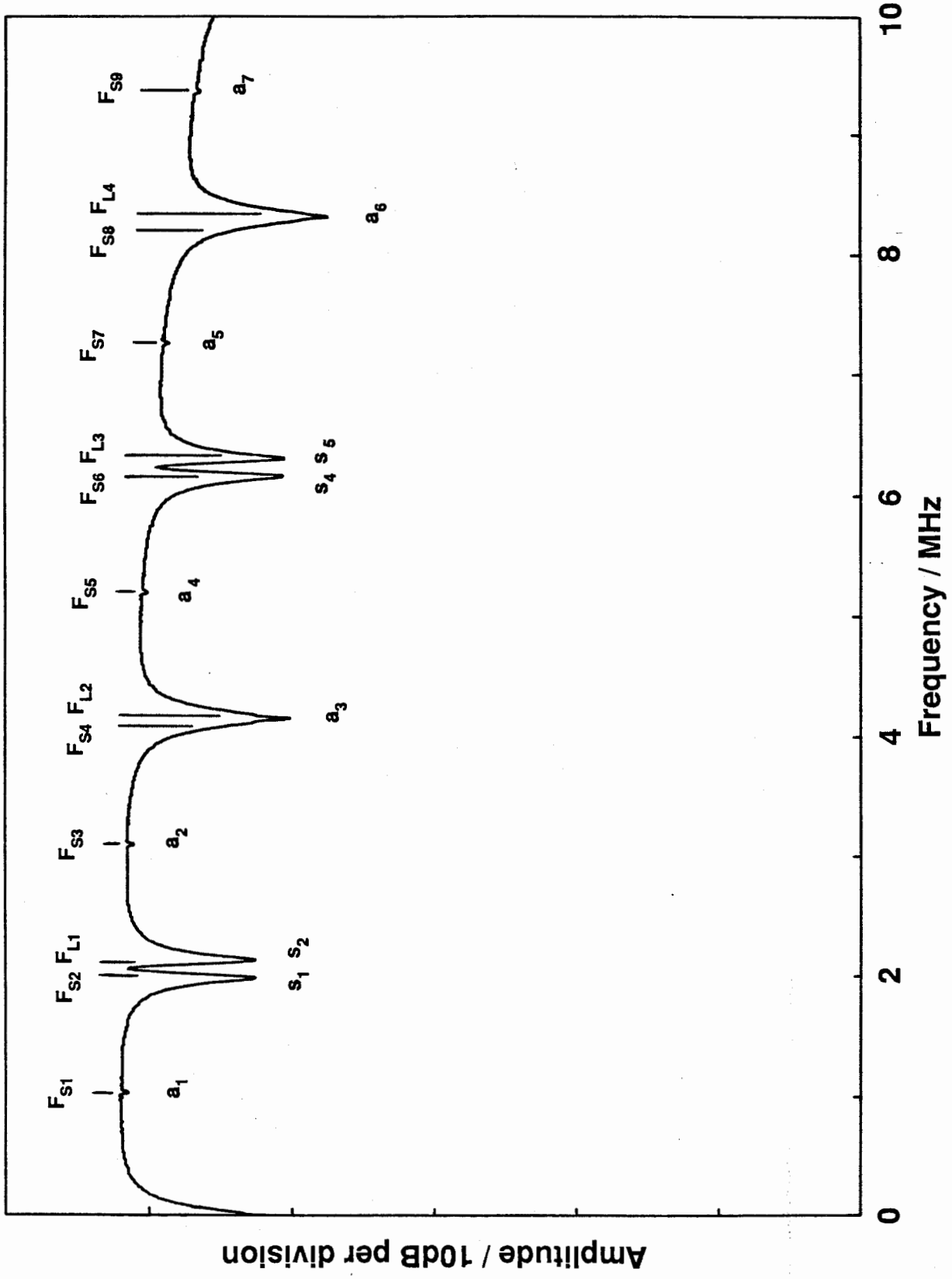

Figure 4.9 **Spectrum of Echoes from 1.6mm Thick Aluminium Plate at θ=2° in pulse echo mode**

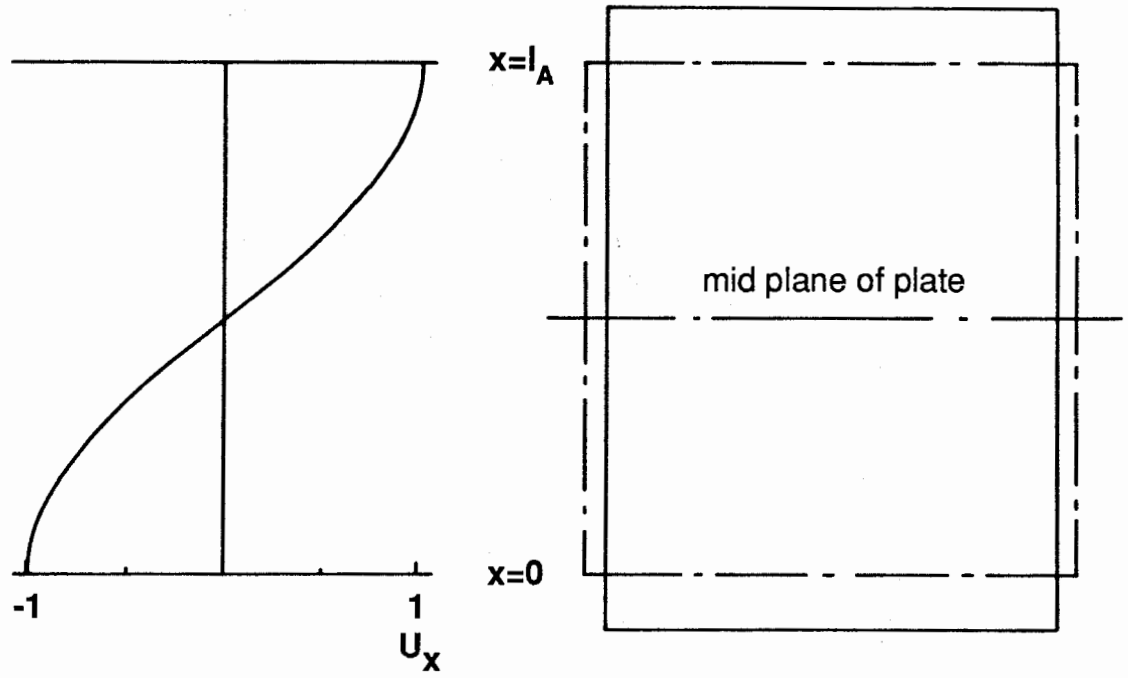

(a) through thickness or longitudinal mode

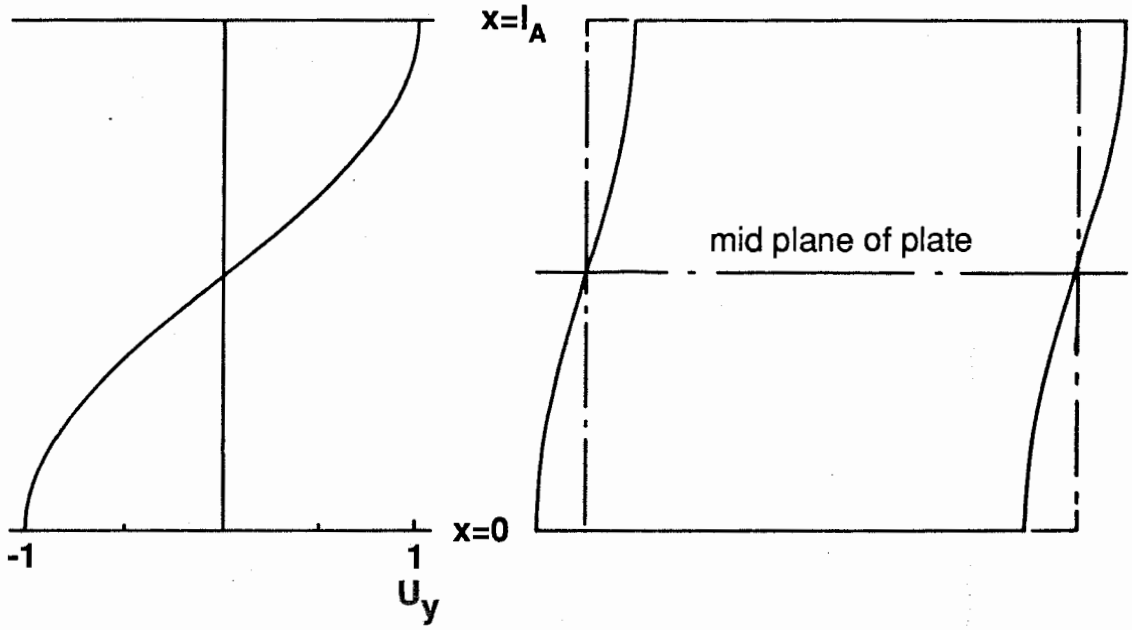

(b) shear mode

Figure 4.10 **First Mode Shape of Plate**
left hand view - through thickness deformation
right hand view - deformed shape of element from plate

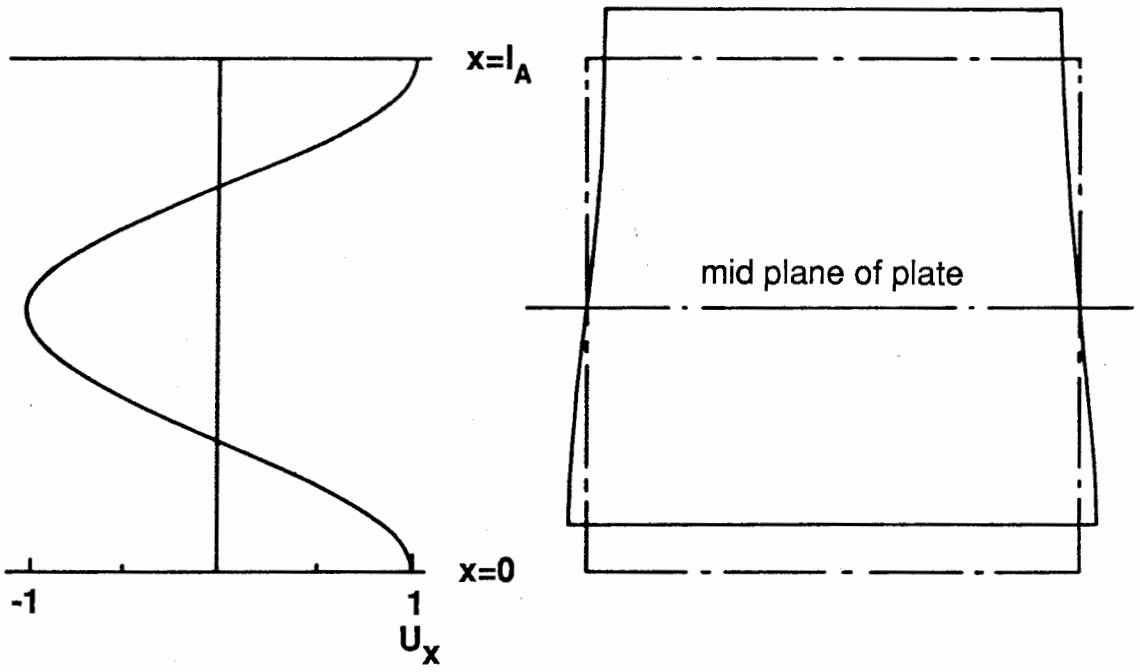

(a) through thickness or longitudinal mode

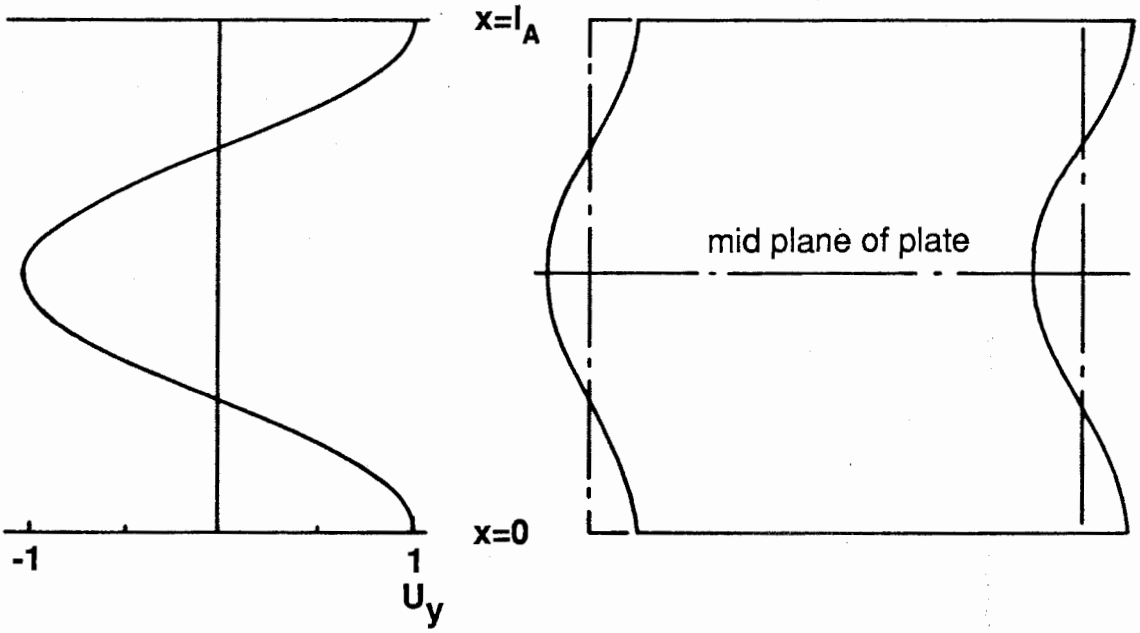

(b) shear mode

Figure 4.11 **Second Mode Shape of Plate**
left hand view - through thickness deformation
right hand view - deformed shape of element from plate

CHAPTER 5

Experimental Results for a Plain Plate at Normal Incidence

1 Introduction

Having predicted the echo pattern and corresponding spectrum which would be obtained in a test on a plain plate, it was then necessary to check the results experimentally.

2 Experimental Set-Up

Figure 5.1 shows a schematic diagram of the apparatus used to digitise the ultrasonic echoes from the specimen under test and to calculate the corresponding spectrum. The transducer was excited and the echoes received and amplified by a Panametrics PR 5052 pulser/receiver. The analogue bandwidth of the system was governed by that of the amplifier in the PR 5052 which is uniform between 1kHz and 35MHz (-3dB points). The received signal was then monitored using a 60 MHz analogue oscilloscope and digitised using a LeCroy 9400 125 MHz digital oscilloscope. The number of digitised points depended on the sampling frequency used and the duration of the transient to be recorded; however, the digitised record, of length T_d, would typically consist of 1,000 to 2,500 points at a 50MHz sampling rate.

The data was averaged in the time domain, the micro-computer being used to store and average the digital data the required number of times, typically between 20-50. The internal trigger of the digital osciloscope was used to trigger the system from the sharply rising first echo from the specimen, this precluded the possibilty of adding errors, due to fluctuations in the time between the synchronising pulses from the PR 5052 and the received echoes, to the averaged data. Errors resulting from trigger "jitter" within the digital osciloscope could not be avoided but were found to negligible.

The spectrum of the time history was carried out by performing ten zoom transforms (Thrane, 1980) on ten consecutive groups of 1,024 data points using a Bruel and Kjaer type 2033 digital spectrum analyser. An example of a complete 10,240 point time history, see figure 5.2, shows that it consists of

the 1,000-2,500 digitised points (of duration T_d) followed by zeroes, which are added to produce the required data length. It is important to note that the ultrasonic echoes have diminished to zero well within the digitised record length (T_d), thus making it possible to increase the number of points with zeroes without producing errors in the calculated spectrum.

The frequency resolution, δf, of a digital spectrum is only dependent on the overall duration of the time record (T) that is transformed (Newland, 1984) and is given by :-

$$\delta f = 1/T = f_S/N \qquad (5.1)$$

where N is the total number of points in the transform i.e. 10,240 and f_S is the sampling frequency.

This shows that the frequency resolution is increased by increasing the duration of the time record. This can be achieved either by increasing the number of points in the transform or by decreasing the sampling frequency. However, if the sampling frequency is less than twice the maximum frequency at which there is significant energy in the spectrum, aliasing (Newland, 1984) of the spectrum will occur, giving invalid results. Table 5.1 gives the frequency resolution and bandwidth available at various sampling frequencies.

Figure 5.3 shows the frequency response of the transducer (10 MHz Nortec, unfocussed with a 1/4" diameter crystal) used for the experimental work. The frequency response was found by taking the spectrum of the top face echo from a large flat block at normal incidence, the block being placed approximately 90 mm from the face of the probe. A maximum occurs in the spectrum at approximately 7 MHz, but the probe produces significant energy between approximately 2 and 10 MHz (-10 dB points). Above approximately 12 MHz there is negligble energy available meaning that the minimum sampling frequency that could be used with this probe, without aliasing of the spectrum occuring, was 25 MHz.

3 Experimental Measured Time History from a Plain Plate at Normal Incidence

3.1 Ultrasonic Beam Structure

Figure 5.4a shows the echoes, from a 4.95 mm thick glass plate approximately 100 mm square, measured using the set-up described in Section 2, with the probe 30 mm away from the plate, in pulse echo mode and at normal incidence. Each echo is clearly resolved, however, in addition to the main echoes (1,2,3 etc.) expected at normal incidence there are also echoes that correspond to those predicted by assuming a plane wave incident at a shallow angle of incidence, see figure 4.4.

In practice an ultrasonic probe consisting of a circular disc of piezo electric crystal does not only produce a plane longitudinal wave as assumed by the pulse propagation model described in Chapter 4. Instead, the ultrasonic pulse structure is complicated by the presence of edge waves (Weight and Hayman, 1978). Figure 5.5 shows the plane and edge waves at two instants as they propagate away from the transducer. The plane wave propagates into the cylindrical region directly in front of the probe, whilst the edge wave propagates as a toroidal shaped wave from the rim of the transducer.

Using a very small diameter (0.1-0.25mm) receiver, it is possible to resolve the plane and edge waves (Weight, 1984). However, when the pulse is is received by a second large probe the received signal is dominated by the effect of the plane wave (Ueda, 1981) and the edge wave is no longer separately resolved. Similarly, when the probe is used in pulse echo mode and the pulse is reflected off a flat target which is larger than the probe diameter, the received signal is also dominated by the effect of the plane wave.

For example, each main echo (1,2,3 etc. on figure 5.4a) from the glass plate, consists of a large bi-polar pulse followed by a smaller series of pulses. The large bi-polar pulse results from the reflection of the plane wave from the transducer, whereas the smaller pulses result from the reflected edge wave. While the plane wave can be normalised to the reflector or target, the edge wave is always at some angle of incidence to the reflector and hence can produce shear waves in the plate by mode conversion.

The effective angle of the edge wave, θ_e, is approximately equal to the angle between the plane wave and a line passing through the intersection of the edge waves on the centre line, point A on figure 5.5, and the intersection of an edge wave and the plane wave, point B on figure 5.5. Using this approximation it can be shown that the effective angle of incidence of the edge wave is approximately 7° for this probe at range of 30 mm.

As the probe to plate distance is increased, the effective angle of incidence of the edge wave is reduced and the wave front produced by the probe becomes a better approximation to a plane wave. Consequently, when the probe to plate distance is increased the magnitude of the shear waves in the plate are reduced, and the echoes, resulting from mode conversion are smaller.

Figure 5.4b shows the echoes from a glass plate using the same probe used for figure 5.4a but at a range of 120 mm. The calculated angle of the edge wave is now reduced to approximately 2°. Whilst the echoes resulting from mode conversion of the edge wave (2a, 2b, 3a etc) can still be seen, they are of a slightly smaller magnitude than those that occured at a range of 30 mm.

The relative arrival times of the main (e.g. 1, 2, 3 etc. in figure 5.4) and the mode converted echoes (e.g. 2a, 2b, 3a etc. in figure 5.4) are not particularly sensitive to changes in the angle of incidence. For example the shear transit time, T_S, in aluminium increases by approximately 3% when the angle of incidence increases from 2° to 7°, see eqn. (4.42).

Figure 5.6 shows the echoes from a 3.2 mm thick aluminium plate, with the probe at a range of 30 mm away from the plate, in pulse echo mode and at normal incidence. In addition to the main echoes (1,2,3 etc.) predicted at normal incidence there are also echoes (2a, 3a etc) that occur at times corresponding to those predicted by assuming a plane wave incident at a shallow angle of incidence, see figure 4.5.

4 Experimentally Measured Spectra of the Plain Plate at Normal Incidence

Figure 5.7 shows the spectrum of a 2.2 mm thick glass plate at normal incidence, together with the predicted frequencies of the longitudinal and

shear modes of the plate given by eqns. (4.43) and (4.44). The probe to plate distance was approximately 90 mm, hence the effective angle, θ_e, of the edge wave was approximately 2°. Below approximately 2 MHz, the minima, corresponding to resonances of the plate, are not clearly resolved because they occur at frequencies that fall below the usable bandwidth of the transducer. However, figure 5.8 shows that in addition to the longitudinal modes of the plate that would be expected at normal incidence, there are also some shear modes.

The shear modes of the plate that are clearly excited occur at frequencies given by eqn. (4.44) with m=3,7,8, and 12 which is in good agreement with the results predicted by assuming an incident plane wave at an angle of 2°, see figure 4.7. This suggests that while the plane wave from the ultrasonic probe is mainly responsible for exciting the longitudinal modes of the plate the edge wave excites the shear modes, since it is incident at a non-normal angle of incidence.

Since the relative arrival times of the main and mode converted echoes are not particularly sensitive to changes in the angle of incidence, at angles close to normal incidence, the resonant frequencies of the plate are also fairly insensitive to changes in angle. This is clearly seen in the dispersion curves, see figure 4.8, there being relatively small changes in frequency (up to 8%) as the angle increases from 1° to 5°.

Figure 5.8 shows the spectrum of the echoes from a 1.6 mm thick aluminium plate at normal incidence, together with the predicted frequencies of the longitudinal and shear modes given by eqns (4.43) and (4.44). Figure 4.5 shows that there is good agreement between the positions of the shear modes, predicted assuming an incident plane wave at an angle of 2°, and the experimental measurements.

Figure 5.8 also shows that the apparent damping of the shear and longitudinal modes of the aluminium plate is different, the longitudinal modes having broader resonant peaks, and hence greater apparent damping, than the shear modes. Whilst the material damping of the aluminium plate will have some effect on the apparent damping its influence is negligible compared to the energy of the ultrasonic pulse that is lost when it is transmitted to or "leaks"

into the water below the plate during its repeated reflections within the plate. This can be demonstrated by backing the plate with air when, since no energy will propagate across the bottom interface, most of the energy is reflected back to the transducer, the remainder being lost due to material damping. Consequently the echoes from the plate decay more slowly, as was demonstrated in Chapter 1 (see figure 1.12a).

When a longitudinal wave is incident on a plate the energy is initially all in the form of a longitudinal wave; however, following mode conversion, some of the energy is contained within the shear wave. As the longitudinal wave is repeatedly reflected, its energy decreases since some energy is lost to the water and some is converted to shear waves.

The energy in the shear waves intially increases, there being no shear waves present before the incident longitudinal wave and then begins to decrease slowly following the mode conversion back to longitudinal waves which "leak" into the water. The overall effect is for the average decay rate of the shear waves to be lower than that of the longitudinal waves; consequently the apparent damping of the shear modes is less than that of the longitudinal modes.

5 Conclusions

It has been shown that in practice both the longitudinal and shear modes of a plate are excited by a pulse from a transducer at normal incidence to the plate, whereas simple theory suggests that only the longitudinal modes are excited at normal incidence (see Chapter 4). The reason for this is that the pulse from a typical ultrasonic transducer does not consist of a plane wave alone, as is assumed by the simple theory, but is complicated by the presence of the edge wave which is incident on the plate at some small angle of incidence (typically $\theta_e < 7°$). Therefore, while the plane wave dominates the echoes in the time domain the effect of the edge wave is also seen.

The position of the echoes in the time domain, resulting from the mode conversion of the incident edge wave, e.g. echoes labelled 2a, 2b etc in figure 5.4, can be predicted using the pulse propagation model described in Chapter 4. It has been shown that there is good agreement between the predicted and

experimentally measured positions of the echoes from the edge wave for both glass (see figures 4.4 and 5.4) and for aluminium plates (see figures 4.5 and 5.6) using this model. The model can also be used to show that the magnitude of the echoes from the edge wave decrease when the angle of incidence decreases which occurs when the transducer to plate distance is increased, see figures 5.4a and 5.4b.

There is also good agreement between the experimentally measured positions of the shear modes in the spectra for the glass and aluminium plate, that occur at normal incidence, and the corresponding spectra predicted by assuming an incident plane wave at an angle of incidence of 2°. It has also been shown that good approximations for the frequencies of the longitudinal and shear modes of the plate, measured at normal incidence, are obtained from eqns. (4.43) and (4.44). However, the experimentally measured and predicted spectra, (for example see the results for a glass plate, figures 5.7 and 4.7 respectively), show that there are some shear modes predicted by eqn (4.44) that are not excited at small angles of incidence.

Frequency Resolution (δf) kHz	Sampling Frequency (f_S) MHz	Nyquist Frequency (f_{ny}) MHz	Bandwidth ($\approx 0.4 f_S$) MHz
2.5	25	12.5	9
5	50	25	19
10	100	50	39

Table 5.1 **Bandwidth and Frequency Resolution of Fast Fourier Transform at Various Sampling Frequencies.**

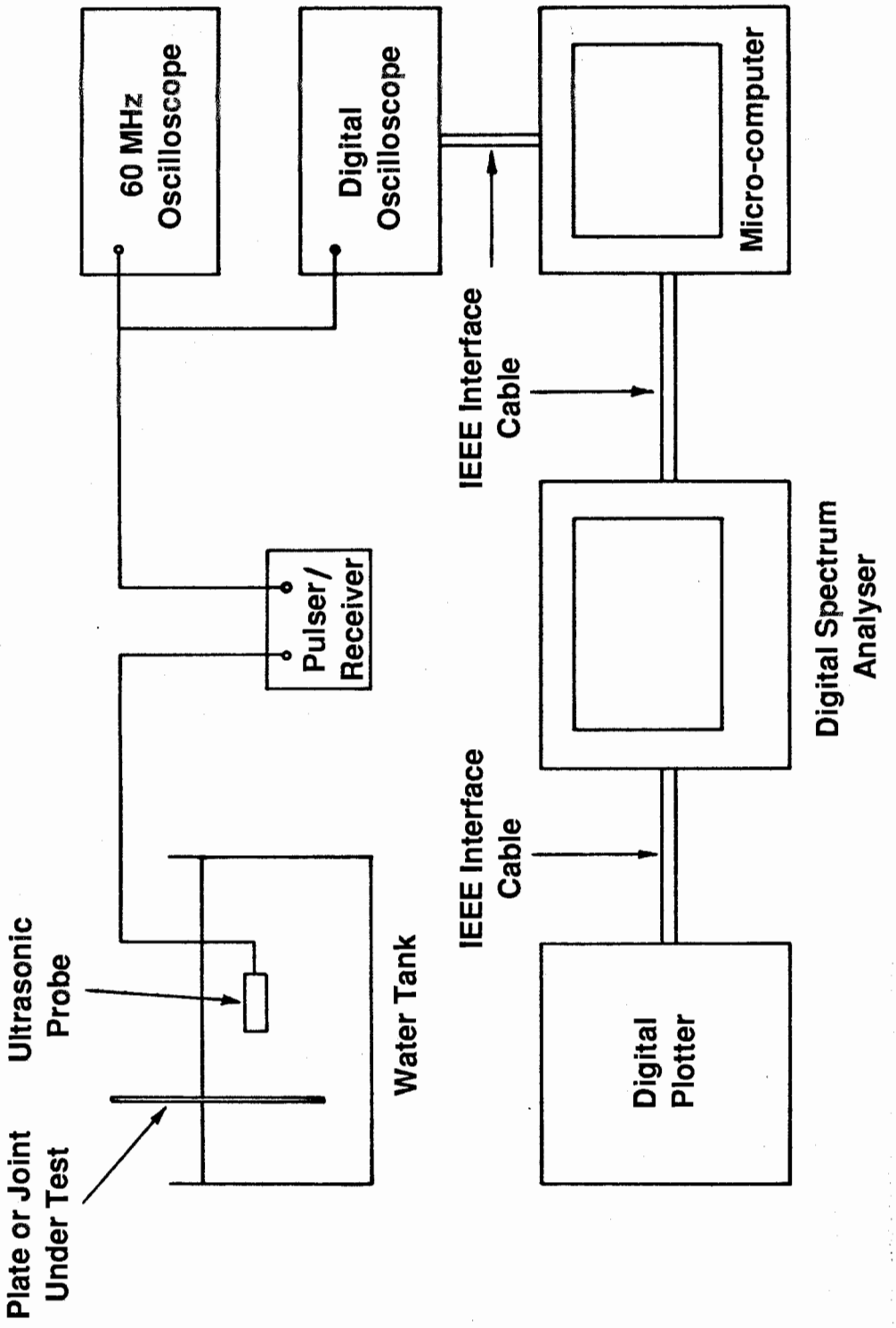

Figure 5.1 **Schematic Diagram of Apparatus**

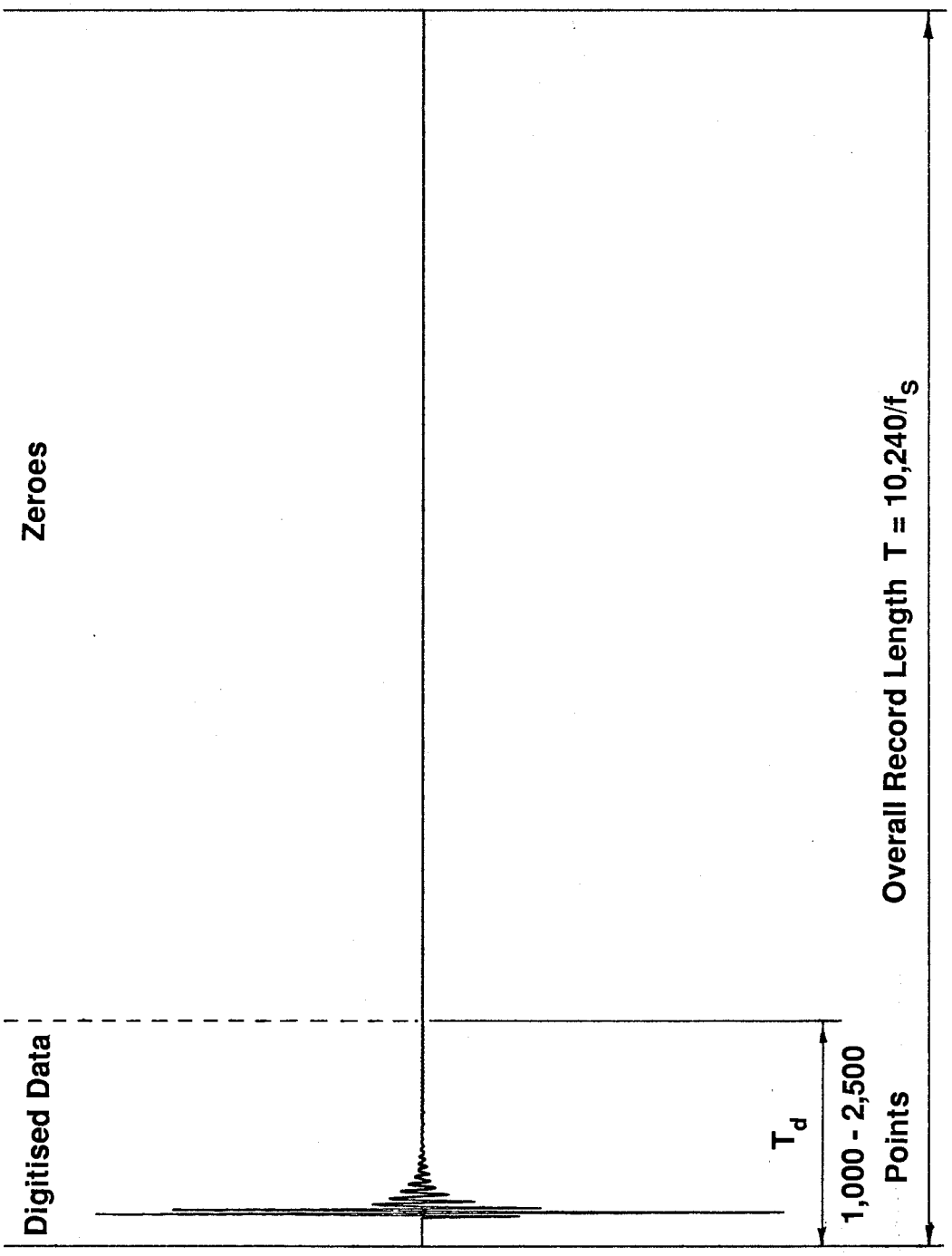

Figure 5.2 **Schematic Representation of Digitised Data and "Added Zeroes"**

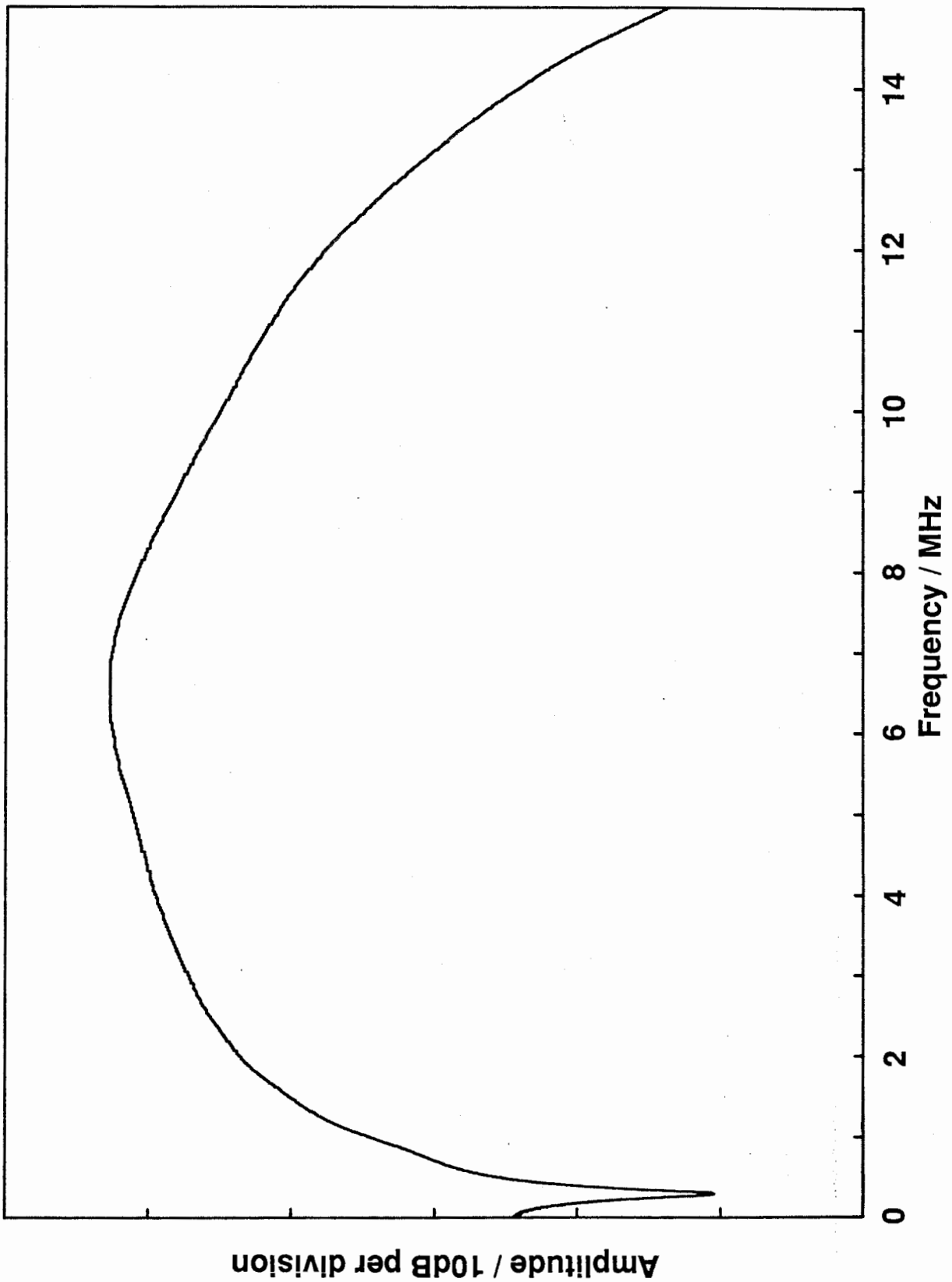

Figure 5.3 **Frequency Response of 10 MHz Nortec Transducer**

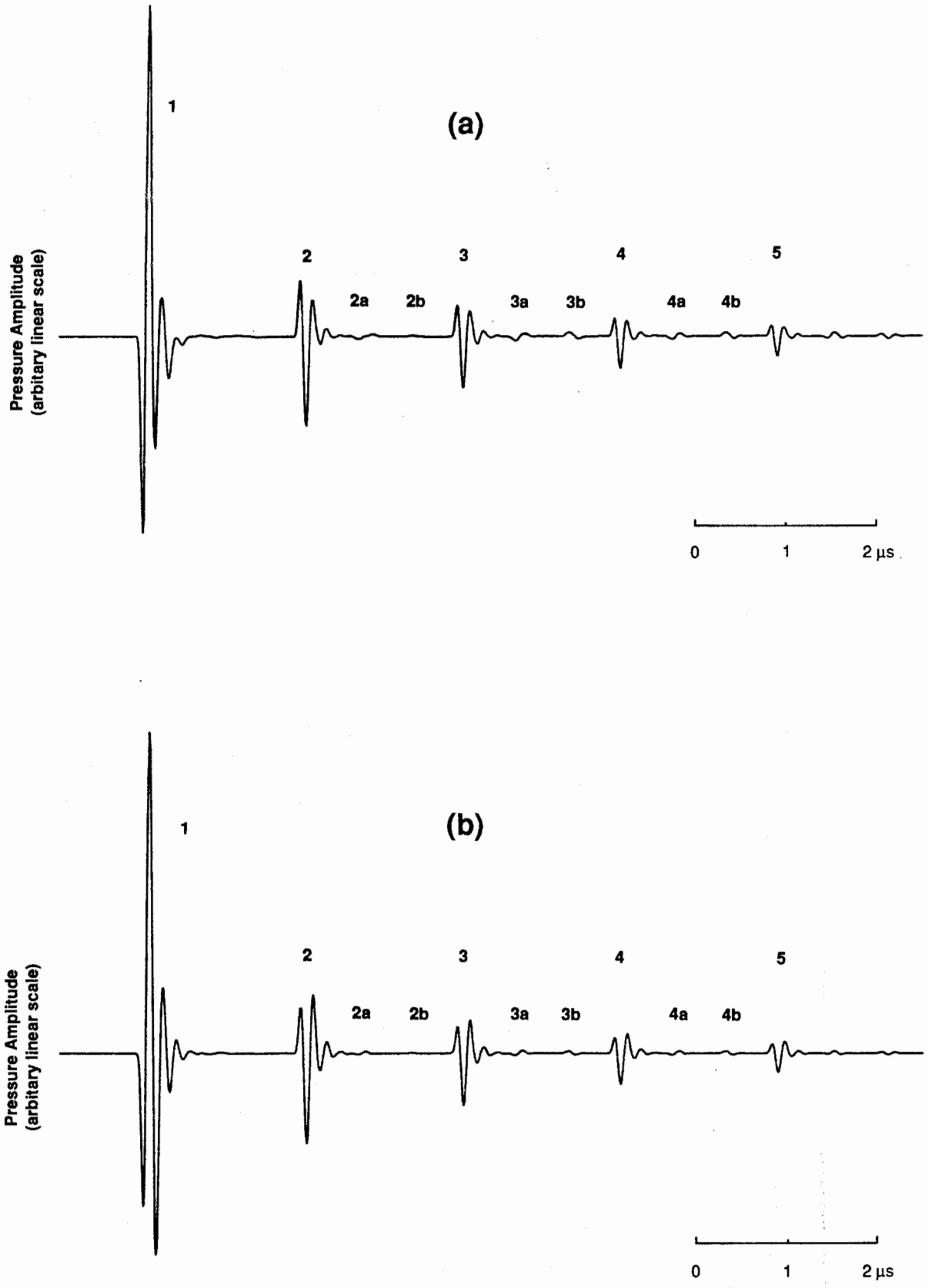

Figure 5.4 **Echoes from a 4.95 mm Thick Glass Plate in Pulse-Echo Mode** (a) probe to plate distance 30 mm (b) probe to plate distance 120 mm

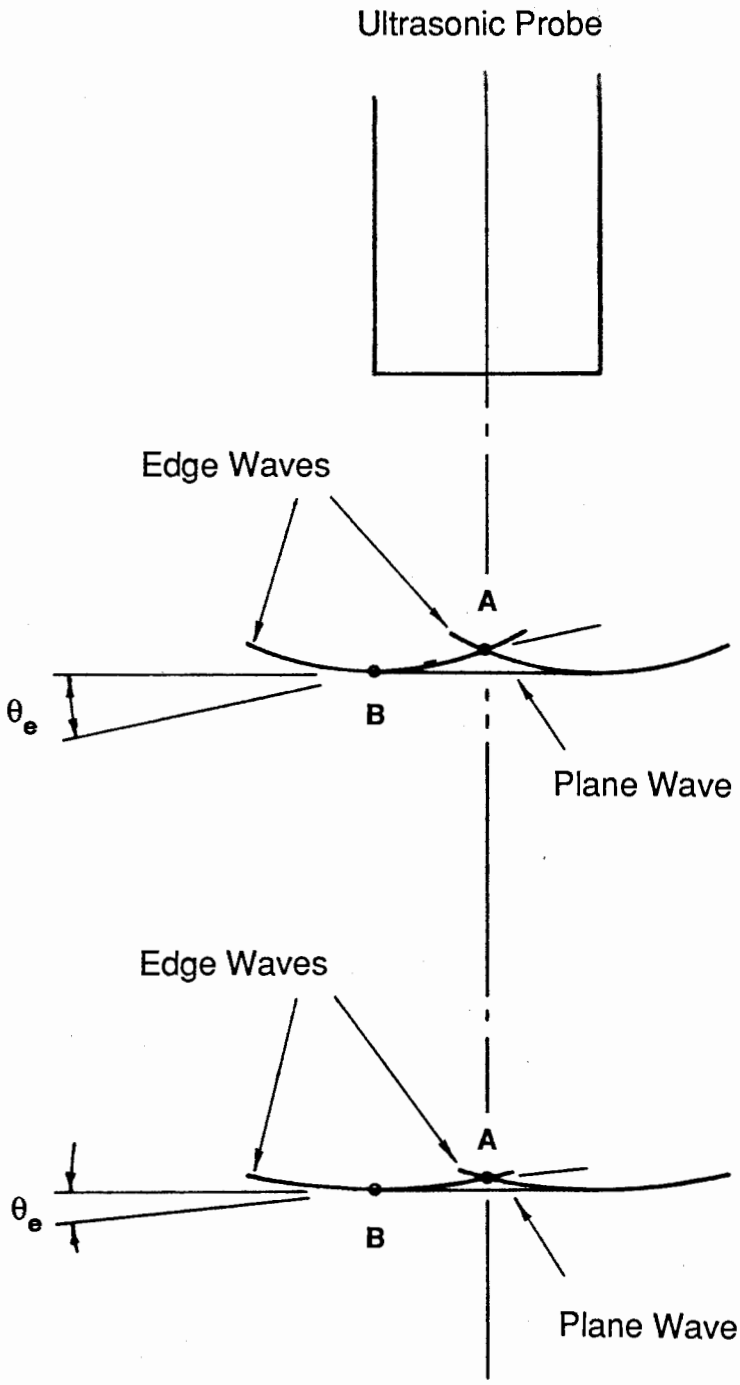

Figure 5.5 **Idealised Representation of the Plane and Edge Waves from a 15 mm Diameter Transducer**

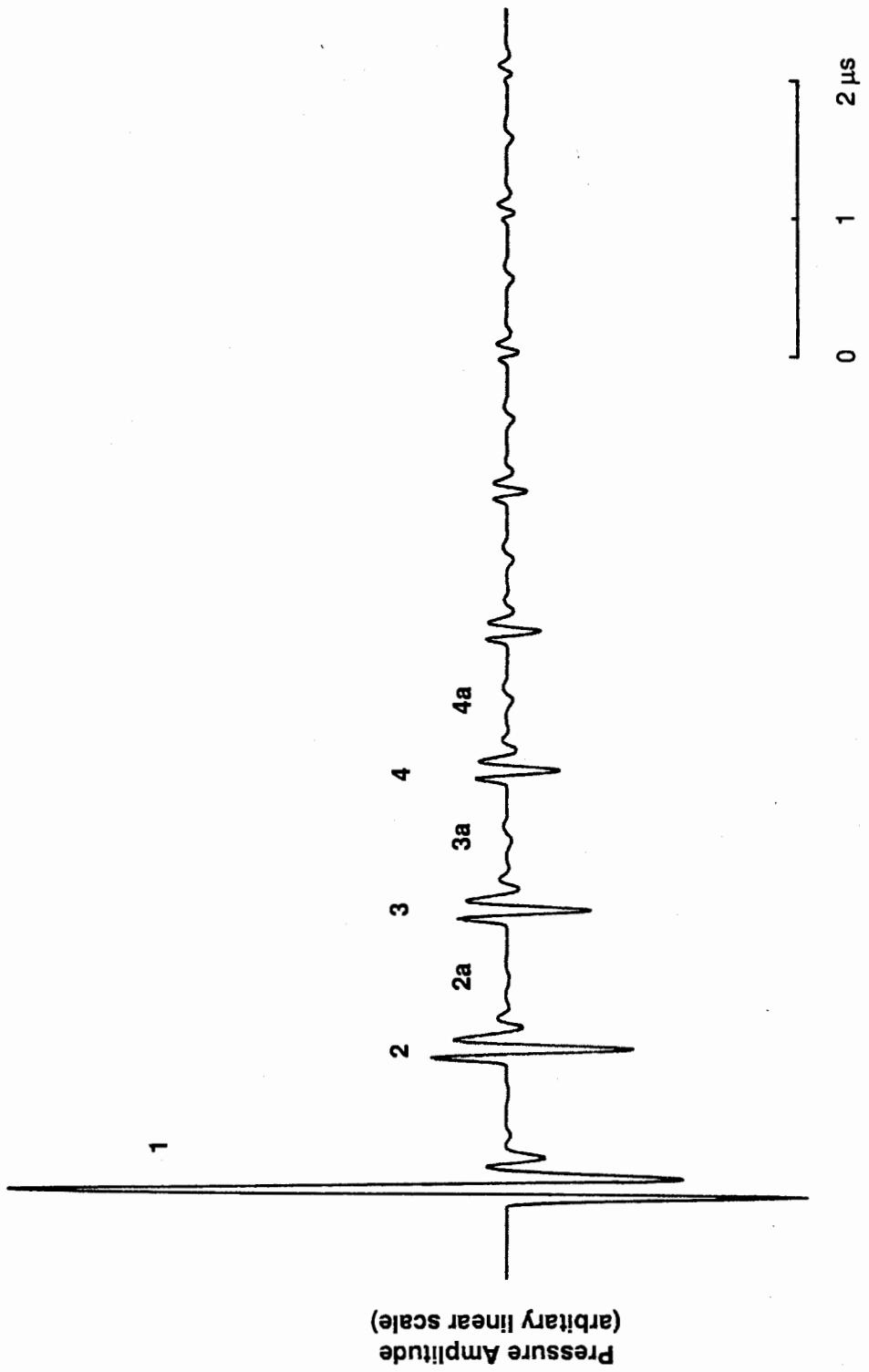

Figure 5.6 **Echoes from a 3.2 mm Thick Aluminium Plate in Pulse-Echo Mode**
(probe to plate distance 30 mm)

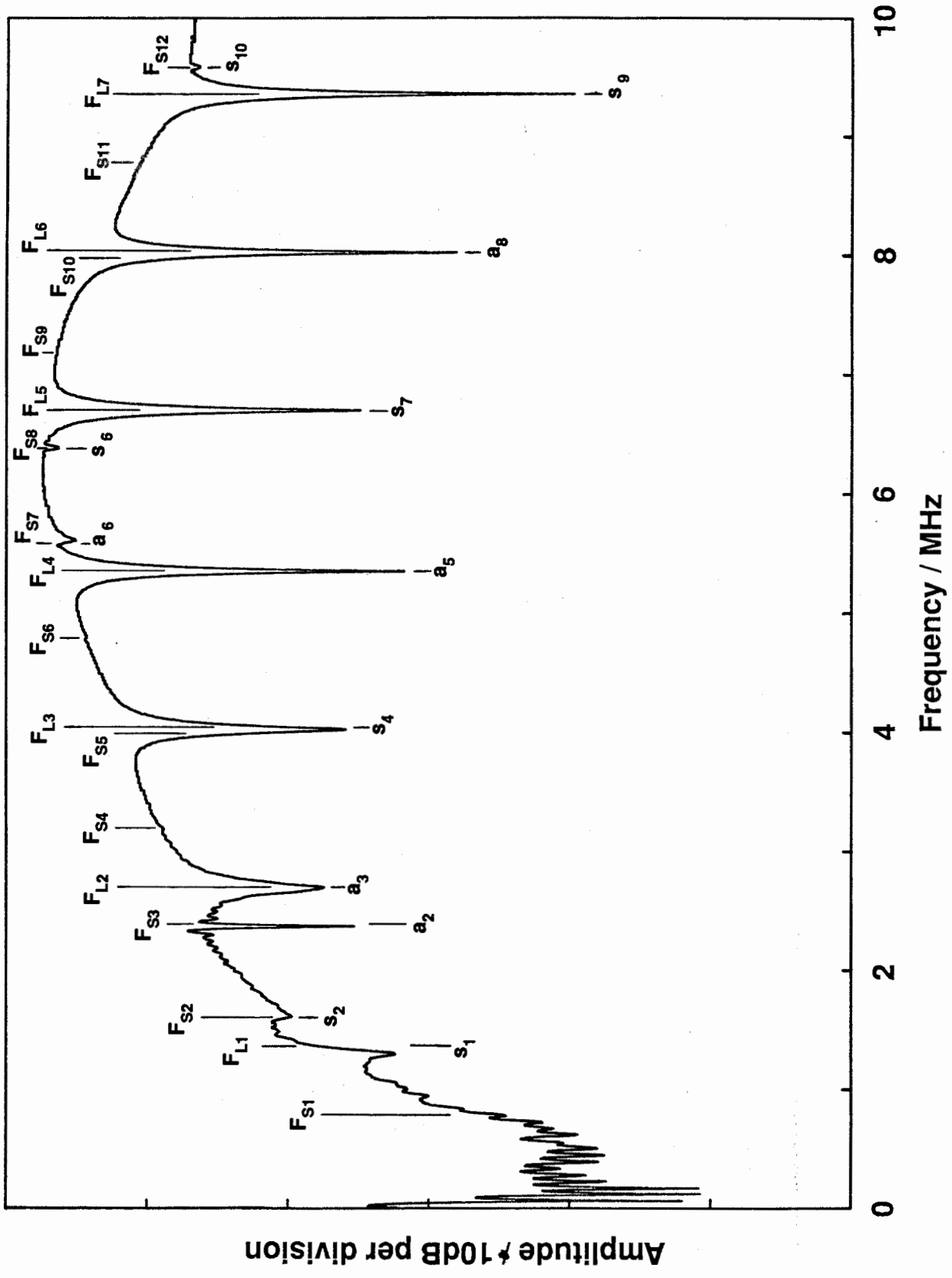

Figure 5.7 **Spectrum of Echoes from a 2.2 mm Thick Glass Plate at Normal Incidence** (in pulse echo mode)

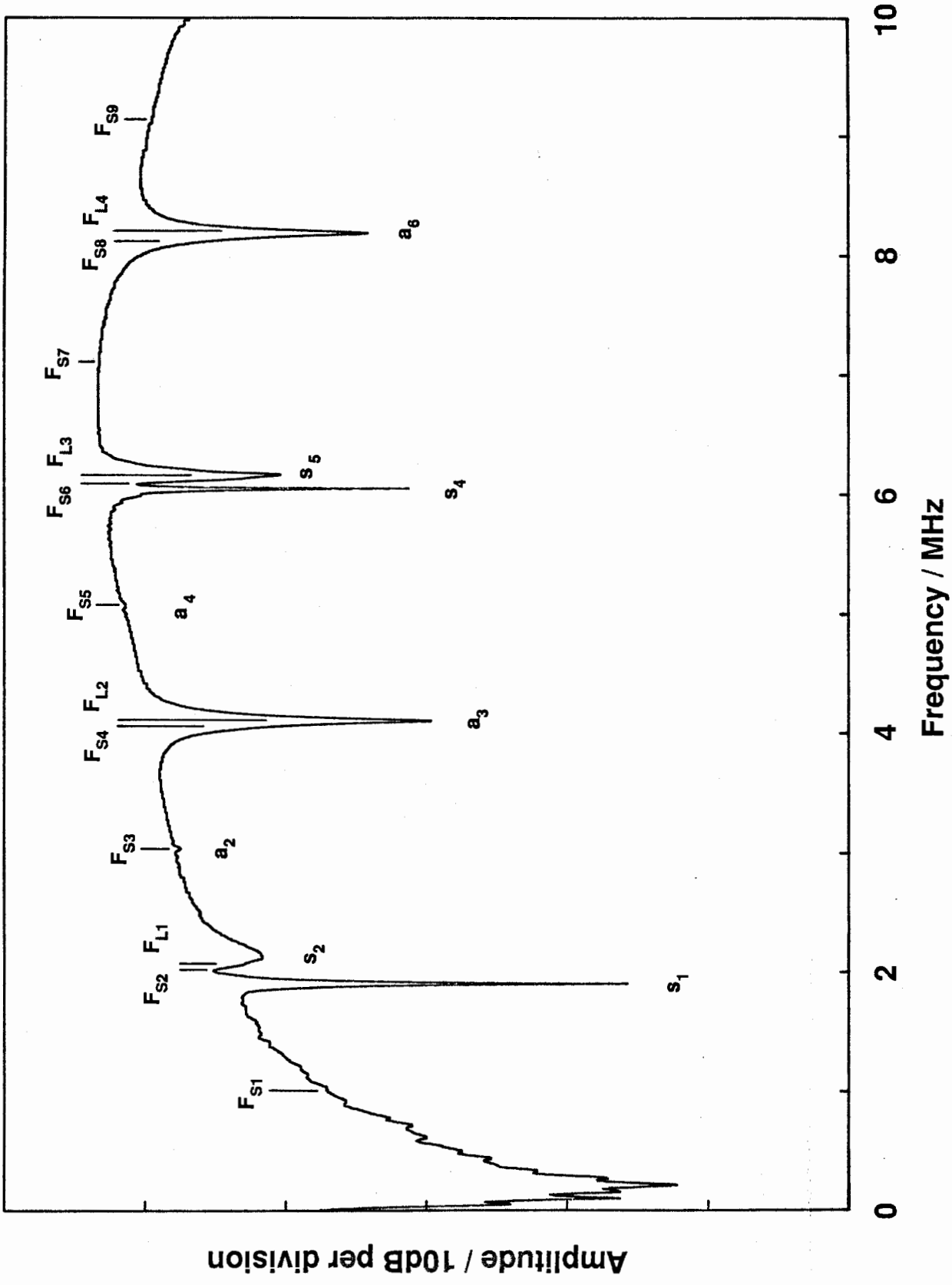

Figure 5.8 **Spectrum of Echoes from a 1.6 mm Thick Aluminium Plate at Normal Incidence** (in pulse echo mode)

CHAPTER 6

Theoretical Model for the Ultrasonic Vibration Characteristics of Adhesive Joints

1 Introduction

In Chapters 4 and 5 it was shown that there was good agreement between the experimentally measured spectrum of a plain plate and the predictions using the pulse propagation model. In order to predict the frequencies of the longitudinal or through thickness modes of the joint it was decided to develop a simple receptance model rather than the pulse propagation model. This was done because the receptance model is computationally more efficient than the pulse propagation model, especially when propagation through more than one layer is to be considered, as is the case in a joint. Also, a similar simple receptance model gave good agreement with the experimentally measured results in the analysis for the Fokker Bond Tester Mk II, see Chapter 3.

2 Description of the Receptance Model for the Joint

The joint was modelled as three solid cylinders in axial vibration joined end-on, see figure 6.1. The lengths of the first and third cylinders, l_1 and l_3, are the thicknesses of the top and bottom adherends respectively, while the length of the second cylinder, l_2, is the thickness of the adhesive. The densities (ρ), loss factors (η) and apparent moduli (E') of the cylinders are those of the adherends or adhesive. The loss (damping) factor of the adhesives used in the predictions was taken as 0.05 (Adams and Coppendale, 1976). Since this is significantly greater than a typical value for the adherends, the damping of the system will be dominated by the adhesive and the exact value used for adherends is not critical. However, the loss factor for the adherends was assumed to be that for aluminium i.e. 0.001 (Lazan, 1968).

The effect of the water couplant on the response of the joint was not modelled. The water has a similar effect on the natural frequencies of the joint to that obtained by grounding the model shown in figure 6.1 via two very weak springs attatched to each adherend. It can readily be shown, Bishop and

Johnson (1960), that this has a negligible effect on the resonant frequencies of the joint.

The water does increase the apparent vibration damping of the joint. This occurs because some of the energy from the ultrasonic pulse is lost when it is transmitted into the water below the plate, in a similar way to that described in Chapter 5 for a plain plate. However, the increase in apparent damping will not significantly change the measured resonant frequencies of the joint.

The model uses the same basic assumptions as the impedance model described by Brekhovskikh (1960) and used by Lloyd and Wadhawani (1978) to predict the response of the joint. However, in the receptance model the variables are more easily related to measurable properties and, more importantly, the mode or deformed shapes of the joint can readily be predicted, thus leading to a better understanding of the frequency response.

The natural frequencies, mode shapes and damping of the longitudinal modes of the complete system were found using receptance analysis (Bishop and Johnson, 1960) in a similar way to that used in the analysis of the Fokker Bond Tester, see Chapter 3. Figure 6.2 shows the natural frequencies of the first eleven longitudinal, or through thickness, modes of a system representing a typical joint used in the aerospace industry with 1.6 mm thick aluminium adherends and a high modulus (Young's Modulus = 4.6 GN/m^2 and apparent modulus (E'_2) = 7.2 GN/m^2) adhesive as a function of adhesive thickness. At low adhesive thicknesses (approximately 0.1 mm), the modes form pairs, except for the first mode which occurs on its own. Lloyd and Wadwhani (1978) referred to the first mode in each pair as the principal peak and the second as the satellite peak.

2.1 First Mode of the Joint

The predicted mode shapes were calculated using the method described by Bishop and Johnson (1960) and assume a unit displacement at the outer surface of the top adherend. Figure 6.3a shows the first mode of the joint with an adhesive thickness of 0.1 mm, the displacement u_x being the motion in the through thickness direction. The mode shape of the first through thickness mode of a plain plate having the same overall thickness as the joint and also

assuming a unit displacement at its outer surface, is shown in figure 6.3b. As can be seen from the figures, the mode shape of the joint is similar to that of the plain plate except that in the joint, the strain, given by the rate of change of displacement with distance, $\partial u_x/\partial x$, is concentrated in the adhesive layer. As the adhesive thickness is decreased, the discontinuity in the mode shape becomes less evident. At very low adhesive thicknesses (less than 0.01 mm) the natural frequency and mode shape of the joint approach those of a plain plate having the same overall thickness as the joint.

At adhesive thicknesses of less than approximately 0.7 mm with a high modulus adhesive, the stiffness of the adherends dominates the frequency of the first mode of the joint. At adhesive thicknesses greater than 0.7 mm the frequency of the first mode is no longer dominated by the stiffness of the adherends and it is possible to model the joint as two rigid masses vibrating in antiphase on a spring as suggested by Schliekelmann (1975). The resonant frequency, f_m, of such a system is given as follows:-

$$f_m = 2\pi \left[E'_2 (l_1 + l_3) / (\rho\, l_1\, l_2\, l_3) \right]^{1/2} \qquad (6.1)$$

where l_1, l_3 are the thicknesses of the top and bottom adherends, ρ is their density, E'_2 is the apparent modulus of the adhesive, and l_2 is the thickness of the adhesive. Since the mass-spring-mass system has only one non-zero resonant frequency this model cannot be used to predict the resonant frequencies of the higher modes of the joint.

2.2 Higher Modes of the Joint

The pairing of modes at low adhesive thickness can be explained by examining the corresponding predicted mode shapes of the joint. The second and third mode shapes of the joint with an adhesive thickness of 0.1 mm are shown in figures 6.4a and 6.4b respectively. Even at low adhesive thicknesses, the adhesive is still the major flexibility in the system since the modulus of the adherends is at least an order of magnitude higher than that of the adhesive. The major difference between the two mode shapes is that in the second mode there is no significant strain in the adhesive while in the third mode there is a rapid change of displacement, and hence high strain, across the adhesive. In

this instance, the calculated strain energy in the adhesive is approximately five hundred times greater in the third mode than in the second. However, the strain energy in the adherends is at least twice that in the adhesive in both modes so it is the adherends which primarily govern the resonant frequencies of the joint. Since the adherends have a similar deformed shape in each of these modes the natural frequencies of the second and third modes of the joint occur close together.

At very low adhesive thicknesses (less than 0.01 mm) the adhesive is no longer the major flexiblity of the system and the modes are no longer paired. Instead, the frequency of the second mode of the joint approaches that of the second mode of a plain plate having the same overall thickness as the joint. Similarly the frequency of the third mode of the joint approaches that of the third mode of a plain plate having the same overall thickness as the joint.

As the adhesive thickness is increased (to above 0.1 mm) the frequencies of all the modes of the joint decrease and the mode pairing ceases to occur, as shown in figure 6.2. The reason for this can also be explained by examining the corresponding mode shapes of the joint. Figure 6.5a and 6.5b show the fourth and fifth mode shapes of the joint with an adhesive thickness of 0.1 mm which occur as a pair (see figure 6.2). Except for the increased strain in the adhesive in the fifth mode compared with the fourth mode the two shapes are similar, the deformed shape of the adherends in both modes corresponding to that of the second mode of a single adherend.

Figures 6.6a and 6.6b show the fourth and fifth mode shapes with an adhesive thickness of 0.4 mm, however, note that there is a significant difference in the scales of the two figures. In the fifth mode the deformed shape of the adherend, which largely determines the frequency of the mode, remains the same as the adhesive thickness is increased. Hence, the resonant frequency of the fifth mode is practically independent of adhesive thickness between 0.1 and 0.4 mm. In the fourth mode, however, the deformed shape of the adherend changes significantly as the adhesive thickness is increased. There is also a substantial increase in strain in the adhesive, the calculated total strain energy in the adhesive increasing by a factor of approximately 400 as the adhesive thickness increases from 0.1 to 0.4 mm.. The deformed shape of the adhesive now becomes a significant factor in determining the resonant

frequency of the joint, (the strain energy in the adhesive now being approximately three times that in the adherend), and the fourth and fifth mode of the joint are no longer paired, see figure 6.2.

Figure 6.7a, b and c show respectively the predicted mode shapes for the second, third and fourth modes of the joint with an adhesive thickness of 0.69 mm. As can be seen from figures 6.7c and 6.6a, the fourth mode shape of the joint changes significantly as the adhesive thickness is increased from 0.4 to 0.69 mm. The calculated strain energy in the adhesive decreases by a factor of approximately 5 and the deformed shape of the adherend now approaches that of the mode shape of the first mode of a single adherend alone. The frequency of the fourth mode, which is again largely determined by deformed shape of the adherends, now approaches that of the second and third modes of the joint which share a similar adherend deformed shape, see figure 6.7a and b.

3 Predicted Changes in Damping of the Joint

The damping of a particular mode was calculated from the width of the resonance peak at the half power points. A convenient method of expressing the damping, in moderately damped systems such as this, is to use the Q factor which is defined as, see Ewins, (1985) :-

$$Q = f_n / (f_{n2} - f_{n1}) \qquad (6.2)$$

where f_n is the resonant frequency of the joint, and f_{n1} and f_{n2} are the frequencies of the half power points i.e. the points with an amplitude 6 dB below the resonant peak. Therefore as the damping, and hence resonant bandwidth increases, the Q factor decreases. The frequency interval between calculated points on the receptance curve was approximately 2 KHz and the bandwidth at the half power points was typically greater than 30 KHz. Therefore there were at least fifteen calculated points around the resonant peak.

The calculated Q factor of the fourth mode is shown as a function of adhesive thickness in Table 6.1. This shows that the damping increases as the adhesive thickness is increased to 0.4 mm and that it then decreases slightly as the thickness is increased further to 0.69 mm. This change in damping is due to a

change in energy dissipated in the adhesive and can be explained by examining the corresponding mode shapes of the joint.

The calculated mode shape of the fourth mode, with an adhesive thickness of 0.1 mm, see figure 6.5a, shows that there is very little strain in the adhesive, the calculated strain energy in the adherends being approximately 200 times greater than that in the adhesive. Consequently there is very little energy dissipated in the adhesive and the damping of the mode is low (the Q factor is 530).

There is a significant increase in the strain in the adhesive of this mode as the adhesive thickness is increased to 0.4 mm, see figure 6.6a. This is accompanied by a large increase in damping, the Q factor for this mode reducing to 20. As the adhesive thickness is increased further to 0.69 mm the strain in the adhesive reduces, see figure 6.7c, and the Q factor increases slightly to 25.

4 Dependence of Resonant Frequencies on Specific Stiffness

So far, only the effect of changes in the thickness of a particular adhesive on the resonant frequencies of the joint have been considered; it is now important to examine the effect of adhesive modulus changes. Figure 6.8 shows the resonant frequency of the first five modes of an adhesive joint with 1.6 mm thick adherends as a function of specific adhesive stiffness, E_S, which is defined as :-

$$E_S = E'_2/l_2 \qquad (6.3)$$

where E'_2 and l_2 are the apparent modulus and the thickness of the adhesive respectively. In figure 6.8 two sets of curves are shown, one representing the typical high modulus adhesive used for the predictions in Section 2 and the other curve a typical low modulus (Young's modulus = 0.7 GN/m^2 apparent modulus (E'_2) = 3.6 GN/m^2) gap filling adhesive. Figure 6.8 shows that, apart from the first mode of the joint, the resonant frequencies are not purely dependent on specific stiffness, but are dependent on adhesive modulus and adhesive thickness separately. However, reducing the modulus at constant

adhesive thickness, or increasing adhesive thickness at constant modulus both cause a decrease in the resonant frequencies of all the modes.

Over the ranges of adhesive modulus and thickness considered here, the first mode is dependent on specific stiffness alone since the two curves representing the different adhesive moduli are coincident, see figure 6.8. In this instance, increasing adhesive thickness has exactly the same effect as decreasing the modulus by the same percentage.

Since the higher resonant frequencies of the joint are dependent on adhesive modulus and thickness separately, provided the resonant frequencies of at least two modes (apart from the first mode) are measured, it should be possible to distinguish a change in adhesive modulus from a change in adhesive thickness.

In contrast, the Fokker Bond Tester, which was discussed in Chapters 2 and 3, monitors the resonant frequencies of the first two modes of a probe coupled to the joint. It was shown that the frequencies of both these modes are practically independent of either modulus or thickness, except when the specific stiffness of is very low. At such low specific adhesive stiffnesses the Fokker Bond Tester is not sensitive to modulus and thickness separately, but to the ratio of adhesive modulus to thickness i.e. to the specific stiffness. Consequently, the instrument is not able to distinguish a change in adhesive thickness from a change in modulus.

5 Other Factors which Influence the Resonant Frequency of a Joint

The resonant frequency of a joint is also dependent on the thickness of the adherends, an increase in their thickness causing a decrease in the resonant frequencies of all the modes. However, the resonant frequencies have a similar general dependence on specific adhesive stiffness to that shown in Figure 6.8 for a joint with 1.6 mm adherends.

The change in frequency of a particular mode produced by a change in thickness of the adherends also depends on the adhesive stiffness. When the specific adhesive stiffness is high (greater than approximately 5×10^4 GN/m^3) the

frequency response of the joint is dominated by the thickness of the adherends, and resonant frequencies approach the asymptotes given by eqn. (4.43) and described in Section 2. Consequently, when the adherend thickness is doubled the overall joint thickness is also approximately doubled and the frequency of each mode is roughly halved.

As the specific adhesive stiffness reduces (less than approximately $2x10^4$ GN/m^3) the resonant frequencies of the joint are no longer dominated by the adherends and the dependence of the resonant frequencies of the joint on the adherend thickness becomes more complex.

The above analysis has also assumed that the top and bottom adherends are the same thickness; if the adherend thicknesses are not equal the frequency response of the joint is more complex. The mode pairing described in Section 2.2, which occurs at low adhesive thicknesses, does not occur in the same regular pattern. However, mode pairing will occur when the deformed shapes of the adherends in consecutive modes are similar.

In practice the thickness of the adherends are likely to be known, and to be uniform over the area to be tested. Consequently changes in the measured spectrum will only result from changes in the properties of the adhesive layer.

Changes in the density of the adhesive layer have a negligble effect on the resonant frequencies of the joint compared with the variations produced by changes in adhesive modulus and thickness. This occurs because the mass of the adhesive layer does not have major effect in determining the resonant frequency of the joint. However, the actual change in resonant frequency due to a variation in adhesive density depends on the adhesive thickness and the mode of the joint. For example larger changes in frequency occur at greater adhesive thicknesses and when there is more deformation in the adhesive. A 10% increase in adhesive density causes a negligble decrease in the frequency of the first mode of less than 0.1%.

The frequency of the higher modes of the joint can be more sensitive to changes in adhesive density, however a 10% change causes less than a 3% change in any of the modes below 10 MHz.

6 Conclusions

A simple receptance model has been used to show how the first eleven through thickness modes a typical joint, with 1.6 mm thick aluminium adherends and a high modulus adhesive, are dependent upon the adhesive thickness. The frequency of each mode was predicted to decrease when the adhesive thickness is increased. Similarly, it has been shown that a reduction in adhesive modulus also reduces the frequency of each mode.

Apart from the first mode, the resonant frequencies of joint are not dependent on the specific stiffness of the adhesive alone, but on the modulus and thickness of the adhesive separately. Consequently, by measuring the frequency of at least two modes (apart from the first mode) it should be possible to distinguish changes in adhesive modulus from variations in adhesive thickness. This is important if the method is to be used to monitor the cohesive properties of adhesive joints.

Adhesive Thickness (l_2) mm	Q Factor	Calculated Total Strain Energy in the Adhesive (relative to that at an Adhesive thickness of 0.1 mm)
0.1	530	1
0.4	20	390
0.7	25	84

Table 6.1 **Predicted Q Factor of the Fourth Mode for Various Thicknesses of Adhesive**

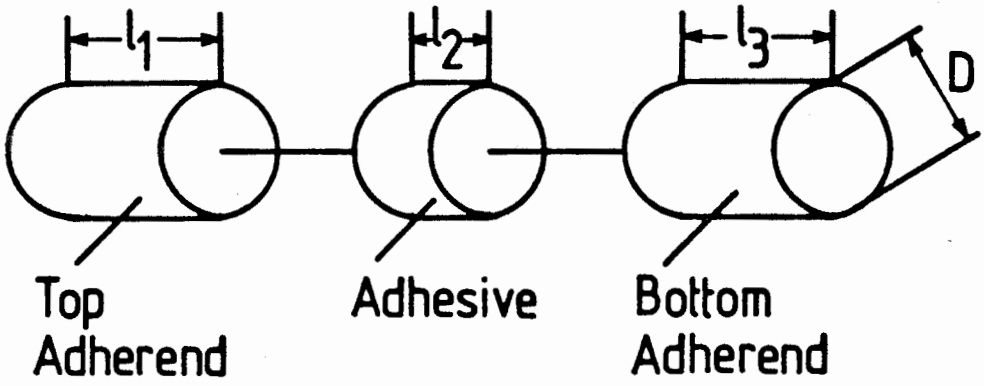

Figure 6.1 Schematic Representation of Model used for the Reception Analysis

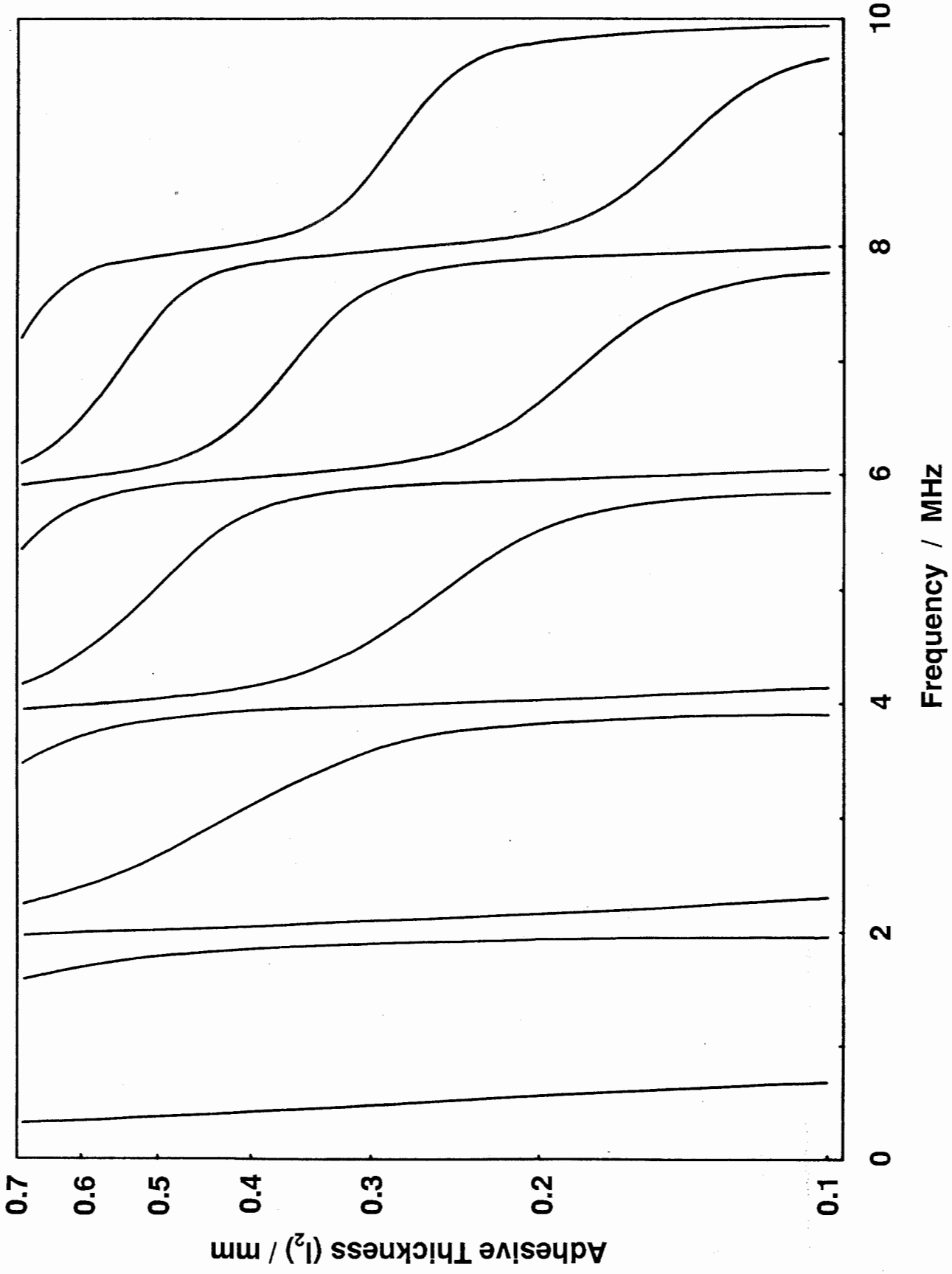

Figure 6.2 **Frequency of First Eleven Through Thickness or Longitudinal Modes of a Joint as a Function of Adhesive Thickness** (1.6 mm thick aluminium adherends)

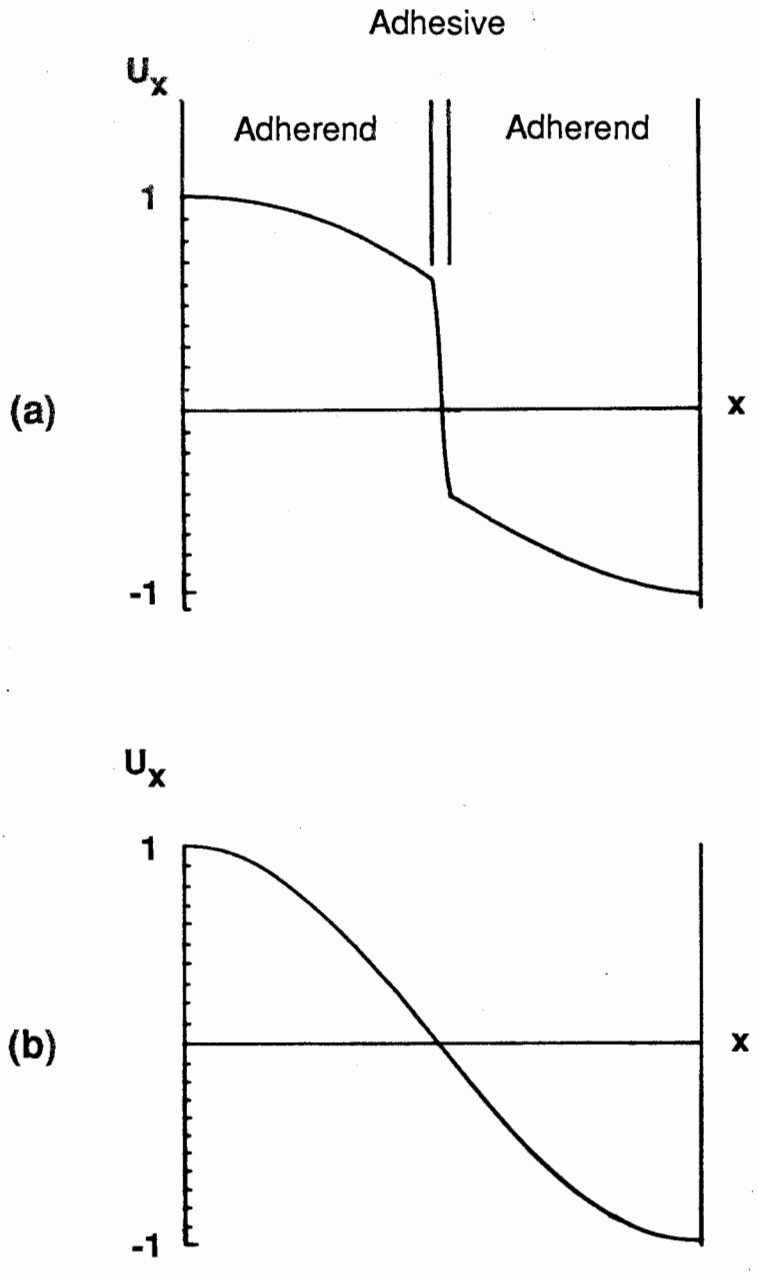

Figure 6.3 **First Longitudinal or Through Thickness Mode Shapes** (a) joint with 0.1 mm thick adhesive (b) plain plate having same overall thickness as the joint

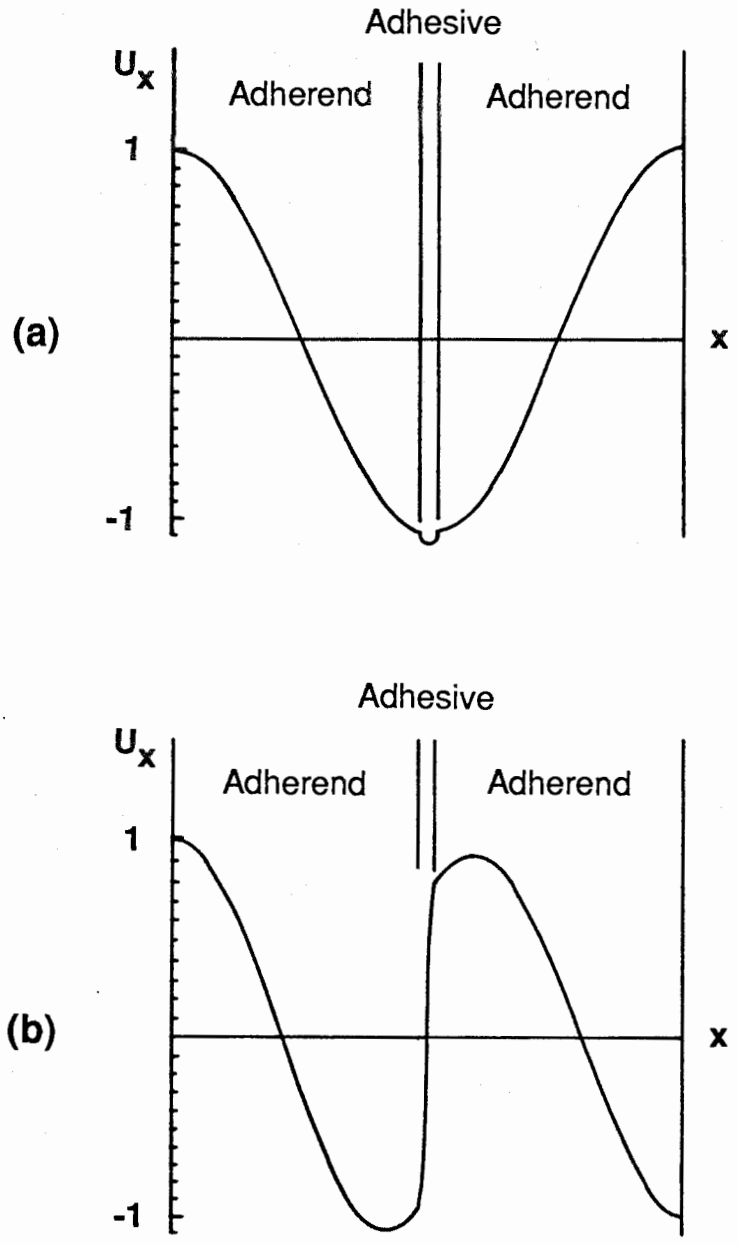

Figure 6.4 **Longitudinal or Through Thickness Mode Shapes of a Joint with 0.1 mm Thick Adhesive** (a) second mode (b) third mode

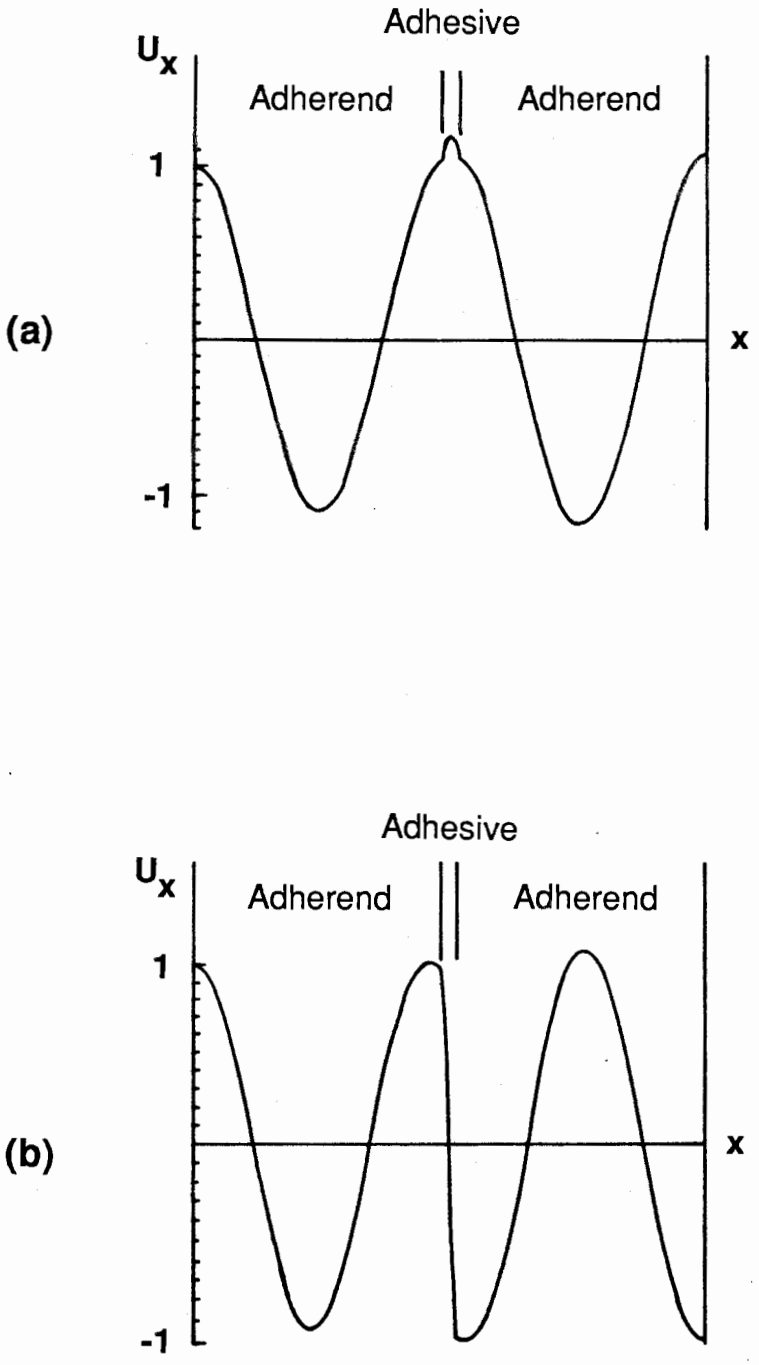

Figure 6.5 **Longitudinal or Through Thickness Mode Shapes of a Joint with 0.1 mm Thick Adhesive** (a) fourth mode (b) fifth mode

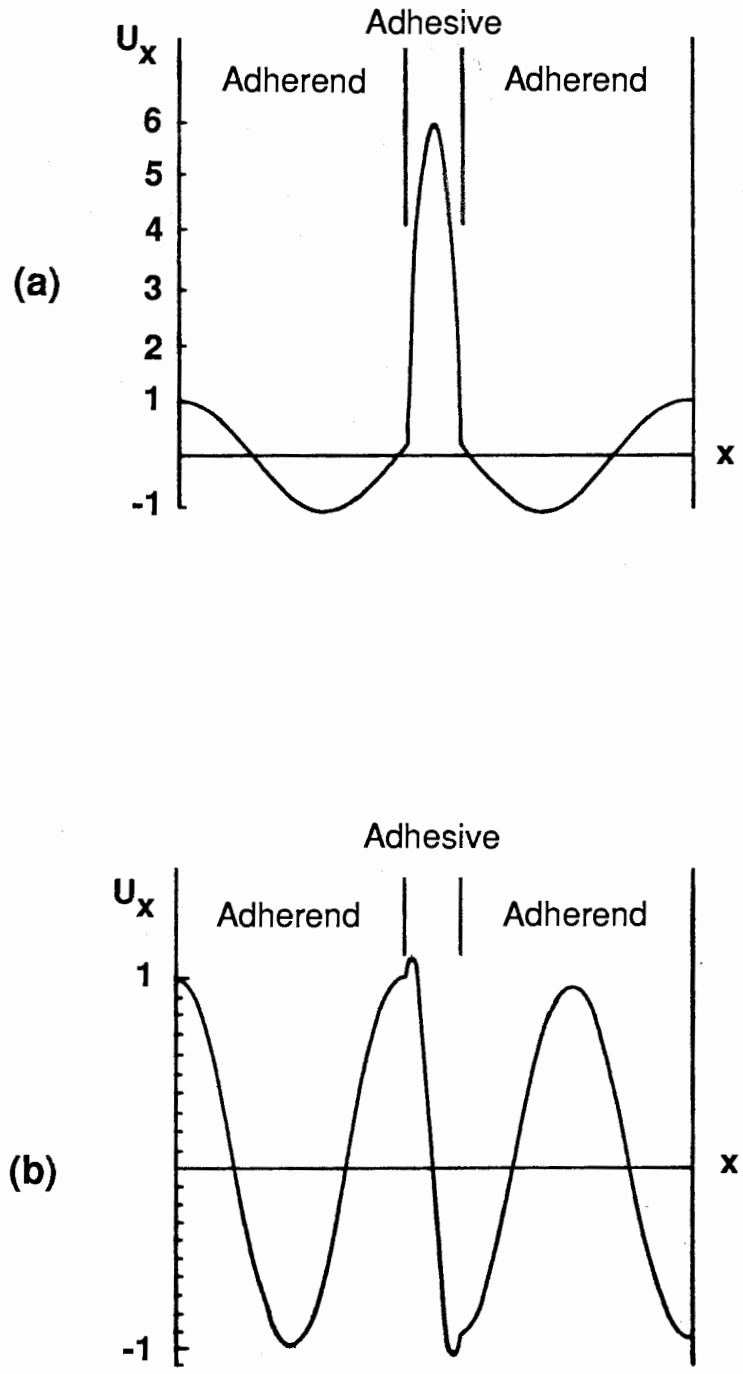

Figure 6.6 **Longitudinal or Through Thickness Mode Shapes of a Joint with 0.4 mm Thick Adhesive** (a) fourth mode (b) fifth mode

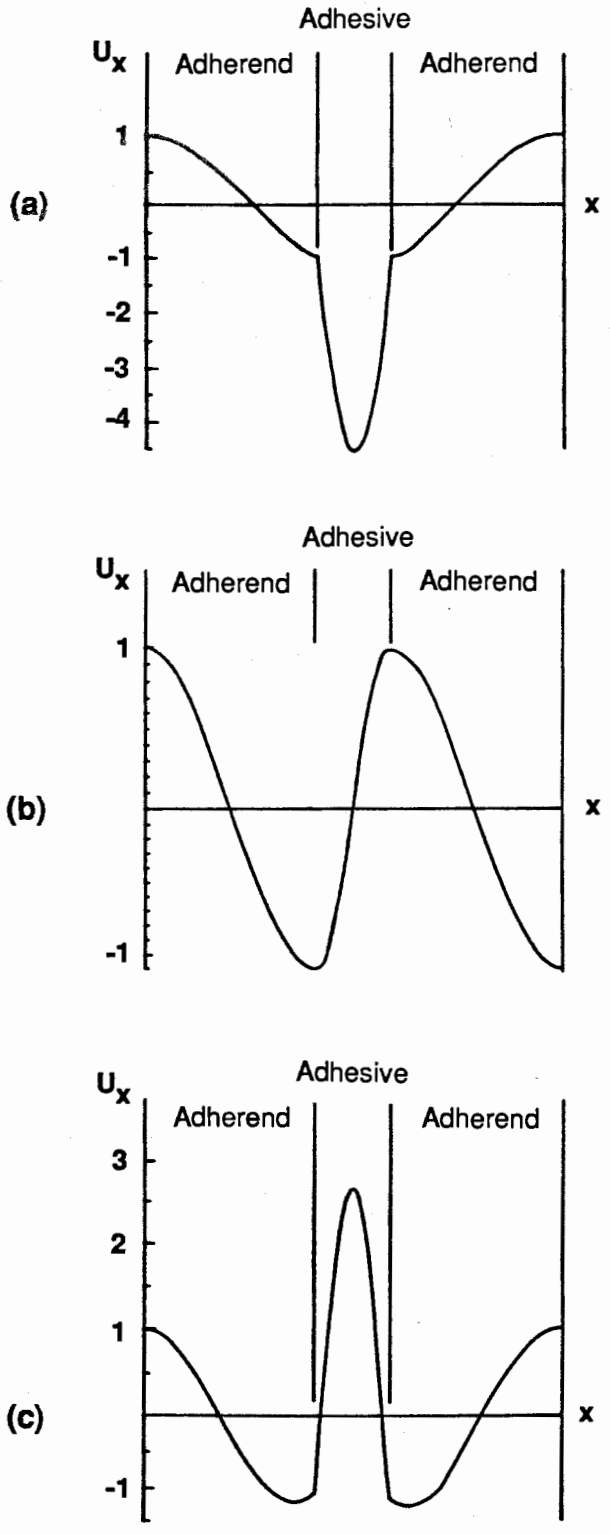

Figure 6.7 **Longitudinal or Through Thickness Mode Shapes of a Joint with 0.69 mm Thick Adhesive** (a) second mode (b) third mode (c) fourth mode

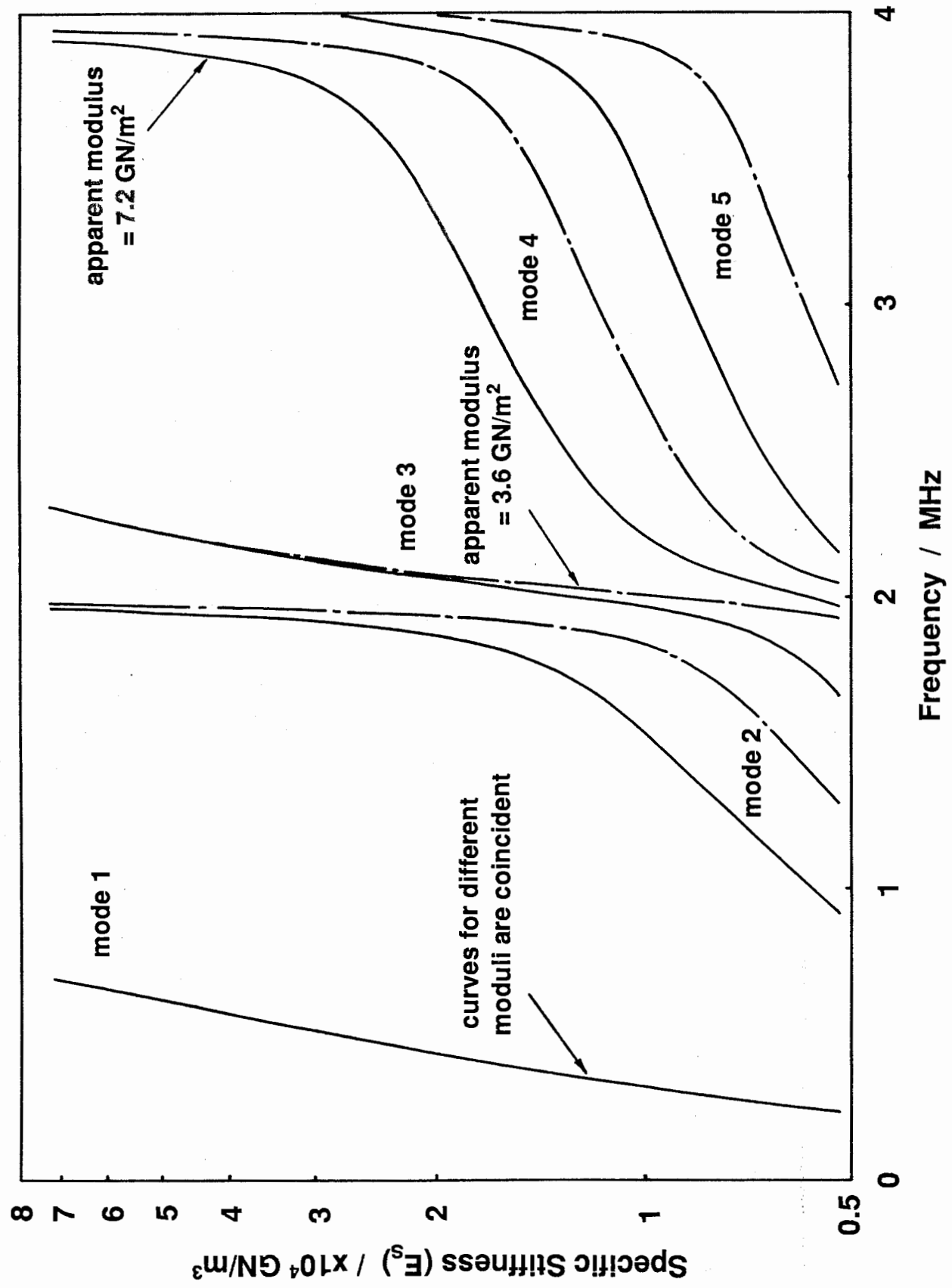

Figure 6.8 **Frequency of First Five Longitudinal or Through Thickness Modes of a Joint as a Function of Specific Adhesive Stiffness** (1.6 mm aluminium adherend)

CHAPTER 7
Experimentally Measured Spectra of Adhesive Joints

1 Introduction

The resonant frequencies of two sets of joints were measured over a wide range of adhesive thicknesses using ultrasonic spectroscopy. The specimens used were single lap joints with nominally 1.6 mm thick aluminium adherends which were prepared by grit blasting and degreasing, making them similar to the joints used in the investigation of the Fokker Bond Tester; details of the adhesives used are given in the Appendix. A typical high modulus epoxy, which would be specified for joints designed to carry high stresses, was used for one set of joints, a rubbery gap filling adhesive being used for the other set. Variations in adhesive thickness were obtained by shimming the joint while it cured.

Two ultrasonic probes were used to test the joints because the bandwidth of the probe described in Chapter 5 (10 MHz Nortec), and used for the work on the plain plate, was insufficient to excite the first mode of the joint which occurs at a frequency of 0.3 to 0.75 MHz. The second probe (a Wells Krautkramer H1N) had a centre frequency of approximately 1 MHz and a useable bandwidth (20 dB below the maximum) of approximately 0.3 to 1.75 MHz, see figure 7.1. It could therefore be used to excite modes of the joint below the useable bandwidth of the higher frequency probe.

Both probes were used in pulse echo mode with the same set-up described in Chapter 5, the probe to joint distance being approximately 90 mm. Figures 7.2 and 7.3 show the measured time histories from a typical joint with 1.6 mm thick aluminium adherends using the low frequency probe (H1N) and the high frequency probe (10 MHz Nortec) respectively. Even when the higher frequency probe was used it was not possible to resolve the echoes from the top of the joint and the top adhesive.

Some authors (Lloyd and Wadhawani, 1978) suggest editing the digitised data from the joint by removing the large echo from the top of the joint that is in anti-phase to the other main echoes. The resonant frequencies of the joint

then appear as maxima in the spectrum since the main echoes then have the same phase.

However, as there was no clear distinction in the time domain between the echo from the top face and the subsequent echoes, the top face echo could not be edited accurately from the remaining echoes. Consequently, the spectrum was calculated without editing the digitised data and the resonant frequencies of the joint occured as minima in the spectra, see Chapter 4.

2 Through Thickness Modes of the Joint

2.1 Dependence of the Resonant Frequencies of a Joint on the Adhesive Thickness

Figure 7.4 shows the predicted and measured frequencies of the first eleven through thickness modes of the single lap joints as a function of adhesive thickness. The joints were made with 1.6 mm thick adherends and a high modulus adhesive (Type B, apparent modulus = 7.2 GN/m^2, see the Appendix). The adhesive thickness of each joint was determined from the overall joint thickness in the area where the test was carried out.

The resonant frequencies of the first mode were determined using the lower frequency probe (HIN) whereas the frequencies of the second mode and above were obtained using the higher frequency probe (10 MHz Nortec). Figure 7.4 shows that there is very good agreement between the predicted and measured values of the through thickness resonant frequencies of the joint. There are less points shown for the first mode than for the higher modes because measurements were only taken at one position in the overlap of the joint. Measurements for the higher modes were typically taken at three positions within the overlap.

Figure 7.5a shows the spectrum, using the high frequency probe, of a typical joint with an adhesive thickness of 0.43 mm. Figure 7.5b shows the spectrum of a similar joint but with an adhesive thickness of 0.53 mm. The frequency of each mode shown in figure 7.5b is less than that of the corresponding mode shown in figure 7.5a owing to the increase in thickness of the adhesive. For example the tenth mode occurs at a frequency of 7.85 MHz in figure 7.5a this then decreases to 7.17 MHz when the adhesive thickness is increased to 0.53

mm (see figure 7.5b). As the adhesive thickness is increased further, to 0.62 mm, the frequency of the tenth mode decreases to 6.55 MHz, see figure 7.5c.

Figure 7.6 shows the predicted and measured frequencies of the first eleven through thickness modes of the joints made with the low modulus adhesive (Type C, apparent modulus = 3.6 GN/m^2, see the Appendix) as a function of adhesive thickness. This shows that for a given adhesive thickness, the resonant frequency of each mode is lower than that made with the high modulus adhesive, see figure 7.4. For example, when the adhesive thickness is 0.43 mm the tenth mode occurs at 6.38 MHz in the case of the low modulus adhesive, and at 7.85 MHz in the case of the high modulus adhesive.

To demonstrate the effect of a change in adherend thickness, figure 7.7 shows the predicted and experimentally measured through thickness resonant frequencies of single lap joints made with the high modulus adhesive and 1.55 mm thick adherends in the range of adhesive thickness of 0.1 to 0.2 mm. The solid curve represents the predicted frequencies for the joints with 1.55 mm thick adherends while the dashed line shows the frequencies for the 1.6 mm thick adherends. Figure 7.7 shows that there is good agreement between the predicted and measured values of the resonant frequencies for both thicknesses of adherend. In addition, figure 7.7 shows that the approximately 3% decrease in thickness of the adherends causes a similar increase in the resonant frequency of all the modes of the joint in this thickness range.

2.2 Damping

In addition to showing how the frequency of the modes change adhesive thickness, figure 7.5 also shows how the apparent damping or widths of the resonant peaks change with adhesive thickness. For example, there is a large increase in the resonant width, and hence damping, of the tenth mode, when the thickness is increased from 0.43 to 0.53 mm, see figure 7.5a and 7.5b. However, when the thickness is increased further to 0.62 mm, see figure 7.5c, the resonant width of the tenth mode does not change significantly.

The spectra shown in figure 7.5 were produced using a sampling frequency of 50 MHz, hence the spacing between the spectral lines is approximately 5 KHz, see table 5.1. Therefore, there are at least ten measured points between the

half power points of each minima seen in figure 7.5, so the observed changes in resonant width are not simply due to inadequate frequency resolution being employed.

The change in damping with thickness is due to a change in the strain energy in the adhesive and can be explained by examining the corresponding mode shapes of the joint, see figure 7.8. In the case of the tenth mode the calculated strain energy in the adhesive increases by a factor of approximately 15 when the adhesive thickness increases from 0.43 to 0.53 mm. When the adhesive thickness is increased further to 0.62 mm the strain energy in the adhesive is approximately halved.

Table 7.1 shows how the predicted damping (Q factor) of the tenth mode, calculated using the method described in Chapter 6, changes as the adhesive thickness is increased. This shows that there is good agreement between the observed changes in damping of the tenth mode and the predicted values, e.g. the predicted Q factor decreases from 256 to 62 when the adhesive thickness is increased from 0.43 to 0.53 mm.

Other modes of the joint, for example the twelfth (see figure 7.5), show a decrease in apparent damping as the adhesive thickness decreases. This is also explained by a change in the strain energy in the adhesive, the strain energy in the twelth mode decreasing as the adhesive thickness increases from 0.43 to 0.62 mm.

2.3 Dependence of the Resonant Frequencies of the Joint on its Cohesive Properties

2.3.1 First Mode of the Joint

Figure 7.9 shows the predicted and measured resonant frequency of the first mode of the joint as a function of specific adhesive stiffness, the experimental results representing data from joints made with both a high and low modulus adhesive. The specific stiffness, E_S, of the joint was calculated from the independently measured apparent modulus and the thickness; the adhesive thickness was determined by measuring the overall joint thickness and subtracting the adherend thicknesses.

It was shown in Chapter 6 that the first through thickness resonant frequency of the joint is not dependent on the adhesive thickness and modulus separately but on the specific adhesive stiffness, defined as the ratio of the apparent adhesive modulus to its thickness. Figure 7.9 shows that there is good agreement between the measured frequencies of the first mode and the frequencies predicted using the receptance model described in Chapter 6. In particular, the measured resonant frequencies of the joints made with the different adhesive moduli fall on the same curve.

The chain line seen in figure 7.9 represents the resonant frequency of the mass-spring-mass model for the first mode of the joint given by eqn. (6.1). This shows that at low specific stiffnesses (less than 10^4 GN/m^3) there is good agreement between the two models: the mass-spring-mass model gives frequencies that are less than 5% higher than those given by the receptance model. However, at higher adhesive stiffnesses, (greater than 10^4 GN/m^3), the mass-spring-mass model gives frequencies that are significantly higher than the receptance model. This occurs because the adherends do not behave as rigid masses at specific adhesive stiffness greater than 10^4 GN/m^3, and the adherend stiffness influences the resonant frequency of the mode. Indeed, at very high adhesive stiffness (greater than approximately 10^6 GN/m^3) the resonant frequency of the first mode approaches that of the first mode of a plain plate having the same overall thickness as the joint (approximately 1 MHz in this case).

2.3.2 Higher Modes of the Joint

Figure 7.10 shows the results, for the sixth and seventh modes, seen in figure 7.4 and 7.6 plotted as a function of specific stiffness instead of thickness. The specific stiffness of each joint was calculated from the measured apparent adhesive modulus and thickness in a similar way to that described above for the first mode of the joint.

As can be seen from figure 7.10, there is good agreement between the measured resonant frequencies of the joint and those predicted using the receptance model described in Chapter 6 for both values of modulus. The other measured modes of the joint also show good agreement with predicted frequencies, (see figure 6.8) but for clarity have not been shown in figure 7.10.

Figure 7.10 also shows that the resonant frequencies of joints having the same specific stiffness, but having different adhesive moduli and thicknesses, are not the same. Consequently it should be possible to distinguish changes in adhesive thickness from those in adhesive modulus by measuring the frequencies of the higher modes of the joint.

3 Shear Modes of the Joint

Although the experimental work was done with the probe at normal incidence, the probes used generated edge waves which have been shown to excite shear modes of the component under test even at normal incidence, see Chapter 5. Consequently, in addition to the through thickness modes of the joint seen in figures 7.5a-c there are also some shear modes of the joint, marked S_A, S_B.

The frequencies of the shear modes of the joint can be predicted using the same model as that used to predict the longitudinal or through thickness modes of the joint described in Chapter 6, the apparent shear moduli of the adhesive and adherend being used instead of the apparent longitudinal moduli. However, in practice, only two of the predicted shear modes are clearly seen in the measured spectra, and it is likely that these appear because they involve a neglible amount of shear deformation in the adhesive, and hence are relatively lightly damped. The shear modes of the joint that involve larger amounts of shear deformation are likely to be heavily damped since the material damping is greater for the shear modes than the longitudinal modes (Madigosky and Fiorito, 1979).

4 Conclusions

It has been shown that there is good agreement between the measured resonant frequencies of the through thickness modes of a joint and the predicted values obtained from the receptance model described in Chapter 6. The model has also been used to explain qualitatively the changes in apparent damping of the resonances that occur as the adhesive stiffness changes.

The results in the first mode show that its resonant frequency is only dependent on the specific stiffness of the adhesive i.e. a given percentage increase in adhesive thickness has exactly the same effect as a given

percentage decrease in modulus (see Chapter 6). It has been demonstrated that, apart from the first mode, the measured resonant frequencies of the joint are dependent on the adhesive modulus and stiffness separately. Therefore, the results confirm that ultrasonic spectroscopy should be able to distinguish changes in adhesive thickness from those in modulus whereas the Fokker Bond Tester cannot, see Chapters 2 and 3.

Adhesive Thickness (l_2) mm	Q Factor	Calculated Total Strain Energy in the Adhesive (relative to that at an Adhesive thickness of 0.43 mm)
0.43	256	1
0.53	62	15.5
0.62	92	6.7

Table 7.1 **Predicted Q Factor of the Tenth Mode for Various Thicknesses of the Adhesive**

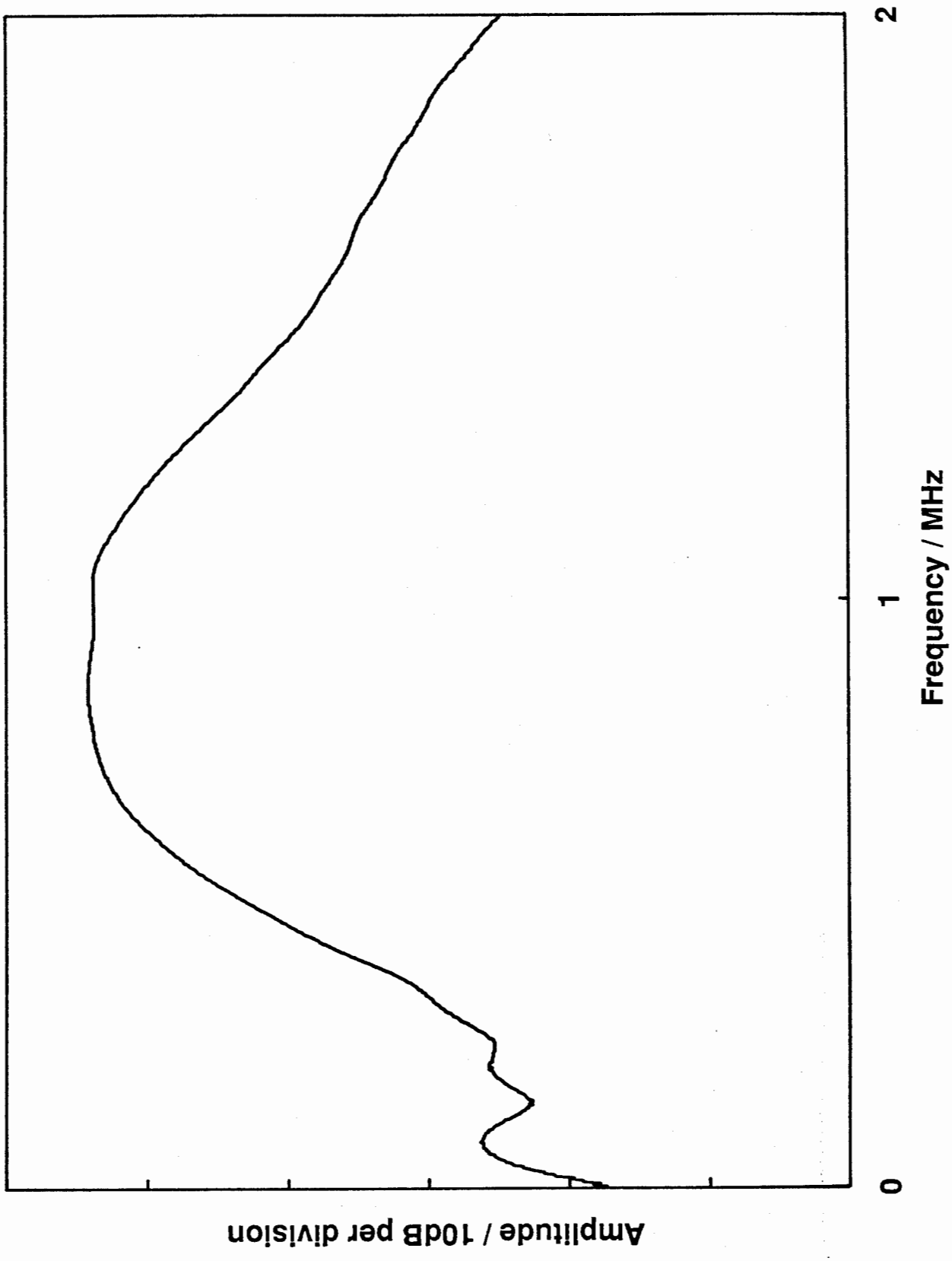

Figure 7.1 **Frequency Response of 1 MHz Krautkramer Transducer**

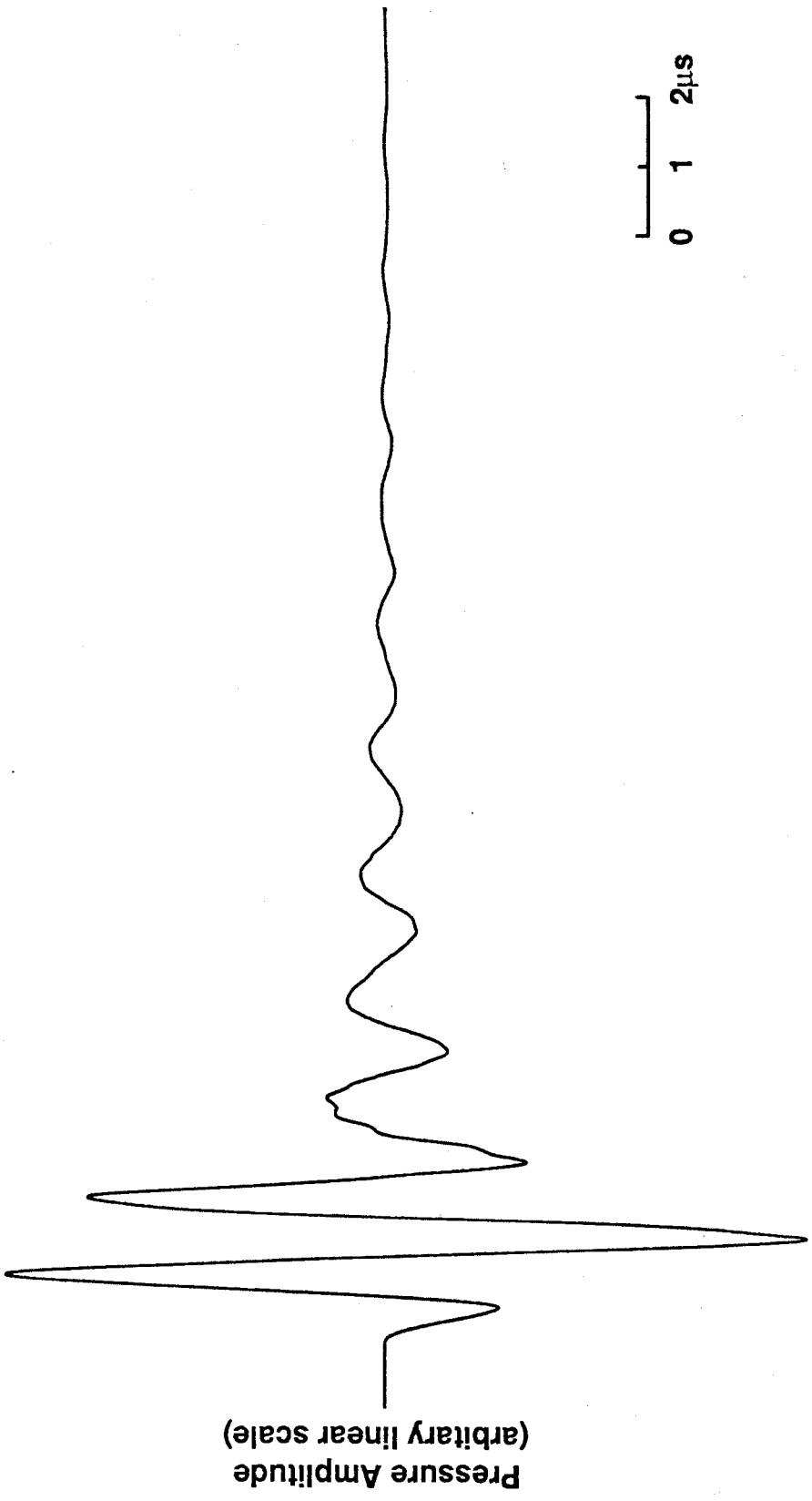

Figure 7.2 **Measured Time History from a Joint having ≈0.2 mm Thick Adhesive using the 1 MHz Probe** (1.6 mm thick adherends)

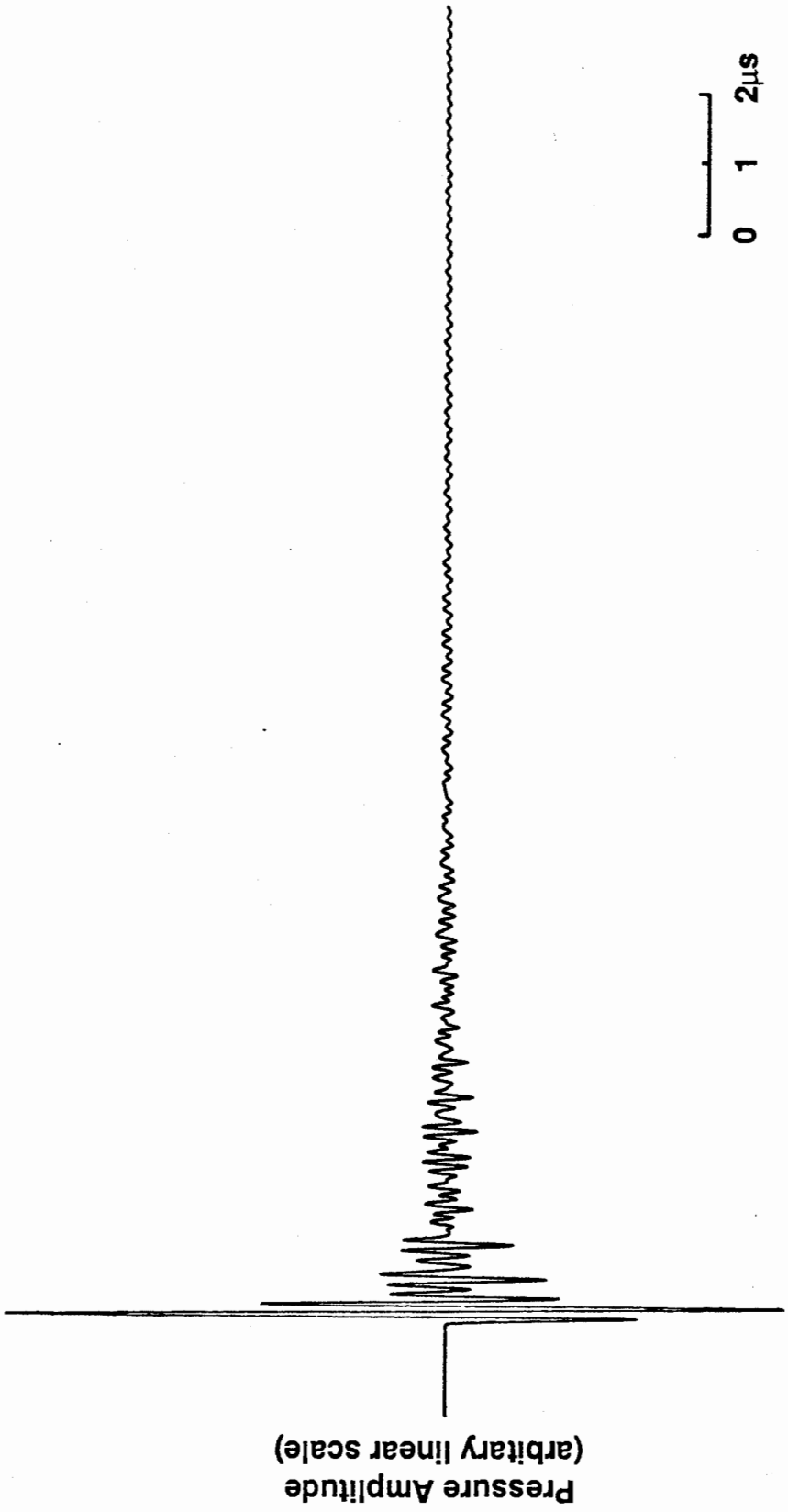

Figure 7.3 **Measured Time History from a Joint having ≈0.2 mm Thick Adhesive using the 10 MHz Probe** (1.6 mm thick adherends)

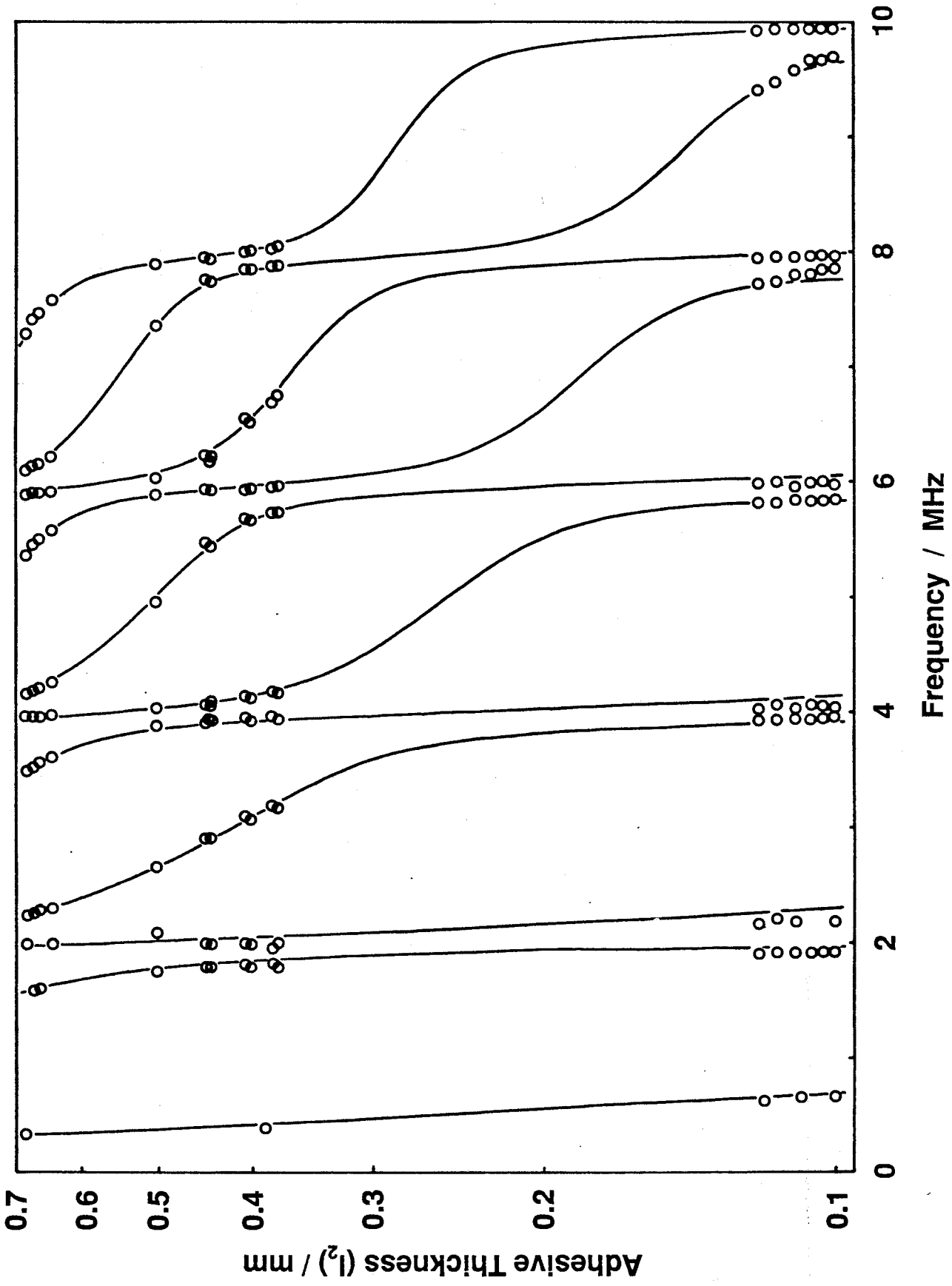

Figure 7.4 **Measured Frequency of First Eleven Through Thickness Modes of a Joint as a Function of Adhesive Thickness**
(1.6 mm thick aluminium adherends and apparent adhesive modulus of 7.2 GN/m^2)

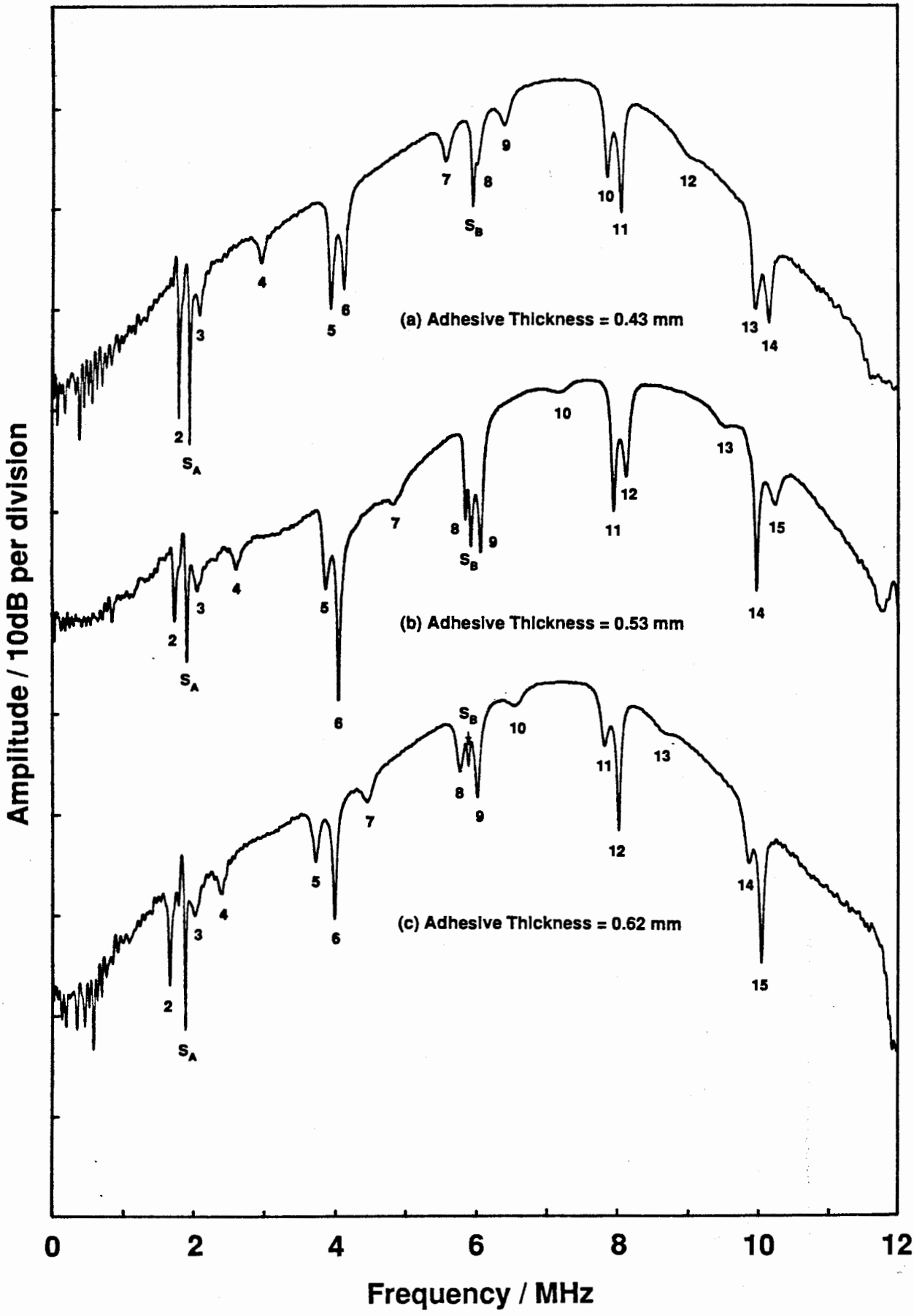

Figure 7.5 **Examples of Measured Spectra** (1.6mm thick aluminium adherends and apparent adhesive modulus of 7.9 GN/m^2)

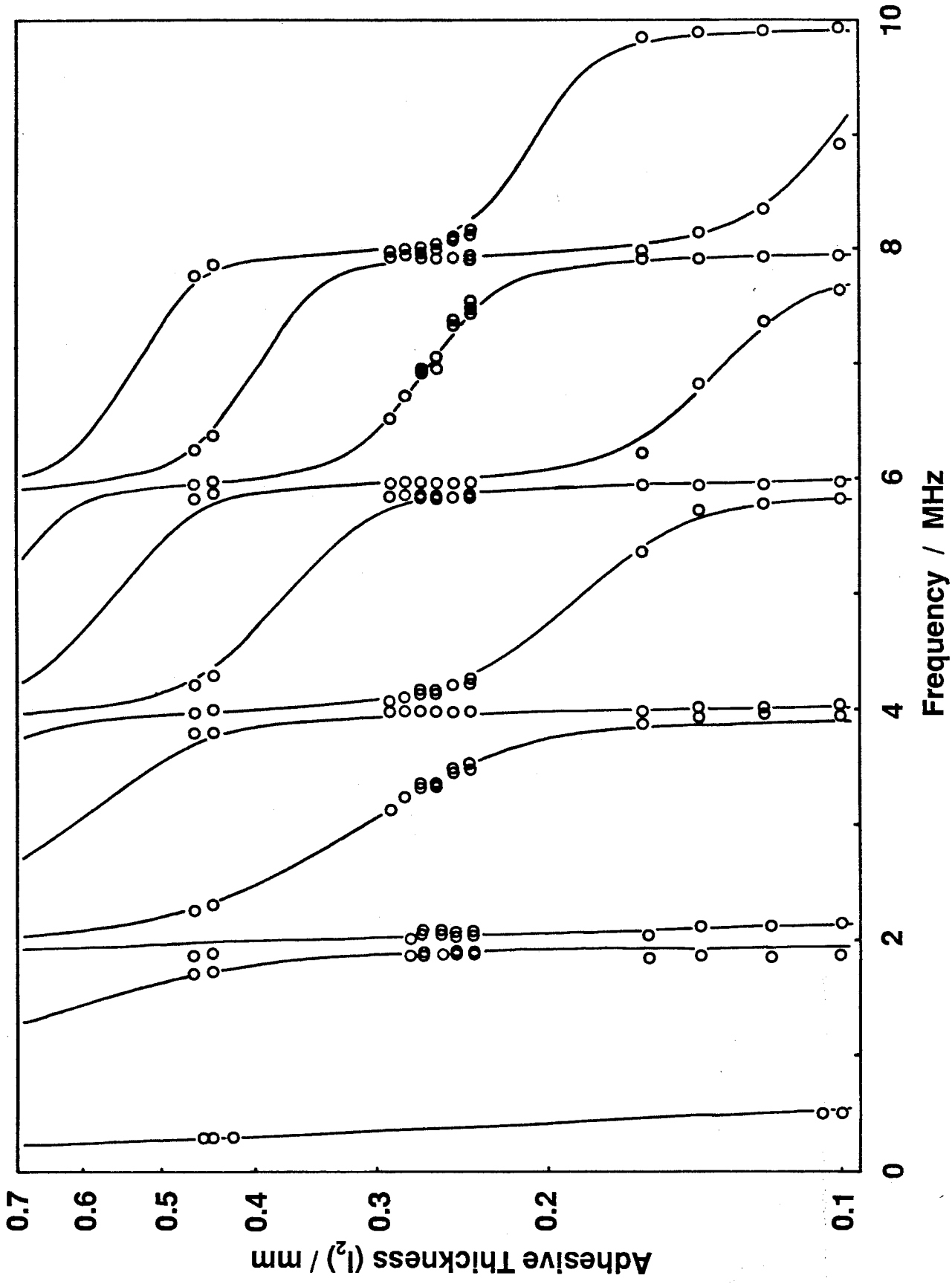

Figure 7.6 **Measured Frequency of First Eleven Through Thickness Modes of a Joint as a Function of Adhesive Thickness**
(1.6 mm thick aluminium adherends and apparent adhesive modulus of 3.6 GN/m^2)

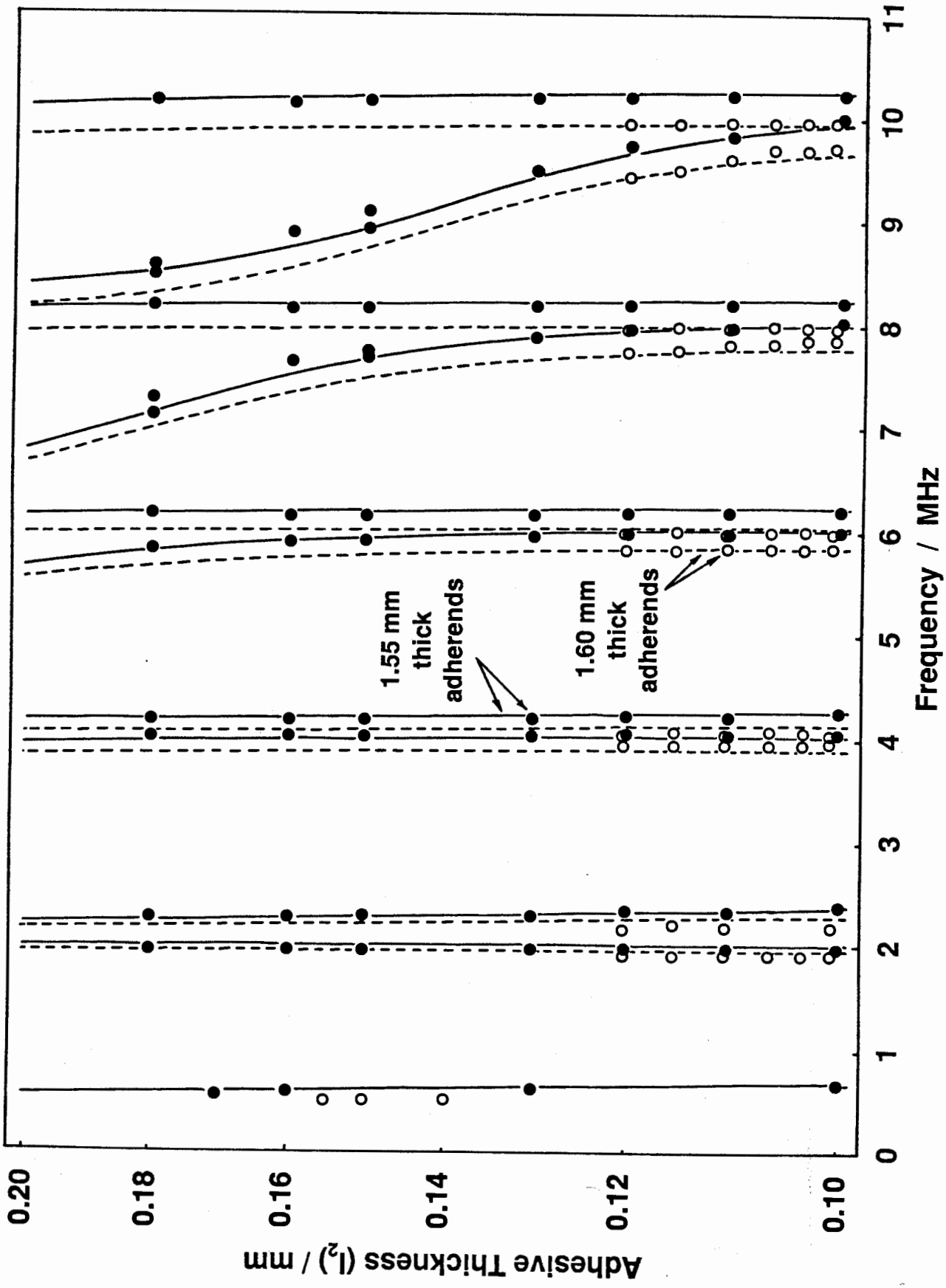

Figure 7.7 **Measured Frequency of First Eleven Through Thickness Modes of a Joint as a Function of Adhesive Thickness**
(apparent adhesive modulus of 7.2 GN/m²)

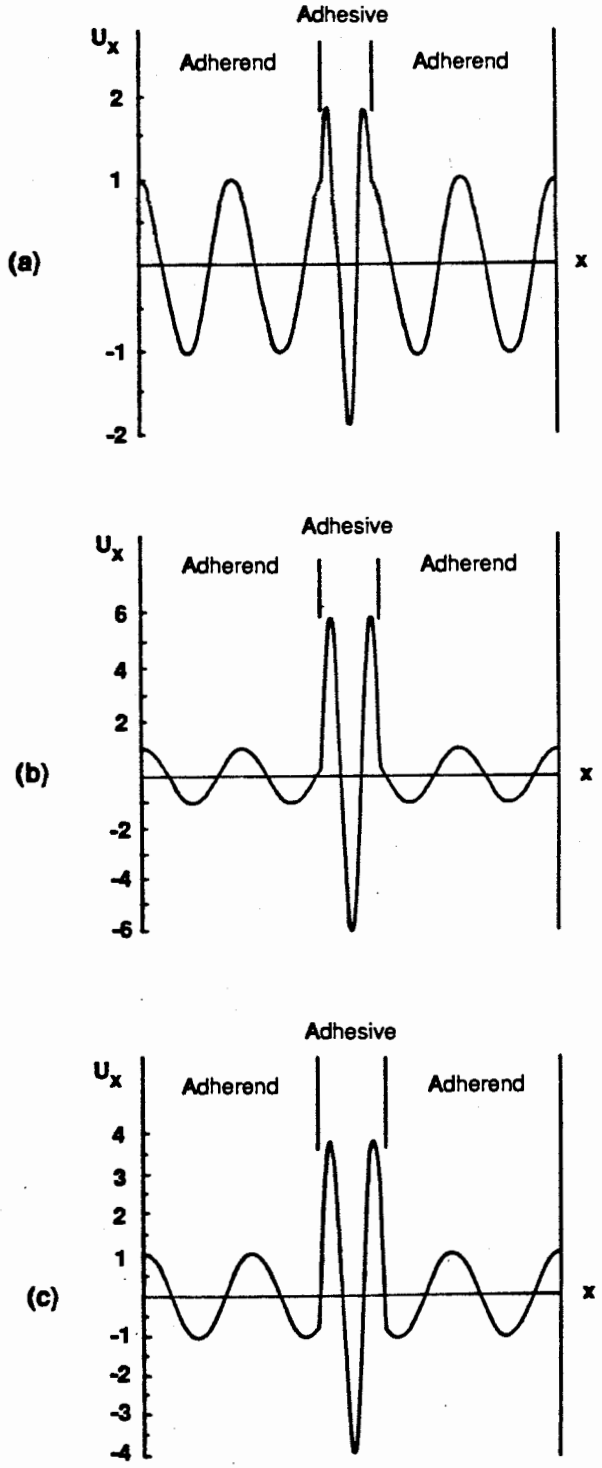

Figure 7.8 **Longitudinal or Through Thickness Mode Shapes of Joint** (a) 0.43 mm thick adhesive (b) 0.53mm thick adhesive (c) 0.62 mm thick adhesive

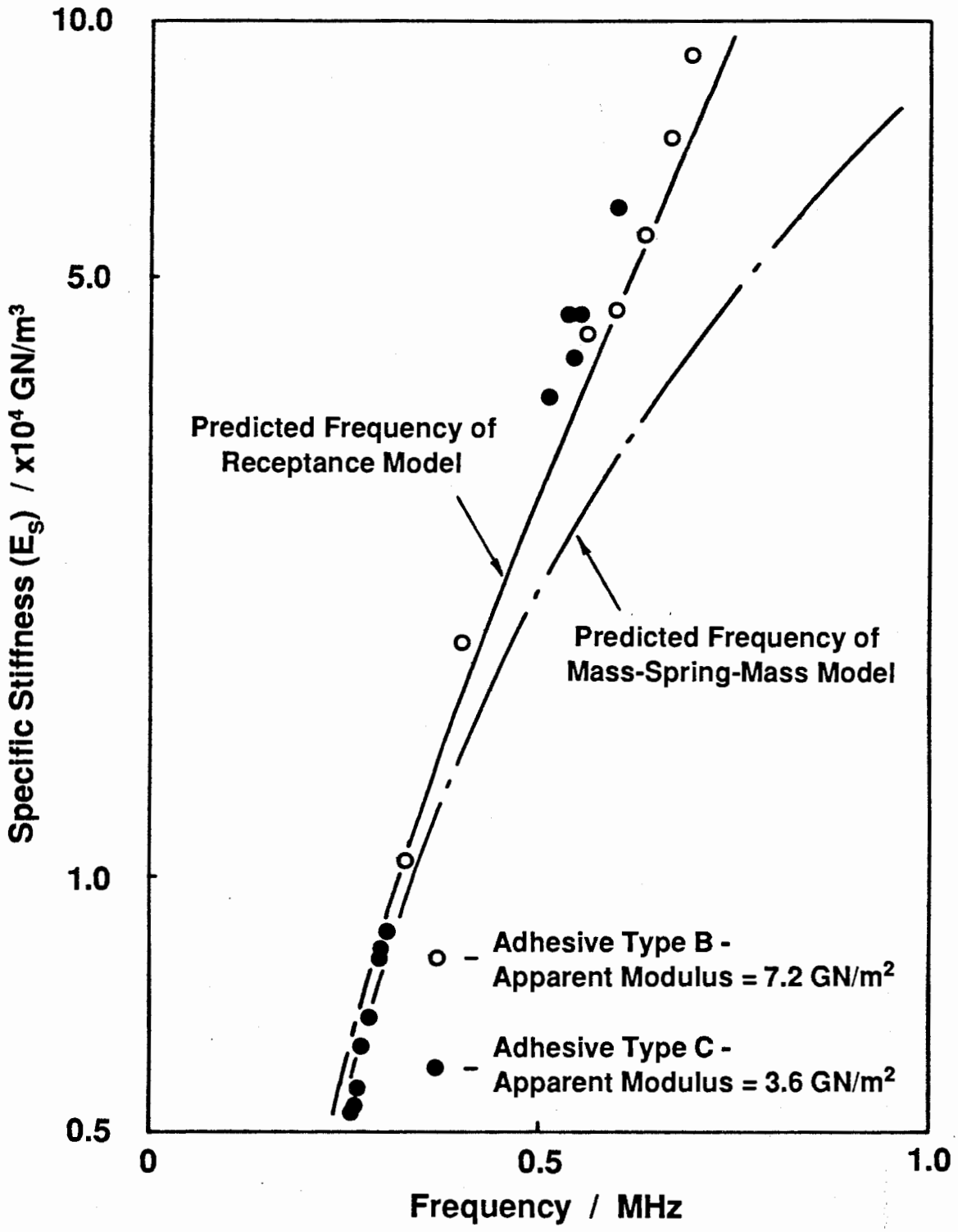

Figure 7.9 Frequency of First Through Thickness Mode of the Joint as a Function of Specific Adhesive Stiffness

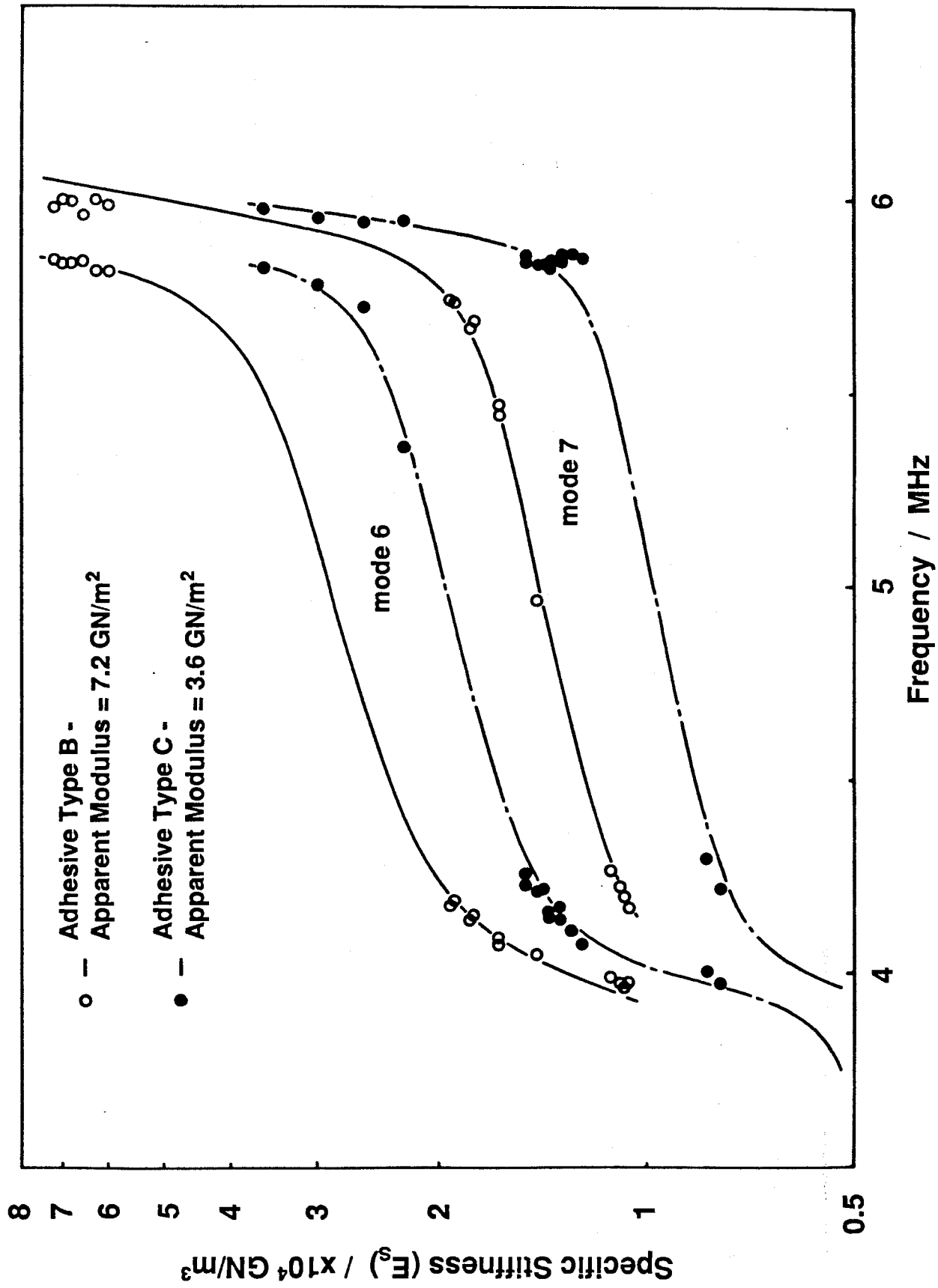

Figure 7.10 Frequency of Sixth and Seventh Through Thickness Modes of the Joint as a Function of Specific Adhesive Thickness

CHAPTER 8

Estimation of the Adhesive Modulus and Thickness from the Measured Resonant Frequencies

1 Introduction

In Chapter 7 it has been shown that there is a good correlation between the predicted spectra, calculated using the independently measured apparent adhesive modulus and thickness, and the experimentally measured spectra. In particular, it was shown that, apart from the first mode, the through thickness resonant frequencies of the joint depend on adhesive modulus and thickness separately. Therefore, by measuring the frequency of at least two modes of the joint it should be possible to determine both the adhesive modulus and thickness.

In order to use ultrasonic spectroscopy for the non-destructive tesing of adhesive joints it is necessary to obtain values for the adhesive modulus and thickness from the experimentally measured spectrum. Therefore, to evaluate the sensitivity of ultrasonic spectroscopy for measuring adhesive modulus and thickness, it was decided that the independently measured values of these properties should be compared with those determined from the measured spectra. No attempt will be made to correlate the changes in the measured spectra with the failure strength of the joint at this stage.

2 Determination of Cohesive Properties from the Measured Spectra

A unique solution for the adhesive modulus and thickness can theoretically be achieved by measuring the frequency of only two modes of the joint. However, the equations for adhesive modulus and thickness are ill conditioned, so any scatter in the experimental results would produce inaccuracies in the calculated values of adhesive modulus and thickness.

Consequently, to increase the accuracy of the calculated adhesive modulus and thickness, the frequencies of more than two modes (apart from the first) are measured. If the frequencies of n (where n is greater than 2) modes are

measured there will be n equations in two variables, the adhesive thickness and modulus. Since there is no solution to the set of n equations, the adhesive modulus and thickness are determined by calculating the square of the error between the predicted and measured values over a range of adhesive thicknesses (l_2) and moduli (E'_2). The values of adhesive modulus and thickness are then taken as those which give the minimum error. The error function, $E_r(E'_2,l_2)$, is defined as follows :-

$$E_r(E'_2,l_2) = \sum_{n=p}^{n=q} [\,(f_n(E'_2,l_2) - f_n^*)^2 / f_n(E'_2,l_2)\,] \qquad (8.1)$$

where $f_n(E'_2,l_2)$ is the predicted resonant frequency of the n^{th} longitudinal mode of the joint, f_n^* is the measured frequency of the n^{th} mode and, p and q are the start and finish modes for the summation procedure. However the modes used in the summation procedure need not be consecutive.

The resonant frequency of some modes of the joint are more dependent on changes in adhesive thickness and modulus than others, which influences the choice of start and finish modes used in eqn. (8.1). For example, figure 7.7 shows that at adhesive thickness of between 0.1-0.2 mm and an apparent modulus of approximately 7.2 GN/m^2 the lowest seven modes are practically independent of adhesive thickness. Consequently, the frequencies of these modes cannot be used successfully to determine the adhesive thickness. However, the eighth and tenth modes show a stronger dependence on adhesive thickness and can be used to determine the adhesive thickness more accurately.

The predicted frequencies, $f_n(E'_2,l_2)$, used in equation (8.1) were calculated for a wide range of adhesive thickness (l_2 = 0.1-0.7 mm) and apparent modulus (E'_2 = 2.8-8 GN/m^2), thus covering the entire range of cohesive properties of the joints used for the results seen in Chapter 7. The interval in adhesive thickness used in the calculations was 0.01 mm and that in the apparent modulus was approximately equal to 0.7 GN/m^2 i.e. 10% of the apparent modulus of the high modulus adhesive.

Table 8.1 shows an example of part of the error matrix, calculated using eqn. (8.1), from the predicted and experimental resonant frequencies for a typical joint. In this instance the experimental values are taken from a joint manufactured using a high modulus adhesive (apparent modulus ≈ 7.2 GN/m^2) and having a bond line thickness of approximately 0.38 mm.

The frequencies of the fourth to the eleventh modes of the joints were used to produce the matrix shown in table 8.1 (i.e. p=4 and q=11 in eqn. (8.1)), since these modes occured at frequencies that were strongly excited by the high frequency (10 MHz Nortec) transducer and hence could be accurately measured. The second and third modes of the joint were also excited by this transducer; however, figure 6.8 shows that the frequencies of these two modes are relatively independent of the adhesive thickness and modulus over a wide range of these properties.

Table 8.1 shows that there is a value of the adhesive thickness which produces a minimum in the error function at each value of modulus, thus forming a "trough" of minima across the error matrix. The adhesive modulus and thickness are taken to be the combination which produces the smallest error throughout the whole matrix. In this instance the minimum error occurs at an apparent modulus of 7.2 GN/m^2 and an adhesive thickness of 0.38 mm.

This procedure was used to determine values of the adhesive modulus and thickness from the experimental results presented in Chapter 7. The calculated values of modulus and thickness were then plotted as functions of the independently measured values.

Figure 8.1 shows the calculated adhesive thicknesses of the joints, manufactured from all the adhesive types (see the Appendix for details), as a function of the independently measured adhesive thicknesses. This shows that the results from all the adhesive types lie close to a line of unit slope passing through the origin.

The lines having gradients of 0.9 and 1.1, seen in figure 8.1, show that the maximum error between the calculated and independently measured bondline thickness is approximately 10%. However, it is important to note that the error involved in the independent measurement of adhesive thickness can equal

or exceed 10%, particularly, when the adhesive thickness is low. For example, although the adhesive thickness was independently determined to an accuracy of greater than 0.02 mm by measuring the overall thickness of the joint, this would result in an error of greater than 10% at bond line thicknesses of below 0.2 mm.

Also, the thicknesses of the joints were found to be non-uniform, there being a difference between the maximum and minimum values of up to 0.1 mm. Since it was difficult to ensure that the spectrum was obtained at exactly the same point at which the thickness was measured, further errors (up to 5%) could be introduced in the independently measured adhesive thickness.

Figure 8.2 shows the calculated adhesive modulus as a function of the value measured independently on a bulk specimen manufactured under the same conditions as the joint (see the Appendix). Since it is more difficult to vary the modulus of the adhesive experimentally than to vary its thickness, the measured values of modulus seen in figure 8.2, form three groups corresponding to the three adhesive moduli detailed in the Appendix. However, figure 8.2 shows that the results from joints having a wide range of adhesive thickness and modulus lie close to the line of unit slope passing through the origin.

In this instance, the maximum error between the calculated apparent modulus and the independently measured value is approximately 20%; the error in the independently measured value of the apparent adhesive moduli is typically less than 3 - 5%, see the Appendix for details.

3 Determination of Adhesive Porosity from Measured Spectra

The results presented so far have only considered changes in the cohesive properties of the adhesive i.e. a change in apparent modulus or thickness of the adhesive, the joints having no other types of defect. It is also important to detect porosity in a joint since it is likely to indicate a fault in the manufacturing process control. Under many circumstances conventional ultrasonic time domain techniques can be used to find porosity; however, when either the impedance of the adhesive is low, or when the adhesive is thin (less

than approximately 0.2 mm), porosity, like disbonds and voids, becomes difficult to detect, see Chapter 1.

Porosity of the adhesive in joints with metallic adherends is typically caused by inadequate degassing of the adhesive, or by air trapped between the adherends when the joint is made. Consequently, the volume of the adhesive in the adhesive layer is reduced. Figure 8.3 shows a typical example of porosity (approximately 25% reduction in area) caused by air trapped between the adherends.

Since the volume of the adhesive is reduced by porosity, the apparent modulus of the adhesive layer, measured over an area which is significantly greater than that of a single bubble, will also be reduced. Similarly, the apparent density of the adhesive layer will also be reduced. For example, 20% porosity of the adhesive causes 20% reduction in apparent modulus and density of the adhesive layer.

Since the frequency response of the joint is relatively insensitive to changes in density of the adhesive (see Chapter 6), small amounts of porosity producing less than a 10% change in density, have a similar effect on the resonant frequencies of the joint to that of a reduction in apparent modulus. Larger amounts of porosity (>10%) have a more complex effect on the resonant frequencies of the joint, and it is no longer possible to model the effect simply by assuming a change in apparent modulus. However, in practice it was found that it was very difficult to distinguish quite large degrees of porosity (approximately 20%) from similar changes in apparent modulus using the resonant frequencies of the joint.

The apparent damping or widths of the resonances (see Chapter 7) were found to be a more reliable indication of porosity than the change in frequency. Figures 8.4a and 8.5b show the spectra from two similar joints, manufactured with the same adhesive, and having similar adhesive thickness. Figure 8.4a shows the spectrum of the joint having no porosity and figure 8.5b shows the spectrum of the joint having approximately 20% porosity. The spectra show that, for example, the apparent damping of the eighth and tenth modes has increased significantly in the presence of porosity. It is also difficult to locate the resonant frequencies of some modes, for example the fourth, where

there is porosity.

This increase in damping appears to effect the modes at higher frequencies more than the lower ones, and is due to an increase in the apparent material damping of the adhesive. This occurs because the ultrasonic pulses are scattered by the air bubbles, thus reducing the amplitude of the echoes received from the joint.

4 Discussion

Figure 8.5 shows the specific stiffness of the joint calculated from the adhesive modulus and thickness, determined using the method described in Section 2, as a function of the adhesive thickness, also determined using the method described in Section 2, for all the joints tested. The curves on figure 8.5 are lines of constant modulus, and represent the values of apparent moduli used to evaluate the error matrix. This shows that joints having similar adhesive stiffness, but manufactured from adhesives with different moduli, and hence having different strengths, can be distinguished clearly using ultrasonic spectroscopy.

In practice, a plot of specific stiffness against adhesive thickness could be used to specify pass and fail limits in a non-destructive test. For example joints which had adhesive thicknesses outside of a predetermined range, regardless of their modulus, could be distinguished and rejected. Similarly, joints with the correct specific stiffness but having a low modulus, perhaps resulting from an incorrect cure cycle, could also be distinguished.

It is important to note that, since it is not possible to resolve echoes from the top and bottom of the adhesive using commonly available ultrasonic transducers, when the adhesive thickness is less than approximately 0.5 mm (see Chapter 1), a similar result cannot be achieved using time domain based techniques. In addition, when the impedance of the adhesive is low relative to the adherends the echoes from the bottom of the adhesive become very small and are difficult to monitor. Changes in the magnitude of echoes from the bottom of the adhesive, due to variations in the cohesive properties, are then easily masked by echoes from other parts of the joint.

It can be readily shown however, that ultrasonic spectroscopy can be used to increase the effective resolution of a typical ultrasonic probe. For example, the maximum useable frequency of the higher frequency probe, used in the experimental work described in Chapter 5 was found to be approximately 10 MHz. From eqn. (4.43) it can be shown that the minimum thickness of an aluminium plate to have its first through thickness resonance at or below 10 MHz is approximately 0.3 mm. However, in the time domain it was found that resolution of the separate echoes from an aluminium plate, using the same probe, became difficult at approximately 1.5 mm (see figure 7.3). Consequently, the minimum thickness of plate that can be distinguished is approximately five times less when the frequency domain is used than when the time domain is used.

Using conventional techniques, it is also difficult to distinguish porosity when the adhesive is thin (<0.5mm) or its impedance is very low. Whilst initial work has shown that it is difficult to quantify the extent of the porosity using ultrasonic spectroscopy, it has been shown that changes in the apparent damping can be used as an indication of its presence. For example, the impedance of the Type C adhesive was low ($\approx 1.9 \times 10^6$ Kg/s.m^2) relative to that of the adherends ($\approx 17.3 \times 10^6$ Kg/s.m^2) and this prevented the joints from being C-Scanned in the conventional manner, see Chapter 1. However, by obtaining the spectrum of the echoes the adhesive modulus and thickness could be determined and porosity could be identified using the apparent damping of the resonances.

To test adhesive thicknesses below the minimum examined here (0.1 mm) the frequencies of modes above 10 MHz need to be measured. This is necessary because the modes in the range 1-10 MHz are practically independent of adhesive thickness at bond line thicknesses less than 0.1 mm, and hence cannot be used to determine the adhesive thickness. However, the modes above 10 MHz are more dependent on changes in adhesive thickness at thin bond lines, and so can be used to determine the adhesive thickness.

5 Conclusions

It has been shown that the cohesive properties of a joint (i.e. the adhesive modulus and thickness) can be independently determined using ultrasonic

spectroscopy. This enables joints which have the same specific adhesive stiffness yet have different adhesive moduli and hence strengths to be distinguished.

Current work has shown that changes in adhesive thickness of approximately 10% and of adhesive modulus of approximately 20% can be detected separately in joints having specific stiffnesses upto $8x10^4$ GN/m^3. However it is likely that these limits could be reduced by using a more sophisticated error function than that employed here (eqn. 8.1). Further work needs to be carried out in this topic.

At present ultrasonic spectroscopy can be used to give a check on the cohesive properties of the adhesive, a change in its modulus or thickness from the "normal" values indicating a fault in the curing process. No attempt has been made to correlate the changes of the spectra with the failure strengths of the joint at this stage. It is therefore esssentially a check on the process control rather than a direct prediction of joint strength. Nevertheless, such a test is valuable since there is at present no means of determining the cohesive properties of a joint non-destructively.

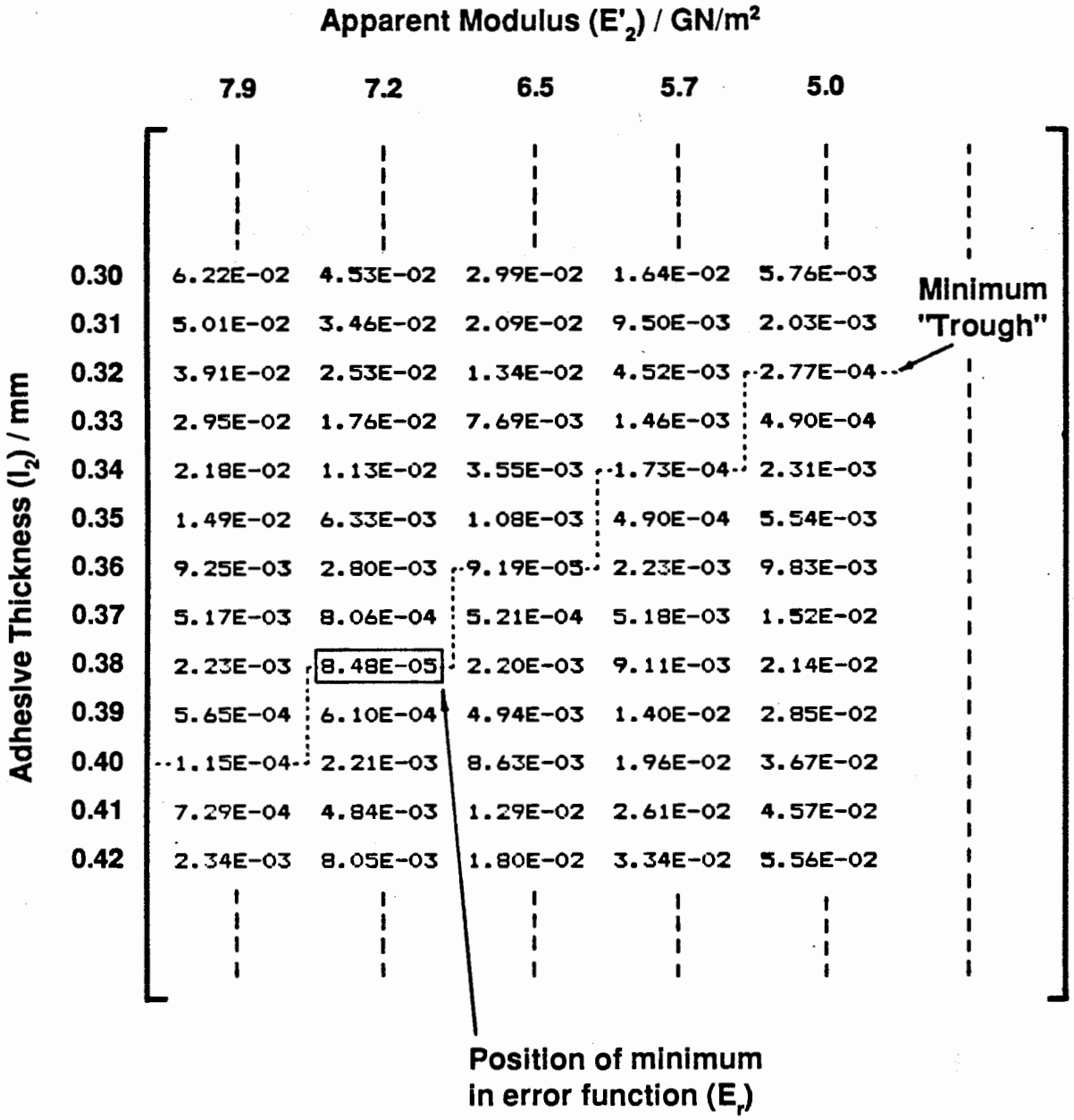

Table 8.1 **Example of Calculated Error Matrix**
(apparent adhesive modulus of 7.2 GN/m^2 and adhesive thickness of 0.38 mm)

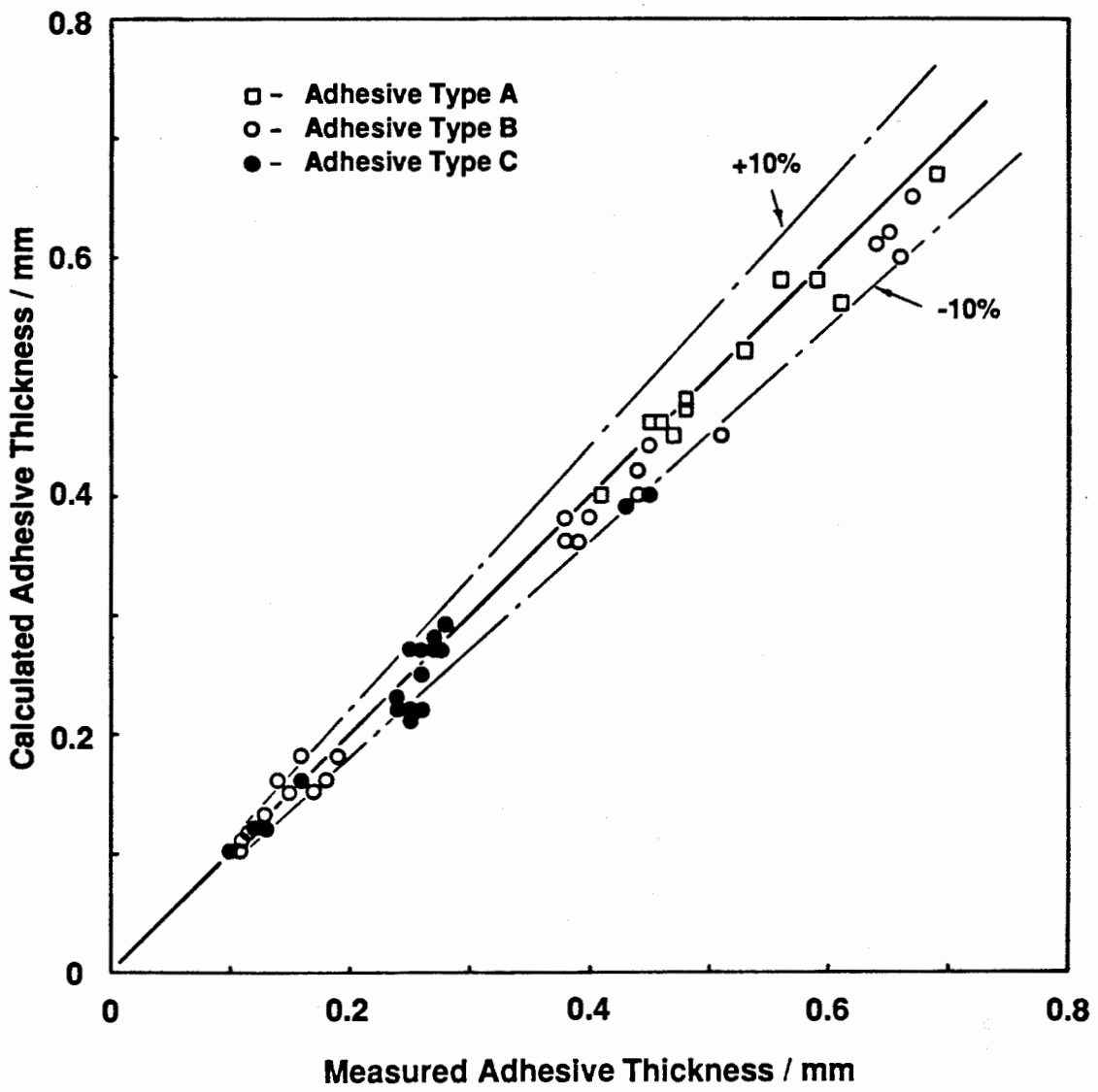

Figure 8.1 Calculated Adhesive Thickness as a Function of the Independently Measured Adhesive Thickness

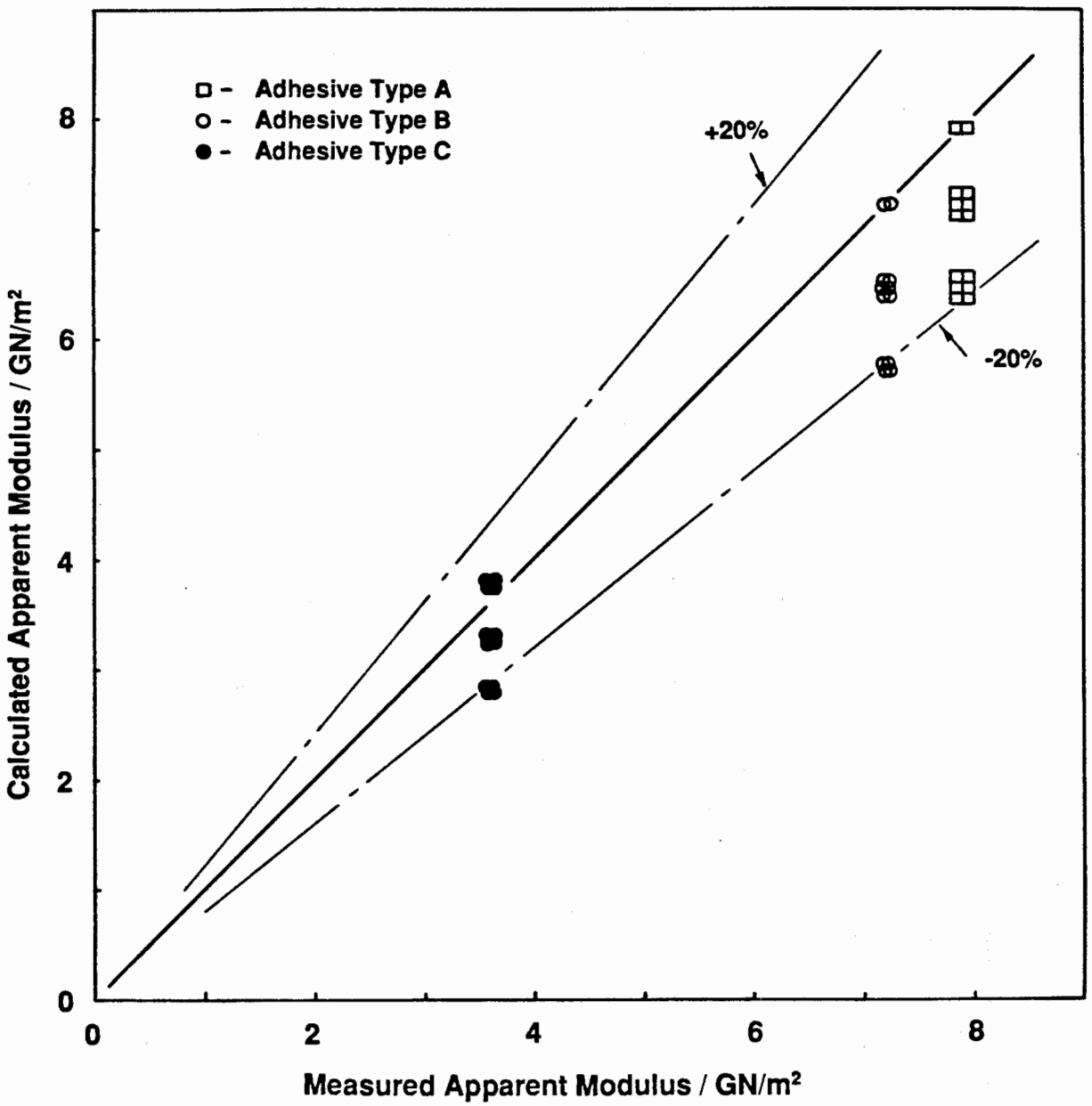

Figure 8.2 Calculated Apparent Adhesive Modulus as a Function of the Independently Measured Adhesive Modulus

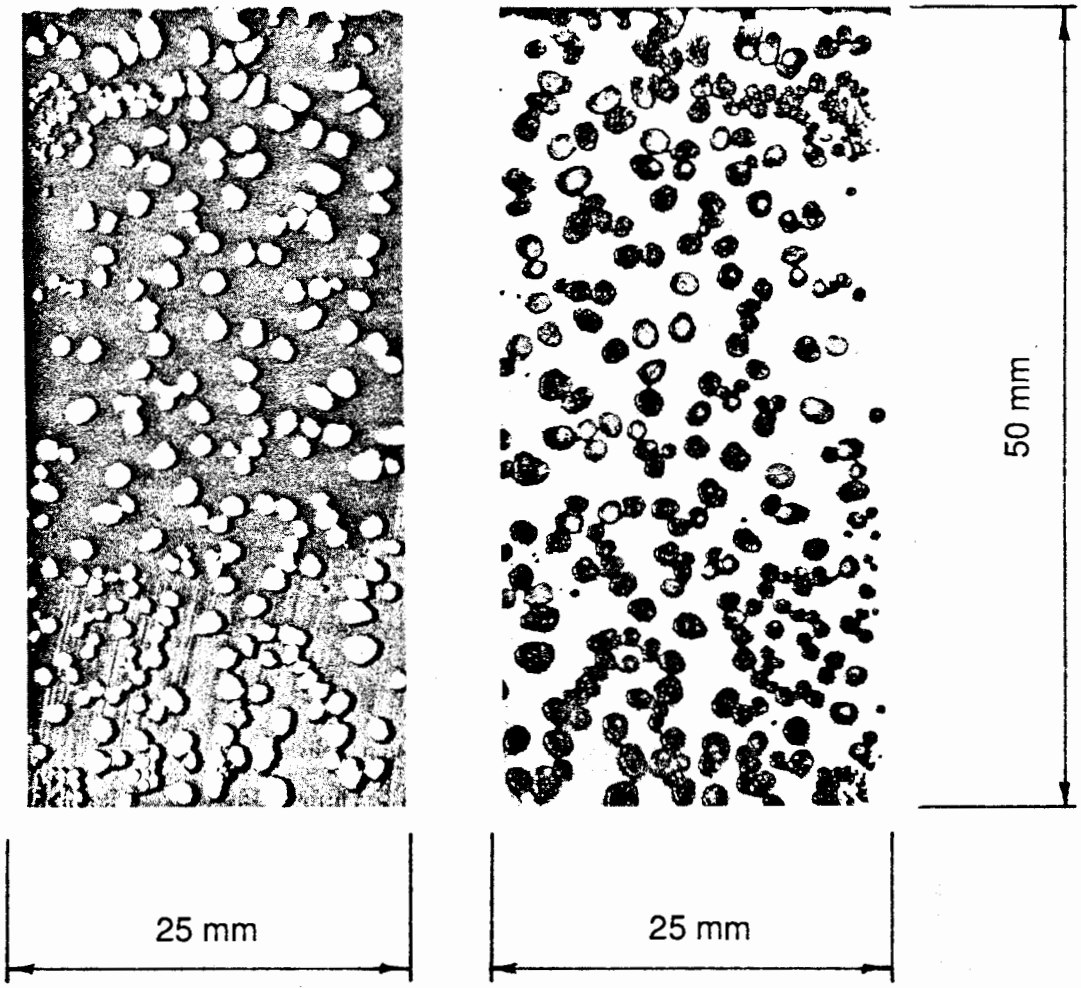

Figure 8.3 **Example of Adhesive Porosity.**
(a) surface of adhesive, (b) surface of adherend.

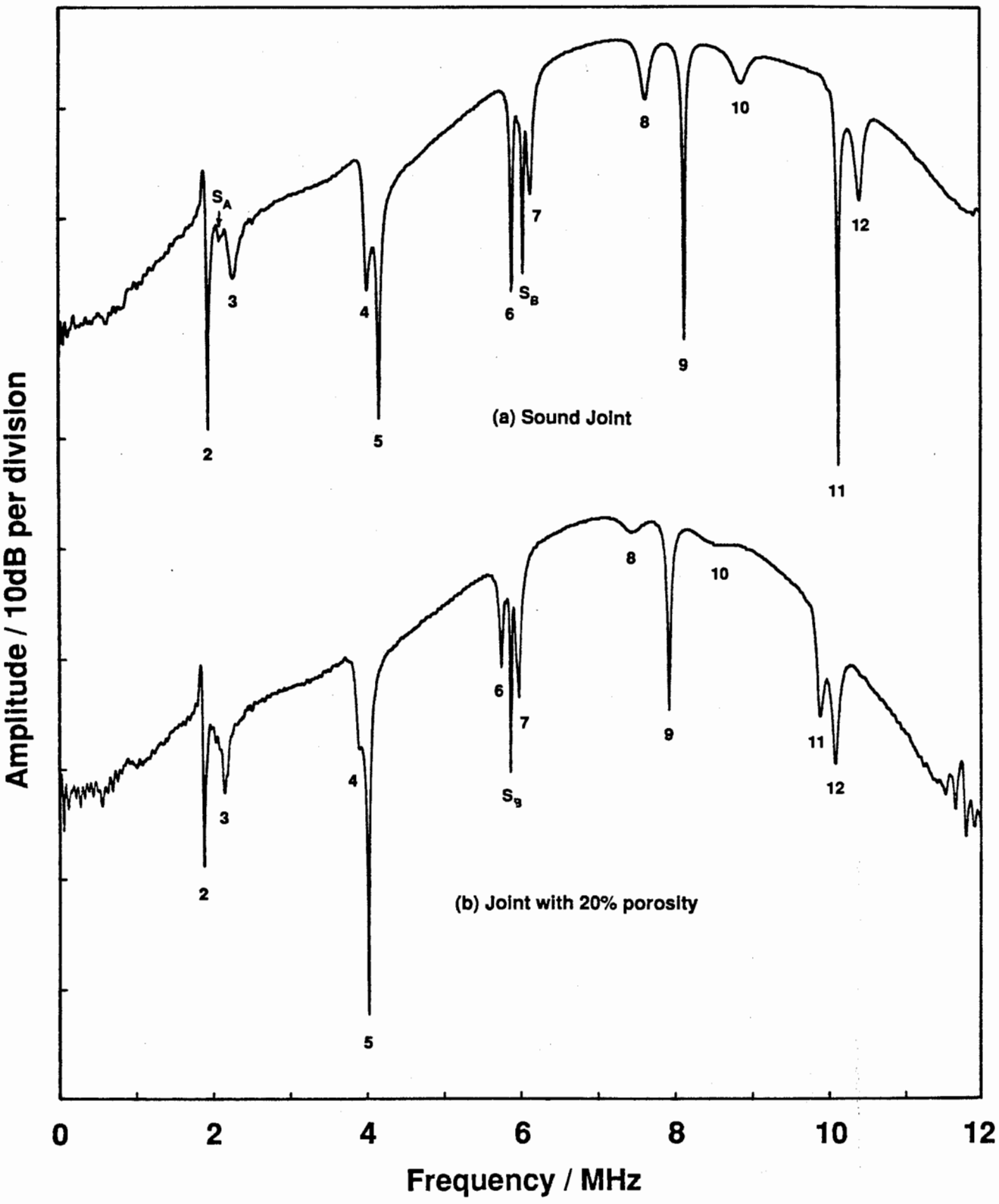

Figure 8.4 Spectra from Joints with and without Adhesive Porosity

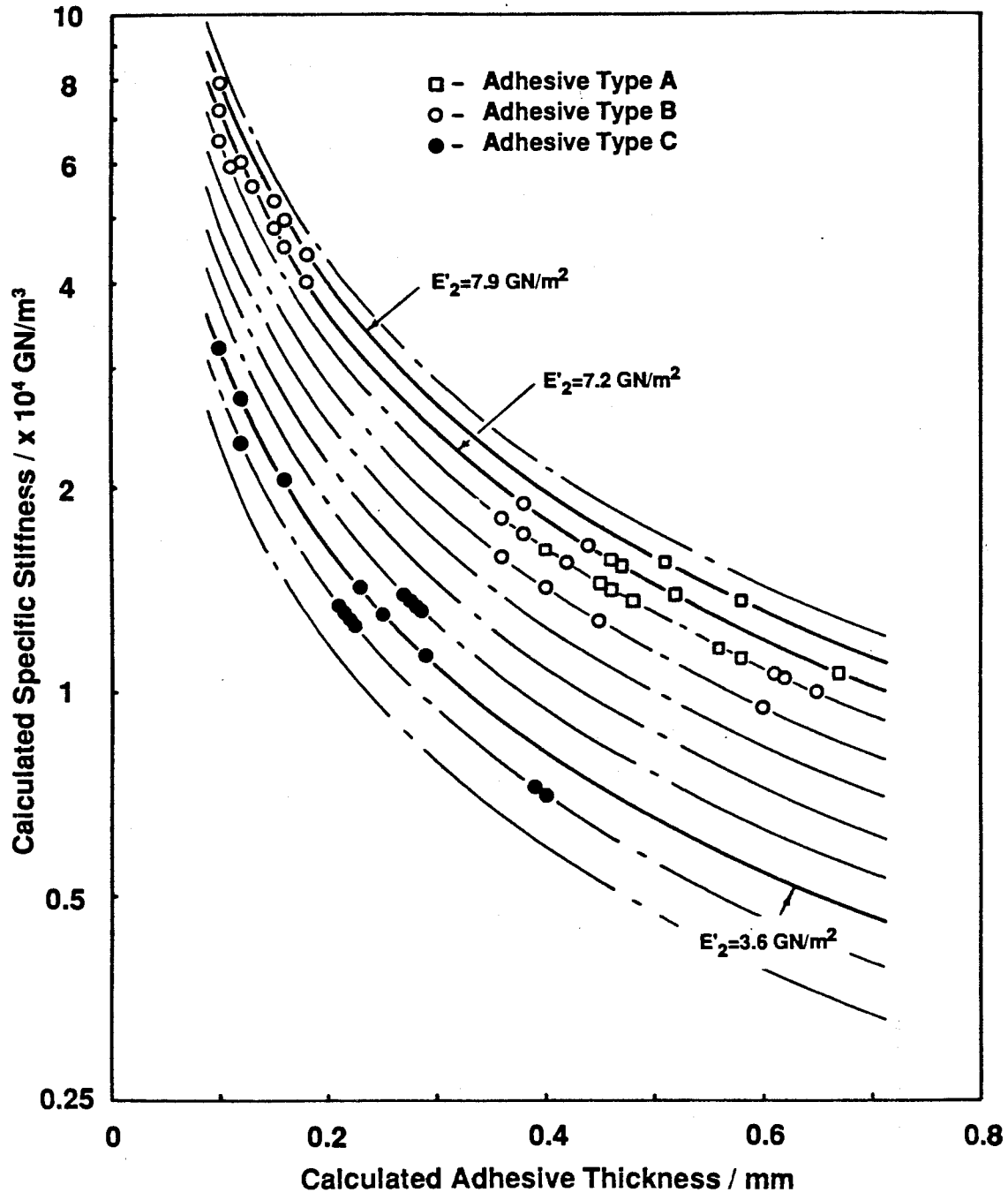

Figure 8.5 Calculated Specific Adhesive Stiffness as a Function of Calculated Adhesive Thickness

PART FOUR

CONCLUSIONS AND FURTHER WORK

CHAPTER 9

The Non-destructive Evaluation of Adhesion Strength

1 Introduction

It has been shown (see Chapter 8) that the basis of a technique to non-destructively evaluate the cohesive strength of a joint has been developed. However, there is still no reliable non-destructive test for the adhesion strength of a bond. Standard practice in the aerospace industry is to exercise great care on the surface preparation of the adherends, or possibly to test the adherend surface prior to bonding (Schliekelmann, 1972; Sutliff, 1978). Whilst this approach has been shown to produce satisfactory results it is widely acknowledged (see, for example, Stone, 1985) that the use of adhesive joints, in more critical areas of a structure, requires a non-destructive test for adhesion strength which can be used after bonding.

It has been shown (Kinloch, 1983) that both surface contamination and the incorrect surface pre-treatment of the adherends are likely to result in poor resistance to environmental attack. Consequently, it is important that a test for adhesion strength should detect both faults after manufacture. Once the joint is in service it is then important to be able to monitor the progress of any environmental degradation which weakens the adhesion layer.

The problems of developing a test for the adhesion strength of the joint are severe since the strength is highly dependent on the properties of the very thin layer (up to 5 μm) between the bulk adhesive and adherends. Whilst no new experimental results are presented here, the model used to examine changes in the cohesive properties of the joint (see Chapter 6) has been modified so that the suitability of methods for the detection of poor adhesion properties can be assessed.

2 Previous work on adhesion

Previous attempts at developing a test for adhesion strength have concentrated on measuring the stiffness of the adhesion zone and relating this

to the failure strength. This was done on the grounds that a defective adhesion layer e.g. resulting from environmental degradation or surface contamination will be more compliant than a correct adhesion layer.

In order to determine the influence of the stiffness of the adhesion layer on the resonant frequencies and amplitudes of the joint, the model described in Chapter 6 was adapted in a similar way to that used by Tattersall (1973) and Lloyd and Wadhwani (1978). Figure 9.1 shows the new model, the adhesion layer being modelled by a spring-damper element between the top adherend and the adhesive. The damping factor for the adhesion layer, η_A, was assumed to be relatively light and to be equal to that of the adherend i.e. 0.001.

It is very difficult to determine a value of adhesion stiffness to use in the model since it is almost impossible to measure it independently. However, the stiffness of a sound adhesion layer can be estimated by assuming that it can be modelled as a plain layer of finite thickness, t_A, having a modulus, E_A, and an area, A, between the adherend and adhesive. The stiffness K_A of such a layer would be given as follows :-

$$K_A = A E_A/t_A \qquad (9.1)$$

The area A, over which the deformation of the joint and the adhesion layer occurs, has been assumed to be equal to that of the ultrasonic probe (Worlton, 1962). The modulus, E_A, of a sound adhesion layer can be estimated as being at least that of the surface oxide, which, if aluminium adherends are assumed, is of the order of 100 GN/m^2. The thickness of the adhesion layer will be approximately equal to that of the oxide (or oxide and primer if a primer is employed). However, the oxide thickness can vary over a large range (0.04 to 2 μm) and is dependent on the type of surface preparation used (Stone,1985; Kinloch, 1983). Consequently, to establish a lower bound of the adhesion stiffness, it has been assumed that the thickness of the layer is no greater than 2 μm. Using these values in eqn. (9.1) gives a value of adhesion layer stiffness between 10^{12} and 10^{13} N/m.

Although it is assumed that a weak adhesion layer will have a lower stiffness,

it is very difficult to determine a typical value of K_A for a defective adhesion zone. In practice it is likely that contamination or incorrect surface preparation will cause only a marginal decrease in the stiffness of the adhesion layer. However, environmental degradation, which causes hydration of the oxide layer and the rupture of secondary bonds at the adhesive/adherend interface (Kinloch, 1983), is likely to cause a greater reduction in the adhesion stiffness.

The lower bound of the adhesion stiffness of a defective adhesion layer can be estimated in a similar way to that used for the sound adhesion layer. In this instance the modulus of the adhesion zone, E_A, is assumed to be equal to that of the adhesive i.e. of the order of 10 GN/m^2 and the thickness of the layer is assumed to be no greater than 0.02 mm (20μm). Using these values in eqn (9.1) and assuming the area (A) is the same as that previously used, produces an estimate of the lower limit for the adhesion stiffness of a defective adhesion zone equal to 5×10^{10} N/m.

The predictions reported in Chapter 6 were made with the assumption that the adhesion stiffness was infinite. Analysis of the model shown in figure 9.1 shows that reducing this stiffness to the value of its estimated lower bound for a good adhesion zone (10^{12} N/m) has a negligible effect on the resonant frequencies of any mode below 10 MHz.

It can be shown that reducing the stiffness to 10^{11} N/m causes small reductions (up to 1%) in the resonant frequencies of some modes. However, no significant change was seen in the first two modes. Therefore, it seems likely that the results of Alers *et al.* (1977), who used changes in frequency of the first mode to predict adhesion quality, were marred by inadequate correction for bond line thickness variations.

The resonant frequencies of the higher modes are more sensitive to changes in adhesion stiffness; however the extent of the change in frequency depends on the particular mode. Figure 9.2 shows how the resonant frequenicies of the eighth and ninth modes varies as a function of adhesion stiffness. This shows that the frequency of the ninth mode is practically independent of adhesion stiffness over a very wide range (10^{10} -10^{15} N/m), whereas the frequency of the eighth mode is more sensitive to stiffness since it decreases by

approximately 1% when the stiffness is reduced to 10^{11} N/m, and by approximately 3% when the stiffness is reduced further to 5 x 10^{10} N/m. However, even when the stiffness is at the lower limit of a defective adhesion zone (5 x 10^{10} N/m) the change in resonant frequency is small, and in practice would easily be masked by changes in the cohesive properties.

The different dependence of the resonant frequencies of the two modes is explained by examining their mode shapes. Figure 9.3 shows the predicted modes shapes of the eighth and ninth modes of the joint assuming that the adhesion stiffness is infinite. Figure 9.3a shows that the strain in the region of the adhesion zone in the eighth mode, given by $\partial u_x/\partial x$, is considerably greater than that in the ninth mode (see figure 9.3b); in this instance the strain across the adhesion zone in the ninth mode is negligble. Consequently, the eighth mode is more sensitive to changes in stiffness of the adesion layer than the ninth mode.

The resonant amplitudes, see Chapter 6, show a more pronounced dependence on adhesion stiffness than the resonant frequencies. As the adhesion stiffness changes from 10^{11} N/m to 10^{10} N/m, the predicted amplitudes of particular modes change by up to approximately 8%. However, there is no obvious pattern to the changes in amplitude, both increases and decreases being predicted. Consequently, in a practical test such changes in amplitude could easily be mistaken for changes in cohesive properties or porosity (see Chapter 8) of the adhesive.

2.1 Environmental Degradation

So far only the effect of changes in the stiffness of the adhesion layer on the frequency response of the joint has been considered. As mentioned earlier, an important mechanism in the degradation of the adhesion strength of a joint is the hydration of the oxide layer. In addition to reducing the modulus of the oxide layer, water also reduces the adhesive modulus, an effect commonly called plasticisation (Kinloch, 1983). In joints with metallic adherends this initially occurs along the adhesion layer owing to the high surface free energies of metals (Kinloch, 1983), and results in a zone of adhesive with a reduced modulus along both interfaces of the adhesive with the adherends.

Since the thickness of such a zone of reduced adhesive modulus is likely to be considerably greater than that of the adhesion layer, the overall change in joint stiffness when the adhesive is exposed to moisture will also be greater than that due to the adhesion layer alone. Indeed, after prolonged exposure to moisture it is likely that the whole of the adhesive layer will have a reduced modulus (Comyn, 1983).

As the size of the zone of reduced adhesive modulus increases it can be modelled as a change in the cohesive properties of the adhesive, in a similar way to that described in Chapters 6, 7 and 8 for bulk changes in adhesive modulus and thickness. Consequently, it is possible that the reduced adhesion strength of a joint due to hydro-thermal degradation or exposure to moisture could be identified more easily as a result of the changes in the cohesive properties of the joint rather than the adhesion properties. However, such a test would only be suitable for use in-service since there would be no significant change in joint stiffness due to moisture immediately after manufacture.

Lloyd and Wadhawani (1978) showed that joints which had been hydro-thermally degraded and failed in the adhesion layer could be identified if the spectra of different groups of echoes were compared. This was achieved by editing the time domain into small groups of echoes and calculating the spectrum of each individual group. The amplitude of the spectra at particular frequencies was then used to distinguish joints with with poor adhesion.

The change in spectra appears to be due to variations in the reflection and transmission coefficients at the adhesive/adherend interface which occur when the joint is subjected to environmental degradation. However, in practice such a technique is only likely to be suitable for joints with very thick adherends and adhesives since otherwise it is very difficult to edit the individual echoes (see Chapters 1 and 7).

3 Areas for Future Work on Adhesion

Although it appears that changes in adhesive stiffness, resulting from contamination or the incorrect surface pretreatment of the adherends, are unlikely to be large enough to affect the modes below 10 MHz, intial work by

other authors suggests that the modes at higher frequencies are more sensitive. For example Nestleroth *et al.* (1985) suggest that the response of the joint between 25-30 MHz can be used to detect more subtle changes in adhesion stiffness. Consequently, this is an area that needs to be investigated further.

Further work is also required for the development of a more detailed model of the adhesion layer. For example, it has been shown that surface contamination permits local slipping, parallel to the plane of the interface, between the adhesive and adherend. This results in a change of the reflection and transmission coefficients (see Chapter 4) for the adhesive/adherend interface (Kuhn and Lutsch, 1961; Graff, 1975). The different reflection and transmission coefficients would then be detected (Rohklin and Marom, 1986) either from the time domain or, more probably, from the frequency domain.

Pilarski (1985) has also shown that the use of interface (Stonely) waves, (see, for example, Graff, 1975), can be used to detect a contaminant between two solids in contact. However, further work needs to be done to determine their sensitivity to contamination in joints, and to find methods for exciting and receiving them in practice.

4 Conclusions

At present there are no non-destructive methods for evaluating the adhesion strength of a joint. The problem is currently overcome by careful control of the surface preparation procedures and possible also by testing the surface of the adherends prior to bonding.

It is possible that the reduction in adhesion strength resulting from hydro-thermal degradation or the ingress of moisture can be detected more easily by the associated reduction in the modulus of the adhesive. However, other work would be required to determine the extent of the change in the modulus of the adhesive and to evaluate the resulting changes in the spectrum.

The detection of surface contamination or incorrect pre-treatment of the adherend surface after bonding is likely to require considerable research effort, though a number of promising areas have been identified. These involve

examining the sensitivity of the through thickness modes of the joint to small changes in adhesive stiffness at frequencies between 25-30 MHz. Also, further work is required to examine the effects of small changes in the reflection and transmission coefficients for the adherend/adhesive interface, and to investigate the use of interface waves for detecting changes in the adhesion layer.

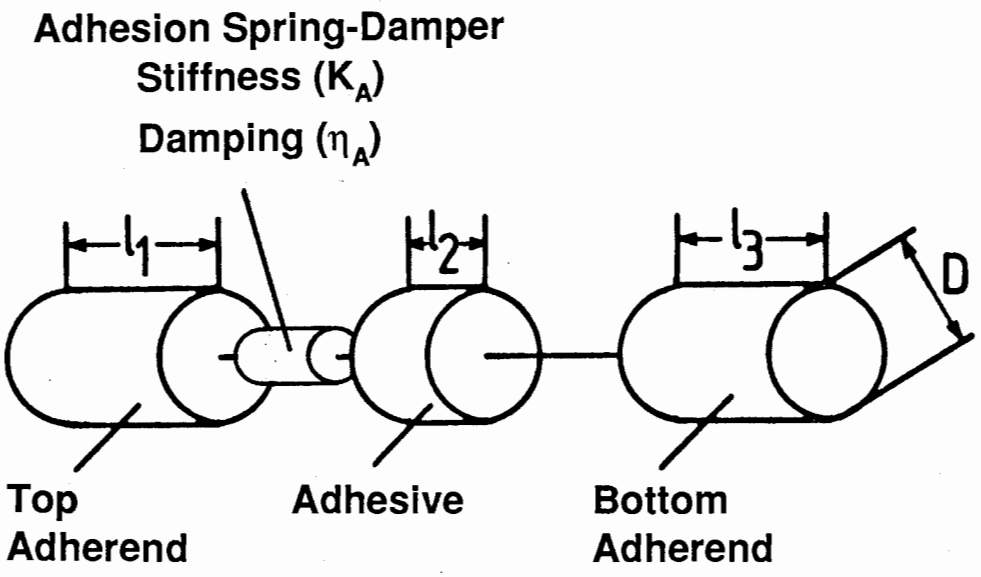

Figure 9.1 Schematic Representation of Model used for the Prediction of Changes in Adhesion Stiffness

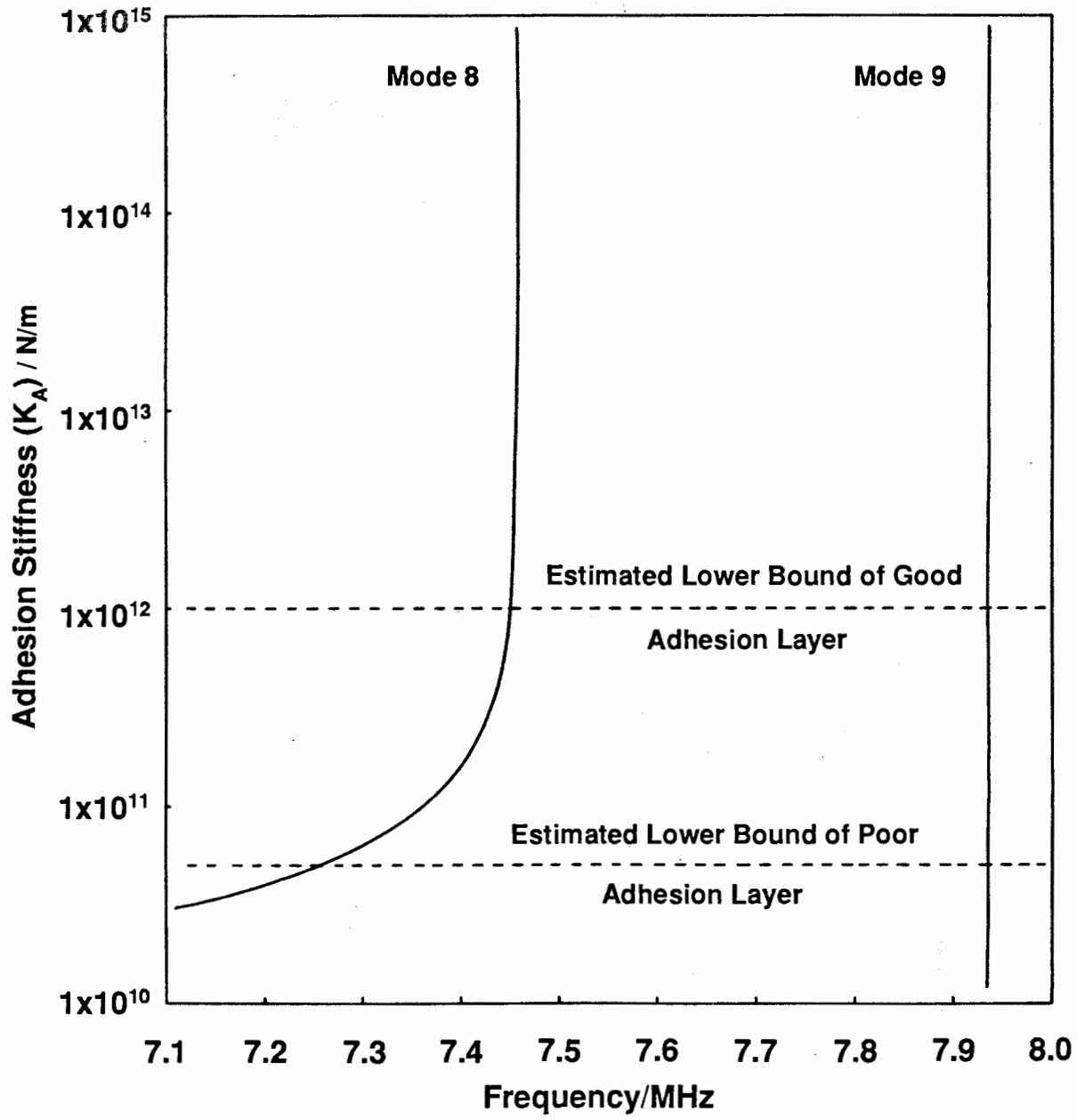

Figure 9.2 Frequency of the Eighth and Ninth Through Thickness Modes of the Joint as a Function of Adhesion Stiffness

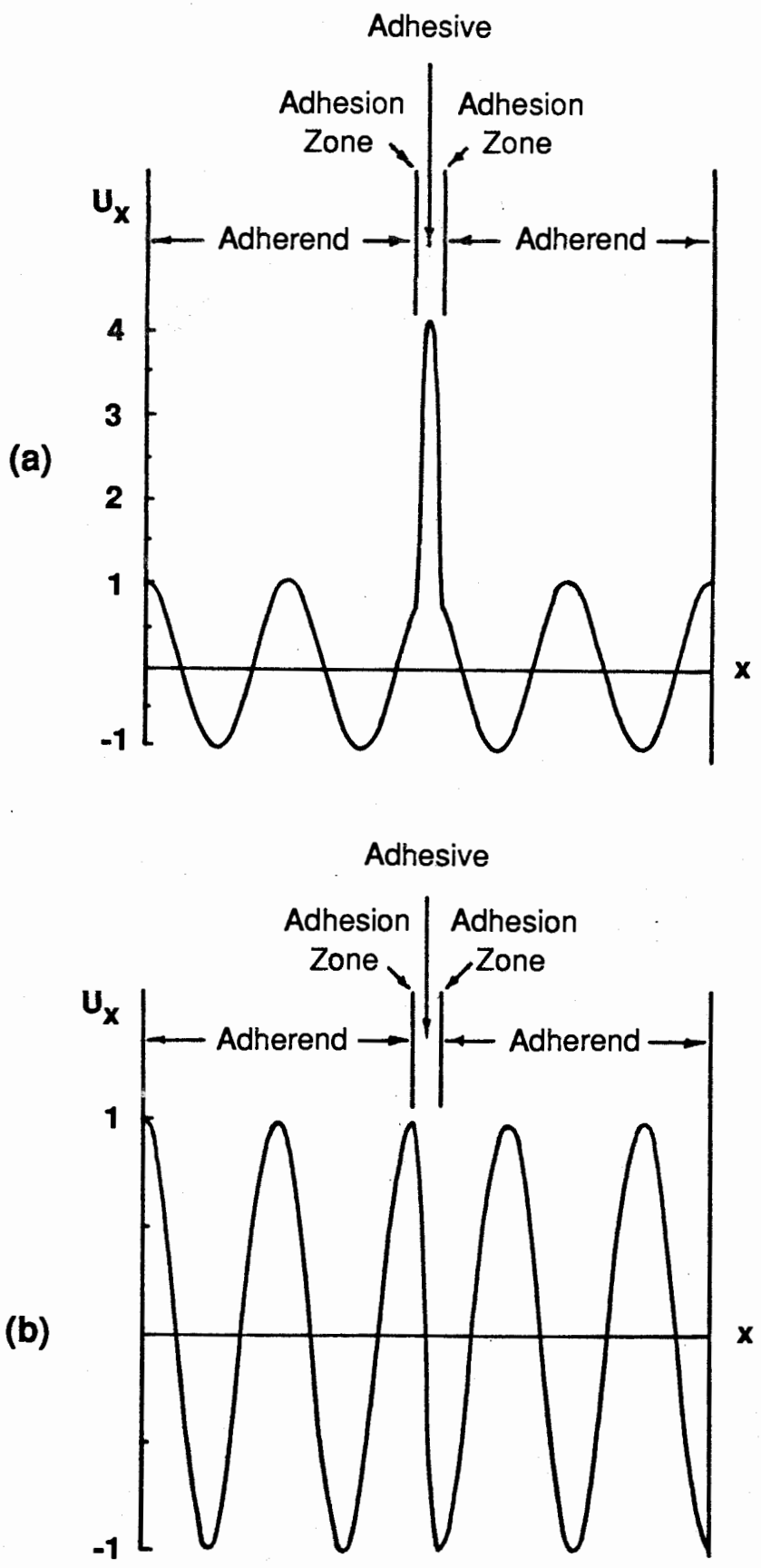

Figure 9.3 **Through Thickness Mode Shapes of the Joint** (a) eighth mode (b) ninth mode

CHAPTER 10
Conclusions

Three main types of defect that are commonly found in adhesive joints have been identified. The first type is complete voids, porosity and disbonds in the adhesive layer. The second type of defect is poor cohesive strength i.e. a weak adhesive layer whilst the final type is low adhesion strength, or a weak bond between the adhesive and the adherends.

A full review of currently available non-destructive testing techniques has shown that there are many methods available for locating voids and disbonds. However, it is important to determine the minimum size of defect to be detected since it is likely to be more difficult and expensive to find small defects, such as adhesive porosity, than it is to find gross voiding of the adhesive. Also, difficulties can be encountered in practice when the adhesive is very thin (<0.1-0.2 mm), or when it changes in thickness across a joint.

The detection of poor cohesive strength is much more difficult than the detection of voids and disbonds in the adhesive. The cohesive strength of an adhesive joint is dependent on many variables such as the adhesive thickness and its modulus and toughness. For example, the modulus of a particular adhesive is typically dependent on the cure cycle and on the correct mixing of hardener and resin yet it can correlate strongly with the cohesive strength of the joint (Alers *et al,* 1977). The dependence of joint strength on adhesive thickness is less clear; however, very thin or thick bondlines can both cause a reduction in strength (Ciba-Geigy, 1982). Consequently, joints which have the same specific adhesive stiffness but different adhesive moduli and thicknesses are likely not to have the same strength.

The review has shown that there is only one commercially available instrument, the Fokker Bond Tester Mk II, that attempts to measure the cohesive strength of a joint. However, an investigation into the sensitivity of the instrument has shown that it is not able to detect typical changes in adhesive modulus and thickness, and hence cohesive strength, unless the specific stiffness, defined as the ratio of apparent adhesive modulus to its

thickness, is less than 1-2 x 10^4 GN/m^3. It has also been shown that even when the instrument is used on joints of very low specific stiffness, it is only sensitive to the ratio of adhesive modulus to thickness, not modulus and thickness spearately. Consequently it is unlikely to give an adequate prediction of cohesive strength. In practice most joints commonly used in engineering primary structure which are made from the higher modulus epoxy adhesives will have specific stiffnesses of 2-3 x 10^4 GN/m^3 or greater. Consequently there is the need for the development of alternative techniques to give a non-destructive prediction the cohesive strength of a joint.

The review identified ultrasonic spectroscopy as a promising technique for the non-destructive evaluation of the cohesive properties of a joint. This technique uses the same basic principle as the Fokker Bond Tester, in that it measures the through thickness resonant frequencies and amplitudes of resonant response of the joint, but it is able to monitor many more modes than the Fokker Bond Tester.

A thorough investigation of ultrasonic spectroscopy has shown that although the first mode of the joint is only sensitive to the ratio of adhesive modulus to thickness i.e. specific stiffness, the higher modes are dependent on the modulus and thickness separately. It has been demonstrated that measurements of the resonant frequencies of a number (eight in the results presented here) of modes of the joint (except the first) can be used to determine the adhesive modulus and thickness separately. Consequently, it is possible to distinguish joints which have a satisfactory specific stiffness but have a low adhesive modulus, perhaps resulting from an incorrect cure cycle, from those which are correctly cured.

The work reported here has shown that changes in adhesive thickness of approximately 10%, and of adhesive modulus of approximately 20%, can be detected separately in joints with specific stiffness of up to 8 x 10^4 GN/m^3. This sensitivity could be increased by measuring the frequencies of more modes of the joint and by refining the calculation procedure. At present, therefore, ultrasonic spectroscopy can be used to give a check on the cohesive properties of the adhesive, a change in its modulus or thickness from the "normal" value indicating a fault in the production process.

It is theoretically possible to obtain similar results to those obtained here using the frequency domain by employing measurements in the time domain. However, changes in the time domain can be very subtle, and to date it has not been possible to distinguish changes in adhesive thickness from those in modulus. One of the main reasons for this is that typical adhesive thicknesses (0.05-0.2 mm) are beyond the resolution of most commercially available ultrasonic probes. This means that the changes in magnitude of the echoes from the top and bottom interface of the adhesive, that could be used to determine its cohesive properties, are masked by the echoes from other parts of the joint which overlap those from the interfaces.

It has also been shown that ultrasonic spectroscopy can be useful for determining the presence of defects such as disbonds, voids and porosity when their detection is difficult using time domain methods i.e. when the adhesive is thin (less than approximately 0.2 mm). Similarly, when the impedance of the adhesive is low, and either the echoes from the bottom of the adhesive are small, or there is a negligible change in the amplitude of echoes in the time domain between a voided and a sound joint, ultrasonic spectroscopy can be used to detect the defect.

At present there are no techniques available to detect poor adhesion strength non-destructively, however, a number of promising areas have been identified which merit further research.

References

Adams, R.D. and Cawley, P., 1985, "Vibration Techniques in Non-destructive Testing", Research Techniques in Non-destructive Testing, Vol. 8, (Academic Press, London) Chap. 7, pp303-360.

Adams, R.D. and Coppendale, J., 1976, "Measurement of the Elastic Moduli of Structural Adhesives by a Resonant Bar Technique", Journal of Mechanical Engineering Science v18 n3, pp149-158.

Adams, R.D., and Peppiatt, N.A., 1974, "Stress Analysis of Adhesive-Bonded Lap Joints", J. Strain Anal. v9, pp185-196.

Adams, R.D., Coppendale, J., and Peppiatt, N.A., 1978, "Failure Analysis of Aluminium-Aluminium Bonded Joints", Adhesion, Vol. 2, (Elsevier Applied Science Publishers) Chap. 7, pp105-120.

Alers, G.A., Flynn, P.L., and Buckley, M.J., 1977, "Ultrasonic Techniques for Measuring the Strength of Adhesive Bonds", Materials Eval. v31, pp77-84.

Bishop, R.E.D., and Johnson, D.C., 1960, "The Mechanics of Vibration", (University Press, Cambridge), Chap. 1, pp1-54.

Benham, P.P., and Warnock, F.V., 1984, "Mechanics of Solids and Structures", (Pitman, London).

Bond, L.J., and Saffari, N., 1984, "Mode-conversion in Ultrasonic Testing", Research Techniques in Non-destructive Testing, Vol. 7, (Academic Press, London), Chap. 5, pp145-189.

Botsco, R.J., 1968, "The Eddy-Sonic Test Method", Mater. Eval. v26, pp21-26.

Brekhovskikh, L.M., 1960, "Waves in Layered Media", (Academic Press, New York).

Canella, G., 1973, "Resonances and Effects of Couplant Layers in Ultrasonic Contact Testing", Mater. Eval. v31, pp61-66.

Cawley, P., 1984, "The Impedance Method of Non-destructive Inspection", NDT Int. v17, pp59-65.

Ciba-Geigy Plastics Division, 1982, "The User's Guide to Adhesives", Publ. A.17d.

Clarke, B., Tiu, W.P., and Sage, G.N., 1983, "Detection of Glue Line Voids in C.F.R.P.", in Symp. Proc. of Environmental Effects on Fibre-Reinforced Plastics, Imperial College, London.

Comyn, J., 1983, "Kinetics and Mechanism of Environmental Attack", in Durability of Structural Adhesives, (Applied Science Pulishers, London), Chapter 3, pp85-131.

Curtis, G.J., 1975, "Acoustic Emission Energy relates to Bond Strength", NDT Int. v8, pp249-257.

Curtis, G.J., 1982, "Non-destructive Testing of Adhesively Bonded Structures with Acoustic Methods", in Ultrasonic Testing - Non Conventional Testing Techniques Ed. J. Szilard, (John Wiley and Sons, Chichester), Chap. 13, pp495-554.

Djordjevic, B.B., and Venables, J.D., 1981, "Non-destructive Evaluation of Bonded Metal and Composite Structures", Proc. 13th Symp. Non-destructive Evaluation, San Antonio.

Evans, G.B., 1985, "40 Years of Structural Adhesive Bonding", Chartered Mechanical Engineer v32 n3, pp23-27.

Ewins, D.J., 1984, "Modal Testing Theory and Practice", (Research Studies Press, Letchworth).

Fagot, H., Albe, F., Smigielski, P., and Arnaud, J.L.,1980, "Holographic Non-destructive Testing of Materials using Pulsed Lasers", Proc. 12th Congress of the International Council of the Aeronautical Sciences (ILAS 80), Session 17, Munich.

Fiorito, R., Madigosky, W., and Uberall, H., 1979, "Resonance Theory of Acoustic Waves Interacting with an Elastic Plate", J. Acoust. Soc. Am. v66, n6, pp1857-1866.

Firestone, F.A., 1948, "Tricks with the Supersonic Reflectoscope", Non-destructive Testing, v7, n2, pp5-20.

Graff, K.F., 1975, "Wave Motion in Elastic Solids", (Clarendon Press, Oxford).

Hagemaier, D.J., 1971, "Bonded Joints and Non-destructive Testing, Bonded Honeycomb Structures-1", Non-destr. Test. v4, pp401-406.

Hagemaier, D.J., 1972, "Bonded Joints and Non-destructive Testing, Bonded Honeycomb Structures-2",Non-destr. Test. v5, pp38-48.

Hagemaier, D.J.,1982, "Automated Ultrasonic Inspection of Adhesive Bonded Structure", Mater. Eval. v40, pp572-578.

Hagemaier, D.J. and Fassbender, R., 1978, "Non-destructive Testing of Adhesively Bonded Structure", SAMPE Quarterly, pp36-58.

Haines, N.F., 1976, "Ultrasonic Spectroscopy", Physics in Technology, v7, n3, pp108-115.

Henneke, E.G., and Reifsnider, K.L., 1982, "Thermography-Applications to the Manufacture and Non-destructive Characterisation of Composites", Proc. Thermosense V, Detroit.

Hill, R., 1977, "The Use of Acoustic Emission for Characterising Adhesive Joint Failure", NDT Int. v10, pp63-72.

Hitchins, D., 1984, "FINEL Reference Manual", Imperial College London.

Izbicki, J.L., Maze, G. and Ripoche, J., 1984, "Etude de la Reemission Libre d'une Plaque Resonnante", Acustica v55, pp27-29.

Kim, D.H., and Sutliff, E.F., 1978, "The Contact Potential Difference (CPD) Measurement Method for Prebond Non-destructive Surface Inspection", Soc. for the Advancement of Materials and Process Engineering (SAMPE) Quarterly, pp59-63.

Kinloch, A.J., 1983, "Durability of Structural Adhesives", (Applied Science Publishers, London), Chap. 1, pp1-39.

Knollman, G.C., Bellin, J.L., and Hartog, J.J., 1982,"Methodology for Macrosonic Debonding of Adhesive Joints", Mater. Eval. v40, pp1057-1063.

Kolsky, H.,1963, "Stress Waves in Solids", (Dover Publ., New York).

Krautkramer, S., and Krautkramer, H., 1983, "Ultrasonic Testing of Materials", (Springer-Verlag, Berlin).

Kuhn, G.J., and Lutsch, A., 1961, "Elastic Wave Mode Conversion at a Solid-Solid Boundary with Transverse Slip", J. Acoust. Soc. Am. v33, n7, pp949-954.

Lange, Yu. Vu., 1976, "Acoustic Amplitude Method of Inspecting Bonding in Laminated Structures", Soviet J. Non-destr. Test. (Engl. Transl.) v12, pp5-11.

Lange, Yu. Vu., 1978, "The Acoustical Spectral Non-destructive Testing Method", Soviet J. Non-destr. Test. (Engl. Transl.) v14, pp193-199.

Lange, Yu. Vu., and Moskovenko, I.B., 1978, "Low Frequency Acoustic NDT Methods", Soviet J. Non-destr. Test. (Engl. Transl.) v14, pp788-797.

Lange, Yu. Vu., and Teumin, I.I., 1971, "Dynamic Flexibility of a Dry Point Contact",Soviet J. Non-destr. Test. (Engl. Transl.) v7, pp157-165.

Lazan, B.J., 1968, "Damping of Materials and Members in Structural Mechanics", (Pergamon Press, Oxford).

Li, M.X., Ding, W.Z., and Chen, J.M., 1982, "Principles of an Acoustic Impedance Method for Detection and Location of Non-Bonds in Adhesive Bonded Multi-layered Joints", NDT Int. v15, pp137-142.

Lloyd, E.A. and Wadhwani, D.S., 1978, "Ultrasonic Spectroscopy and the Detection of Hydrothermal Degradation in Adhesive Bonds", in Proceedings of 1st Int. Symp. on Ultrasonic Materials Characterisation, Gaithsburg Md., Issued 1980.

Lloyd, E.A., Wadhwani, D.S., and Brown, A.F., 1979, "Non-destructive Testing of Adhesive-Bonded Joints", proc. 9th World Conference on NDT, Melbourne.

Lord, R.J., 1985, "In-service Nondestructive Inspection of Fighter and Attack Aircraft", Mater. Eval. v43, pp733-739.

Madigosky, W. and Fiorito, R., 1979, "Modal Resonance Analysis of Acoustic Transmission and Reflection Losses in Viscoelastic Plates", J. Acoust. Soc. Am., v65, n5, pp1105-1115.

Martin, B.G., Hagemaier, D.J., and Fassbender, R.H., 1979, "Interference Effects in Using the Ultrasonic Pulse-Echo Technique on Adhesively Bonded Metal Panels", Mater. Eval., pp81-88.

Maze, G., Izibicki, J.L., Ripoche, J., Nagl, A., Uberall, H., and Yoo, K.B., 1986, "Transient acoustic scattering from layers and plates", J. Acoust. Soc. Am., v80, n1, pp295-301.

McLaughlin, P.V., McAssey, E.V., and Dietrich, R.C., 1980, "Non-destructive Examination of Fibre Composite Structures by Thermal Field Techniques", NDT Int. v13, pp56-62.

Newland, D.E., 1984, "Introduction to Random Vibration and Spectroscopic Analysis", (Longman, New York).

Nestleroth, J.B., Rose, J.L., Subramanian, K., 1985, "Feature Mapping for Anomaly Identification in Composite Materials and Adhesive Bonds", in proc. 11th World Conference on NDT, Las Vegas, pp1359-1365.

Phelan, C.S., 1972, "A Critical Analysis of Two Stage Non-destructive Testing using Harmonic and Interfacing Resonant Frequency Systems", in proc. Applied Polymer Symposium No.19, (John Wiley and Sons, New York), pp423-439.

Pilarski, A., 1985, "Ultrasonic Evaluation of the Adhesion Degree in Layered Joints", Mater. Eval. v43, pp765-770.

Pitts, L.E., Thomas, J.P., and Mayer, W.G., 1976, "Theoretical Similarities of Rayleigh and Lamb Modes of Vibration", J. Acoust. Soc. Am., v60, n2, pp374-377.

Pye, C.J., and Adams, R.D., 1981, "Detection of Damage in Fibre Reinforced Plastics using Thermal Fields generated during Resonant Vibration", NDT Int. v14, pp111-118.

Reynolds, W.N., and Wells, G.M., 1984, "Video Compatible Thermography", Br. J. Non-destr. Test. v26, pp40-43.

Rienks, K.J., 1972, "Fokker Bond Tester Model 70 Operation Manual", Royal Netherlands Aircraft Factories Fokker, Report no. R-1498.

Rivenez, J., 1984, "Determination Non-destructive de la Resistance de Joints Colles par Analyse Fine d'Echos Ultrasonores", in proc. 3rd European Conf. on NDT, Florence.

Rohklin, S.I., and Marom, D., 1986, "Study of Adhesive Bonds using Low Frequency Obliquely Incident Ultrasonic Waves", J. Acoust. Soc. Am. v80, n2, pp585-590.

Rose, J.L., 1984, "Elements of a Feature-based Ultrasonic Inspection System", Mater. Eval. v42, pp210-218.

Rose, J.L., Avioli, M.J., and Bilgram, R., 1983, "A Feasibility Study on the Non-destructive Evaluation of an Adhesively Bonded Metal to Metal Bond: Ultrasonic Pulse Echo Approach", Br. J. Non-destr. Test. v25, pp67-71.

Rose, J.L., and Meyer, P.A., 1973, "Ultrasonic Procedures for Predicting Adhesive Bond Strength", Mater. Eval., pp109-115.

Rothe, A., 1986, "Excitation of Lamb Waves in a Thin Plate with Short Ultrasonic Pulses", M.Sc. Thesis, Mech. Eng. Dept., Imperial College, London.

Schliekelmann, R.J., 1972, "The Non-destructive Testing of Adhesive Bonded Metal-to-metal Joints - 1", Non-Destr. Test. v5, pp79-86.

Schliekelmann, R.J., 1975, "Non-destructive Testing of Bonded Joints, Recent Developments in Testing Systems", Non-destr. Test., v8, pp100-110.

Schliekelmann, R.J., 1979, "Non-destructive Testing of Adhesive Bonded Joints", AGARD-LS-102, Chap. 8, pp8.1-8.37.

Schoch, A., 1952, "Der Schalldurchgang durch Platten", Acustica, v2, pp1-17.

Sendeckyj, G.P., 1983, "NDE Techniques for Composite Laminates" AGARD-CP-355, Chap. 2, pp1-22.

Stone, D.E.W., 1985, "Non-destructive Methods of Characterising the Strength of Adhesive-Bonded Joints", Tech. Memo MAT/STR 1065, Royal Aircraft Establishment.

Szilard, J., 1982, "Review of Conventional Testing Techniques", in Ultrasonic Testing - Non Conventional Testing Techniques,Ed. J. Szilard, (John Wiley and Sons, Chichester), Chap. 2, pp25-52.

Tattersall, H.G., 1973, "The Ultrasonic Pulse-Echo Technique as Applied to Adhesion Testing", J. Phys., v6, pp819-832.

Thrane, N., 1980, "Zoom-FFT", in Digital Signal Analysis - Using Digital Filters and FFT Techniques, (published by Bruel and Kjaer, 1981), pp121-160.

Tretout, H., Maurer, A., David, M., Juengling, K., Pepin, Ph., 1985, "Advanced Water Squirter System for Composite Materials Inspection and Application and Industrial Quality Control", in proc. 11th World Conference on NDT, Las Vegas, pp1396-1403.

Ueda, M., and Ichikawa, H., 1981, "Analysis of an echo signal reflected from a weakly scattering volume by a discrete model of the medium", J. Acoust. Soc. Am., v70, n6, pp1768-1775.

Worlton, D.C., 1961, "Experimental Confirmation of Lamb Waves Megacycle Frequencies", J. Appd. Phys., v32, n6, pp967-971.

Weight, J.P., 1984, "New Transducers for High Resolution Ultrasonic Testing", NDT Int. v17, pp3-8.

Weight, J.P., and Hayman, A., 1978, "Observation of the Propagation of Very Short Ultrasonic Pulses and their Reflections by Small Targets", J. Acoust. Soc. Am. v63, n2, pp396-404.

Wilkinson, C.T., 1982, "A Comparison of NDT Assessment for Quality Control and the Subsequent NDT Ability to Follow Ageing Degradation of Adhesive Bonded Joints in Aluminium Alloy", British Aerospace Aircraft Group, Hatfield, Chester Division, Final Report MOD Contract A93f/65.

Ying, C.F., and Li, M.X., 1979, "A Phenomenological Investigation into the Working Principle of the Fokker Bond Tester", Acta Acustica v1, pp44-51.

Zienkiewicz, O.C., 1971, "The Finite Element Method in Engineering Science", (McGraw Hill, New York).

APPENDIX

Details of Adhesives and Modulus Determination

1 Description of the Adhesives

In order achieve a range of adhesive modulus it was decided to add an ATBN rubber (HYCAR 1300X16 manufactured by BF Goodrich Chemical UK) in different proportions to typical epoxy resins. Three different adhesive mixes, refered to here as adhesive Types A, B and C, were used to represent the range of adhesive modulus likely to be encountered in practice.

The Type A adhesive was a typical epoxy resin, MY750 (manufactured by Ciba-Geigy), with no added rubber. This represented an adhesive with the highest modulus likely to be used in practice, the Young's Modulus being approximately 5 GN/m^2. The Type B adhesive comprised the same epoxy resin, MY750, mixed with a small proportion of the rubber (13% by mass). This was used to represent an adhesive having a 10% reduction in modulus compared to Type A. It had a moderately high modulus but was typical of the modulus that might be expected if a high modulus adhesive had been slightly mis-cured. The Type C adhesive was made by mixing a large proportion of rubber (62% by mass) with a different epoxy resin, GY292 (Ciba-Geigy), which had a lower modulus than MY750. This then represented either a rubbery, gap filling adhesive, or an adhesive having the modulus that might be expected if an epoxy adhesive had been very poorly cured.

In each instance a hardener, HY932 (Ciba-Geigy), was added to the base resin, or mixture of resin and rubber. Although other hardeners could be used, it was found that HY932 gave the most satisfactory working viscosity, usable life and cure cycle for the adhesives. The proportion of hardener used was 30%, by mass, of the base resin. The adhesive mixes were then thoroughly degassed in a vacuum chamber before being cured at 120°C for 3 hours.

2 Measurement of Adhesive Modulus

2.1 Basic Method

It was decided to determine the modulus of the adhesive by measuring the longitudinal wave velocity in the bulk specimen. This was done, using a pulse

from an ultrasonic probe, so that the stress state in the bulk specimen was similar to that in the adhesive of the joint during its through thickness vibration. The modulus (E'_2) can then be calculated from the longitudinal wave velocity, c_2, and the density of the adhesive, ρ_2, as follows :-

$$E'_2 = c_2^2 \rho_2 \qquad (A.1)$$

However, in this instance eqn. (A.1) gives an effective or apparent modulus rather than a true Young's Modulus of the adhesive. This occurs because the wavelength in the adhesive (≈2 mm at 1MHz) is less than the dimensions of the bulk specimen perpendicular to the path of the incident wave (Kolsky, 1963). Therefore, the deformation of the adhesive is likely to be confined to a small area compared to the area of the bulk specimen. Consequently, there will be a constraining effect from the surrounding undeformed material and the modulus will appear higher than the true Young's modulus.

The Young's (E) and apparent (E') moduli are related via the Poisson's ratio (ν) as follows (Kolsky, 1963) :-

$$E' = E(1-\nu) / [(1-2\nu)(\nu+1)] \qquad (A.2)$$

For example, the Young's modulus and Poisson's Ratio of aluminium are 68.9 GN/m^2 and 0.355 respectively; therefore using eqn. (A.2), the apparent modulus can be calculated as 113 GN/m^2. This is in good agreement with the value of apparent modulus of 111 GN/m^2 which was calculated, using eqn. (A.1), from wave velocity (6400 m/s), measured on a bulk specimen, and the density (2720 kg/m^3).

The apparent modulus can also differ from the true Young's modulus because the apparent modulus is measured dynamically rather than statically. Consequently, viscoelastic materials, such as many polymers and adhesives, appear to become more rigid as the measurement frequency increases.

2.2 Measurement of the Wave Velocity in the Adhesive

The wave velocity in the adhesive was measured from bulk specimens

(approximately 3 x 30 x 100 mm) of the adhesive which were manufactured at the same time as the joints. The longitudinal velocity in the adhesive, c_2, can be conveniently determined from the through thickness resonant frequencies of the bulk specimen. These frequencies, F_{Ln}, occur when the thickness, l_2, is equal to an integer number of half wavelengths (see eqn. (1.6)). By rearranging eqn. (1.6) it can readily be shown that the product of resonant frequency and thickness is a simple linear function of the mode number, n, i.e. :-

$$F_{Ln} \cdot l_2 = n \cdot c_2 / 2 \qquad (A.3)$$

Consequently, by plotting the mode number against the product of measured frequency and thickness the longitudinal velocity, over a considerable frequency range, can be determined from the gradient of the graph.

Figure A.1 shows a typical example of a spectrum between 0-6 MHz from a bulk specimen of adhesive Type A, obtained using the technique described in Chapter 5. Figure A.2 shows the product of resonant frequency, obtained from figure A.1, and thickness plotted as a function of mode number. This shows that the points lie very close to the line representing a longitudinal velocity of 2610 m/s. Since the experimental points do not significantly deviate from the line as the frequency is increased, it can be assumed that the longitudinal velocity is practically independent of frequency in the range of measurement of 0.5-5 MHz.

Figure A.2 also shows the results for the Type B and C adhesives, the longitudinal velocities corresponding to 2520 m/s and 1850 m/s respectively. Whilst the longitudinal velocity for the Type B adhesive appears to be independent of frequency, the results for the Type C adhesive show some deviation from the line representing a longitudinal velocity of 1850 m/s. This apparent increase in longitudinal velocity with frequency (approximately 3% over the frequency range 300 kHz to 3 MHz) is probably due to the viscoelastic nature of the Type C adhesive.

The accuracy of the measured longitudinal velocity is controlled by the measurement errors in the resonant frequency and the thickness. The error in the resonant frequency, provided the damping is not too great and it becomes difficult to determine the position of the minimum, is equal to the spacing

between spectral lines in the spectrum (2.5 kHz in this instance). Consequently, the percentage error in the measured resonant frequency is less than 0.3%.

The thickness of the bulk specimen (approximately 3 mm) was determined to an accuracy of greater than 0.02 mm, thus giving an error of approximately 0.7%. However, the thickness of the specimens was found to be non-uniform, there being a taper of up to 0.1 mm in 60 mm. Consequently, since it was difficult ensure that the spectrum was obtained at exactly the same point at which the measurement was taken, further errors of up to 0.3% could be introduced. Therefore, the maximum error in longitudinal velocity was 1.3%. The density of the adhesive was determined from the mass and volume of the bulk specimen after having machined its edges to obtain a regular shape. The errors in the measured mass and volume of the bulk specimen were approximately 0.2% and 0.8% respectively; the overall error in the density was therefore approximately 1%.

The apparent modulus of the adhesive could therefore be determined, using eqn. (A.1), to an accuracy of approximately 3-4% from the measured adhesive properties. The measured adhesive properties and the apparent moduli, determined using the above method, for all three adhesive types are shown in table A.1. The variation of the adhesive properties between different batches of the same adhesive type were found to be within the experimental measurement error.

3 Determination of Adhesive Modulus at Low Frequencies

Table A.1 also shows the adhesive modulus (E_{res}) measured using the resonant bar technique at frequencies of approximately 5 kHz (Adams and Coppendale, 1976) on 3 mm thick sections of adhesive cut from the bulk specimens. Adams and Coppendale showed that provided the adhesive thickness used was greater than approximately 1 mm, the measured modulus (E_{res}) approached the true Young's modulus for the adhesive. If, however the modulus was frequency dependent over the frequency range 0-5 kHz the measured modulus would not be the same as the static modulus.

For adhesive Types A and B the ratio between the apparent (measured between

500 kHz and 5 MHz) and resonant bar modulus (measured at around 5 kHz) is approximately 1.5, which corresponds to a typical Poisson's ratio for such adhesives of approximately 0.34 (Adams *et al.*, 1978), see eqn. (A.2). Therefore the modulus of the Type A and B adhesives appears to be effectively independent of frequency over a wide frequency range (from 5 kHz to 5 MHz).

The modulus of the Type C adhesive is more dependent on frequency there being a significant increase in the ratio of the apparent to the resonant bar modulus, to approximately 5, compared to the Type A and B adhesives. This indicates that there is a large increase in the stiffness of the adhesive as the frequency rises from 5 kHz to 300 kHz. This frequency dependent behaviour results from the large proportion of rubber (62% by mass) used in this adhesive. Figure A.2 shows that while there is a small (approximately 3%) increase in longitudinal velocity between 300 kHz and 3 MHz the frequency dependent behaviour of the adhesive is less pronounced than at lower frequencies and therefore it is not significant in the spectroscopy predictions.

Adhesive Type	Base Resin	% mass of rubber	Longitudinal Velocity (c_2) m/s error≈1%	Density (ρ_2) kg/m^3 error≈1%	Apparent Modulus (E'_2) GN/m^2 error≈3%	Resonant Bar Modulus (E_{res}) GN/m^2 error≈5%
A	MY750	0	2610	1170	7.9	5.2
B	MY750	13	2520	1130	7.2	4.6
C	GY292	62	1850	1050	3.6	0.7

Table A.1 Measured Adhesive Properties

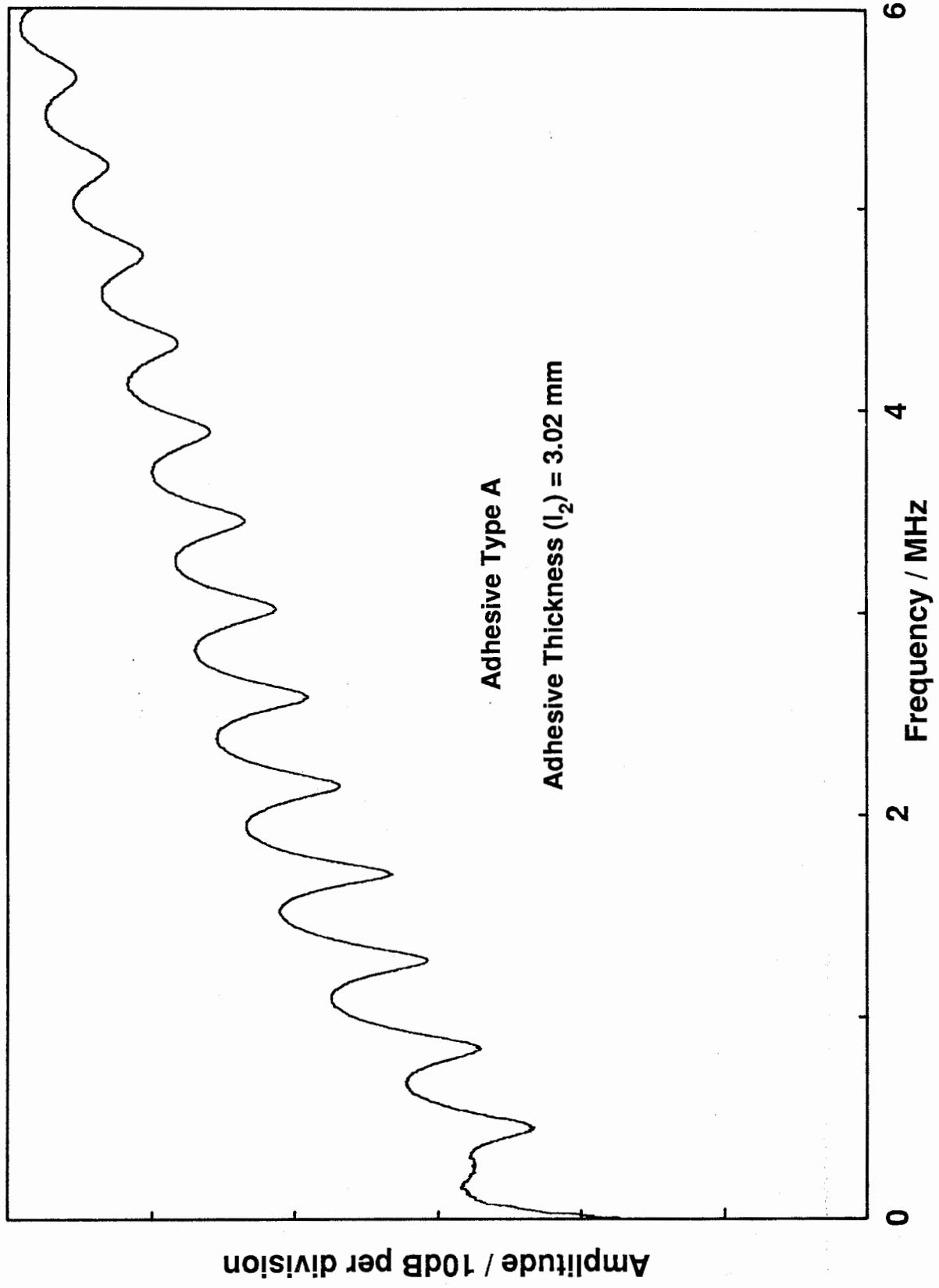

Figure A.1 **Example of Spectrum from a Bulk Specimen of Adhesive Type A**

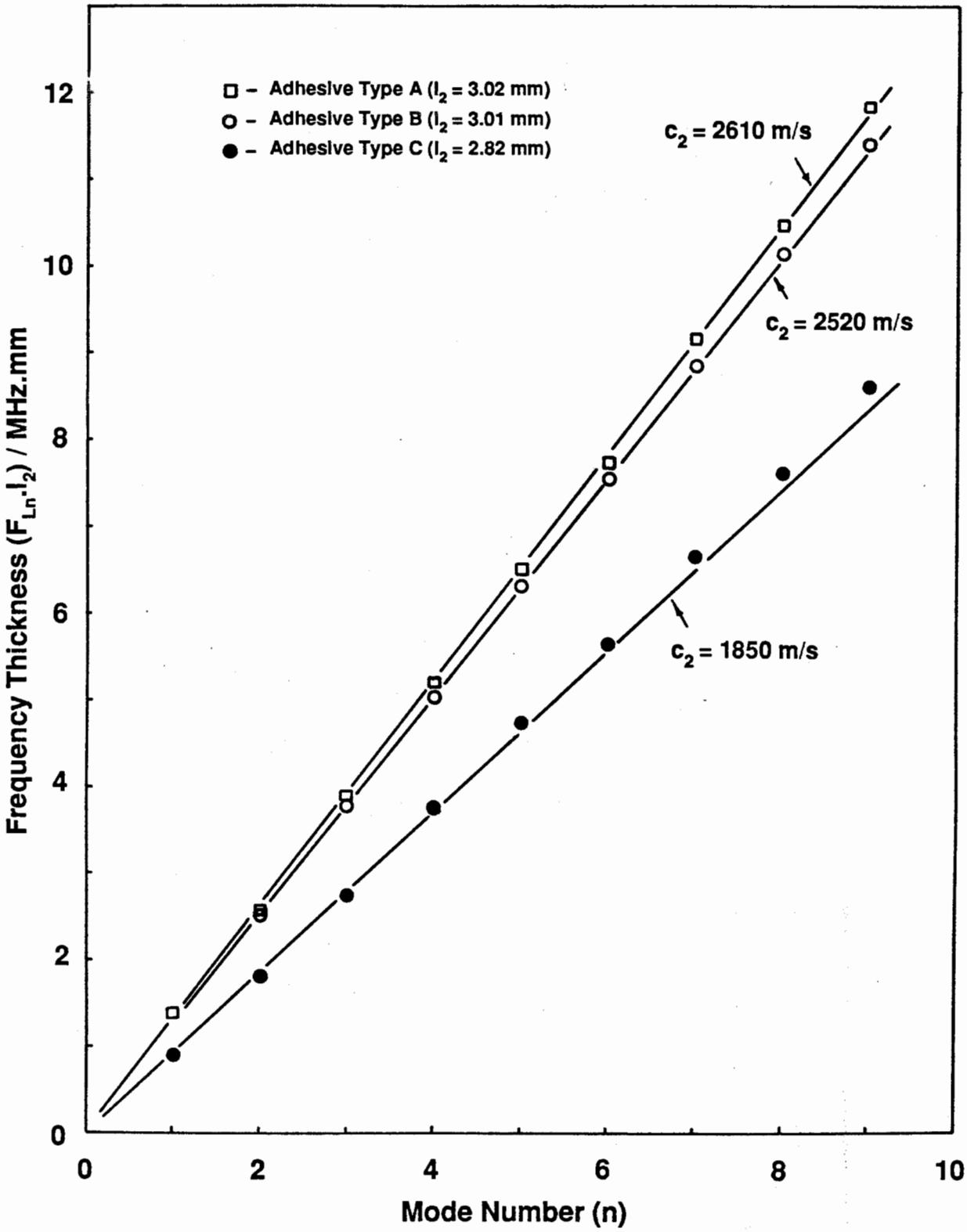

Figure A.2 Measured Product of Resonant Frequency and Thickness as Function of the Mode Number